Proteomic Signatures of Epidermal Growth Factor Receptor Signaling

By

Matthew Vaughn Myers

Dissertation

Submitted to the Faculty of the

Graduate School of Vanderbilt University

in partial fulfillment of the requirements

for the degree of

DOCTOR OF PHILOSOPHY

in

Biochemistry

May 2012

Nashville, Tennessee

Approved:

Professor Daniel C. Liebler

Professor Jennifer A. Pietenpol

Professor Carlos L. Arteaga

Professor Graham F. Carpenter

Professor Robert J. Coffey

To my wonderful parents William and Claryn Myers and to my soulmate Erin

ACKNOWLEDGEMENTS

Professor Daniel Liebler who, as my mentor, has given me support and encouragement during all my years of graduate research and helped me develop as a scientist. I thank him for the opportunity to be part of his research group and learn from his scientific creativity, which was integral through all stages of my research and enabled me to achieve my final educational goal.

Thank you to the outstanding committee members, Dr. Carlos Arteaga, Dr. Graham Carpenter, Dr. Robert Coffey, and Dr. Jennifer Pietenpol, who provided support and guidance throughout the years. All of my current and former colleagues; the friendly atmosphere in the laboratory made my days as a graduate student enjoyable and no less interesting.

I greatly appreciate the support and encouragement of my family throughout this long effort. Without them I would not have been inspired to become the man I am today. I also would like to express my gratitude and love to my better half, whose patience, encouragement, and humor helped me through my most difficult moments in my career as a graduate student. I'm truly indebted.

TABLE OF CONTENTS

LIST OF TABLES

LIST OF FIGURES

CHAPTER I

INTRODUCTION

Overview

Signaling networks and pathways regulate a variety of essential cellular functions. Identifying molecular responses to changes in signaling events is crucial not only for understanding the molecular mechanisms intrinsic to a signaling pathway, but also for evaluating the biological processes driving phenotypes. Activities of pathways are controlled by posttranslational modification of key pathway intermediates, such as signaling receptors and their downstream effectors, which undergo reversible phosphorylation and other modifications. Direct analysis of phosphorylated proteins is the most commonly employed method to assess signaling networks. Antibody and mass spectrometry-based techniques have proven useful to monitor phosphorylation events. However, these approaches are complicated by the transient nature of protein posttranslational modifications, their low abundance relative to unmodified proteins, potential artifacts due to uncontrolled pre-analytical variables or specificity of available antibodies. Given these considerations, more robust approaches to measure signaling networks are needed to overcome the challenges of direct phosphoproteome analyses.

The epidermal growth factor receptor (EGFR) is one of the most extensively studied receptor tyrosine kinases and represents a nexus of biological signaling events and influences a broad range of biological processes. Upon receptor activation, signal transduction occurs by recruitment of adaptor proteins and downstream kinases. Given EGFR involvement in multiple biological processes, it is not surprising that mutations and aberrant expression of the receptor have been linked to a number of human cancers types and can modify responsiveness to EGFR inhibiting drugs. Despite the rapid growth of information about EGFR signaling networks, identification of robust molecular markers linking network status and therapeutic response remains an ongoing challenge. We asked whether changes in global protein expression levels could produce distinct protein signatures indicative of a cellular response to EGFR drug modulation.

The work described in this dissertation presents results demonstrating the potential for monitoring signaling pathway changes through global protein responses. I hypothesize that changes in global protein expression signatures are indicative of a distinct response to drug treatment. Using two clinically available EGFR-targeted inhibitors (gefitinib and cetuximab), the EGFR signaling axis was modulated in human cancer cells and differences in protein expression were compared between treatments. The resulting changes represent a signature of differential protein expression and were assessed in multiple cancer cell lines, tissue models and human tissue samples. The following chapters detail a mass spectrometry-based approach for identifying and quantifying

changes in global protein signatures in response to EGFR perturbation. In addition, a comparison between two quantitative mass spectrometry methods for detecting phosphorylated proteins is discussed. The remainder of Chapter I will provide background on EGFR biology, discuss the role of the receptor in cancer, address variability in response to treatment, and outline the rationale for the approach described herein.

The Epidermal Growth Factor Receptor

Structure and organization

The epidermal growth factor receptor (EGFR) is a 170 kDa transmembrane glycoprotein that is one of the four members of the ErbB family of protein tyrosine kinase receptors along with ErbB2, ErbB3 and ErbB4 (HER2, 3 and 4 respectively) (1-3). A key mediator in many signaling pathways, EGFR regulates complex biological processes such as growth, differentiation, motility and cell death. As seen in Figure I-1A, EGFR is composed of several functional domains including: the extracellular (EC) domain, transmembrane domain, juxtamembrane domain, tyrosine kinase domain and the carboxy-terminal tail (2). The EC portion of the receptor has cysteine-rich regions, is highly glycosylated, and is capable of binding several different ligands including EGF, HB-EGF, epigen, amphiregulin, epiregulin, transforming growth factor alpha (TGF-α), and betacellulin (Figure I-1A). Binding of ligand to this EC domain induces the formation of homodimers with another EGFR molecule or heterodimers with

other members of the c-ErbB receptor tyrosine kinase family (4). This EC portion consists of four sub-domains referred to as L1, CR1, L2, and CR2 (Figure I-1C). Ligands bind between sub-domains L1 and L2 when the receptor adopts an extended confirmation to create a ligand binding pocket (5). The CR1 and CR2 domains consist of small modules

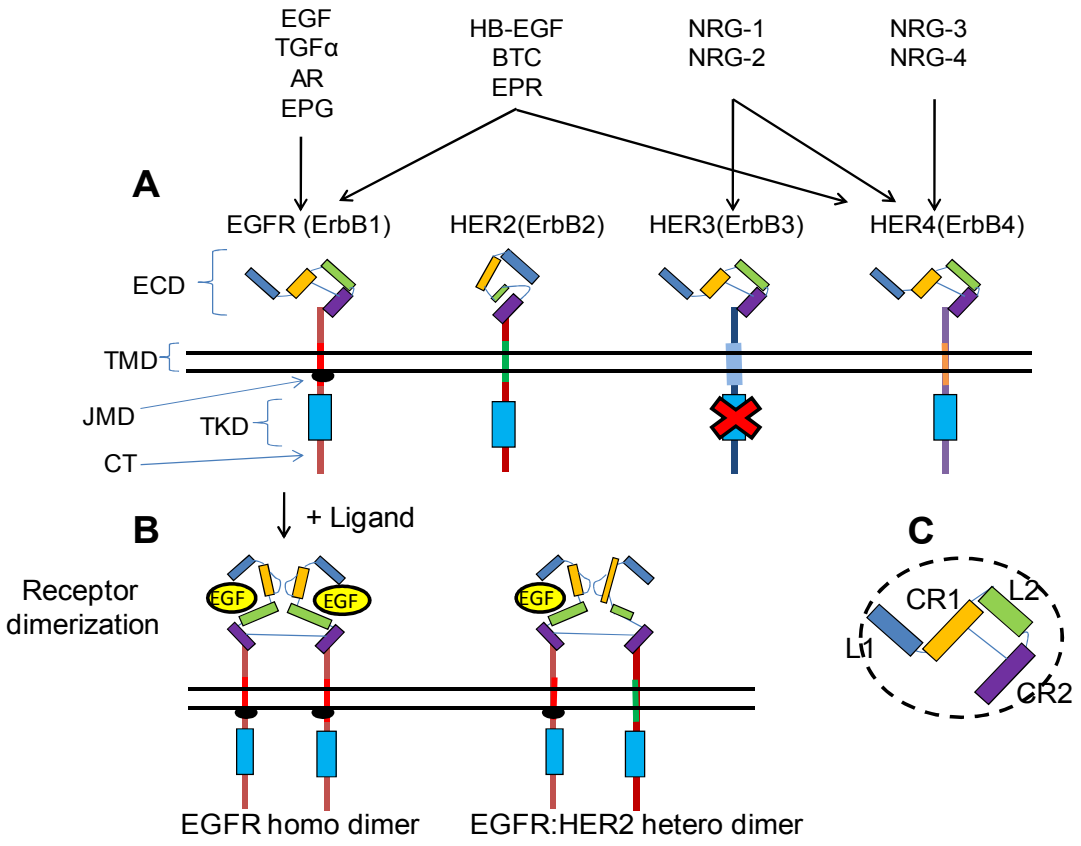

Figure I-1 Schematic of EGFR, ErbB family members, receptor dimerization and extracellular domain. ECD = extracellular domain, TMD = transmembrane domain, JMD = juxtamembrane domain, TKD = tyrosine kinase domain and CT = carboxy-terminal tail. A) Identifies the domains and ligands for EGFR and the other ErbB family members. HER2 binds no ligand, while HER3 has no active kinase domain. EGF = epidermal growth factor, TGF-α = transforming growth factor alpha, AR = amphiregulin, EPG = epigen, BTC betacellulin, EPR = epiregulin, NRG1-4 = neuregulin. B) Illustrates ligand binding and receptor homo-/hetero- dimerization. C) Enlarged view of the extracellular sub-domains of EGFR (L1-2) = ligand binding, (CR1-2) = cysteine rich domains.

containing disulfide bonds, and a large loop protruding from the back of the CR1 domain, which makes contact with the CR1 domain of other receptors and is necessary for dimerization (6, 7) (Figure I-1B).

Receptor activation

Upon dimerization, the intrinsic tyrosine kinase activity of the receptor is activated (8, 9) and catalyzes the transfer of the γ-phosphate of bound ATP—to autophosphorylate several specific sites (e.g., Y992, Y1045, Y1068, Y1148 and Y1173) in the cytoplasmic tail (CT) as well as endogenous substrates (10-12). The ATP binding pocket sits between an N-terminal lobe and a larger C-terminal lobe within the kinase domain (13). The internal phosphorylated residues serve as docking sites for Shc, Grb2, Src, phospholipase C and a host of other adapter proteins and activators of intracellular substrates (14-16)—typically with phosphotyrosine binding (PTB) and Src homology (SH2) domains (17-20). These recruited partners can be subsequently phosphorylated through the activated TKD of EGFR and form multi-component signaling complexes that activate intracellular signaling pathways.

Numerous reviews have addressed the pathways involved in EGFR receptor signaling (21-24). For example, Shc and Grb2 recruitment to the tyrosine phosphorylated receptor activates the Ras/Raf mitogen-activated protein kinase (MAPK) pathway—through a Grb2–bound exchange factor SOS—ultimately regulating transcription factors such as Elk-1 and c-fos (15). Another example is

the activation of the phosphatidylinositol 3-kinase (PI3K)/Akt signaling pathway (Figure I-2) through EGFR binding protein Gab1 (25, 26). These and other

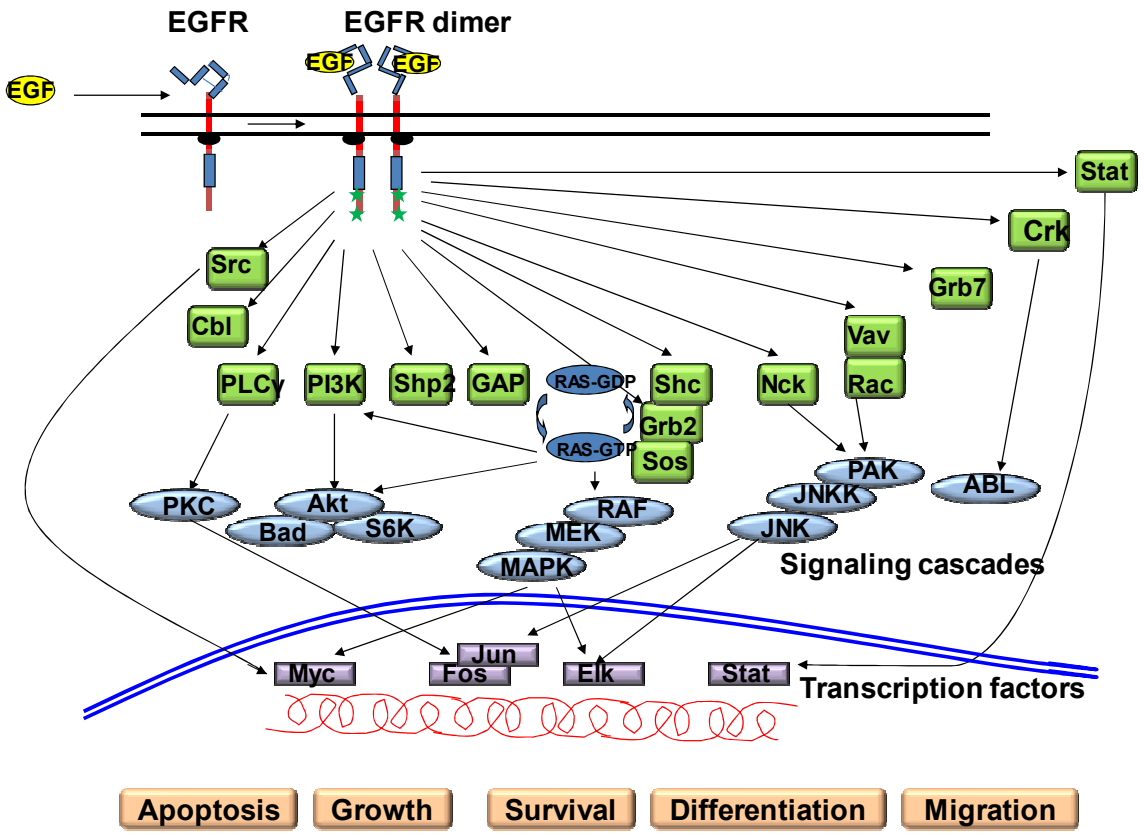

Figure I-2. EGFR signaling. Upon ligand binding, EGFR adopts an extended conformation allowing the receptor to dimerize through Domain II (CR1) of the EC portion of the receptor. Subsequent autophosphorylation (green stars) of residues in the cytoplasmic tail of the receptor occurs and present themselves as docking sites for adapter proteins. These adapter proteins and enzymes form multi-component signaling complexes capable of mediating downstream signaling events responsible for an array of biological processes.

EGFR-driven pathways regulate biological processes from cellular proliferation and gene expression to inhibition of apoptosis and survival (16, 27).

Additional mechanisms of receptor activation

In addition to EGFR activation by canonical ligand binding, receptor signaling can also be influenced via alternative mechanisms of transactivation (Figure I-3). Cytokines such as growth hormone and prolactin have been

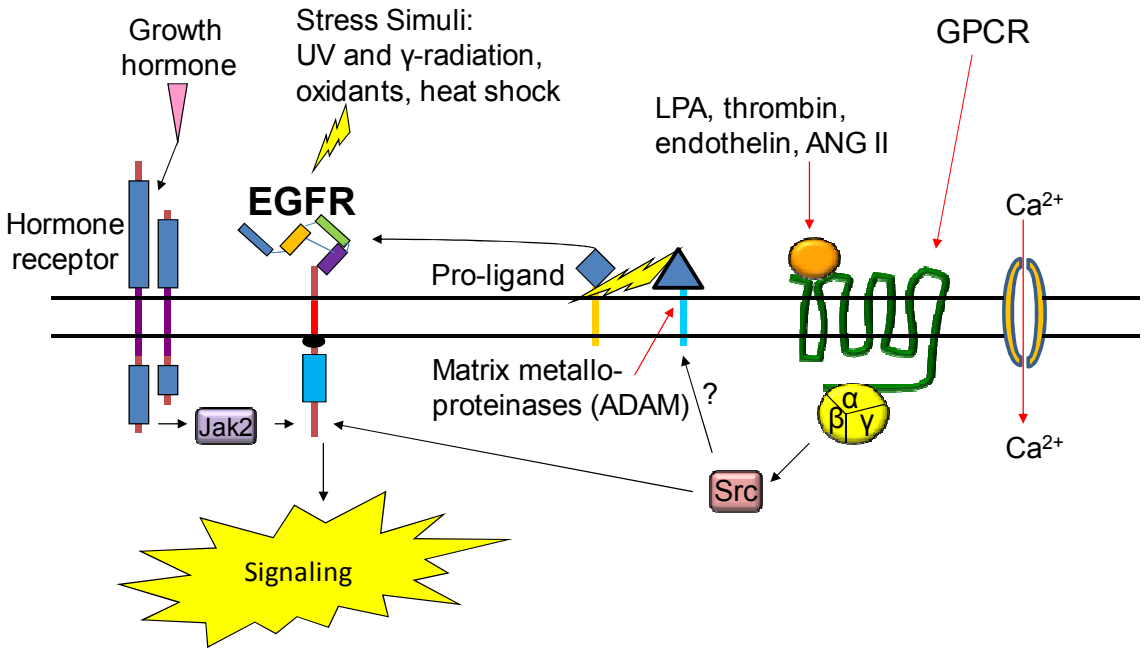

Figure I-3. Alternate methods of receptor activation. Schematic illustrating non-canonical mechanisms of EGFR activation. In addition to a number of stress stimuli, the growth hormone receptors and g-protein coupled receptors (GPCR) have been demonstrated to indirectly activate EGFR.

observed to indirectly activate EGFR through Janus tyrosine kinase (Jak2) which phosphorylates tyrosine residues within the CT domain of EGFR promoting GRB2 association, MAP kinase activation, and c-Fos induction (28, 29}. Additionally, EGFR has been found to be exploited by G-protein coupled receptor (GPCR)

mitogenic signaling involving assorted ligands including lysophosphatidic acid (LPA), endothelin, and angiotensin II (30, 31).

These activated GPCRs stimulate metalloproteinases capable of cleaving membrane bound EGF-like ligands and releasing them for enhanced receptor signaling (32). In addition, activated GPCRs indirectly activate the non-receptor tyrosine kinase Src, which can phosphorylate various residues on EGFR leading to increased receptor signaling (33-35). In some cells, particularly those of the nervous system, EGFR intracellular signaling pathways can be evoked by cellular changes in electrical activity. Moreover, angiotensisn II has been reported to induce Ca^{2+}-dependent trasnsactivation of EGFR (36). In PC-12 cells, an influx of Ca^{2+} through membrane depolarization results in increased levels of EGFR phosphorylation, while growth factor and insulin receptor phosphorylation remains unaffected (37, 38). This is believed to occur indirectly via a Src-activation mechanism similar to that for activated GPCR (39, 40). Other non-canonical means of EGFR activation include stress stimuli such as UV radiation (41, 42), gamma radiation (43), oxidants (44) and heat shock (45).

EGFR: Cancer and Targeted Inhibitors

EGFR expression in cancer

EGFR is found expressed or overexpressed in several human cancers including: non-small cell lung cancer (NSCLC) (46, 47), head and neck (48, 49), breast (50, 51), colorectal (52), prostate (53), gliomas (54), and bladder cancer

(55). Increased expression of EGFR has been associated with advanced tumor stages, resistance to traditional therapies, poor prognosis in patients and increased metastasis (56-60).

EGFR inhibitors

These findings led a surge in clinical focus on EGFR as a target for drug development, as demonstrated by the FDA approval of five drugs directed at this tyrosine kinase receptor from 2003-2007, including gefitinib and cetuximab, which will be further addressed in this section. Both of these drugs have been approved for the treatments of cancer including colorectal cancer (CRC), head and neck cancer, and non-small cell lung cancer (NSCLC). While both gefitinib and cetuximab target EGFR specifically, these two types of inhibitors block EGFR activation by different mechanisms (Figure I-4). Cetuximab is a chimeric (human:mouse), monoclonal antibody directed at the EC domain and competes for binding sites with endogenous ligands (61). Cetuximab binding to Domain III (L2) prohibits conformational changes and dimerization of the receptor monomer and results in the downregulation from the membrane surface, thus inhibiting further EGFR signaling (62, 63). Cetuximab treatment, in cell cultures with human cancer cells, exhibits growth inhibition, decreased angiogenesis and induction of apoptosis (64-66) and is characterized similarly *in vivo* by tumor regression, inhibited growth and angiogenesis, and increasing tumor sensitivity to radioresponse (61, 67-71). Gefitinib, however, is a small-molecule receptor

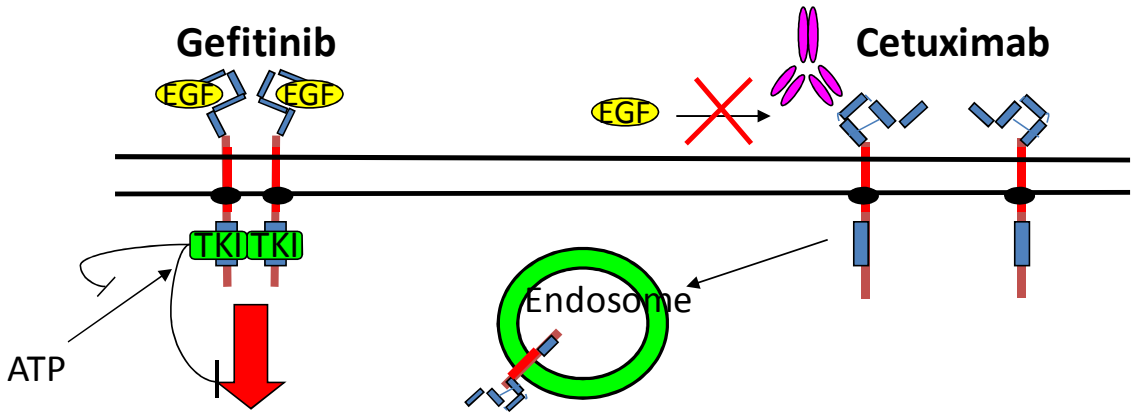

Figure I-4. Schematic of EGFR inhibition with gefitinib and cetuximab. TKI = tyrosine kinase inhibitor, EGF epidermal growth factor receptor. Gefitinib competes for binding near the ATP binding site inhibiting activation of the tyrosine kinase domain. Cetuximab binds to domain III (L2) of the extracellular portion of the receptor inhibiting dimerization and resulting in receptor down regulation.

tyrosine kinase inhibitor (TKI) designed to penetrate the cell membrane and compete with adenosinetriphosphate (ATP) for binding to the tyrosine kinase domain of EGFR (72). Similar to studies with cetuximab, studies both *in vitro* and *in vivo* demonstrated the ability of gefitinib to suppress tumorigenesis in mouse models and increase radiosensitivity (73-76).

Variable Response to EGFR-targeted Therapies

EGFR overexpression

Despite the broad importance of EGFR as a therapeutic target, varying responses to EGFR-targeted drugs *in vitro* and *in vivo* imply varying degrees and alternative mechanisms of signaling pathway activation and thus present a

significant clinical problem in assessing efficacy of therapy. There are multiple methods by which EGFR can become activated implying interplay of signaling mechanisms resulting in variable responses. Certainly, overexpression of EGFR is the most evident mechanism of increased receptor signaling and occurs several cancer types including glioma, colorectal, esophageal, and breast cancers (50, 54, 56, 57). However, conflicting reports in the literature make EGFR overexpression an inconsistent predictor of response to EGFR inhibiting drugs. For example, studies from esophageal and metastatic colorectal cancer patients reported by Janmaat et al. (77) and Yen et al. (78) have demonstrated a correlation between increased EGFR expression and gefitinib or cetuximab sensitivity, whereas studies in a number of cancer cell lines by Ciardiello et al. (79) and in patients with advanced colon cancer by Cascinu et al. (80) reported no significant correlation.

Heterodimerization and cross-talk with heterologous receptors

Extensive evidence supports heterodimerization with other ErbB receptors or cross-talk of EGFR with heterologous receptors as additional mechanisms of enhanced receptor activation, providing another possible explanation for the varying responses to EGFR inhibitor treatment. Reported overexpression of Her2 and Her3 was associated with resistance to gefitinib, but not to cetuximab in HNSCC cell lines (81). Cell models of liver metastases from gastric cancers with gefitinib resistance show EGFR and HER2 co-expression with an increase in EGFR expression over gefitinib-sensitive cell lines (82). Conversely, NSCLC and

breast cancer cell lines with HER2 overexpression showed increased sensitivity to gefitinib (83, 84). In addition, similar results were reported in breast cancer tumors by Hirch et al., who noted increased sensitivity to gefitinib in tumors overexpressing HER2 (85). Similar studies by Patel et al. in human xenograft models of gastric carcinoma showed that cetuximab treatment decreased EGFR-HER2 signaling and resulted in tumor growth inhibition (86). Again, discrepancies in the literature emphasize the complex nature of signaling responses and support the need for additional metrics of response to EGFR-inhibiting therapies.

Numerous examples in the literature link cross-talk of EGFR and heterologous receptor signaling pathways to human cancers (87-90). In pancreatic ductal adenocarcinomas and colon cancers, co-expression of the insulin-like growth factor receptor (IGR) and EGFR correlated with poor outcome (91, 92). Furthermore, studies in NSCLC cells and glioblastomas describe a role for the insulin-like growth factor receptor in a mechanism of resistance to gefitinib (93, 94). Additional mechanisms of cross-talk between EGFR signaling and the receptor tyrosine kinase c-Met (hepatocyte growth factor receptor) have been reported *in vitro* and *in vivo* (95, 96) with increased Met activation associated with resistance to gefitinib and anti-epidermal growth factor antibodies in lung cancer cells and to gefitinib in glioblastoma multiform mouse models (97,98, 99). In patients treated with cetuximab for metastatic colorectal cancer, c-MET overexpression significantly correlated with shorter progression-free survival and overall survival (100). These findings describe the interplay of EGFR with other

signaling pathways to influence the outcome of response to EGFR-targeted inhibitors.

Feedback loops

Signaling through autocrine feedback loops involving one or more EGFR ligands co-expressed with EGFR add an additional layer of complexity to EGFR signaling. Increased expression of EGF, TGF-α, or other EGF-like proteins has been noted in colorectal carcinoma and in advanced gliomas (101, 102) and expression of EGF, TGF-α, or amphiregulin correlates with poor prognosis or lowered survival in patients with breast and lung adenocarcinomas (103-106). In contrast, increased gene expression of amphireguiln and epiregulin was associated with longer progression free survival in patients with metastatic colorectal cancer (107). HNSCC cell lines with increased amphiregulin expression were significantly more likely to be growth inhibited by both gefitinib and cetuximab than those that produced minimal or no amphiregulin (108).

EGFR and downstream mutations

A large body of evidence indicates that responses to EGFR-targeted drugs are affected by EGFR mutations. Mutations affect intrinsic sensitivity or resistance at the level of the target receptor. EGFRvIII is an example of a truncated form of the receptor due to a deletion of exons 2 through 7, which results in a loss of amino acid residues 6 to 276 of the receptor EC domain (109); this variant of EGFR is constitutively active and is not downregulated by

endocytosis (110, 111). Overexpression of EGFRvIII has been noted in NSCLC and prostate cancer tissue (112, 113), and in studies *in vitro* and *in vivo* involving glioblastoma cells. EGFRvIII expression correlates with enhanced tumorgenicity in breast cancers and HNSCC (114-116). No significant response to cetuximab or gefitinib treatment was observed in HNSCC or in glioblastoma cells expressing EGFRvIII (116, 117). Activating mutations in the kinase domain, including L858R or deletion of residues l746-750 have been repeatedly found in non-small cell lung cancers and sensitize patients to gefitinib drug treatments (118, 119).

An interesting observation is the occurrence (either prior to or post-gefitinib treatment) of a T790M point mutation in NSCLC patients, which confers resistance to treatment with gefitinib (120-122). Furthermore, recent laboratory studies have suggested that the antitumor effect of cetuximab is not affected by the EGFR mutations, including the TKI-resistance mutation T790M (122, 123). However, it should also be noted that not all activating mutations in the kinase domain of EGFR (e.g., L861Q) similarly affect sensitivity to inhibition of the receptor tyrosine kinase by gefitinib (124).

Finally, some mutations or alterations in downstream signaling components are negative predictors of response to EGFR targeted therapies and afffect outcomes to drug treatments. Mutations in KRAS constitutively activate MAPK signaling and block cellular response to EGFR inhibiting drugs (120, 125, 126). Similarly, mutations in PIK3CA also confer resistance to the effects of EGFR inhibition by cetuximab (127-129).

Increased receptor and receptor ligand expression, cross-talk with HER2 or other receptors, co-expression of EGFR mutants, and mutations affecting downstream signaling components are all mechanisms that can alter EGFR signaling output and potentially modify response to EGFR inhibitors. These alternate modes of EGFR activation and highly variable responses observed for EGFR-targeting drugs highlight the need for robust molecular markers linking signaling network status and therapeutic response. Despite the complexity of EGFR-driven signaling pathways, endpoints and biomarkers linked to clinical responses are ultimately most needed to guide clinical application. Indeed, skin rash remains one of the most effective early indicators of clinical response to EGFR inhibitors (130).

Strategies for Assessing Response to EGFR-targeted Drugs

Monitoring phosphorylation events

Given the complex nature of EGFR signaling, direct analysis of phosphoprotein intermediates in signaling networks presents a logical analysis approach. Antibody-based methods are most commonly used for identifying protein and phosphoprotein changes in response to drugs. Numerous studies have employed immunohistochemical analysis of tissues to detect changes in response to treatment (131-133), although the lack of a standardized scoring system and subjective appraisal of staining make this method prone to inconsistencies. Additionally, western blot analysis is a convenient technique for

monitoring changes in total protein or phosphorylation status of a given signaling system (73, 134). Both techniques can be cumbersome when analyzing numerous targets. Protein and phosphoprotein analyses in tumor tissues by reverse phase protein arrays represent a new high through-put approach to identify putative signatures for EGFR inhibitor responses (135-138). A major drawback shared by all of these detection methods is the reliance on antibody specificity and limited availability of specific reagents to detect many target proteins.

Recently, mass spectrometry (MS)-based proteomic approaches aimed at the detection of protein phosphorylation have proven useful in the investigation of cellular signaling events (139-141) and have been shown to identify protein phosphorylation changes in response to drug treatments (142). Studies in cell models using global phosphoproteomics and targeted analysis of EGF pathway phosphoprotein intermediates have provided the most comprehensive analyses of EGFR-driven signaling networks (139, 143-145). Due to the low abundance of phosphorylation modifications relative to unmodified proteins, these methods typically require affinity techniques to enrich phosphorylated proteins and peptides for MS analysis (139, 141, 142, 146).

Cell culture models enable well-controlled experiments to study the status of phosphoprotein signaling networks. However, analysis of tissue specimens is complicated by sample heterogeneity, the transient nature and potential instability of phosphorylation modifications and limiting amounts of available tissue. In addition, acquisition practices for biopsies and surgical resections do

not permit rigorous control of preanalytical variables, such as ischemic time and temperature, which trigger stress responses that may obscure the status of network intermediates *in vivo* (147-149). These considerations suggest a need for robust assays capable of detecting signaling changes in response to EGFR drug treatments in patient tissue samples.

MS-based approaches: global shotgun proteomic analysis

While mass spectrometry approaches using phosphoproteomic techniques have proven useful in elucidating molecular mechanisms of drug response, the limitations involved in analyzing modified proteins demonstrates the value of additional assays to assess signaling changes. Shotgun proteomics, a method first described by Yates et al. (150), is now routinely used to identify the proteins present in complex biological mixtures (151, 152, 153l, 154). Shotgun proteomics (Figure I-5) involves digestion of a protein mixture into a collection of peptides subsequently separated on-line with a tandem mass spectrometer (151). Tandem mass spectra (MS/MS), which encode the peptide sequences, are collected for as many peptides as possible, and the resulting peptide identifications are searched against databases to identify the proteins in the original mixture (151, 155).

A critical element of shotgun proteomic analysis is the separation of peptides and proteins using multidimensional separation techniques to fractionate the complex peptide mixtures prior to MS/MS analysis (156). Each fraction presents a simplified peptide mixture for tandem MS analysis enabling acquisition of MS/MS spectra for lower abundance peptides. A variety of separation

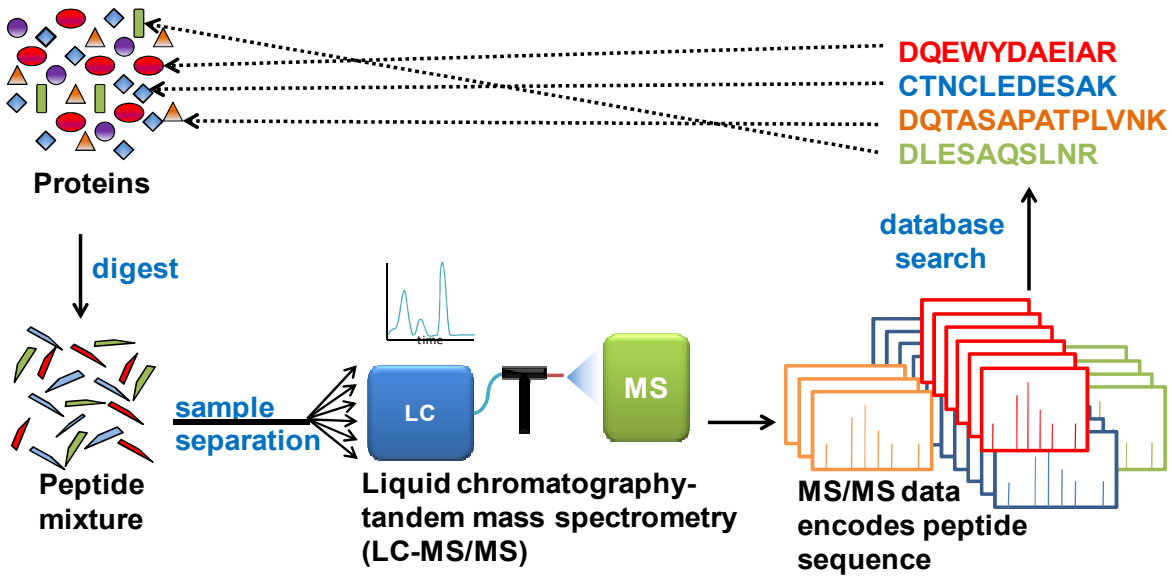

Figure I-5. Shotgun proteomics workflow. Proteins in sample are digested to peptide mixtures which are separated into multiple fractions before reverse-phase liquid chromatography tandems mass spectrometry analysis. Each MS/MS spectrum collected encodes a peptide sequence. Observed spectra are searched against a database to identify peptide sequences. Identified peptide sequences are mapped to proteins.

techniques from gel-enhanced protein separation (157), to strong-cation exchange (158), to isoelectric focusing (159) have been reported as the first dimension of separation in conjunction with shotgun proteomic analysis.

The collection of identified peptide sequences is then assembled into an inventory of proteins that can account for the peptide identifications. Because the likelihood of collecting an MS/MS spectrum of a peptide increases with the amount of the peptide in a sample, the numbers of MS/MS spectra that map to each protein provide a preliminary estimate of the amount of each protein in the sample (160, 161) (Figure I-6). Therefore, comparison of the MS/MS datasets

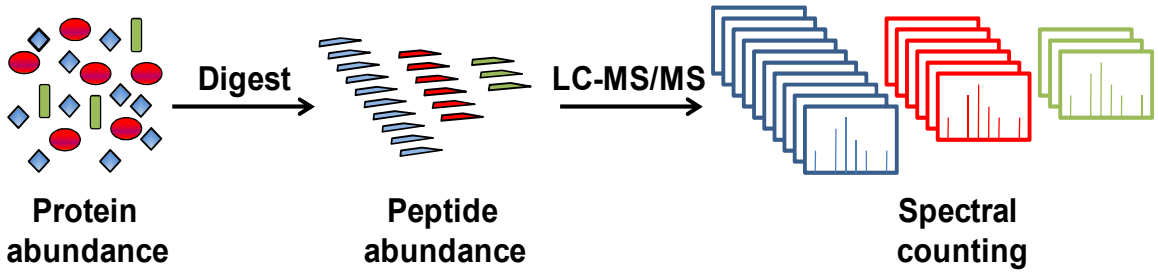

Figure I-6. Estimating protein abundance using spectral counting. The amount of peptides present in a digested protein sample correlates to the protein abundance. Thus, spectral counting approximates protein abundance based on observed peptides

from differentially treated cells (e.g., treated versus non-treated) or different tissue specimens (e.g., normal vs. cancer) facilitates the identification of proteome differences, which are distinct to one treatment or tissue type versus another. Global shotgun mass spectrometry-based techniques have been used to identify protein expression profiles in small systems such as proteins involved in a specific signaling network, and have proven robust enough to identify protein changes at the cellular and tissue levels (144, 162, 163). In addition, mass spectrometry approaches have reported distinct proteome profiles for cancer cells responsive or non-responsive to both gefitinib and cetuximab treatments (164-166).

MS-based approaches: targeted MRM analyses

Current approaches in the field of mass spectrometry also allow for quantitation of differentially expressed proteins. Previous studies have demonstrated the use of liquid chromatography-multiple reaction monitoring

mass spectrometry (MRM) as an invaluable tool for quantifying protein expression changes in complex biological systems (141, 167, 168). MRM analyses using a triple quadrupole mass spectrometer (Figure I-7) involves

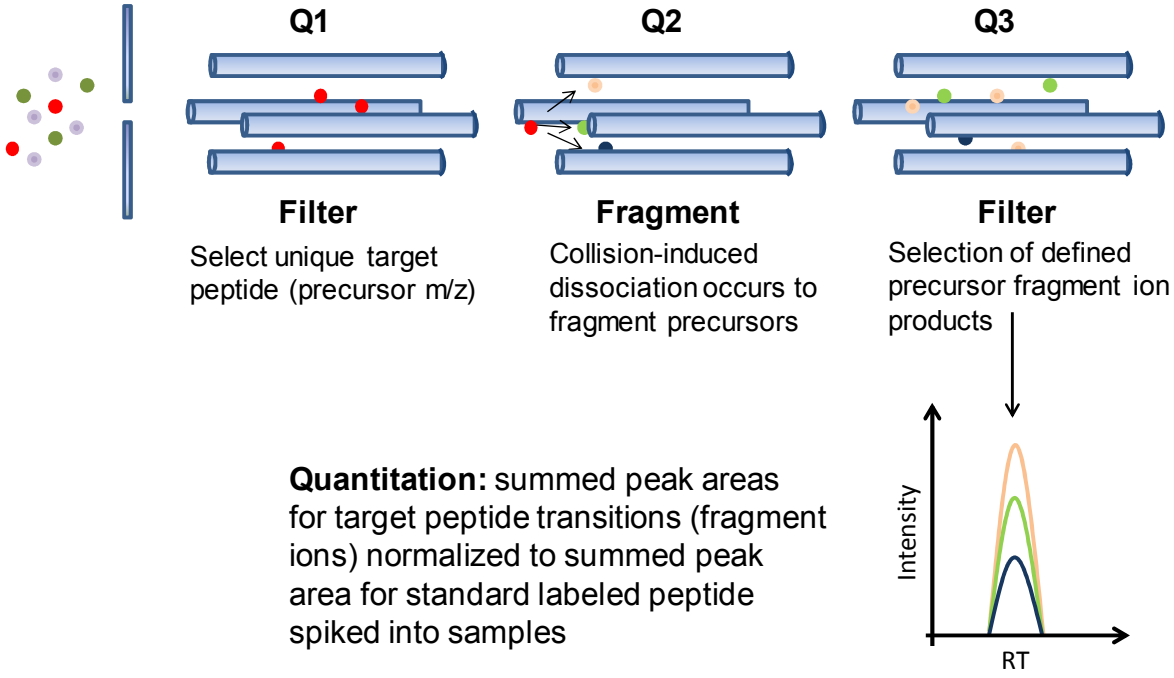

Figure I-7. Quantifying using MRM on a triple quadrupole mass spectrometer. Peptides unique to the protein of interest are selected in Q1, fragmented in Q2 and multiple fragment ion transitions are monitored for each peptide in Q3. Peak areas for each individual transition are summed and normalized to transition peak areas summed for a reference standard.

selecting an ion of interest (precursor) with the first mass filter Q1 and induces fragmentation in Q2 by collisional excitation with a neutral gas in a pressurized collision cell. The resulting 'product ions' (i.e., the fragmentation products of the selected precursor) are mass analyzed using the third quadrupole (Q3) (169,

170). This approach provides a selective method for measuring specific peptides and their corresponding protein. Targeted MS analysis using MRM enhances the lower detection limit for peptides by up to 100-fold by allowing rapid and continuous monitoring exclusively for the specific ions of interest (170). Modern triple quadrupole mass spectrometers are especially well suited to this type of analysis taking only 10–30 ms to survey each precursor-product transition, enabling large numbers of such transitions to be monitored during chromatographic elution into the mass spectrometer, with consequent high multiplexing capability.

Target peptides selected for MRM analysis should be unique (proteotypic) peptide sequences (typically 7-23 amino acids) and possess features that enhance chemical stability (170, 171). Peptide selection is often based upon results obtained during LC-MS/MS shotgun experiments (172); however, *in silico* methods of protein digestion and peptide selection are also available (173).

Contrary to antibody-based quantitation methods where antibody availability and specificity are often limiting, an LC-MRM-MS approach facilitates configuration of an assay for essentially any protein. Quantitation by these methods is typically achieved using stable isotope dilution (SID), in which labeled peptides are spiked into samples as internal standards for the corresponding endogenous peptide (168, 174). Application of this approach has proven sensitive enough to broach challenging quantitation problems including protein quantification at single-digit copy numbers in cells (172) and near ng/ml concentration in plasma (174, 175). Moreover, LC-MRM-MS in concert with

antibody-based enrichment techniques can achieve even greater levels of sensitivity (176, 177).

SID methods allow for the absolute quantitation of targeted peptides, but large-scale experiments are often costly ($500-$1000 per peptide) owing to the need for multiple isotopically labeled reagents (172, 178, 179}. However, recent studies reporting “label free” methods demonstrate quantitative data comparable to SID-based measurements and provide alternative means for quantifying protein expression changes without the need for costly labeled peptides for each target (168, 171). The LRP approach described by Zhang et al.—while not providing absolute quantitation—uses a single isotopically labeled peptide as a reference for all target analytes, and the data suggests the LRP method as a suitable approach for use in preclinical studies to rapidly screen large numbers of protein candidates at a fraction of the cost of configuring SID-LC-MRM-MS assays.

Research Objectives and Approach

Question and objectives

My research addresses the broad question of how to analyze responses to EGFR-modulating drugs. The major hypothesis to be tested is can changes in global protein expression levels produce distinct protein signatures indicative of a cellular response to EGFR-targeted drugs. Chapters II and III describes the mass spectrometry-based approach for identifying and quantifying global protein

changes resulting from EGFR stimulation and inhibition. The major objectives of this dissertation research were:

1. Establish a model system of EGFR activation and inhibition in human cancer cells using clinically relevant EGFR-targeting inhibitors
2. Apply global proteomic profiling to identify protein inventories for each treatment condition in the model system (proliferating, EGF-stimulated, gefitinib- or cetuximab- treated)
3. Develop a candidate signature of differentially expressed proteins indicative of a specific response to EGFR modulation and validate with targeted analysis
4. Test the candidate signature in multiple cell and tissue models to assess applications of this approach for future studies

A secondary goal of this research is to apply a new method to quantify protein modification changes to EGFR. The major focus of this work was to assess the performance of a newly developed MS-based quantitation method to detect phosphorylation changes on EGFR. Chapter IV compares the performance characteristics of two quantitative mass spectrometry approaches (internal reference peptide (IRP) and stable isotope dilution (SID)) at quantifying changes in EGFR phosphorylation. Initial studies are presented along with suggestions for future studies using overall findings in this dissertation.

Approach

To test the hypothesis that changes in global protein expression levels produce distinct protein signatures indicative of a cellular response to EGFR-targeted drugs, shotgun proteomic analysis were first employed to generate protein inventories for differentially treated A431 cells. Proteomic datasets were compared and protein differences were identified between treatment conditions. These protein differences constitute potential stimulation and inhibition signatures in response to EGFR modulation. A set of proteins whose expression was changed by EGF and reversed by both gefitinib and cetuximab comprised a candidate "EGFR inhibition signature", which was further verified by multiple reaction monitoring (MRM) analyses. This EGFR inhibition signature was then tested in 3 other models: 1) a comparison of DiFi (EGFR inhibitor-sensitive) and HCT116 (EGFR-resistant) cell lines, 2) in formalin-fixed, paraffin-embedded (FFPE) mouse xenograft DiFi and HCT116 tumors, and 3) in frozen tissue biopsies from a patient with the gastric hyperproliferative disorder Ménétrier's disease, who was treated with cetuximab. The results validated a multiprotein EGFR inhibition signature in all three models and illustrate the utility of protein expression changes as surrogate measures of signaling network activation and inhibition.

References

1. Cohen, S., Carpenter, G., and King, L. (1980) Epidermal growth factor-receptor-protein kinase interactions. Co-purification of receptor and epidermal growth factor-enhanced phosphorylation activity. *J. Biol. Chem.* **255**, 4834-4842.

2. Jorissen, R. N., Walker, F., Pouliot, N., Garrett, T. P. J., Ward, C. W., Burgess, A. W., and Graham, C. (2003) Epidermal growth factor receptor: Mechanisms of activation and signalling. *The EGF Receptor Family*, 33-55, Academic Press, Burlington.

3. Cohen, S., Ushiro, H., Stoscheck, C., and Chinkers, M. (1982) A native 170,000 epidermal growth factor receptor-kinase complex from shed plasma membrane vesicles. *J. Biol. Chem.* **257**, 1523-1531.

4. Cochet, C., Kashles, O., Chambaz, E. M., Borrello, I., King, C. R., and Schlessinger, J. (1988) Demonstration of epidermal growth factor-induced receptor dimerization in living cells using a chemical covalent cross-linking agent. *J. Biol. Chem.* **263**, 3290-3295.

5. Greenfield, C., Hiles, I., Waterfield, M. D., Federwisch, M., Wollmer, A., Blundell, T. L., and McDonald, N. (1989) Epidermal growth factor binding induces a conformational change in the external domain of its receptor. *EMBO J.* **8**, 4115-4123.

6. Garrett, T. P. J., McKern, N. M., Lou, M., Elleman, T. C., Adams, T. E., Lovrecz, G. O., Zhu, H.-J., Walker, F., Frenkel, M. J., Hoyne, P. A., Jorissen, R. N., Nice, E. C., Burgess, A. W., and Ward, C. W. (2002) Crystal Structure of a Truncated Epidermal Growth Factor Receptor Extracellular Domain Bound to Transforming Growth Factor [alpha]. *Cell* **110**, 763-773.

7. Ogiso, H., Ishitani, R., Nureki, O., Fukai, S., Yamanaka, M., Kim, J.-H., Saito, K., Sakamoto, A., Inoue, M., Shirouzu, M., and Yokoyama, S. (2002) Crystal Structure of the Complex of Human Epidermal Growth Factor and Receptor Extracellular Domains. *Cell* **110**, 775-787.

8. Thiel, K. W., and Carpenter, G. (2007) Epidermal growth factor receptor juxtamembrane region regulates allosteric tyrosine kinase activation. *Proceedings of the National Academy of Sciences* **104**, 19238-19243.

9. Red Brewer, M., Choi, S. H., Alvarado, D., Moravcevic, K., Pozzi, A., Lemmon, M. A., and Carpenter, G. (2009) The Juxtamembrane Region of the EGF Receptor Functions as an Activation Domain. *Mol. Cell* **34**, 641-651.

10. Downward, J., Parker, P., and Waterfield, M. D. (1984) Autophosphorylation sites on the epidermal growth factor receptor. *Nature* **311**, 483-485.

11. Voldborg, B. R., Damstrup, L., Spang-Thomsen, M., and Poulsen, H. S. (1997) Epidermal growth factor receptor (EGFR) and EGFR mutations, function and possible role in clinical trials. *Ann. Oncol.* **8**, 1197-1206.

12. Fan, Y. X., Wong, L., and Johnson, G. R. (2005) EGFR kinase possesses a broad specificity for ErbB phosphorylation sites, and ligand increases catalytic-centre activity without affecting substrate binding affinity. *Biochem. J.* **392**, 417-423.

13. Zhang, X., Gureasko, J., Shen, K., Cole, P. A., and Kuriyan, J. (2006) An Allosteric Mechanism for Activation of the Kinase Domain of Epidermal Growth Factor Receptor. *Cell* **125**, 1137-1149.

14. Batzer, A. G., Rotin, D., Urena, J. M., Skolnik, E. Y., and Schlessinger, J. (1994) Hierarchy of binding sites for Grb2 and Shc on the epidermal growth factor receptor. *Mol. Cell. Biol.* **14**, 5192-5201.

15. Prenzel, N., Fischer, O. M., Streit, S., Hart, S., and Ullrich, A. (2001) The epidermal growth factor receptor family as a central element for cellular signal transduction and diversification. *Endocrine-related cancer* **8**, 11-31.

16. Normanno, N., De Luca, A., Bianco, C., Strizzi, L., Mancino, M., Maiello, M. R., Carotenuto, A., De Feo, G., Caponigro, F., and Salomon, D. S. (2006) Epidermal growth factor receptor (EGFR) signaling in cancer. *Gene* **366**, 2-16.

17. O'Bryan, J. P. (1999) The PTB domain: a modular domain with multiple function. *Current opinion in drug discovery & development* **2**, 505-518.

18. Rojas, M., Yao, S., Donahue, J. P., and Lin, Y. Z. (1997) An alternative to phosphotyrosine-containing motifs for binding to an SH2 domain. *Biochem. Biophys. Res. Commun.* **234**, 675-680.

19. Zhou, M. M., Ravichandran, K. S., Olejniczak, E. F., Petros, A. M., Meadows, R. P., Sattler, M., Harlan, J. E., Wade, W. S., Burakoff, S. J., and Fesik, S. W. (1995) Structure and ligand recognition of the phosphotyrosine binding domain of Shc. *Nature* **378**, 584-592.

20. Kavanaugh, W. M., and Williams, L. T. (1994) An alternative to SH2 domains for binding tyrosine-phosphorylated proteins. *Science* **266**, 1862-1865.

21. Schlessinger, J. (2000) Cell signaling by receptor tyrosine kinases. *Cell* **103**, 211-225.

22. Schlessinger, J., and Bar-Sagi, D. (1994) Activation of Ras and other signaling pathways by receptor tyrosine kinases. *Cold Spring Harb. Symp. Quant. Biol.* **59**, 173-179.

23. Yarden, Y., and Sliwkowski, M. X. (2001) Untangling the ErbB signalling network. *Nat Rev Mol Cell Biol* **2**, 127-137.

24. Marmor, M. D., Skaria, K. B., and Yarden, Y. (2004) Signal transduction and oncogenesis by ErbB/HER receptors. *International Journal of Radiation Oncology*Biology*Physics* **58**, 903-913.

25. Rodrigues, G. A., Falasca, M., Zhang, Z., Ong, S. H., and Schlessinger, J. (2000) A Novel Positive Feedback Loop Mediated by the Docking Protein Gab1 and Phosphatidylinositol 3-Kinase in Epidermal Growth Factor Receptor Signaling. *Mol. Cell. Biol.* **20**, 1448-1459.

26. Alessi, D. R., and Cohen, P. (1998) Mechanism of activation and function of protein kinase B. *Current Opinion in Genetics & Development* **8**, 55-62.

27. Hackel, P. O., Zwick, E., Prenzel, N., and Ullrich, A. (1999) Epidermal growth factor receptors: critical mediators of multiple receptor pathways. *Curr. Opin. Cell Biol.* **11**, 184-189.

28. Yamauchi, T., Ueki, K., Tobe, K., Tamemoto, H., Sekine, N., Wada, M., Honjo, M., Takahashi, M., Takahashi, T., Hirai, H., Tushima, T., Akanuma, Y., Fujita, T., Komuro, I., Yazaki, Y., and Kadowaki, T. (1997) Tyrosine phosphorylation of the EGF receptor by the kinase Jak2 is induced by growth hormone. *Nature* **390**, 91-96.

29. Shida, D., Kitayama, J., Mori, K., Watanabe, T., and Nagawa, H. (2005) Transactivation of Epidermal Growth Factor Receptor Is Involved in Leptin-Induced Activation of Janus-Activated Kinase 2 and Extracellular Signal-Regulated Kinase 1/2 in Human Gastric Cancer Cells. *Cancer Res.* **65**, 9159-9163.

30. Prenzel, N., Zwick, E., Daub, H., Leserer, M., Abraham, R., Wallasch, C., and Ullrich, A. (1999) EGF receptor transactivation by G-protein-coupled receptors requires metalloproteinase cleavage of proHB-EGF. *Nature* **402**, 884-888.

31. Daub, H., Ulrich Weiss, F., Wallasch, C., and Ullrich, A. (1996) Role of transactivation of the EGF receptor in signalling by G-protein-coupled receptors. *Nature* **379**, 557-560.

32. Ohtsu, H., Dempsey, P. J., and Eguchi, S. (2006) ADAMs as mediators of EGF receptor transactivation by G protein-coupled receptors. *American Journal of Physiology - Cell Physiology* **291**, C1-C10.

33. Andreev, J., Galisteo, M. L., Kranenburg, O., Logan, S. K., Chiu, E. S., Okigaki, M., Cary, L. A., Moolenaar, W. H., and Schlessinger, J. (2001) Src and Pyk2 Mediate G-protein-coupled Receptor Activation of Epidermal Growth Factor Receptor (EGFR) but Are Not Required for Coupling to the Mitogen-activated Protein (MAP) Kinase Signaling Cascade. *J. Biol. Chem.* **276**, 20130-20135.

34. Luttrell, L. M., Rocca, G. J. D., van Biesen, T., Luttrell, D. K., and Lefkowitz, R. J. (1997) GÎ²Î³ Subunits Mediate Src-dependent Phosphorylation of the Epidermal Growth Factor Receptor. *J. Biol. Chem.* **272**, 4637-4644.

35. Dikic, I., Tokiwa, G., Lev, S., Courtneidge, S. A., and Schlessinger, J. (1996) A role for Pyk2 and Src in linking G-protein-coupled receptors with MAP kinase activation. *Nature* **383**, 547-550.

36. Eguchi, S., Numaguchi, K., Iwasaki, H., Matsumoto, T., Yamakawa, T., Utsunomiya, H., Motley, E. D., Kawakatsu, H., Owada, K. M., Hirata, Y., Marumo, F., and Inagami, T. (1998) Calcium-dependent Epidermal Growth Factor Receptor Transactivation Mediates the Angiotensin II-induced Mitogen-activated Protein Kinase Activation in Vascular Smooth Muscle Cells. *J. Biol. Chem.* **273**, 8890-8896.

37. Rosen, L. B., and Greenberg, M. E. (1996) Stimulation of growth factor receptor signal transduction by activation of voltage-sensitive calcium channels. *Proceedings of the National Academy of Sciences* **93**, 1113-1118.

38. Zwick, E., Daub, H., Aoki, N., Yamaguchi-Aoki, Y., Tinhofer, I., Maly, K., and Ullrich, A. (1997) Critical Role of Calcium- dependent Epidermal Growth Factor Receptor Transactivation in PC12 Cell Membrane Depolarization and Bradykinin Signaling. *J. Biol. Chem.* **272**, 24767-24770.

39. Biscardi, J. S., Maa, M.-C., Tice, D. A., Cox, M. E., Leu, T.-H., and Parsons, S. J. (1999) c-Src-mediated Phosphorylation of the Epidermal Growth Factor Receptor on Tyr845 and Tyr1101 Is Associated with Modulation of Receptor Function. *J. Biol. Chem.* **274**, 8335-8343.

40. Maretzky, T., Zhou, W., Huang, X. Y., and Blobel, C. P. (2011) A transforming Src mutant increases the bioavailability of EGFR ligands via stimulation of the cell-surface metalloproteinase ADAM17. *Oncogene* **30**, 611-618.

41. Zheng, Z. S., Chen, R. Z., and Prystowsky, J. H. (1993) UVB radiation induces phosphorylation of the epidermal growth factor receptor, decreases EGF binding and blocks EGF induction of ornithine decarboxylase gene expression in SV40-transformed human keratinocytes. *Exp. Dermatol.* **2**, 257-265.

42. Warmuth, I., Harth, Y., Matsui, M. S., Wang, N., and DeLeo, V. A. (1994) Ultraviolet Radiation Induces Phosphorylation of the Epidermal Growth Factor Receptor. *Cancer Res.* **54**, 374-376.

43. Schmidt-Ullrich, R. K., Mikkelsen, R. B., Dent, P., Todd, D. G., Valerie, K., Kavanagh, B. D., Contessa, J. N., Rorrer, W. K., and Chen, P. B. (1997) Radiation-induced proliferation of the human A431 squamous carcinoma cells is dependent on EGFR tyrosine phosphorylation. *Oncogene* **15**, 1191-1197.

44. Knebel, A., Rahmsdorf, H. J., Ullrich, A., and Herrlich, P. (1996) Dephosphorylation of receptor tyrosine kinases as target of regulation by radiation, oxidants or alkylating agents. *EMBO J.* **15**, 5314-5325.

45. Lin, R. Z., Hu, Z.-W., Chin, J. H., and Hoffman, B. B. (1997) Heat Shock Activates c-Src Tyrosine Kinases and Phosphatidylinositol 3-Kinase in NIH3T3 Fibroblasts. *J. Biol. Chem.* **272**, 31196-31202.

46. Garcia de Palazzo, I. E., Adams, G. P., Sundareshan, P., Wong, A. J., Testa, J. R., Bigner, D. D., and Weiner, L. M. (1993) Expression of Mutated Epidermal Growth Factor Receptor by Non-Small Cell Lung Carcinomas. *Cancer Res.* **53**, 3217-3220.

47. Chang, J. W.-C., Liu, H.-P., Hsieh, M.-H., Fang, Y.-F., Hsieh, M.-S., Hsieh, J.-J., Chiu, Y.-T., Tsai, H.-Y., Chen, Y.-H., Chen, Y.-T., Hsu, H.-Y., Chen, Y.-T., Tsai, S.-F., Chen, Y.-R., Hsi, B.-L., and Huang, S.-F. (2008) Increased epidermal growth factor receptor (EGFR) gene copy number is strongly associated with EGFR mutations and adenocarcinoma in non-small cell lung cancers: A chromogenic in situ hybridization study of 182 patients. *Lung Cancer* **61**, 328-339.

48. Maurizi, M., Almadori, G., Ferrandina, G., Distefano, M., Romanini, M. E., Cadoni, G., Benedetti-Panici, P., Paludetti, G., Scambia, G., and Mancuso, S. (1996) Prognostic significance of epidermal growth factor receptor in laryngeal squamous cell carcinoma. *Br. J. Cancer* **74**, 1253-1257.

49. Sweeny, L., Dean, N. R., Magnuson, J. S., Carroll, W. R., Helman, E. E., Hyde, S. O., Desmond, R. L., and Rosenthal, E. L. (2011) EGFR expression in advanced head and neck cutaneous squamous cell carcinoma. *Head Neck*, n/a-n/a.

50. Badovinac-Crnjevic, T., Jakic-Razumovic, J., Podolski, P., Pleština, S., Šarčević, B., Munjas, R., and Vrbanec, D. (2010) Significance of epidermal growth factor receptor expression in breast cancer. *Med. Oncol.*, 1-8.

51. Gumuskaya, B., Alper, M., Hucumenoglu, S., Altundag, K., Uner, A., and Guler, G. (2010) EGFR expression and gene copy number in triple-negative breast carcinoma. *Cancer Genet. Cytogenet.* **203**, 222-229.

52. Italiano, A., Saint-Paul, M. C., Caroli-Bosc, F. X., Fransois, E., Bourgeon, A., Benchimol, D., Gugenheim, J., and Michiels, J. F. (2005) Epidermal growth factor receptor (EGFR) status in primary colorectal tumors correlates with EGFR expression in related metastatic sites: biological and clinical implications. *Ann. Oncol.* **16**, 1503-1507.

53. Peraldo-Neia, C., Migliardi, G., Mello-Grand, M., Montemurro, F., Segir, R., Pignochino, Y., Cavalloni, G., Torchio, B., Mosso, L., Chiorino, G., and Aglietta, M. (2011) Epidermal Growth Factor Receptor (EGFR) mutation analysis, gene expression profiling and EGFR protein expression in primary prostate cancer. *BMC Cancer* **11**, 31.

54. Bredel, M., Pollack, I. F., Hamilton, R. L., and James, C. D. (1999) Epidermal growth factor receptor expression and gene amplification in high-grade non-brainstem gliomas of childhood. *Clin. Cancer Res.* **5**, 1786-1792.

55. Mellon, K. W., Chris; Kelly, Peter; Horne, C. H. Wilson; Neal, David E (1995) Bladder Cancer: Long-Term Outcome Related to Epidermal Growth Factor Receptor Status in Bladder Cancer. *J. Urol.*, 919–925.

56. Spano, J. P., Lagorce, C., Atlan, D., Milano, G., Domont, J., Benamouzig, R., Attar, A., Benichou, J., Martin, A., Morere, J. F., Raphael, M., Penault-Llorca, F., Breau, J. L., Fagard, R., Khayat, D., and Wind, P. (2005) Impact of EGFR expression on colorectal cancer patient prognosis and survival. *Ann. Oncol.* **16**, 102-108.

57. Hanawa, M., Suzuki, S., Dobashi, Y., Yamane, T., Kono, K., Enomoto, N., and Ooi, A. (2006) EGFR protein overexpression and gene amplification in squamous cell carcinomas of the esophagus. *Int. J. Cancer* **118**, 1173-1180.

58. Sainsbury, J. R., Malcolm, A. J., Appleton, D. R., Farndon, J. R., and Harris, A. L. (1985) Presence of epidermal growth factor receptor as an indicator of poor prognosis in patients with breast cancer. *J. Clin. Pathol.* **38**, 1225-1228.

59. Sainsbury, J. R., Farndon, J. R., Needham, G. K., Malcolm, A. J., and Harris, A. L. (1987) Epidermal-growth-factor receptor status as predictor of early recurrence of and death from breast cancer. *Lancet* **1**, 1398-1402.

60. Watzka, S. B., Rauscher-Pötsch, I., Nierlich, P., Setinek, U., Köstler, W. J., Pötschger, U., Müller, M. R., and Attems, J. (2010) Concordance between epidermal growth factor receptor status in primary non-small-cell lung cancer and metastases: a post-mortem study. *Eur. J. Cardiothorac. Surg.* **38**, 34-37.

61. Ng, M., and Cunningham, D. (2004) Cetuximab (Erbitux) – an emerging targeted therapy for epidermal growth factor receptor-expressing tumours. *Int. J. Clin. Pract.* **58**, 970-976.

62. Sunada, H., Magun, B. E., Mendelsohn, J., and MacLeod, C. L. (1986) Monoclonal antibody against epidermal growth factor receptor is internalized without stimulating receptor phosphorylation. *PNAS* **83**, 3825-3829.

63. Mendelsohn, J. (2002) Targeting the Epidermal Growth Factor Receptor for Cancer Therapy. *J. Clin. Oncol.* **20**, 1-13.

64. Meira, D. D., Nóbrega, I., de Almeida, V. H., Mororó, J. n. S., Cardoso, A. M., Silva, R. L. A., Albano, R. M., and Ferreira, C. G. (2009) Different antiproliferative effects of matuzumab and cetuximab in A431 cells are associated with persistent activity of the MAPK pathway. *Eur. J. Cancer* **45**, 1265-1273.

65. Liska, D., Chen, C.-T., Bachleitner-Hofmann, T., Christensen, J. G., and Weiser, M. R. (2010) HGF Rescues Colorectal Cancer Cells from EGFR Inhibition via MET Activation. *Clin. Cancer Res.* **17**, 472-482.

66. Wu, X., Fan, Z., Masui, H., Rosen, N., and Mendelsohn, J. (1995) Apoptosis induced by an anti-epidermal growth factor receptor monoclonal antibody in a human colorectal carcinoma cell line and its delay by insulin. *The Journal of Clinical Investigation* **95**, 1897-1905.

67. Ciardiello, F., Bianco, R., Damiano, V., De Lorenzo, S., Pepe, S., De Placido, S., Fan, Z., Mendelsohn, J., Bianco, A. R., and Tortora, G. (1999) Antitumor Activity of Sequential Treatment with Topotecan and Anti-Epidermal Growth Factor Receptor Monoclonal Antibody C225. *Clin. Cancer Res.* **5**, 909-916.

68. Milas, L., Mason, K., Hunter, N., Petersen, S., Yamakawa, M., Ang, K., Mendelsohn, J., and Fan, Z. (2000) In Vivo Enhancement of Tumor Radioresponse by C225 Antiepidermal Growth Factor Receptor Antibody. *Clin. Cancer Res.* **6**, 701-708.

69. Droller, M. J. (2000) Anti-epidermal growth factor receptor antibody C225 inhibits angiogenesis in human transitional cell carcinoma growing orthotopically in nude mice. *J. Urol.* **164**, 594.

70. Baselga, J. (2001) The EGFR as a target for anticancer therapy: focus on cetuximab. *Eur. J. Cancer* **37, Supplement 4**, 16-22.

71. Reynolds, N. A., and Wagstaff, A. J. (2004) Cetuximab: In the Treatment of Metastatic Colorectal Cancer. *Drugs* **64**, 109-118.

72. Shah, S. R., Walsh, T. L., Williams, C. B., and Soefje, S. A. (2003) Gefitinib (ZD1839, Iressa): a selective epidermal growth factor receptor-tyrosine kinase inhibitor. *Journal of Oncology Pharmacy Practice* **9**, 151-160.

73. Helfrich, B. A., Raben, D., Varella-Garcia, M., Gustafson, D., Chan, D. C., Bemis, L., Coldren, C., Barón, A., Zeng, C., Franklin, W. A., Hirsch, F. R., Gazdar, A., Minna, J., and Bunn, P. A. (2006) Antitumor Activity of the Epidermal Growth Factor Receptor (EGFR) Tyrosine Kinase Inhibitor Gefitinib (ZD1839, Iressa) in Non-Small Cell Lung Cancer Cell Lines Correlates with Gene Copy Number and EGFR Mutations but not EGFR Protein Levels. *Clin. Cancer Res.* **12**, 7117-7125.

74. Baselga, J., and Averbuch, S. D. (2000) ZD1839 ('Iressa') as an Anticancer Agent. *Drugs* **60**, 33-40.

75. Anne E. G. Lenferink, J. F. S., Laura K. Shawver, Robert J. Coffey, James T. Forbes, and Carlos L. Arteaga (2000) Blockade of the epidermal growth factor receptor tyrosine kinase suppresses tumorigenesis in MMTV/Neu + MMTV/TGF-α bigenic mice. *PNAS* **97**, 9609–9614.

76. Geoerger, B., Gaspar, N., Opolon, P., Morizet, J., Devanz, P., Lecluse, Y., Valent, A., Lacroix, L., Grill, J., and Vassal, G. (2008) EGFR tyrosine kinase inhibition radiosensitizes and induces apoptosis in malignant glioma and childhood ependymoma xenografts. *Int. J. Cancer* **123**, 209-216.

77. Janmaat, M. L., Gallegos-Ruiz, M. I., Rodriguez, J. A., Meijer, G. A., Vervenne, W. L., Richel, D. J., Van Groeningen, C., and Giaccone, G. (2006) Predictive factors for outcome in a phase II study of gefitinib in second-line treatment of advanced esophageal cancer patients. *J. Clin. Oncol.* **24**, 1612-1619.

78. Yen, L. C., Uen, Y. H., Wu, D. C., Lu, C. Y., Yu, F. J., Wu, I. C., Lin, S. R., and Wang, J. Y. (2010) Activating KRAS mutations and overexpression of epidermal growth factor receptor as independent predictors in metastatic colorectal cancer patients treated with cetuximab. *Ann. Surg.* **251**, 254-260.

79. Ciardiello, F., Caputo, R., Bianco, R., Damiano, V., Fontanini, G., Cuccato, S., De Placido, S., Bianco, A. R., and Tortora, G. (2001) Inhibition of Growth Factor Production and Angiogenesis in Human Cancer Cells by ZD1839 (Iressa), a Selective Epidermal Growth Factor Receptor Tyrosine Kinase Inhibitor. *Clin. Cancer Res.* **7**, 1459-1465.

80. Cascinu, S., Berardi, R., Salvagni, S., Beretta, G. D., Catalano, V., Pucci, F., Sobrero, A., Tagliaferri, P., Labianca, R., Scartozzi, M., Crocicchio, F., Mari, E., and Ardizzoni, A. (2007) A combination of gefitinib and FOLFOX-4 as first-line treatment in advanced colorectal cancer patients. A GISCAD multicentre phase II

study including a biological analysis of EGFR overexpression, amplification and NF-kB activation. *Br. J. Cancer* **98**, 71-76.

81. Erjala, K., Sundvall, M., Junttila, T. T., Zhang, N., Savisalo, M., Mali, P., Kulmala, J., Pulkkinen, J., Grenman, R., and Elenius, K. (2006) Signaling via ErbB2 and ErbB3 Associates with Resistance and Epidermal Growth Factor Receptor (EGFR) Amplification with Sensitivity to EGFR Inhibitor Gefitinib in Head and Neck Squamous Cell Carcinoma Cells. *Clin. Cancer Res.* **12**, 4103-4111.

82. Yokoyama, H., Ikehara, Y., Kodera, Y., Ikehara, S., Yatabe, Y., Mochizuki, Y., Koike, M., Fujiwara, M., Nakao, A., Tatematsu, M., and Nakanishi, H. (2006) Molecular basis for sensitivity and acquired resistance to gefitinib in HER2-overexpressing human gastric cancer cell lines derived from liver metastasis. *Br. J. Cancer* **95**, 1504-1513.

83. Hirata, A., Hosoi, F., Miyagawa, M., Ueda, S.-i., Naito, S., Fujii, T., Kuwano, M., and Ono, M. (2005) HER2 Overexpression Increases Sensitivity to Gefitinib, an Epidermal Growth Factor Receptor Tyrosine Kinase Inhibitor, through Inhibition of HER2/HER3 Heterodimer Formation in Lung Cancer Cells. *Cancer Res.* **65**, 4253-4260.

84. Moasser, M. M., Basso, A., Averbuch, S. D., and Rosen, N. (2001) The Tyrosine Kinase Inhibitor ZD1839 ("Iressa") Inhibits HER2-driven Signaling and Suppresses the Growth of HER2-overexpressing Tumor Cells. *Cancer Res.* **61**, 7184-7188.

85. Hirsch, F. R., Varella-Garcia, M., and Cappuzzo, F. (2009) Predictive value of EGFR and HER2 overexpression in advanced non-small-cell lung cancer. *Oncogene* **28**, S32-S37.

86. Patel, D., Bassi, R., Hooper, A., Prewett, M., Hicklin, D. J., and Kang, X. (2009) Anti-epidermal growth factor receptor monoclonal antibody cetuximab inhibits EGFR/HER-2 heterodimerization and activation. *Int. J. Oncol.* **34**, 25-32.

87. van der Veeken, J., Oliveira, S., Schiffelers, R. M., Storm, G., van Bergen En Henegouwen, P. M., and Roovers, R. C. (2009) Crosstalk between epidermal growth factor receptor- and insulin-like growth factor-1 receptor signaling: implications for cancer therapy. *Current cancer drug targets* **9**, 748-760.

88. Hu, J., Jo, M., Cavenee, W. K., Furnari, F., VandenBerg, S. R., and Gonias, S. L. (2011) Crosstalk between the urokinase-type plasminogen activator receptor

and EGF receptor variant III supports survival and growth of glioblastoma cells. *Proceedings of the National Academy of Sciences* **108**, 15984-15989.

89. Karamouzis, M. V., Konstantinopoulos, P. A., and Papavassiliou, A. G. (2009) Targeting MET as a strategy to overcome crosstalk-related resistance to EGFR inhibitors. *The Lancet Oncology* **10**, 709-717.

90. Hu, T., and Li, C. (2010) Convergence between Wnt-beta-catenin and EGFR signaling in cancer. *Molecular Cancer* **9**, 236.

91. Valsecchi, M. E., McDonald, M., Brody, J. B., Hyslop, T., Freydin, B., Yeo, C. J., Solomides, C., Peiper, S. C., and Witkiewicz, A. K. (2011) Epidermal growth factor receptor and insulinlike growth factor 1 receptor expression predict poor survival in pancreatic ductal adenocarcinoma. *Cancer*, n/a-n/a.

92. Takahari, D., Yamada, Y., Okita, N. T., Honda, T., Hirashima, Y., Matsubara, J., Takashima, A., Kato, K., Hamaguchi, T., Shirao, K., Shimada, Y., and Shimoda, T. (2009) Relationships of insulin-like growth factor-1 receptor and epidermal growth factor receptor expression to clinical outcomes in patients with colorectal cancer. *Oncology* **76**, 42-48.

93. Morgillo, F., Kim, W.-Y., Kim, E. S., Ciardiello, F., Hong, W. K., and Lee, H.-Y. (2007) Implication of the Insulin-like Growth Factor-IR Pathway in the Resistance of Nonâ€“small Cell Lung Cancer Cells to Treatment with Gefitinib. *Clin. Cancer Res.* **13**, 2795-2803.

94. Chakravarti, A., Loeffler, J. S., and Dyson, N. J. (2002) Insulin-like Growth Factor Receptor I Mediates Resistance to Anti-Epidermal Growth Factor Receptor Therapy in Primary Human Glioblastoma Cells through Continued Activation of Phosphoinositide 3-Kinase Signaling. *Cancer Res.* **62**, 200-207.

95. Puri, N., and Salgia, R. (2008) Synergism of EGFR and c-Met pathways, cross-talk and inhibition, in non-small cell lung cancer. *Journal of carcinogenesis* **7**, 9.

96. Wang, X., Li, K., Chen, H., Wang, D., Zhang, Y., and Bai, C. (2010) Does hepatocyte growth factor/c-Met signal play synergetic role in lung cancer? *Journal of Cellular and Molecular Medicine* **14**, 833-839.

97. Engelman, J. A., Zejnullahu, K., Mitsudomi, T., Song, Y., Hyland, C., Park, J. O., Lindeman, N., Gale, C.-M., Zhao, X., Christensen, J., Kosaka, T., Holmes, A. J., Rogers, A. M., Cappuzzo, F., Mok, T., Lee, C., Johnson, B. E., Cantley, L. C., and Jänne, P. A. (2007) MET Amplification Leads to Gefitinib Resistance in Lung Cancer by Activating ERBB3 Signaling. *Science* **316**, 1039-1043.

98. Yamada, T., Takeuchi, S., Kita, K., Bando, H., Nakamura, T., Matsumoto, K., and Yano, S. (2011) Hepatocyte Growth Factor Induces Resistance to Anti-epidermal Growth Factor Receptor Antibody in Lung Cancer. *Journal of Thoracic Oncology* **Publish Ahead of Print**, 10.1097/JTO.1090b1013e3182398e3182369.

99. Jun, H. J., Acquaviva, J., Chi, D., Lessard, J., Zhu, H., Woolfenden, S., Bronson, R. T., Pfannl, R., White, F., Housman, D. E., Iyer, L., Whittaker, C. A., Boskovitz, A., Raval, A., and Charest, A. (2011) Acquired MET expression confers resistance to EGFR inhibition in a mouse model of glioblastoma multiforme. *Oncogene*.

100. Inno, A., Di Salvatore, M., Cenci, T., Martini, M., Orlandi, A., Strippoli, A., Ferrara, A. M., BagalÃ , C., Cassano, A., Larocca, L. M., and Barone, C. (2011) Is There a Role for IGF1R and c-MET Pathways in Resistance to Cetuximab in Metastatic Colorectal Cancer? *Clinical Colorectal Cancer* **10**, 325-332.

101. Tang, P., Steck, P. A., and Yung, W. K. A. (1997) The autocrine loop of TGF-Î±/EGFR and brain tumors. *J. Neurooncol.* **35**, 303-314.

102. Messa, C., Russo, F., Caruso, M. G., and Di Leo, A. (1998) EGF, TGF-alpha, and EGF-R in human colorectal adenocarcinoma. *Acta Oncol.* **37**, 285-289.

103. Mizukami, Y., Nonomura, A., Noguchi, M., Taniya, T., Koyasaki, N., Saito, Y., Hashimoto, T., Matsubara, F., and Yanaihara, N. (1991) Immunohistochemical study of oncogene product ras p21, c-myc and growth factor EGF in breast carcinomas. *Anticancer Res.* **11**, 1485-1494.

104. Tateishi, M., Ishida, T., Mitsudomi, T., Kaneko, S., and Sugimachi, K. (1990) Immunohistochemical Evidence of Autocrine Growth Factors in Adenocarcinoma of the Human Lung. *Cancer Res.* **50**, 7077-7080.

105. Yarden, Y. (2001) The EGFR family and its ligands in human cancer: signalling mechanisms and therapeutic opportunities. *Eur. J. Cancer* **37**, 3-8.

106. Ishikawa, N., Daigo, Y., Takano, A., Taniwaki, M., Kato, T., Hayama, S., Murakami, H., Takeshima, Y., Inai, K., Nishimura, H., Tsuchiya, E., Kohno, N., and Nakamura, Y. (2005) Increases of Amphiregulin and Transforming Growth Factor-Î± in Serum as Predictors of Poor Response to Gefitinib among Patients with Advanced Non-Small Cell Lung Cancers. *Cancer Res.* **65**, 9176-9184.

107. Khambata-Ford, S., Garrett, C. R., Meropol, N. J., Basik, M., Harbison, C. T., Wu, S., Wong, T. W., Huang, X., Takimoto, C., Godwin, A. K., Tan, B. R., Krishnamurthi, S. S., Burris, I. H., Poplin, E. A., Hidalgo, M., Baselga, J., Clark, E. A., and Mauro, D. J. (2007) Expression of epiregulin and amphiregulin and K-ras mutation status predict disease control in metastatic colorectal cancer patients treated with cetuximab. *J. Clin. Oncol.* **25**, 3230-3237.

108. Yonesaka, K., Zejnullahu, K., Lindeman, N., Homes, A. J., Jackman, D. M., Zhao, F., Rogers, A. M., Johnson, B. E., and Jänne, P. A. (2008) Autocrine Production of Amphiregulin Predicts Sensitivity to Both Gefitinib and Cetuximab in EGFR Wild-type Cancers. *Clin. Cancer Res.* **14**, 6963-6973.

109. Wong, A. J., Ruppert, J. M., Bigner, S. H., Grzeschik, C. H., Humphrey, P. A., Bigner, D. S., and Vogelstein, B. (1992) Structural alterations of the epidermal growth factor receptor gene in human gliomas. *Proc. Natl. Acad. Sci. U. S. A.* **89**, 2965-2969.

110. Montgomery, R. B., Moscatello, D. K., Wong, A. J., Cooper, J. A., and Stahl, W. L. (1995) Differential Modulation of Mitogen-activated Protein (MAP) Kinase/Extracellular Signal-related Kinase Kinase and MAP Kinase Activities by a Mutant Epidermal Growth Factor Receptor. *J. Biol. Chem.* **270**, 30562-30566.

111. Huang, H. J. S., Nagane, M., Klingbeil, C. K., Lin, H., Nishikawa, R., Ji, X.-D., Huang, C.-M., Gill, G. N., Wiley, H. S., and Cavenee, W. K. (1997) The Enhanced Tumorigenic Activity of a Mutant Epidermal Growth Factor Receptor Common in Human Cancers Is Mediated by Threshold Levels of Constitutive Tyrosine Phosphorylation and Unattenuated Signaling. *J. Biol. Chem.* **272**, 2927-2935.

112. Tang, C. K., Gong, X.-Q., Moscatello, D. K., Wong, A. J., and Lippman, M. E. (2000) Epidermal Growth Factor Receptor vIII Enhances Tumorigenicity in Human Breast Cancer. *Cancer Res.* **60**, 3081-3087.

113. Olapade-Olaopa, E. O., Moscatello, D. K., MacKay, E. H., Horsburgh, T., Sandhu, D. P. S., Terry, T. R., Wong, A. J., and Habib, F. K. (1999) Evidence for

the differential expression of a variant EGF receptor protein in human prostate cancer. *Br. J. Cancer* **82**, 186-194.

114. R Nishikawa, X. D. J., R C Harmon, C S Lazar, G N Gill, W K Cavenee, and H J Huang (1994) A mutant epidermal growth factor receptor common in human glioma confers enhanced tumorigenicity. *PNAS* **91**, 7727–7731.

115. Ge, H., Gong, X., and Tang, C. K. (2002) Evidence of high incidence of EGFRvIII expression and coexpression with EGFR in human invasive breast cancer by laser capture microdissection and immunohistochemical analysis. *Int. J. Cancer* **98**, 357-361.

116. Sok, J. C., Coppelli, F. M., Thomas, S. M., Lango, M. N., Xi, S., Hunt, J. L., Freilino, M. L., Graner, M. W., Wikstrand, C. J., Bigner, D. D., Gooding, W. E., Furnari, F. B., and Grandis, J. R. (2006) Mutant Epidermal Growth Factor Receptor (EGFRvIII) Contributes to Head and Neck Cancer Growth and Resistance to EGFR Targeting. *Clin. Cancer Res.* **12**, 5064-5073.

117. Learn, C. A., Hartzell, T. L., Wikstrand, C. J., Archer, G. E., Rich, J. N., Friedman, A. H., Friedman, H. S., Bigner, D. D., and Sampson, J. H. (2004) Resistance to Tyrosine Kinase Inhibition by Mutant Epidermal Growth Factor Receptor Variant III Contributes to the Neoplastic Phenotype of Glioblastoma Multiforme. *Clin. Cancer Res.* **10**, 3216-3224.

118. Taron, M., Ichinose, Y., Rosell, R., Mok, T., Massuti, B., Zamora, L., Mate, J. L., Manegold, C., Ono, M., Queralt, C., Jahan, T., Sanchez, J. J., Sanchez-Ronco, M., Hsue, V., Jablons, D., Sanchez, J. M., and Moran, T. (2005) Activating Mutations in the Tyrosine Kinase Domain of the Epidermal Growth Factor Receptor Are Associated with Improved Survival in Gefitinib-Treated Chemorefractory Lung Adenocarcinomas. *Clin. Cancer Res.* **11**, 5878-5885.

119. Chou, T.-Y., Chiu, C.-H., Li, L.-H., Hsiao, C.-Y., Tzen, C.-Y., Chang, K.-T., Chen, Y.-M., Perng, R.-P., Tsai, S.-F., and Tsai, C.-M. (2005) Mutation in the Tyrosine Kinase Domain of Epidermal Growth Factor Receptor Is a Predictive and Prognostic Factor for Gefitinib Treatment in Patients with Non-Small Cell Lung Cancer. *Clin. Cancer Res.* **11**, 3750-3757.

120. Pao, W., Miller, V. A., Politi, K. A., Riely, G. J., Somwar, R., Zakowski, M. F., Kris, M. G., and Varmus, H. (2005) Acquired Resistance of Lung

Adenocarcinomas to Gefitinib or Erlotinib Is Associated with a Second Mutation in the EGFR Kinase Domain. *PLoS Med* **2**, e73.

121. Gazdar, A. F. (2009) Activating and resistance mutations of EGFR in non-small-cell lung cancer: role in clinical response to EGFR tyrosine kinase inhibitors. *Oncogene* **28**, S24-S31.

122. Wu, J.-Y., Yang, C.-H., Hsu, Y.-C., Yu, C.-J., Chang, S.-H., Shih, J.-Y., and Yang, P.-C. (2010) Use of Cetuximab After Failure of Gefitinib in Patients With Advanced Nonâ€“Small-Cell Lung Cancer. *Clinical Lung Cancer* **11**, 257-263.

123. Perez-Torres, M., Guix, M., Gonzalez, A., and Arteaga, C. L. (2006) Epidermal Growth Factor Receptor (EGFR) Antibody Down-regulates Mutant Receptors and Inhibits Tumors Expressing EGFR Mutations. *J. Biol. Chem.* **281**, 40183-40192.

124. Kancha, R. K., Peschel, C., and Duyster, J. (2011) The Epidermal Growth Factor Receptor-L861Q Mutation Increases Kinase Activity without Leading to Enhanced Sensitivity Toward Epidermal Growth Factor Receptor Kinase Inhibitors. *Journal of Thoracic Oncology* **6**, 387-392

125. Benvenuti, S., Sartore-Bianchi, A., Di Nicolantonio, F., Zanon, C., Moroni, M., Veronese, S., Siena, S., and Bardelli, A. (2007) Oncogenic Activation of the RAS/RAF Signaling Pathway Impairs the Response of Metastatic Colorectal Cancers to Antiâ€“Epidermal Growth Factor Receptor Antibody Therapies. *Cancer Res.* **67**, 2643-2648.

126. Baker, J. B., Dutta, D., Watson, D., Maddala, T., Munneke, B. M., Shak, S., Rowinsky, E. K., Xu, L. A., Harbison, C. T., Clark, E. A., Mauro, D. J., and Khambata-Ford, S. (2011) Tumour gene expression predicts response to cetuximab in patients with KRAS wild-type metastatic colorectal cancer. *Br. J. Cancer* **104**, 488-495.

127. Rebucci, M., Peixoto, P., Dewitte, A., Wattez, N., De Nuncques, M. A., Rezvoy, N., Vautravers-Dewas, C., Buisine, M. P., Guerin, E., Peyrat, J. P., Lartigau, E., and Lansiaux, A. (2011) Mechanisms underlying resistance to cetuximab in the HNSCC cell line: role of AKT inhibition in bypassing this resistance. *Int. J. Oncol.* **38**, 189-200.

128. Jhawer, M., Goel, S., Wilson, A. J., Montagna, C., Ling, Y.-H., Byun, D.-S., Nasser, S., Arango, D., Shin, J., Klampfer, L., Augenlicht, L. H., Soler, R. P., and

Mariadason, J. M. (2008) PIK3CA Mutation/PTEN Expression Status Predicts Response of Colon Cancer Cells to the Epidermal Growth Factor Receptor Inhibitor Cetuximab. *Cancer Res.* **68**, 1953-1961.

129. Perrone, F., Lampis, A., Orsenigo, M., Di Bartolomeo, M., Gevorgyan, A., Losa, M., Frattini, M., Riva, C., Andreola, S., Bajetta, E., Bertario, L., Leo, E., Pierotti, M. A., and Pilotti, S. (2009) PI3KCA/PTEN deregulation contributes to impaired responses to cetuximab in metastatic colorectal cancer patients. *Ann. Oncol.* **20**, 84-90.

130. Perez-Soler, R., and Saltz, L. (2005) Cutaneous Adverse Effects With HER1/EGFR-Targeted Agents: Is There a Silver Lining? *J. Clin. Oncol.* **23**, 5235-5246.

131. Albanell, J., Rojo, F., Averbuch, S., Feyereislova, A., Mascaro, J. M., Herbst, R., LoRusso, P., Rischin, D., Sauleda, S., Gee, J., Nicholson, R. I., and Baselga, J. (2002) Pharmacodynamic Studies of the Epidermal Growth Factor Receptor Inhibitor ZD1839 in Skin From Cancer Patients: Histopathologic and Molecular Consequences of Receptor Inhibition. *J. Clin. Oncol.* **20**, 110-124.

132. Hirsch, F. R., Dziadziuszko, R., Thatcher, N., Mann, H., Watkins, C., Parums, D. V., Speake, G., Holloway, B., Bunn, P. A., and Franklin, W. A. (2008) Epidermal growth factor receptor immunohistochemistry. *Cancer* **112**, 1114-1121.

133. Gori, S., Sidoni, A., Colozza, M., Ferri, I., Mameli, M. G., Fenocchio, D., Stocchi, L., Foglietta, J., Ludovini, V., Minenza, E., De Angelis, V., and Crinò, L. (2009) EGFR, pMAPK, pAkt and PTEN status by immunohistochemistry: correlation with clinical outcome in HER2-positive metastatic breast cancer patients treated with trastuzumab. *Ann. Oncol.* **20**, 648-654.

134. Richards, K. N., Zweidler-McKay, P. A., Van Roy, N., Speleman, F., Trevino, J., Zage, P. E., and Hughes, D. P. M. (2010) Signaling of ERBB receptor tyrosine kinases promotes neuroblastoma growth in vitro and in vivo. *Cancer* **116**, 3233-3243.

135. Hennessy, B. T., Lu, Y., Gonzalez-Angulo, A. M., Carey, M. S., Myhre, S., Ju, Z., Davies, M. A., Liu, W., Coombes, K., Meric-Bernstam, F., Bedrosian, I., McGahren, M., Agarwal, R., Zhang, F., Overgaard, J., Alsner, J., Neve, R. M., Kuo, W. L., Gray, J. W., Borresen-Dale, A. L., and Mills, G. B. (2010) A Technical Assessment of the Utility of Reverse Phase Protein Arrays for the Study of the

Functional Proteome in Non-microdissected Human Breast Cancers. *Clin Proteomics* **6**, 129-151.

136. Pernas, F. G., Allen, C. T., Winters, M. E., Yan, B., Friedman, J., Dabir, B., Saigal, K., Mundinger, G. S., Xu, X., Morris, J. C., Calvo, K. R., Van Waes, C., and Chen, Z. (2009) Proteomic Signatures of Epidermal Growth Factor Receptor and Survival Signal Pathways Correspond to Gefitinib Sensitivity in Head and Neck Cancer. *Clin. Cancer Res.* **15**, 2361-2372.

137. Pierobon, M., Calvert, V., Belluco, C., Garaci, E., Deng, J., Lise, M., Nitti, D., Mammano, E., Marchi, F. D., Liotta, L., and Petricoin, E. (2009) Multiplexed Cell Signaling Analysis of Metastatic and Nonmetastatic Colorectal Cancer Reveals COX2-EGFR Signaling Activation as a Potential Prognostic Pathway Biomarker. *Clin Colorectal Cancer* **8**, 110-117.

138. Tsavachidou-Fenner, D., Tannir, N., Tamboli, P., Liu, W., Petillo, D., Teh, B., Mills, G. B., and Jonasch, E. (2011) Gene and protein expression markers of response to combined antiangiogenic and epidermal growth factor targeted therapy in renal cell carcinoma. *Ann. Oncol.* **21**, 1599-1606.

139. Zhang, Y., Wolf-Yadlin, A., Ross, P. L., Pappin, D. J., Rush, J., Lauffenburger, D. A., and White, F. M. (2005) Time-resolved Mass Spectrometry of Tyrosine Phosphorylation Sites in the Epidermal Growth Factor Receptor Signaling Network Reveals Dynamic Modules. *Mol. Cell. Proteomics* **4**, 1240-1250.

140. Hinsby, A. M., Olsen, J. V., and Mann, M. (2004) Tyrosine Phosphoproteomics of Fibroblast Growth Factor Signaling. *J. Biol. Chem.* **279**, 46438-46447.

141. Wolf-Yadlin, A., Hautaniemi, S., Lauffenburger, D. A., and White, F. M. (2007) Multiple reaction monitoring for robust quantitative proteomic analysis of cellular signaling networks. *PNAS* **104**, 5860-5865.

142. Rexer, B. N., Ham, A. J. L., Rinehart, C., Hill, S., de Matos Granja-Ingram, N., Gonzalez-Angulo, A. M., Mills, G. B., Dave, B., Chang, J. C., Liebler, D. C., and Arteaga, C. L. (2011) Phosphoproteomic mass spectrometry profiling links Src family kinases to escape from HER2 tyrosine kinase inhibition. *Oncogene* **30**, 4163-4174.

143. Thelemann, A., Petti, F., Griffin, G., Iwata, K., Hunt, T., Settinari, T., Fenyo, D., Gibson, N., and Haley, J. D. (2005) Phosphotyrosine signaling networks in epidermal growth factor receptor overexpressing squamous carcinoma cells. *Mol Cell Proteomics* **4**, 356-376.

144. Pandey, A., Podtelejnikov, A. V., Blagoev, B., Bustelo, X. R., Mann, M., and Lodish, H. F. (2000) Analysis of receptor signaling pathways by mass spectrometry: Identification of Vav-2 as a substrate of the epidermal and platelet-derived growth factor receptors. *PNAS* **97**, 179-184.

145. Guo, A., Villen, J., Kornhauser, J., Lee, K. A., Stokes, M. P., Rikova, K., Possemato, A., Nardone, J., Innocenti, G., Wetzel, R., Wang, Y., MacNeill, J., Mitchell, J., Gygi, S. P., Rush, J., Polakiewicz, R. D., and Comb, M. J. (2008) Signaling networks assembled by oncogenic EGFR and c-Met. *PNAS* **105**, 692-697.

146. Li, X., Gerber, S. A., Rudner, A. D., Beausoleil, S. A., Haas, W., Villén, J., Elias, J. E., and Gygi, S. P. (2007) Large-Scale Phosphorylation Analysis of Î±-Factor-Arrested Saccharomyces cerevisiae. *J. Proteome Res.* **6**, 1190-1197.

147. Espina, V., Edmiston, K. H., Heiby, M., Pierobon, M., Sciro, M., Merritt, B., Banks, S., Deng, J., VanMeter, A. J., Geho, D. H., Pastore, L., Sennesh, J., Petricoin, E. F., 3rd, and Liotta, L. A. (2008) A portrait of tissue phosphoprotein stability in the clinical tissue procurement process. *Mol Cell Proteomics* **7**, 1998-2018.

148. Espina, V., Mueller, C., Edmiston, K., Sciro, M., Petricoin, E. F., and Liotta, L. A. (2009) Tissue is alive: New technologies are needed to address the problems of protein biomarker pre-analytical variability. *Proteomics Clin Appl* **3**, 874-882.

149. Silvestri, A., Colombatti, A., Calvert, V. S., Deng, J., Mammano, E., Belluco, C., De Marchi, F., Nitti, D., Liotta, L. A., Petricoin, E. F., and Pierobon, M. (2010) Protein pathway biomarker analysis of human cancer reveals requirement for upfront cellular-enrichment processing. *Lab. Invest.* **90**, 787-796.

150. Link, A. J., Eng, J., Schieltz, D. M., Carmack, E., Mize, G. J., Morris, D. R., Garvik, B. M., and Yates, J. R. (1999) Direct analysis of protein complexes using mass spectrometry. *Nat Biotech* **17**, 676-682.

151. Washburn, M. P., Wolters, D., and Yates, J. R. (2001) Large-scale analysis of the yeast proteome by multidimensional protein identification technology. *Nat Biotech* **19**, 242-247.

152. Taylor, S. W., Fahy, E., Zhang, B., Glenn, G. M., Warnock, D. E., Wiley, S., Murphy, A. N., Gaucher, S. P., Capaldi, R. A., Gibson, B. W., and Ghosh, S. S. (2003) Characterization of the human heart mitochondrial proteome. *Nat Biotech* **21**, 281-286.

153. Omenn, G. S., States, D. J., Adamski, M., Blackwell, T. W., Menon, R., Hermjakob, H., Apweiler, R., Haab, B. B., Simpson, R. J., Eddes, J. S., Kapp, E. A., Moritz, R. L., Chan, D. W., Rai, A. J., Admon, A., Aebersold, R., Eng, J., Hancock, W. S., Hefta, S. A., Meyer, H., Paik, Y.-K., Yoo, J.-S., Ping, P., Pounds, J., Adkins, J., Qian, X., Wang, R., Wasinger, V., Wu, C. Y., Zhao, X., Zeng, R., Archakov, A., Tsugita, A., Beer, I., Pandey, A., Pisano, M., Andrews, P., Tammen, H., Speicher, D. W., and Hanash, S. M. (2005) Overview of the HUPO Plasma Proteome Project: Results from the pilot phase with 35 collaborating laboratories and multiple analytical groups, generating a core dataset of 3020 proteins and a publicly-available database. *PROTEOMICS* **5**, 3226-3245.

154. Cravatt, B. F., Simon, G. M., and Yates Iii, J. R. (2007) The biological impact of mass-spectrometry-based proteomics. *Nature* **450**, 991-1000.

155. Tabb, D. L., Fernando, C. G., and Chambers, M. C. (2007) MyriMatch: Highly Accurate Tandem Mass Spectral Peptide Identification by Multivariate Hypergeometric Analysis. *J. Proteome Res.* **6**, 654-661.

156. Liu, H., Lin, D., and Yates, J. R., 3rd (2002) Multidimensional separations for protein/peptide analysis in the post-genomic era. *Biotechniques* **32**, 898, 900, 902 passim.

157. Blagoev, B., Ong, S. E., Kratchmarova, I., and Mann, M. (2004) Temporal analysis of phosphotyrosine-dependent signaling networks by quantitative proteomics. *Nat. Biotechnol.* **22**, 1139-1145.

158. Wolters, D. A., Washburn, M. P., and Yates, J. R., 3rd (2001) An automated multidimensional protein identification technology for shotgun proteomics. *Anal. Chem.* **73**, 5683-5690.

159. Cargile, B. J., Sevinsky, J. R., Essader, A. S., Stephenson, J. L., Jr., and Bundy, J. L. (2005) Immobilized pH gradient isoelectric focusing as a first-dimension separation in shotgun proteomics. *J Biomol Tech* **16**, 181-189.

160. Liu, H., Sadygov, R. G., and Yates, J. R. (2004) A Model for Random Sampling and Estimation of Relative Protein Abundance in Shotgun Proteomics. *Anal. Chem.* **76**, 4193-4201.

161. Old, W. M., Meyer-Arendt, K., Aveline-Wolf, L., Pierce, K. G., Mendoza, A., Sevinsky, J. R., Resing, K. A., and Ahn, N. G. (2005) Comparison of Label-free Methods for Quantifying Human Proteins by Shotgun Proteomics. *Mol. Cell. Proteomics* **4**, 1487-1502.

162. Diamandis, E. P. (2004) Mass Spectrometry as a Diagnostic and a Cancer Biomarker Discovery Tool. *Mol. Cell. Proteomics* **3**, 367-378.

163. Drew, J. E., Rucklidge, G. J., Duncan, G., Lufty, A., Farquharson, A. J., Reid, M. D., Russell, W. R., Morrice, P. C., Arthur, J. R., and Duthie, G. G. (2005) A proteomics approach to identify changes in protein profiles in pre-cancerous colon. *Biochem. Biophys. Res. Commun.* **330**, 81-87.

164. Loeffler-Ragg, J., Skvortsov, S., Sarg, B., Skvortsova, I., Witsch-Baumgartner, M., Mueller, D., Lindner, H., and Zwierzina, H. (2005) Gefitinib-responsive EGFR-positive colorectal cancers have different proteome profiles from non-responsive cell lines. *Eur. J. Cancer* **41**, 2338-2346.

165. Skvortsov, S., Sarg, B., Loeffler-Ragg, J., Skvortsova, I., Lindner, H., Werner Ott, H., Lukas, P., Illmensee, K., and Zwierzina, H. (2004) Different proteome pattern of epidermal growth factor receptor-positive colorectal cancer cell lines that are responsive and nonresponsive to C225 antibody treatment. *Mol Cancer Ther* **3**, 1551-1558.

166. Ying-Tao, Z., Yi-Ping, G., Lu-Sheng, S., and Yi-Li, W. (2005) Proteomic analysis of differentially expressed proteins between metastatic and non-metastatic human colorectal carcinoma cell lines. *Eur. J. Gastroenterol. Hepatol.* **17**, 725-732.

167. Kondrat, R. W., McClusky, G. A., and Cooks, R. G. (1978) Multiple reaction monitoring in mass spectrometry/mass spectrometry for direct analysis of complex mixtures. *Anal. Chem.* **50**, 2017– 2021.

168. Addona, T. A., Abbatiello, S. E., Schilling, B., Skates, S. J., Mani, D. R., Bunk, D. M., Spiegelman, C. H., Zimmerman, L. J., Ham, A.-J. L., Keshishian, H., Hall, S. C., Allen, S., Blackman, R. K., Borchers, C. H., Buck, C., Cardasis, H. L., Cusack, M. P., Dodder, N. G., Gibson, B. W., Held, J. M., Hiltke, T., Jackson, A., Johansen, E. B., Kinsinger, C. R., Li, J., Mesri, M., Neubert, T. A., Niles, R. K., Pulsipher, T. C., Ransohoff, D., Rodriguez, H., Rudnick, P. A., Smith, D., Tabb, D. L., Tegeler, T. J., Variyath, A. M., Vega-Montoto, L. J., Wahlander, A., Waldemarson, S., Wang, M., Whiteaker, J. R., Zhao, L., Anderson, N. L., Fisher, S. J., Liebler, D. C., Paulovich, A. G., Regnier, F. E., Tempst, P., and Carr, S. A. (2009) Multi-site assessment of the precision and reproducibility of multiple reaction monitoring-based measurements of proteins in plasma. *Nat Biotech* **27**, 633-641.

169. Rifai, N., Gillette, M. A., and Carr, S. A. (2006) Protein biomarker discovery and validation: the long and uncertain path to clinical utility. *Nat Biotech* **24**, 971-983.

170. Keshishian, H., Addona, T., Burgess, M., Kuhn, E., and Carr, S. A. (2007) Quantitative, Multiplexed Assays for Low Abundance Proteins in Plasma by Targeted Mass Spectrometry and Stable Isotope Dilution. *Mol. Cell. Proteomics* **6**, 2212-2229.

171. Zhang, H., Liu, Q., Zimmerman, L. J., Ham, A.-J. L., Slebos, R. J. C., Rahman, J., Kikuchi, T., Massion, P. P., Carbone, D. P., Billheimer, D., and Liebler, D. C. (2011) Methods for Peptide and Protein Quantitation by Liquid Chromatography-Multiple Reaction Monitoring Mass Spectrometry. *Mol. Cell. Proteomics* **10**.

172. Kirkpatrick, D. S., Gerber, S. A., and Gygi, S. P. (2005) The absolute quantification strategy: a general procedure for the quantification of proteins and post-translational modifications. *Methods* **35**, 265-273.

173. MacLean, B., Tomazela, D. M., Shulman, N., Chambers, M., Finney, G. L., Frewen, B., Kern, R., Tabb, D. L., Liebler, D. C., and MacCoss, M. J. (2010) Skyline: an open source document editor for creating and analyzing targeted proteomics experiments. *Bioinformatics* **26**, 966-968.

174. Kuzyk, M. A., Smith, D., Yang, J., Cross, T. J., Jackson, A. M., Hardie, D. B., Anderson, N. L., and Borchers, C. H. (2009) Multiple Reaction Monitoring-based, Multiplexed, Absolute Quantitation of 45 Proteins in Human Plasma. *Mol. Cell. Proteomics* **8**, 1860-1877.

175. Keshishian, H., Addona, T., Burgess, M., Mani, D. R., Shi, X., Kuhn, E., Sabatine, M. S., Gerszten, R. E., and Carr, S. A. (2009) Quantification of Cardiovascular Biomarkers in Patient Plasma by Targeted Mass Spectrometry and Stable Isotope Dilution. *Mol. Cell. Proteomics* **8**, 2339-2349.

176. Whiteaker, J. R., Zhao, L., Anderson, L., and Paulovich, A. G. (2009) An Automated and Multiplexed Method for High Throughput Peptide Immunoaffinity Enrichment and Multiple Reaction Monitoring Mass Spectrometry-based Quantification of Protein Biomarkers. *Mol. Cell. Proteomics* **9**, 184-196.

177. Anderson, N. L., Jackson, A., Smith, D., Hardie, D., Borchers, C., and Pearson, T. W. (2009) SISCAPA Peptide Enrichment on Magnetic Beads Using an In-line Bead Trap Device. *Mol. Cell. Proteomics* **8**, 995-1005.

178. Barr, J. R., Maggio, V. L., Patterson, D. G., Jr., Cooper, G. R., Henderson, L. O., Turner, W. E., Smith, S. J., Hannon, W. H., Needham, L. L., and Sampson, E. J. (1996) Isotope dilution--mass spectrometric quantification of specific proteins: model application with apolipoprotein A-I. *Clin. Chem.* **42**, 1676-1682.

179. Gerber, S. A., Rush, J., Stemman, O., Kirschner, M. W., and Gygi, S. P. (2003) Absolute quantification of proteins and phosphoproteins from cell lysates by tandem MS. *PNAS* **100**, 6940-6945.

CHAPTER II

CELL MODELS FOR EGFR ACTIVATION AND INHIBITION AND INITIAL EVALUATION OF GLOBAL PROTEIN EXPRESSION CHANGES

Introduction

The overarching question asked in this project is whether differences in global protein expression levels could indicate cellular responses to EGFR modulation. This project required a model system in which activation and inhibition of EGFR could be established according to well-defined criteria in the field. Subsequent proteomic analyses of activated and inhibited states would enable a test of the hypothesis that protein expression patterns indicate the activation state of the system. I chose two well-established cell models for EGFR biochemistry and cell biology. DiFi and A431 cells were treated with epidermal growth factor (EGF) and two clinically-available EGFR inhibitors, gefitinib and cetuximab, to manipulate the EGFR signaling axis. Initial studies established culture and treatment conditions, extraction methods and verification of EGFR activation by western blotting to detect EGFR autophosphorylation and activation of downstream targets.

Once the A431 model was established, an initial global proteome analysis was performed with a shotgun proteomics platform that combines polyacrylamide gel electrophoresis and reverse phase LC-MS/MS. Comparison of these datasets indicated proteins that differed significantly in expression between treatment

conditions. Protein expression differentials were further verified by multiple reaction monitoring (MRM) mass spectrometry analyses. Results demonstrate proof-of-concept for the implementation of this platform to identify and verify global protein changes resulting from different responses to drug treatments. However, analysis of the data also suggested that longer exposure duration and modifications to the proteomic analysis platform would yield a more useful response signature. The second phase of this work is described in Chapter III.

Experimental Procedures

Materials and reagents

Iodoacetamide, ammonium bicarbonate, sodium molybdate, β-glycerophosphate, sodium molybdate, sodium orthovanadate, 4-(2-aminoethyl)benzenesulfonyl fluoride, aprotinin, leupeptin, betastatin, pepstatin A, dimethyl sulfoxoide, and sodium dodecyl sulfate (SDS) (all >99.0% purity) were purchased from Sigma (St. Louis, MO). Dithiothreitol was from Bio-Rad (Hercules, CA). 2,2,2-Trifluoroethanol (TFE) was from Acros (Geel, Belgium). C-Terminal isotopically labeled β-actin peptide (GYSFTTTAE*R) containing U-$^{13}C_6$, U-$^{15}N_4$-arginine was obtained from New England Peptide at 99% isotopic purity and 95% chemical purity. Fetal bovine serum (FBS) was from Atlas Biologicals (Fort Collins, CO). Mass spectrometry grade trypsin (Trypsin Gold) was purchased from Promega (Madison, WI). HPLC grade water and acetonitrile (ACN) were from Mallinckrodt Baker (Phillipsburg, NJ). Phosphate buffered

saline, Dulbecco's modified eagle medium (DMEM), improved minimal essential medium (IMEM), McCoy's 5A medium, NuPAGE® MOPS and MES SDS running buffer, NuPAGE® LDS sample buffer, NuPAGE® 10% Bis-tris gels and polyvinylidene difluoride membrane were from Invitrogen (Carlsbad, CA). Epidermal growth factor (EGF), transforming growth factor-alpha (TGF-α), EGFR, pY1173, pY998, SHC, pSHC (Y317), HER2, pHER2 (Y1248), HER3 and pHER3 (Y1289) antibodies (#8916LF, 4267s, 4407s, 2432, 2431s, 2242, 2247s, 4754 and 4791s, respectively) were purchased from Cell Signaling Technologies (Danvers, MA). β-Actin antibody (#ab8224) was from AbCam (Cambridge, MA). 4G10 antibody (#05-1050X) was from Milipore (Billerica, MA). AlexaFluor® 680-conjugated fluorescent secondary antibodies were obtained from Molecular Probes (Eugene, OR). Trifluoroacetic acid (TFA), formic acid (FA), urea and tris-carboxyethylphosphine (TCEP) were purchased from Thermo Fisher Scientific. Gefitinib and cetuximab were gifts from Dr. Carlos Arteaga and Dr. Robert Coffey, respectively, both at Vanderbilt University.

Cell culture

A431 human epithelial carcinoma cells were provided by Dr. Carlos Arteaga at Vanderbilt University (Nashville, TN) or were purchased from ATCC (Manassas, VA). A431 cells were maintained in IMEM supplemented with 10% FBS. DiFi human colorectal carcinoma cells were provided by Dr. Robert Coffey at Vanderbilt University and were maintained in DMEM and supplemented with 10% FBS. All cell lines were cultured at 37°C in 5% CO_2. After treatment, all

cells were harvested on ice using cold magnesium and calcium free phosphate buffered saline supplemented with a phosphatase inhibitor cocktail (1.0 mM sodium orthovanadate, 1.0 mM sodium molybdate, 1.0 mM sodium fluoride, and 10 mM of β-glycerophosphate). Cells were pelleted at 1,000 rpm at 4°C and pellets were flash frozen in liquid nitrogen.

Proliferating cells were grown to 70-75% confluency before collection, while serum-starved cells were grown to ~60-65% confluency before incubation overnight in serum-free media before subsequent treatment. Cells co-treated with EGF and either cetuximab or gefitinib were preincubated with the indicated concentrations of the inhibitor for 30 minutes prior to EGF stimulation. Pellets were resuspended and lysed in either modified RIPA buffer (50 mM Tris-HCl, 150 mM NaCl, 1% Igepal, 0.5% sodium deoxycholate, and 0.1% sodium dodecyl sulfate, 50 mM DTT), NETN buffer (0.5% Igepal, 20 mM Tris-HCl, 100 mM NaCl, and 50 mM DTT), or Laemelli buffer (2% SDS, 125 mM Tris-HCl, and 5% glycerol) supplemented with 50 mM DTT, phosphatase inhibitor cocktail (see above) and protease inhibitor cocktail (0.5 μM AEBSF, 10 mM aprotinin, 1.0 mM leupeptin, 5.0 μM bestatin and 1.0 μM pepstatin). Lysates were kept for 20 minutes on ice before sonication with five one-second pulses at 30 watts and 20% output. The lysate was centrifuged at 13,000 x g and the total protein concentration of the supernatant was determined using a bicinchoninic acid assay from Pierce with bovine serum albumin used as protein standard.

Western blot analysis

Equivalent sample loads were normalized for total protein concentration before reducing with dithiothreitol and adding NuPAGE® LDS sample buffer. The samples were then boiled for 7 minutes at 90°C. All denatured samples then were resolved on NuPAGE® 10% Bis-Tris gels at 160 V for ~65 minutes in either MOPS or MES SDS running buffer (Invitrogen). Proteins were electrophoretically transferred from the gel to a polyvinylidene difluoride membrane for 3 h at 35 V in a cold room. Membranes were probed overnight at 4°C using indicated primary antibody. AlexaFluor® 680-labeled goat anti-rabbit and goat anti-mouse secondary antibodies were used to detect the corresponding primary antibodies. Immunoreactive proteins were visualized using the Odyssey™ Infrared IYmaging System and Odyssey software as described by the manufacturer (Li-Cor, Lincoln, NE).

In-gel digestion and MS sample preparation

Cell pellets were lysed in RIPA buffer and resolved on NuPAGE® 10% Bis-Tris gels as described in previous section. Gels were stained with Colloidal Coomassie Blue (Invitrogen). Fifteen fractions from the top of gel to the bottom were excised and chopped into 1-mm cubes and placed in 0.5-mL Eppendorf tubes containing 100 µL of 100 mM ammonium bicarbonate, pH 8.0. Samples were reduced with 10 µl of 45 mM dithiothreitol for 20 min at 55 °C and alkylated with 10 µL of 100 mM iodoacetamide for 20 min at room temperature in the dark. Samples were destained with two washes of 100 µL of 50% acetonitrile and 50

mM ammonium bicarbonate. The gel pieces were then dehydrated with 100% acetonitrile and digested with Trypsin Gold from Promega (25 µl of 0.01 µg/µL Trypsin Gold) in 25 mM ammonium bicarbonate) overnight at 37 °C. The peptides for each fraction were extracted with two portions of 60% acetonitrile in water and 0.1% trifluoroacetic acid. Samples were evaporated *in vacuo* and reconstituted with 0.1% formic acid in water.

Cell preparation for LC-MRM MS analyses

A431 cell pellets were resuspended and lysed in 100 µL of ammonium bicarbonate (100 mM, pH 8.0) and 100 µL of TFE and then incubated with mixing at 60°C for 60 min and at 1000 rpm on an Eppendorf Thermomixer before sonicating at 30 watts and 20% output for 10 one-second pulses. Protein concentration was measured with the bicinchoninic acid assay and equivalent sample aliquots were reduced with 40 mM TCEP and 100 mM DTT with mixing at 60°C for 30 min at 1000 rpm on the Eppendorf Thermomixer and then were incubated at ambient temperature in the dark with 200 mM iodoacetamide. Samples were diluted with 50 mM ammonium bicarbonate, pH 8.0 (to 10% TFE) before adding Trypsin Gold at a 1:50 (w/w) ratio and incubating overnight at 37ºC with shaking. Aliquots of digested samples corresponding to 200 µg protein were lyophilized. Samples were resuspended in 1 mL water, vortex-mixed vigorously, and desalted with Sep-Pak® 100 mg, C-18 columns (Waters) on a vacuum manifold. After washing the columns with water, peptides were eluted with 80% ACN and the solution was evaporated to dryness *in vacuo.* Samples were

reconstituted in 0.1% (v/v) aqueous formic acid to a final concentration of 0.5 μg/μL and the isotopically labeled β-actin peptide reference standard was spiked in at a concentration of 20 fmol/μL.

Reverse phase LC-MS/MS

LC-MS/MS analyses were performed on an LTQ-XL mass spectrometer from Thermo Fisher Scientific (Waltham, MA) equipped with an Eksigent nanoLC 1D plus pump and Eksigent autosampler (Dublin, CA). Peptides were resolved on 100 μm × 11 cm fused-silica capillary column (Polymicro Technologies, LLC Phoenix, AZ) packed with 5 μm, 300 Å Jupiter C-18 resin (Phenomenex, Torrance, CA) with an in-line solid-phase extraction column (pre-column, 100 μm × 6 cm) packed with the same C-18 resin (using a frit generated with liquid silicate Kasil similar to that previously described (1). LC was carried out at ambient temperature over 85 min using a gradient mixture of 0.1% (v/v) FA in water (solvent A) and 0.1% (v/v) FA in ACN (solvent B). A 10 min load period using 100% solvent A at 1 μL/min was followed by an elution gradient (600 nL/min) from 2-25% solvent B in 30 min, 25-90% solvent B over 15 min, and held at 90% solvent B for 17 min before returning to 2% solvent B to equilibrate column. Peptides eluting from the capillary tip were introduced into the LTQ source in micro-electrospray mode with a capillary voltage of ~2 kV. A full scan was obtained for eluting peptides in the range of 400–2000 amu followed by four data-dependent MS/MS scans of the most intense ions. MS/MS spectra were recorded using dynamic exclusion of previously analyzed precursors for 60 s with a repeat

of 1 and a repeat duration of 1. MS/MS spectra were generated by collision-induced dissociation of the peptide ions at normalized collision energy of 35% to generate a series of b- and y-ions as major fragments.

Liquid chromatography-multiple reaction monitoring (MRM)-MS

MRM analyses were performed on a TSQ Vantage triple quadrupole mass spectrometer from Thermo-Fisher Scientific (Waltham MA) equipped with an Eksigent NanoLC-ultra 1D Plus pump (Dublin CA) and a capillary column and pre-column similar to that described above. The mobile phase consisted of the gradient mixture of solvent A and solvent B used for LC-MS/MS analysis. Sample solution (2 µL) containing 0.5 ng/µL peptide mixture (based on protein concentration) were loaded for 15 min onto the column using 100% solvent A at 1 µL/min followed by a gradient elution (400 nL/min) from 3–20% solvent B over 7 min, 20–60% solvent B over 35 min, 60–95% solvent B in 6 min and held at 95% for 11 min before returning to 3% solvent B. MRM analyses of target peptides and β-actin peptides (isotope labeled and endogenous) were performed using a 1300 V electrospray voltage, 210 °C capillary temperature, and −5 V skimmer offset. Both Q1 and Q3 were set at unit resolution FWHM 0.7 Da and collision gas (He) pressure in Q2 was held at 1.5 mTorr. Scan width was 0.004 *m/z* and scan time was 10 ms for all analyses. Collision energy for each peptide was calculated using the open source software Skyline (2). Instrument quality control assessment was done as described previously (3).

Quantitative analyses were done by the method described recently (3) using U-$^{13}C_6$, U-$^{15}N_4$-arginine β-actin (BA) peptide (GYSFTTTAE*R) as the reference standard. At least four MRM transitions were monitored for target peptides and the standard. Signature peptides for each protein measured were required to be between 7-25 amino acids long and were selected based on uniqueness and chemical stability. Although priority was given to peptides that were previously identified in the shotgun data set with high MS/MS spectral quality, additional peptides were selected by *in silico* analysis of the target protein sequences. Peptides containing cysteine or methionine residues were not excluded and cysteines were present as carboxyamidomethylated derivatives following treatment with iodoacetamide during sample work-up. Peptide uniqueness was confirmed by BLAST searching sequences against the UniProt database. Skyline software was used to extract and integrate transition peak areas for each target peptide (2). Summed peak areas for target peptide transitions were divided by the summed peak area for the reference standard peptide transitions to give normalized peak area (NPA) and coefficient of variations (CVs) were calculated across replicates for each treatment. For MRM analyses in cell culture experiments, three replicate cell cultures were analyzed for each cell culture and treatment.

Data analysis

The “ScanSifter” algorithm v1.0.5 read MS/MS spectra stored as centroided peak lists from Thermo RAW files and transcoded them to mzData files

(4). Only MS/MS scans were written to the mzData files; MS scans were excluded. If 90% of the intensity of a MS/MS spectrum appeared at a lower *m/z* than that of the precursor ion, a single precursor charge was assumed; otherwise the spectrum was processed under both double and triple precursor charge assumptions. MS/MS spectra were assigned to peptides from the IPI Human database version 3.33 (September 7, 2007; 67837 sequence entries) by the MyriMatch algorithm, version 1.1.0 (5). The sequence database was doubled to contain each sequence in both normal and reversed orientations, enabling false discovery rate (FDR) estimation. MyriMatch was configured to expect all cysteines to bear carboxamidomethyl modifications and to allow for the possibility of oxidation of methionines. Candidate peptides were required to feature trypsin cleavages or protein termini at both ends, though any number of missed cleavages was permitted. A precursor error of 1.25 *m/z* was allowed, but fragment ions were required to match within 0.5 *m/z*. The IDPicker algorithm v1.6.1 (6) filtered the identifications for each reverse phase liquid chromatography run to include the largest set for which a 5% peptide-level identification FDR could be maintained, as described by Qian et al. (7). Indistinguishable proteins were recognized and grouped, and parsimony rules were applied to generate a minimal list of proteins (Protein groups) that explained all of the peptides that passed our entry criteria (6). This approach uses bipartite graph analysis to derive a minimal list of protein identifications with shared clusters of peptides. These identifications were pooled for each gel sample set (15 fractions). Proteins were required to have at least two different peptide sequences observed within a gel sample set.

FDR for peptide identifications were computed by the formula (8): FDR = (2 × reverse)/(forward + reverse). The algorithm reported the number of spectra and number of distinct sequences observed for each protein and protein group in each sample set.

Statistical analyses

Comparisons of protein abundance from shotgun datasets were made with spectral count data (9) using QuasiTel, a statistical software modeling package (10). QuasiTel uses a quasi-likelihood method based on Poisson distribution—commonly used for count data (11)—and applies a regression model to compare spectral count data. This statistical model was used to perform pair-wise comparisons between two treatment conditions (4 replicates per condition) which generated a single combined inventory of protein identifications (Comparison dataset). The model also uses F-tests to compute p-values and the FDR method to correct for multiple hypothesis comparisons of identified proteins (12). Thresholds were set for p-values (≤0.05), total spectral counts (7), and spectral count $\log_2$ rate ratios (fold changes, ≥ 1.5) generated by this model and were used as criteria to filter comparison datasets. Significance of measured differences for target proteins of MRM analytes was determined with two-tailed unpaired *t* test using Prism 5.0 (GraphPad Software, San Diego, CA).

Results

Evaluation of cell lysis buffers

Initial studies established optimal conditions for preparation and analysis of EGFR activation status in cell models. The DiFi human colorectal cancer cell line was derived from a colon cancer patient harboring an adenomatous polyposis coli gene (APC) mutation—frequently found in hereditary colorectal cancers—and demonstrates both gene amplification and protein overexpression of the EGF receptor (13, 14). Figure II-1 shows western blot analysis of DiFi cells lysed under three different conditions with RIPA, NETN, and Laemmli buffers. Cells were cultured in media containing no serum for approximately 18 h before

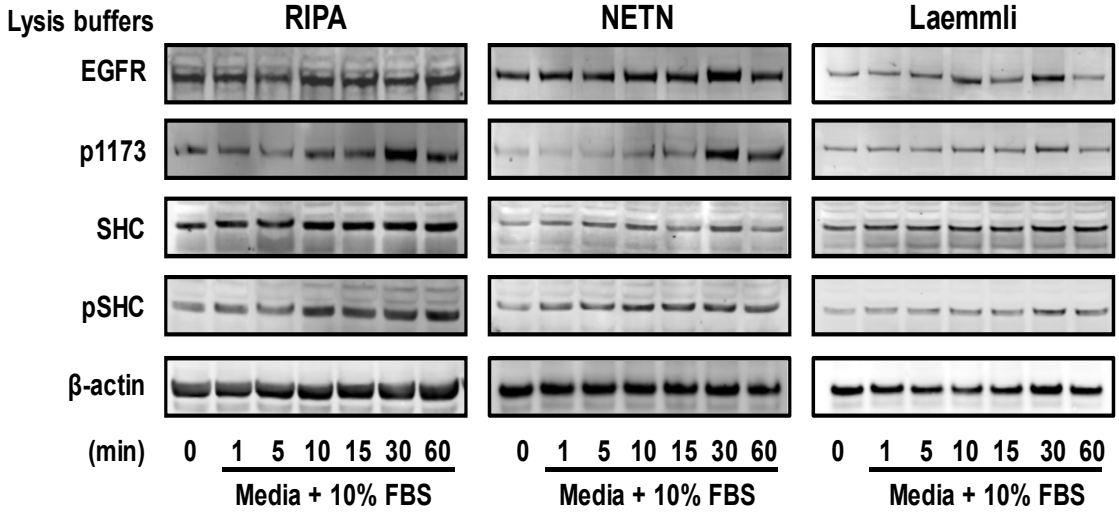

Figure II-1. Lysis buffer evaluation. DiFi cells were serum-starved overnight before incubation with media plus 10% FBS for indicated times. RIPA, NETN and Laemmli buffers (left to right) were used to lyse treated samples. Immunoblots were performed for total EGFR, EGFR phosphorylation at pY1173, total and phosphorylated SHC. β-Actin was used as a loading control.

addition of media plus 10% serum for indicated times. Total EGFR and EGFR phosphorylation status as well as expression of an effector protein SHC (p52 isoform) and its Y317 phosphorylated form were assessed in equally loaded (50 µg/lane) samples for each buffer condition.

For each lysis condition, total EGFR and SHC were detected at relatively unchanging levels across treatments with an exception noted in the Laemmli conditions for EGFR at the 30 minute time-point. Using RIPA and NETN buffers, both the phosphorylated form of EGFR (p1173) and SHC (pSHC) showed an increase in signal with increasing incubation time with media plus serum with a maximum signal detected for both phosphoproteins at the 30 minute time-point. Phosphorylation signals detected from Laemmli lysed cells were weak relative to RIPA- and NETN-lysed samples and did not show dramatic changes with increasing serum incubation time noted for the other two buffers; however, maximal phosphorylation signal detection for both p1173 and pSHC was still observed at the 30 minute time-point. RIPA lysis resulted in stronger signals for both total and phospho signals relative to NETN and Laemmli buffers and, based on these results, was selected as the lysis buffer for the remainder of the western blotting and LC MS/MS experiments.

Activation of EGFR in DiFi cells

As stated in Chapter I, there are several ligands that bind to and stimulate the EGFR influencing receptor activation. Using the two EGFR-specific ligands epidermal growth factor (EGF) and transforming growth factor-α (TGF-α), DiFi

cells were treated with 10 nM concentrations of each ligand to assess the extent of receptor and effector activation at varying time-points (Figure II-2). All treated cells were serum-starved overnight prior to treatment with ligand for the indicated times, while proliferating cells were cultured and collected in media containing 10% FBS.

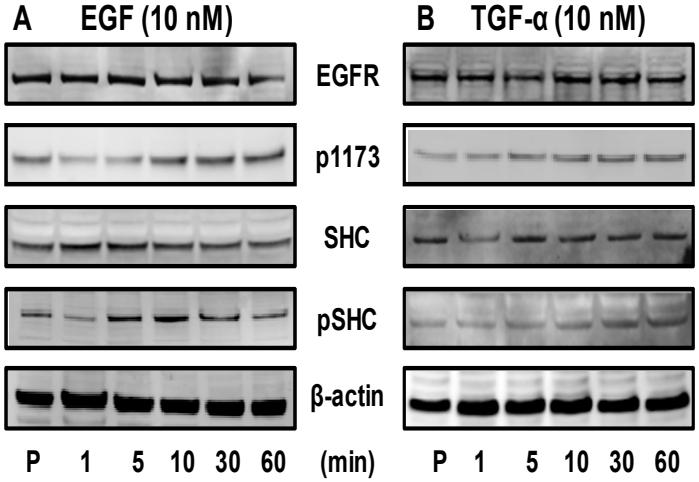

Figure II-2. EGFR stimulation in DiFi cells (10 nM). Treated DiFi cells were serum-starved overnight before being treated with (A) 10 nM EGF or (B) 10 nM TGF-α for indicated times. Proliferating cells (P) were not serum starved and serve as a reference control for basal level signaling. Immunoblots were performed for total EGFR, EGFR phosphorylation at pY1173, total SHC and pSHC. β-Actin was used as a loading control.

Over the course of 60 min, total EGFR, SHC and β-actin levels remained largely unchanged during both EGF and TGF-α treatments, while the phosphorylated forms (p1173 and pSHC) showed signal increases with increasing ligand incubation time (Figure II-2A and B). Cells treated with EGF displayed a time-dependent increase of phosphorylation signal detected for p1173, with maximal signal occurring between 30 and 60 minutes while pSHC signals peaked

around the 10 and 30 minute timepoints before tapering off at 60 min (Figure II-2A). Although TGF-α treatment increased phosphoprotein signals detected in DiFi cells, these samples did not demonstrate changes as extreme as those noted for EGF-treated DiFi cells (Figure II-2.B). Analogous experiments performed with 30 nM concentrations of EGF and TGF-α can be seen in Figure II-3. Similar trends were observed using the increased ligand concentrations; however, larger differences were noted for p1173 and pSHC between proliferating and 30 nM stimulated conditions when compared to 10 nM treatments.

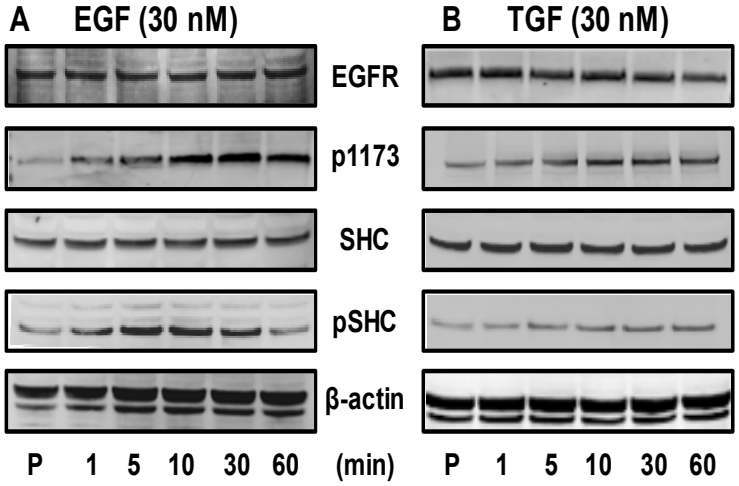

Figure II-3. EGFR stimulation in DiFi cells (30 nM). Treated DiFi cells were serum-starved overnight before being treated with (A) 30 nM EGF or (B) 30 nM TGF-α 30 nM EGF for indicated times. Proliferating cells (P) were not serum starved and serve as a reference control for basal level signaling. Immunoblots were performed for total EGFR, sites of EGFR phosphorylation at pY1173, total SHC and pY998 SHC phosphorylation. β-Actin was used as a loading control.

Both Figures II-2 and II-3 illustrate a greater increase in receptor activation—monitored via phosphorylation of Y1173 and SHC—in cells treated with EGF than those treated with TGF-α. Reports that DiFi cells not only secrete measurable levels of TGF-α, but also up-regulate TGF-α gene expression in

response to exogenous TGF-α (15) could indicate a cellular dependency on TGF-α, which might explain the lesser extent of activation compared to EGF treatments. Having noted that the 30 minute time-point typically displayed maximal phosphorylated protein signals and that the 30 nM treatments resulted in increased receptor activation, subsequent experiments were stimulated using these conditions.

Modulation of EGFR signaling in DiFi and A431 cell lines

Having developed a reproducible system for EGFR stimulation, the next experiments focused on the application of clinically used EGFR-targeted inhibitors gefitinib and cetuximab to inhibit receptor activation and subsequent downstream signaling. Figure II-4 shows western blot analysis of DiFi cells treated with increasing concentrations of cetuximab (Figure II-4A) and gefitinib (Figure II-4B). All treated cells were serum starved overnight prior to EGF or inhibitor plus EGF co-treatment. After treatment with 30 nM EGF for 30 minutes, EGFR phosphorylation at residues Y998 and Y1173 increased dramatically over proliferating cell levels, as did global phosphotyrosine levels detected using the anti-phosphotyrosine antibody 4G10. Increasing concentrations of both cetuximab and gefitinib lead to a decrease of EGFR phosphorylation at Y1173 and Y998 relative to EGF-only stimulated cells. At the concentrations used, the tyrosine kinase inhibitor gefitinib produced a more profound inhibition of EGFR

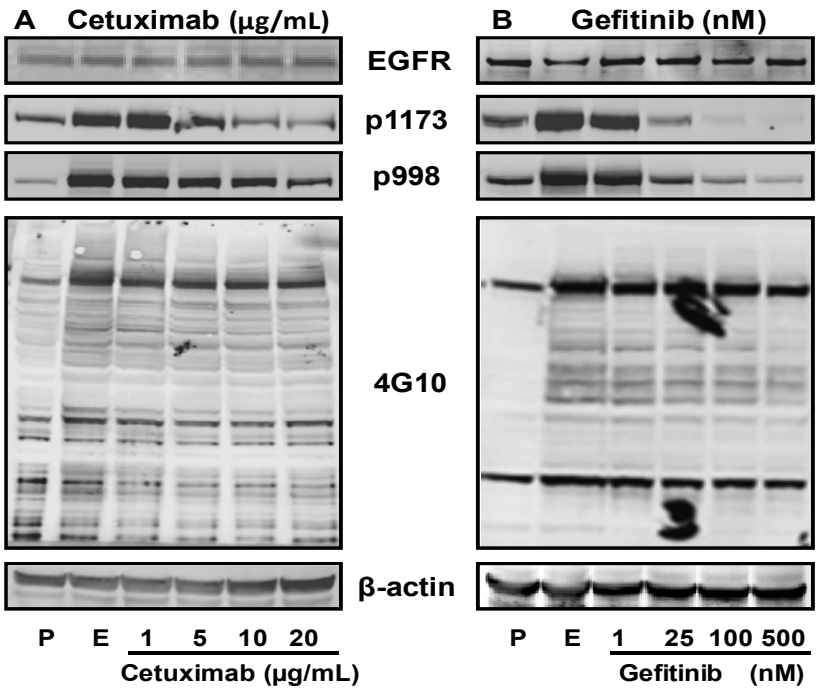

Figure II-4. EGFR modulation in DiFi cells. Proliferating cells (P) were not serum-starved and serve as a reference control for basal level signaling. EGF stimulated (E) and EGF plus (A) cetuximab (10 μg/mL) or (B) gefitinib (500 nM) for indicated times. DiFi cells were serum-starved overnight before indicated treatement for 30 min. Immunoblots were performed for total EGFR, sites of EGFR phosphorylation at pY1173 and pY998, and total tyrosine phosphorylation (4G10). β-Actin was used as a loading control.

phosphorylation than did the ligand binding domain inhibitor cetuximab. The highest concentration of cetuximab (20 μg/mL) reduced EGFR phosphorylation to approximately basal levels (Figure II-4.A) whereas gefitinib at 250 nM abolished both Y1173 and Y998 phosphorylation signals almost completely (Figure II-4.B). Similarly, total tyrosine phosphorylation was diminished well below EGF stimulated levels upon addition of both inhibitors, although not quite to basal level. The dark bands at the top of the 4G10 western blots migrate at approximately 175 kDa and likely represent detection of phosphorylated EGFR as well as

phosphorylated Her2, Her3 and Her4, thus explaining the relative lack of decrease upon addition of increasing concentrations of both gefitinib and cetuximab.

A431 cells are epidermoid carcinoma cells, which are characterized by EGFR gene amplification and protein overexpression—similar to DiFi cells—in addition to harboring a p53 mutation. A431 cells were treated as described above for DiFi cells and the western blot analysis can be seen in Figure II-5. Results for EGFR, p1173 and 4G10 were analogous to those observed for DiFi cell experiments; however, DiFi cells appeared to have a higher level of basal phosphorylation relative to A431 cells when equal protein loads were used.

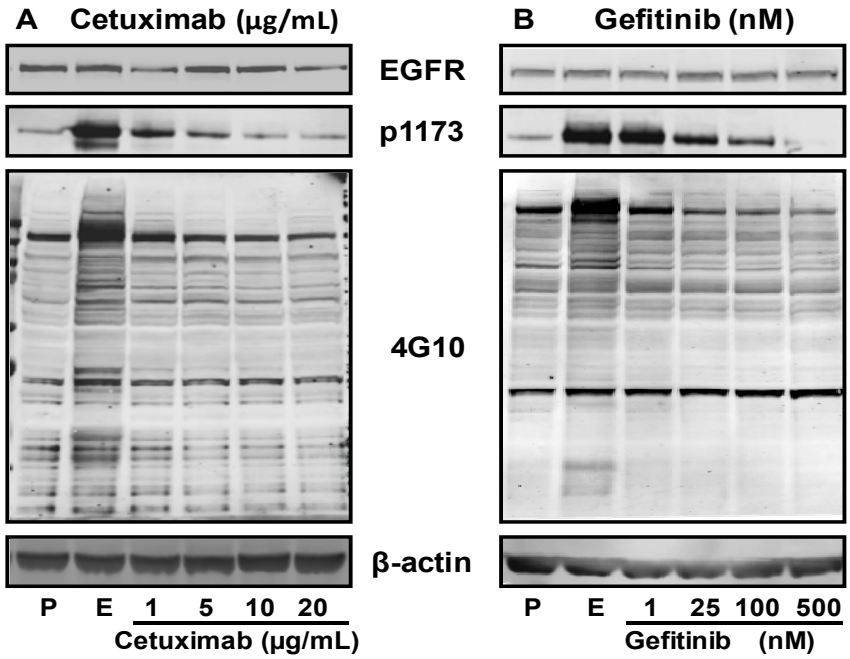

Figure II-5. EGFR modulation in A431 cells. Proliferating cells (P) were not serum starved and serve as a reference control for basal level signaling. EGF stimulated (E) and EGF plus plus (A) cetuximab (10 µg/mL) or (B) gefitinib (500 nM) for indicated times. A431 cells were serum-starved overnight before indicated treatment for 30 min. Immunoblots were performed for total EGFR, EGFR phosphorylation at pY1173 and total tyrosine phosphorylation (4G10). β-Actin was used as a loading control.

These results are in agreement with another report that EGFR in DiFi cells displays higher basal levels of tyrosine phosphorylation relative to other cell lines (16). Figures A1 and A2 (Appendix A) show control experiments for each cell line for both cetuximab and gefitinib inhibitors respectively. DMSO vehicle control showed no effect on treated samples, and—contrary to a report that cetuximab causes autophosphorylation of residue Y1173 of EGFR (17)—these experiments illustrate no increase of 1173 phosphorylation in response to cetuximab treatment.

Monitoring other ErbB receptors

As discussed in Chapter I, EGFR can dimerize with multiple ErbB family members such as human epidermal growth factor receptors 2 and 3 (HER2 and HER3 respectively). Figure II-6 shows western blot analysis assessing total HER2 and HER3 expression as well as phosphorylation status (pY1248 and pY1289 respectively) in response to EGFR stimulation and inhibition. Both cell lines express detectable levels of HER2 and HER3 that demonstrate increased phosphorylated upon addition of EGF ligand. However, the pHER2 signal increase appears to be less drastic in DiFi cells. Treatment with either cetuximab or gefitinib diminished pHER2 and pHER3 signals to basal (proliferating) levels in both cell lines.

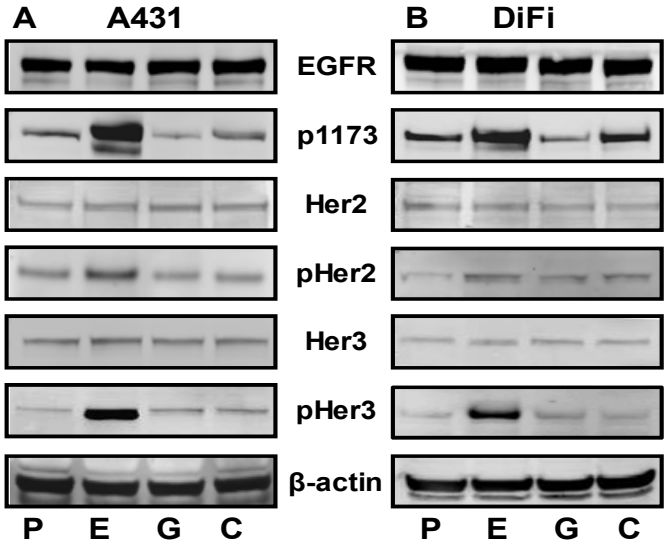

Figure II-6. ErbB expression in A431 and DiFi cells. Proliferating (P), EGF stimulated (E), EGF plus gefitinib (500 nM) co-treatment (G), EGF plus cetuximab (10 μg/mL) co-treatment (C). All treated (A) A431 and (B) DiFi cells were serum-starved for 18 h before 30 minute incubation with indicated treatment. Immunoblots were performed for total EGFR, Her2, and Her3 as well as phosphorylated forms of each receptor and total tyrosine phosphorylation (4G10). β-Actin was used as a loading control.

The combined results illustrate a larger differential between EGF stimulated and inhibited EGFR—as well as the adapter protein SHC—in A431 cells than in DiFi cells. These data, taken together with reports that DiFi cells secrete TGF-α and demonstrate increased basal levels of signaling relative to other cell lines (15, 16), support the use of A431 cells as a model system of EGFR perturbation for further proteomic analysis.

GeLC-MS analysis of A431 cells

Shotgun proteome analyses were performed on each of the four A431 treatment conditions described above: proliferating cells, EGF treated (30 nM),

EGF and gefitinib treated or EGF and cetuximab treated. A schematic of the experimental work-flow is shown in Figure II-7. This analysis platform combines SDS-PAGE gel separation with LC-MS/MS analysis of peptides from the

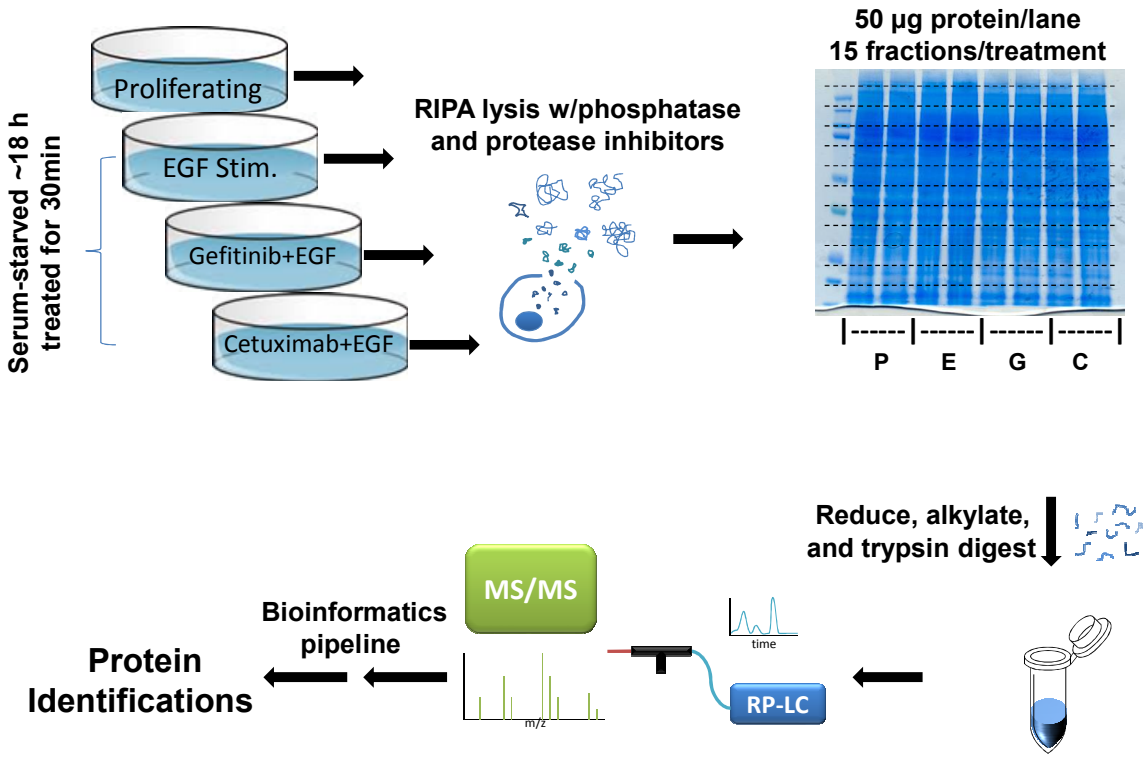

Figure II-7. Schematic of experimental work flow. P=proliferating. All treated cells were serum-starved for 18 h before incubation for 30 min with EGF (E=30 nM) or gefitinib (G=500 nM) plus EGF, or cetuximab (C=10 µg/mL) plus EGF. Equal protein loads were resolved on a polyacrylamide gel and fractionated samples (15) were trypsin digested, reduced and alkylated before reconstitution for reverse-phase liquid chromatography tandem mass spectrometry analysis.

fractionated proteins and is thus termed “GeLC-MS”. In-gel trypsin digests were performed and peptides extracted from gel fractions were analyzed by data-dependent LC-MS/MS. A summary of the global protein analysis is shown in

Table II-1. Values displayed are averaged data from 3 separate cultures per treatment condition. Confident spectral IDs (numbers of spectra matched to database sequences at 5% FDR) and similar values for protein groups (numbers of indistinguishable protein identifications supported by the identified peptides)

Table II-1 Summary of proteomic shotgun analysis. The table lists confident identifications (spectra successfully matched to database sequences at 5% FDR), protein groups (indistinguishable protein identifications supported by the identified peptides), and %CV of replicate analysis for each of the four treatment conditions (proliferating, 30 nM EGF, 30 nM EGF plus 500 nM gefitinib and 30 nM EGF plus 10 µg/mL cetuximab,). Protein group numbers are averages of three separate cultures per treatment. A 5% peptide-level FDR and minimum two distinct peptides were required for confident protein identification. *A protein group is defined by a set of proteins that cannot be distinguished based on the peptide identifications. A single protein is chosen to represent each protein group.

	Proliferating	EGF Stimulated	Gefitinib + EGF	Cetuximab + EGF
Confident spectral IDs	**40267**	**46945**	**54882**	**48867**
Protein groups	**3377**	**3486**	**3697**	**3564**
Protein group CV(%)	**16.8**	**12.8**	**13.3**	**16.2**

and protein group CVs under 17% illustrate reasonable variation across biological replicates. Figure A3 (Appendix A) shows the distribution of peptides identified across all fractions for each of the treatment conditions with fractions 3-8 typically displaying the highest number of confident identifications. Of note from the A431 cell proteomic datasets were confident protein identifications for EGFR, HER2 and HER4, although no peptides unique to HER3 were identified.

Dataset comparisons, data filtering and identification of significant differences in protein expression

Next, protein expression datasets from the four A431 cell conditions were compared to identify proteins whose levels were different between EGF-stimulated conditions and either proliferating or EGFR-inhibited conditions. Protein expression was compared on the basis of spectral counts using QuasiTel, a quasi-likelihood modeling software package (10). QuasiTel performed pair-wise comparison between two treatment conditions based on protein spectral counts and variance across replicate analyses and computed p-values and rate ratios (fold changes) for detected proteins.

Pair-wise comparisons were made between 1) proliferating and EGF stimulated cells, 2) EGF-stimulated and gefitinib plus EGF-treated cells and 3) EGF stimulated and cetuximab plus EGF-treated cells (Table II-2). To control the

Table II-2. Protein identifications and protein FDR of comparison datasets. Pair-wise comparison of the proteomic datasets for EGF (30 nM) versus proliferating, EGF versus gefitinib (500 nM) plus EGF and EGF versus cetuximab (10 µg/mL) plus EGF were generated using QuasiTel. The three resulting comparison datasets were filtered to require ≥6 spectra for each protein per replicate.

Comparison	EGF-stimulated vs. Proliferating	EGF-stimulated vs. Gefitinib + EGF	EGF-stimulated vs. Cetucimab + EGF
Proteins	**2298**	**2488**	**2393**
Protein FDR (%)	**2.2**	**1.7**	**1.7**

protein-level FDR, comparisons were limited to proteins with ≥6 spectral counts per protein across replicates. The three comparison datasets were further filtered

to contain only proteins with quasi p-values ≤ 0.05 and fold changes ≥ 1.5. This resulted in 42, 60 and 31 differential protein identifications for EGF vs. Proliferating, EGF vs. Gefitinib/EGF and EGF vs. cetuximab/EGF comparisons respectively. Figures A4-A6 (Appendix A) list the HUGO names of proteins up regulated (red) and down-regulated (green)—with respect to EGF treatment—at selected cut-offs in each comparison dataset.

MRM verification of protein expression differences in A431 cells

Changes in protein expression were verified via MRM analyses using the labeled reference peptide (LRP) method described recently (3). Expression was quantified by normalizing target peptide signals to a labeled β-actin peptide standard. A431 cells were treated as described for western blot analysis and global proteomic experiments; however, cell lysis and sample preparations were modified to account for the lack of polyacrilamide gel fractionation (see experimental section). The targeted MS data generated by MRM analyses for 11 selected proteins are displayed in Figure II-8. MRM data were from analyses of 3 separate cultures for each treatment and the normalized peak area (NPA) for a single, proteotypic peptide is shown for each protein. CVs calculated (across replicate analysis for each treatment condition) from NPA values were below 30% for all monitored peptides with the majority of CV values falling below 17%. The peptide sequences, HUGO name, normalized peak areas, and CVs for the MRM data in Figure II-8 can be found in Table A1 in Appendix A.

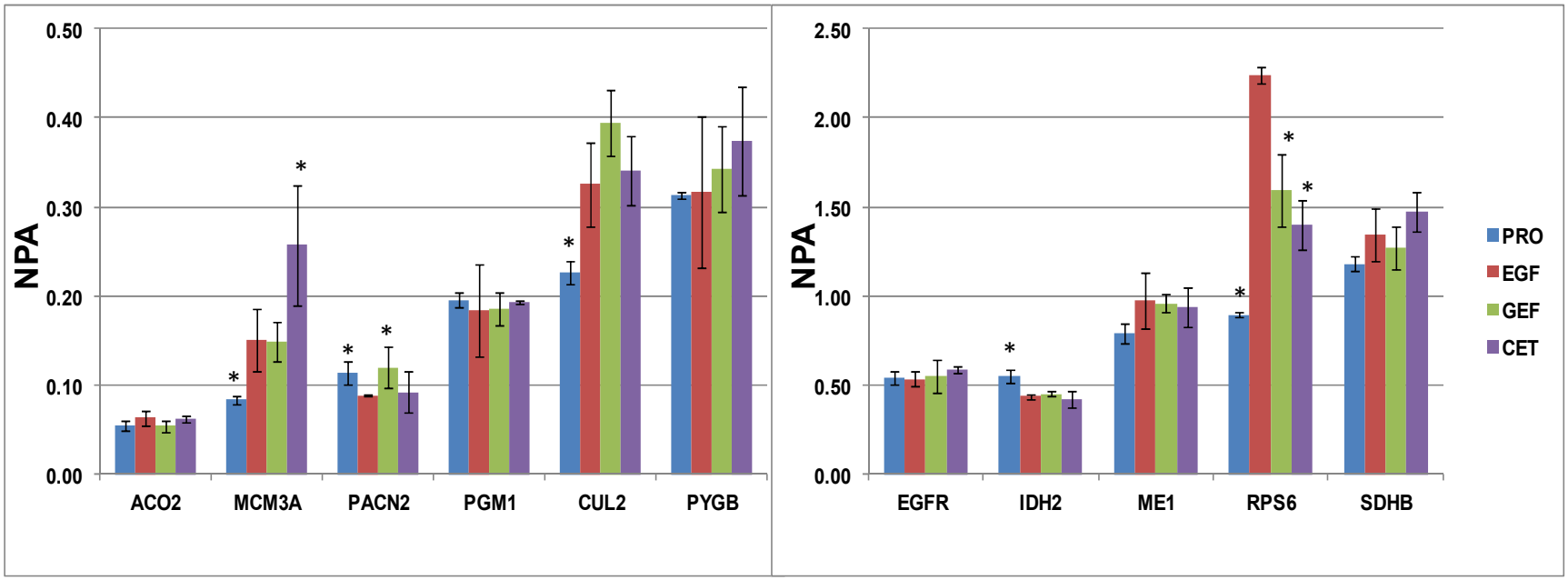

Figure II-8. MRM analysis of differential proteins. MRM data shows normalized peak area (NPA) quantified from one unique peptide for each target protein across three separate cultures. Pro = proliferating cells, EGF=EGF-stimulated (30 nM) for 30 min, GEF=gefitinib (500 nM) and EGF-treated for 30 min, CET=cetuximab (10 ug/mL) and EGF-treated for 30 min. ACO2 = aconitase 2, MCM3A=minichromosome maintenance complex component 3, PACN2=protein kinase C and casein kinase substrate in neurons 2, PGM1=phosphoglucomutyase 1, CUL2=cullin 2, PYGB=glycogen phosphorylase (brain), EGFR=epidermal growth factor receptor, IDH2=isocitrate dehydrogenase 2, ME1=malic enzyme 1, RPS6=ribosomal protein S6, and SDHB=succinate dehydrogenase subunit beta. (*) Denotes significant difference between EGF-treated A431 cells as determined by Student's two-tailed, unpaired t-test.

In agreement with spectral count data, signals for both cullin 2 (CUL2) and ribosomal protein S6 (RPS6) displayed an EGF-induced increase relative to proliferating cells. However, when treated with gefitinib or cetuximab, only RPS6 signals were significantly decreased below levels observed in EGF only stimulated samples. Minichromosomal maintenance complex associated protein 3 (MCM3A), in concordance with spectra count comparison, was detected at higher levels in cetuximab-treated samples than in EGF-treated samples. Moreover, peptide signals detected for MCM3A were significantly lower in proliferating samples than in EGF-stimulated cells. Also in agreement with findings from spectral count comparisons, was a significantly higher signal in proliferating cells compared to EGF-treated cells for isocitrate dehydrogenase 2 (IDH2) and protein kinase C and casein kinase substrate 2 (PACSN2). MRM analyses detected no significant differences between EGF only and EGF plus inhibitor treatments for EGFR (in agreement with western blots), aconitase 2 (ACO2), phosphoglucomutase 1 (PGM1), glycogen phosphorylase B (PYGB), malic enzyme (ME1) and succinate dehydrogenase beta (SDHB) peptide signals. Since several proteins identified as significantly different in the shotgun datasets (e.g., phosphoglucomutase, succinate dehydrogenase, malic enzyme, isocitrate dehydrogenase and glycogen phosphorylase) participate in a variety of metabolic pathways, I hypothesized that other proteins involved in these metabolic processes might be differentially expressed as well. Figures A7, A8, and A9 in Appendix A show expanded panels of targeted assays designed to monitor other proteins involved in three metabolic pathways including glycolysis, tricarboxylic

acid (TCA) cycle and pentose phosphate pathway (PPP) respectively. Tables A2-4 list the targeted peptide sequences, precursor *m/z,* NPA, standard deviation and CV for greater than 30 proteins involved in glycolysis, the TCA cycle and PPP respectively. While not all of these proteins were identified in the global LC-MS/MS studies, MRM analysis identified significant differences between treatments for 12 of the 32 targeted proteins. Of the 12 differentially expressed proteins, nine of these were identified in initial shotgun experiments (DERA, G6PD, TKT, PGD, CS, MDH2, PCK2 and PC); and six of those 12 (PGD, G6PD, CS, MDH2, PCK2 and PC) only narrowly failed to meet the applied filtering criteria.

Discussion

Direct analysis of phosphorylated receptor proteins and their downstream effectors is the most commonly employed method to assess signaling networks. This approach is complicated by the transient nature of protein post-translational modifications, their low abundance relative to unmodified proteins and potential artifacts due to uncontrolled preanalytical variables. The described studies ask whether changes in protein expression could indicate changes in the status of a signaling network. A test of this hypothesis requires an experimental model in which EGFR activation and inhibition can be reproducibly demonstrated by widely accepted criteria. These results clearly demonstrate that EGF treatment of A431 and DiFi cells stimulate EGFR phosphorylation and activation of associated

substrates, as well as global tyrosine phosphorylation. The results also demonstrate that cetuximab and gefitinib treatments inhibit these responses. A preliminary proteomic analysis by GeLC-MS identified large proteome inventories, although differences in protein expression between the treatments were modest, yet were verified by MRM analyses.

For the described experiments, it was important to establish a reproducible model system of EGFR stimulation and inhibition. EGFR and phosphorylated EGFR (activated) expression was assessed in DiFi colorectal carcinoma and A431 squamous cell carcinoma cells in response to receptor modulation. DiFi cells displayed higher basal levels of activated EGFR and decreased response to EGFR stimulation and inhibition relative to A431 cells. Based on these findings and an extensive literature background (18-22), the A431 cell model was selected as the principal experimental system to study EGFR-driven signaling events.

Whereas the goal of this work was to evaluate the feasibility of using global protein expression changes as indicators of response to EGFR drug treatment and not to define a cellular mechanism or specific protein signature, applying this method to mechanistic studies of signaling pathways necessitates consideration of the unique biology intrinsic to the model selected. For example, detection of Her2, Her3, and Her4 expression by either western blotting and/or shotgun mass spectrometry, which is consistent with previously published reports for the epidermoid carcinoma cell line (23, 24), leads to questions about the overall contributions of these receptors in affecting the EGFR signaling pathway of

interest. Moreover, A431 cells harboring mutant p53 will undoubtedly show different protein changes than those cell lines possessing wild-type p53.

LC-MS/MS analysis of differentially treated A431 cells reproducibly generated large, proteomic datasets for each condition. Pair-wise comparison of the datasets highlighted significant differences in protein expression profiles. An interesting point to note from these experiments is that, although gefitinib and cetuximab are both inhibitors of the EGFR receptor, the majority of the differential proteins identified—at the selected cut-offs—were observed to have more spectral counts (i.e. higher protein abundance) in inhibitor-treated conditions relative to EGF only conditions. This same trend holds true when comparing EGF stimulated and proliferating datasets.

MRM was successfully used to quantify > 40 proteins, 10 of which were identified as significantly different in shotgun experiments; one of these was EGFR. Of the 10 proteins targeted, 5 were verified as having significant changes consistent with observations from global analysis. CVs were calculated for each of the four treatments per protein and only one was greater than 30%; the majority fell below 17% (see supplemental tables in Appendix A). Use of the MRM approach to target multiple proteins in three metabolic pathways (glycolysis, TCA cycle and PPP) illustrates the ease and versatility of this approach to develop targeted assays that can elaborate on initial screening results from shotgun analysis. For example, this pathway-directed approach detected significant changes in several proteins that were either not detected in shotgun analyses or did not meet the filtering requirements applied to comparison datasets.

Although several differential proteins were successfully confirmed using targeted LC-MRM MS methods, the results obtained from these studies highlights potential points for refinement of experimental design. For example, statistical analysis of 4 replicate datasets might be approaching the limits for the statistical model suggesting potential benefits from the use of more replicates to strengthen statistical analysis. In addition, the use of 30 minute treatment time-points—while adequate for detection of a few significant protein differences—may not be adequate to allow development of a robust protein expression signature. This work was done while the shotgun analysis platforms in our laboratory were undergoing development and the GeLC-MS method was replaced for many applications by a method in which protein digests are fractionated by isoelectric focusing (IEF) and the fractions are analyzed by LC-MS/MS. Application of this latter platform is described in Chapter III.

The main objective for this work was to assess the feasibility of using global protein expression signatures to indicate a response to drug treatment. These studies establish proof-of-concept experiments for using shotgun (LC-MS/MS) and targeted (LC-MRM) mass spectrometry platforms to identify global protein changes in EGFR modulated cells.

Acknowledgments

I thank Dr. Robert Coffey and Dr. Carlos Arteaga for the cell lines and EGFR inhibitors.

References

1. Licklider, L. J., Thoreen, C. C., Peng, J., and Gygi, S. P. (2002) Automation of nanoscale microcapillary liquid chromatography-tandem mass spectrometry with a vented column. *Anal. Chem.* **74**, 3076-3083.

2. MacLean, B., Tomazela, D. M., Shulman, N., Chambers, M., Finney, G. L., Frewen, B., Kern, R., Tabb, D. L., Liebler, D. C., and MacCoss, M. J. (2010) Skyline: an open source document editor for creating and analyzing targeted proteomics experiments. *Bioinformatics* **26**, 966-968.

3. Zhang, H., Liu, Q., Zimmerman, L. J., Ham, A.-J. L., Slebos, R. J. C., Rahman, J., Kikuchi, T., Massion, P. P., Carbone, D. P., Billheimer, D., and Liebler, D. C. (2011) Methods for Peptide and Protein Quantitation by Liquid Chromatography-Multiple Reaction Monitoring Mass Spectrometry. *Mol. Cell. Proteomics* **10**.

4. Ma, Z.-Q., Tabb, D. L., Burden, J., Chambers, M. C., Cox, M. B., Cantrell, M. J., Ham, A.-J. L., Litton, M. D., Oreto, M. R., Schultz, W. C., Sobecki, S. M., Tsui, T. Y., Wernke, G. R., and Liebler, D. C. (2011) Supporting Tool Suite for Production Proteomics. *Bioinformatics*.

5. Tabb, D. L., Fernando, C. G., and Chambers, M. C. (2007) MyriMatch: Highly Accurate Tandem Mass Spectral Peptide Identification by Multivariate Hypergeometric Analysis. *J. Proteome Res.* **6**, 654-661.

6. Zhang, B., Chambers, M. C., and Tabb, D. L. (2007) Proteomic Parsimony through Bipartite Graph Analysis Improves Accuracy and Transparency. *J. Proteome Res.* **6**, 3549-3557.

7. Qian, W.-J., Liu, T., Monroe, M. E., Strittmatter, E. F., Jacobs, J. M., Kangas, L. J., Petritis, K., Camp, D. G., and Smith, R. D. (2004) Probability-Based Evaluation of Peptide and Protein Identifications from Tandem Mass Spectrometry and SEQUEST Analysis: The Human Proteome. *J. Proteome Res.* **4**, 53-62.

8. Elias, J. E., and Gygi, S. P. (2007) Target-decoy search strategy for increased confidence in large-scale protein identifications by mass spectrometry. *Nat Meth* **4**, 207-214.

9. Liu, H., Sadygov, R. G., and Yates, J. R. (2004) A Model for Random Sampling and Estimation of Relative Protein Abundance in Shotgun Proteomics. *Anal. Chem.* **76**, 4193-4201.

10. Li, M., Gray, W., Zhang, H., Chung, C. H., Billheimer, D., Yarbrough, W. G., Liebler, D. C., Shyr, Y., and Slebos, R. J. C. (2010) Comparative Shotgun Proteomics Using Spectral Count Data and Quasi-Likelihood Modeling. *J. Proteome Res.* **9**, 4295-4305.

11. Breslow, N. (1990) Further studies in the variability of pock counts. *Stat. Med.* **9**, 615-626.

12. Pawluk-Kolc, M., Zieba-Palus, J., and Parczewski, A. (2006) Application of false discovery rate procedure to pairwise comparisons of refractive index of glass fragments. *Forensic Sci. Int.* **160**, 53-58.

13. Gross, M. E., Zorbas, M. A., Danels, Y. J., Garcia, R., Gallick, G. E., Olive, M., Brattain, M. G., Boman, B. M., and Yeoman, L. C. (1991) Cellular Growth Response to Epidermal Growth Factor in Colon Carcinoma Cells with an Amplified Epidermal Growth Factor Receptor Derived from a Familial Adenomatous Polyposis Patient. *Cancer Res.* **51**, 1452-1459.

14. Olive, M., Untawale, S., Coffey, R. J., Siciliano, M. J., Wildrick, D. M., Fritsche, H., Pathak, S., Cherry, L. M., Blick, M., Lointier, P., and et al. (1993) Characterization of the DiFi rectal carcinoma cell line derived from a familial adenomatous polyposis patient. *In Vitro Cell. Dev. Biol.* **29A**, 239-248.

15. Untawale, S., Zorbas, M. A., Hodgson, C. P., Coffey, R. J., Gallick, G. E., North, S. M., Wildrick, D. M., Olive, M., Blick, M., Yeoman, L. C., and Boman, B. M. (1993) Transforming Growth Factor-Î± Production and Autoinduction in a Colorectal Carcinoma Cell Line (DiFi) with an Amplified Epidermal Growth Factor Receptor Gene. *Cancer Res.* **53**, 1630-1636.

16. Cunningham, M. P., Thomas, H., Fan, Z., and Modjtahedi, H. (2006) Responses of human colorectal tumor cells to treatment with the anti-epidermal growth factor receptor monoclonal antibody ICR62 used alone and in combination with the EGFR tyrosine kinase inhibitor gefitinib. *Cancer Res.* **66**, 7708-7715.

17. Mandic, R., Rodgarkia-Dara, C. J., Zhu, L., Folz, B. J., Bette, M., Weihe, E., Neubauer, A., and Werner, J. A. (2006) Treatment of HNSCC cell lines with the EGFR-specific inhibitor cetuximab (Erbitux) results in paradox phosphorylation of tyrosine 1173 in the receptor. *FEBS Lett.* **580**, 4793-4800.

18. Wahl, M., and Carpenter, G. (1988) Regulation of epidermal growth factor-stimulated formation of inositol phosphates in A-431 cells by calcium and protein kinase C. *J. Biol. Chem.* **263**, 7581-7590.

19. Xu, Y., Guo, D.-F., Davidson, M., Inagami, T., and Carpenter, G. (1997) Interaction of the Adaptor Protein Shc and the Adhesion Molecule Cadherin. *J. Biol. Chem.* **272**, 13463-13466.

20. Bianco, R., Shin, I., Ritter, C. A., Yakes, F. M., Basso, A., Rosen, N., Tsurutani, J., Dennis, P. A., Mills, G. B., and Arteaga, C. L. (2003) Loss of PTEN//MMAC1//TEP in EGF receptor-expressing tumor cells counteracts the antitumor action of EGFR tyrosine kinase inhibitors. *Oncogene* **22**, 2812-2822.

21. Mariner, D. J., Davis, M. A., and Reynolds, A. B. (2004) EGFR signaling to p120-catenin through phosphorylation at Y228. *J. Cell Sci.* **117**, 1339-1350.

22. Kim, S.-H., Song, Y.-C., Kim, S.-H., Jo, H., and Song, Y.-S. (2009) Effect of Epidermal Growth Factor Receptor Inhibitor Alone and in Combination with Cisplatin on Growth of Vulvar Cancer Cells. *Ann. N. Y. Acad. Sci.* **1171**, 642-648.

23. Song, J.-y., Lee, S.-w., Hong, J. P., Chang, S. E., Choe, H., and Choi, J. (2009) Epidermal growth factor competes with EGF receptor inhibitors to induce cell death in EGFR-overexpressing tumor cells. *Cancer Lett.* **283**, 135-142.

24. Ono, M., Hirata, A., Kometani, T., Miyagawa, M., Ueda, S.-i., Kinoshita, H., Fujii, T., and Kuwano, M. (2004) Sensitivity to gefitinib (Iressa, ZD1839) in non-small cell lung cancer cell lines correlates with dependence on the epidermal growth factor (EGF) receptor/extracellular signal-regulated kinase 1/2 and EGF receptor/Akt pathway for proliferation. *Molecular Cancer Therapeutics* **3**, 465-472.

CHAPTER III

PROTEIN EXPRESSION SIGNATURES FOR INHIBITION OF EPIDERMAL GROWTH FACTOR RECEPTOR-MEDIATED SIGNALING

Introduction

The main objective of this work was to determine whether protein expression signatures can represent the effects of drugs on a signaling network. The experiments detailed in Chapter II establish a foundation for this body of work and provide proof-of-concept for using the described approach to test the proposed hypothesis that changes in global protein expression levels can produce distinct protein signatures indicative of a cellular response to EGFR modulation.

However, the lack of a robust protein expression differential for EGFR activation and inhibition in the initial studies suggested the need for modifications in the experimental approach described in Chapter II. Accordingly, four changes were made to the experimental approach: 1) the treatment period was extended from 30 minutes to 4 hours; 2) the number of replicate datasets used for global proteomic comparisons was increased from four to six; 3) the initial polyacrylamide gel fractionation of proteins was replaced with isoelectric focusing of peptides on pH gradient gel strips following tryptic digestion; and 4) initial starting material for each sample was increased from 100 µg to 200 µg of protein.

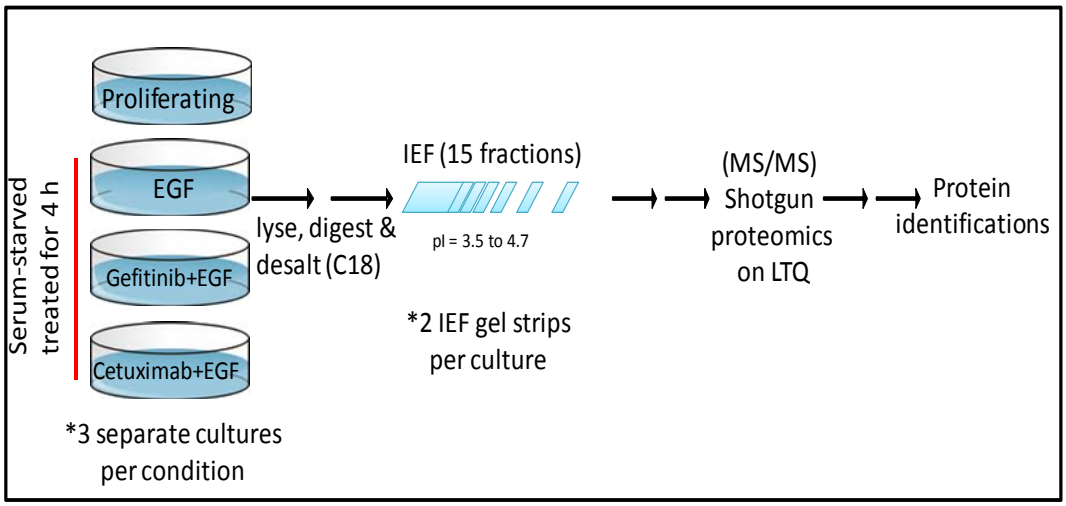

Figure III-1. Schematic of sample work flow. Proliiferating, EGF treated (30 nM) or EGFR inhibitor and EGF co-treated A431 cells (500 nM gefitinib or 10 µg/mL cetuximab) were either serum starved and treated with 30 nM EGF or co-treated with EGFR inhibitors and EGF. Trypsin digested samples were resolved using immobilized pH gradient gel strips (3.5-4.7) and isoelectric focusing. Gel strips were cut into 15 fractions and a total of six replicates (three separate cultures and two gel strips per culture) were analyzed using liquid chromatography tandem mass spectrometry.

Differentially treated A431 cells were analyzed with a standardized shotgun proteomics platform that combines peptide isoelectric focusing and LC-MS/MS (1, 2). Comparison of these A431 proteomic datasets indicated proteins that differed significantly in expression between treatment conditions and constitute potential stimulation and inhibition signatures. A set of proteins whose expression was changed by EGF and reversed by both gefitinib and cetuximab comprised a candidate “EGFR inhibition signature”, which was further verified by multiple reaction monitoring (MRM) analyses. The EGFR inhibition signature was then monitored in three other models: 1) a comparison of DiFi (EGFR inhibitor-sensitive) and HCT116 (EGFR-resistant) cell lines, 2) in formalin-fixed, paraffin-embedded (FFPE) mouse xenograft DiFi and HCT116 tumors, and 3) in

frozen tissue biopsies from a patient with the gastric hyperproliferative disorder Ménétrier's disease, who was treated with cetuximab. The results validated a multiprotein EGFR inhibition signature in all three models and illustrate the utility of protein expression changes as surrogate measures of signaling network activation and inhibition.

Experimental Procedures

Materials and reagents

Iodoacetamide, ammonium bicarbonate, sodium molybdate, β-glycerophosphate, sodium molybdate, sodium orthovanadate, 4-(2-Aminoethyl)benzenesulfonyl fluoride, aprotinin, leupeptin, betastatin, pepstatin A, dimethyl sulfoxoide, and sodium dodecyl sulfate (all >99.0% purity) were purchased from Sigma (St. Louis, MO). Dithiothreitol was from Bio-Rad (Hercules, CA); 2,2,2-trifluoroethanol (TFE) was from Acros (Geel, Belgium). C-terminal isotopically labeled β-actin (BA) peptide (GYSFTTTAE*R) containing U-$^{13}C_6$, U-$^{15}N_4$-arginine was obtained from New England Peptide at 95% chemical purity. Fetal bovine serum (FBS) was from Atlas Biologicals (Fort Collins, CO). Mass spectrometry grade trypsin (Trypsin Gold) was purchased from Promega (Madison, WI). HPLC grade water and acetonitrile (ACN) were from Mallinckrodt Baker (Phillipsburg, NJ). Phosphate buffered saline, Dulbecco's modified eagle medium (DMEM), improved minimal essential medium (IMEM), McCoy's 5A medium, NuPAGE® MOPS and MES SDS running buffer, NuPAGE® LDS sample buffer, NuPAGE® 10% Bis-tris gels and polyvinylidene difluoride

membrane were from Invitrogen (Carlsbad, CA). Epidermal growth factor (EGF), EGFR, pY1173, pY998, Jagged 1, c-Jun, caspase 3 and PARP antibodies (#8916LF, 4267s, 4407s, 2641, 2620, 9165, 9542 and 9662 respectively) were purchased from Cell Signaling Technologies (Danvers, MA). Claudin 4 and β-actin antibody (#ab53156 and ab8224 respectively) were from AbCam (Cambridge, MA). 4G10 antibody (#05-1050X) was from Milipore (Billerica, MA). AlexaFluor® 680-conjugated fluorescent secondary antibodies were obtained from Molecular Probes (Eugene, OR). Trifluoroacetic acid (TFA), formic acid (FA), urea and tris-carboxyethylphosphine were purchased from Thermo Fisher Scientific. Gefitinib and cetuximab were gracious gifts from Dr. Carlos Arteaga and Dr. Robert Coffey respectively, both at Vanderbilt University. Sub-X was from Surgipath (Richmond, IL).

Frozen gastric epithelial biopsy specimens were obtained from were obtained from Dr. Robert Coffey at Vanderbilt University from a previous study (3), which was a single-arm clinical trial to explore the effectiveness of a 4-week course of cetuximab in patients with clinically and histologically confirmed Ménétrier's disease. This prospective, open-label trial was approved by the Vanderbilt University Medical Center Institutional Review Board (IRB), and all participants provided written informed consent. DiFi and HCT116 derived mouse xenograft tumor samples were a gift from Dr. Charles Manning and a previous study (4); tissues were obtained as archival FFPE sections.

Cell culture

A431 human epithelial carcinoma cell lines were either a gift from Dr. Carlos Arteaga at Vanderbilt University (Nashville, TN) or purchased from ATCC (Manassas, VA). A431 cells were maintained in IMEM supplemented with 10% FBS. DiFi human colorectal carcinoma cells were a gift from Dr. Robert Coffey at Vanderbilt University and were maintained in DMEM and supplemented with 10% FBS. HCT116 human colorectal carcinoma cells were from ATCC and were maintained in McCoy's 5A medium also supplemented with 10% FBS. All cell lines were cultured at 37°C in 5% CO^2. Proliferating cells were grown to 70-75% confluency before collection, while all treated cells were grown to ~60-65% confluency before incubation overnight in serum-free media. These serum-starved cells were then either treated with 30 nM EGF only for 4 h (EGF Stimulated), or preincubated with 500 nM gefitinib or 10 μg/mL cetuximab (unless otherwise noted) for 30 minutes before treatment with 30 nM EGF for 4 h in the presence of the inhibitors (gefitinib treated and cetuximab treated respectively), or pre-treated with DMSO (DMSO control) before EGF stimulation. All cells were harvested on ice using cold magnesium and calcium free phosphate buffered saline and supplemented with a phosphatase inhibitor cocktail (1.0 mM sodium orthovanadate, 1.0 mM sodium molybdate, 1.0 mM sodium fluoride, and 10mM of β-glycerophosphate). Cells were pelleted by centrifugation at 500 x g at 4°C and pellets were flash frozen in liquid nitrogen.

Western blot analysis

Cell pellets were resuspended and lysed in a modified RIPA buffer (50 mM Tris-HCl, 150 mM NaCl, 1% Igepal, 0.5% sodium deoxycholate, and 0.1% sodium dodecyl sulfate) supplemented with phosphatase inhibitor cocktail (see concentrations in previous section) and protease inhibitor cocktail (0.5 μM AEBSF, 10 mM aprotinin, 1.0 mM leupeptin, 5.0 μM bestatin and 1.0 μM pepstatin). Lysates sat for 20 minutes on ice before sonication with five one second pulses at 30 watts and 20% output. The lysate was centrifuged at 12,000 rpm and the total protein concentration of the supernatant was determined using a bicinchoninic acid assay from Pierce with bovine serum albumin used as protein standard. Equivalent samples loads were normalized for total protein concentration before reducing with dithiothreitol and adding NuPAGE® LDS sample buffer. The samples were then boiled for 7 minutes at 90°C.

Serial tissue biopsies from a Ménétrier's disease patient treated with cetuximab were provided as lysates generated using the TFE and ammonium bicarbonate protocol (described in the following section). Prior to western blot analysis, aliquots of MD biopsy lysates were lyophilized and resuspended in HPLC water a total of three times in order to remove residual traces of TFE before resuspending tissue lysate in RIPA buffer. All denatured samples were then resolved using NuPAGE® 10% Bis-Tris gels at 160 V for ~65 minutes in either MOPS or MES SDS running buffer (Invitrogen). Proteins were electrophoretically transferred from the gel to a polyvinylidene difluoride membrane for 3 h at 35 V at 4°C.

Membranes were probed using EGFR, pY1173, pY998, Jagged 1, c-Jun, Claudin 4, 4G10, caspase 3, PARP or β-actin primary antibodies overnight at 4°C. AlexaFluor® 680-labeled goat anti-rabbit and goat anti-mouse secondary antibodies were used to detect the corresponding primary antibodies. Immunoreactive proteins were visualized using the Odyssey™ Infrared IYmaging System and Odyssey software as described by the manufacturer (Li-Cor, Lincoln, NE).

Cell and tissue preparation for MS analyses

A431, DiFi, and HCT116 cell pellets were resuspended and lysed in 100 µL of ammonium bicarbonate (100 mM, pH 8.0) and 100 µL of TFE and incubated at 60°C for 60 min at 1000 rpm on an Eppendorf Thermomixer before sonicating at 30 watts and 20% output for 10 one second pulses. Protein concentration was assessed using Pierce bicinchoninic acid assay and manufacturer's protocol. Equivalent sample aliquots were reduced with 40 mM Tris-carboxyethylphosphine and 100 mM dithiothriotol at 60°C for 30 min at 1000 rpm on the Eppendorf Thermomixer then incubated at ambient temperature in the dark with 200 mM iodoacetamide. Samples were diluted with 50 mM ammonium bicarbonate, pH 8.0 (to 10% TFE) before adding Trypsin Gold at a 1:50 (w:w) ratio and incubating overnight at 37ºC with shaking (400 rpm). 200 µg aliquots of digested samples were frozen and dried down *in vacuo*. Samples were resuspended in 1 mL HPLC water, vortexed vigorously, and desalted using Sep-Pak® 100 mg, C-18 columns from Waters and a vacuum manifold. After washing with HPLC water, peptides

were eluted with 80% ACN and dried *in vacuo.* Aliquots of A431 lysate for use with LC-MS/MS studies were also subjected to a subsequent separation method described in the *Isoelectric focusing of peptides* section. Dried sample aliquots for LC-MRM-MS analysis were reconstituted in 0.1% (v:v) FA in water to obtain a final concentration of 0.5 µg/µL, and the isotopically labeled β-actin peptide was spiked in at a concentration of 20 fmol/µL.

DiFi and HCT116 derived mouse xenograft tumor samples were a gift from Dr. Charles Manning at Vanderbilt University. These xenografts are from a study published by Dr. Manning and colleagues in *Clinical Cancer Research* in 2008 and should be referenced for experimental details (4). All xenograft samples were acquired as formalin-fixed paraffin embedded tumor blocks from DiFi and HCT116 derived xenografts. Three 30 µm slices were cut from each tumor block and placed into a single 1.5 mL Eppendorf tube. Paraffin was removed with three washes in 1 mL of Sub-X, and sample rehydration was achieved with three 1 mL washes each of 100, 85, and 70% ethanol in HPLC water. To complete the antigen retrieval process, samples were heated for 1 h at 80 °C in 100 µL ammonium bicarbonate (100 mM).

Human tissue biopsies from a patient with Ménétrier's disease (MD) were obtained from Dr. Robert Coffey at Vanderbilt University. The sample set originates from a single patient treated with cetuximab and consists of 3 separate tissue biopsies for each of the following time points: baseline (control), 1 day, 1 week, 1 month and 4 months after initial cetuximab treatment. The samples were flash-frozen and came from a patient involved in a previously published study

from 2009 in *Science and Translational Medicine* which should be referenced for specific details (3).

DiFi and HCT116 derived mouse tumor xenograft samples were acquired as FFPE tumor blocks. Three 30 µm slices were cut from each tumor block and placed into a single 1.5 mL Eppendorf tube. These were processed as described previously (2). Rehydrated mouse xenograft samples and Menetrier's disease lysates were prepared for LC-MRM-MS analysis using the TFE and ammonium bicarbonate protocol described previously for cell lines; however, the tissue samples were sonicated 3 times at 30 watts and 20% output continuously for 20s both before and after 60 min incubation in 50mM ammonium bicarbonate with 50% TFE.

Isoelectric focusing of peptides

A431 tryptic peptide mixtures (200µg) were resuspended in 155 µL of 6M urea. Samples were loaded into sample loading wells of the ZOOM IPGRunner cassette. 10cm ZOOM strips with immobilized pH gradient gel from 3.5-4.7 were placed into cassette and allowed to incubate with samples at room temperature for 1 h. Cassette was placed into a ZOOM IPGRunner cell, connected to a power supply and run for 15 minutes at 175 V, ramped from 175 V to 2000 V over 45 minutes, and held at 2000 V for 105 minutes. The gel strips were then cut into 15 fractions (4 mm pieces), and placed in separate wells of a 96-well enzyme-linked immunosorbent assay (ELISA) plate. Peptides were eluted from the strips as follows: 200 µL of 0.1% FA in water for 15 min; 200 µL of 50% acetonitrile

(ACN)/0.1% FA for 15 min; 200 µL of 100% ACN/0.1% FA for 15 min. Extracted peptides for each fraction were pooled, evaporated *in vacuo*, resuspended in 1 ml of 0.1% trifluoroacetic acid (TFA) and desalted over a 96-well, C18 Oasis hydrophilic-lipophilic balance 30 µm (µElution) plate (Waters Corp.). After washing with HPLC water and step-wise elution (200 µL of 30% ACN/0.1% TFA, 200 µL 70% ACN/0.1% TFA, and 200 µL of 100% ACN/0.1% TFA), peptide eluate for each IGP strip fraction were pooled, evaporated *in vacuo*, resuspended in 100 µL of 0.1% (v/v) FA in water and placed in sample vials for LC-MS/MS analysis.

Reverse phase LC-MS/MS

LC-MS/MS analyses were performed on an LTQ-XL mass spectrometer from Thermo-Fisher Scientific (Waltham, MA) equipped with an Eksigent nanoLC 1D plus pump and Eksigent autosampler (Dublin, CA) analogous to those described in the Reverse phase LC-MS/MS section in Chapter II. The only difference being that five data-dependent scans of the most intense ions were acquired after the initial full scan as opposed to only four collected in experiments described in Chapter II.

MRM analyses

Targeted MRM experiments were performed on a TSQ Vantage triple quadrupole mass spectrometer from Thermo-Fisher Scientific (Waltham MA) equipped with an Eksigent 1D Plus NanoLC pump (Dublin CA). Studies were conducted as described in Liquid chromatography-multiple reaction monitoring-mass spectrometry (LC-MRM-MS) section in Chapter II.

Data analysis

The “ScanSifter” algorithm v2.0.4 read tandem mass spectra stored as centroided peak lists from Thermo RAW files and transcoded them to mzData files. Only MS/MS scans were written to the mzData files; MS scans were excluded. If 90% of the intensity of a tandem mass spectrum appeared at a lower *m/z* than that of the precursor ion, a single precursor charge was assumed; otherwise the spectrum was processed under both double and triple precursor charge assumptions. Tandem mass spectra were assigned to peptides from the IPI Human database version 3.56 (2009-05-05 with 76591 entries) by the MyriMatch algorithm, version 1.6.33 (5). The sequence database was doubled to contain each sequence in both normal and reversed orientations, enabling false discovery rate estimation. MyriMatch was configured to expect all cysteines to bear carboxamidomethyl modifications and to allow for the possibility of oxidation on methionines. Candidate peptides were required to feature trypsin cleavages or protein termini at both ends, though any number of missed cleavages was permitted. A precursor error of 1.25 *m/z* was allowed, but fragment ions were required to match within 0.5 *m/z*. The IDPicker algorithm v2.6.1 (6) filtered the identifications for each reverse phase liquid chromatography run to include the largest set for which a 5% peptide-level identification false discovery rate could be maintained, as described by Qian *et al.* (7). Indistinguishable proteins were recognized and grouped, and parsimony rules were applied to generate a minimal list of proteins (Protein groups) that explained all of the peptides that passed the entry criteria (6). This approach uses bipartite graph analysis to derive a minimal

list of protein identifications with shared clusters of peptides. These identifications were pooled for each IEF sample set (15 fractions). Proteins were required to have at least two different peptide sequences observed within an IEF sample set. False discovery rates (FDR) for peptide identifications were computed by the formula (8): FDR = (2 × reverse)/(forward + reverse). The algorithm reported the number of spectra and number of distinct sequences observed for each protein and protein group in each sample set.

Statistical analyses

As described in the Statistical analyses section of Chapter II, comparison of protein spectral count data between treatments was carried out using the statistical modeling software package QuasiTel (9). This statistical model was used to perform pair-wise comparisons between two treatment conditions (6 replicates per condition) which generated a single combined inventory of protein identifications (Comparison dataset). Comparison datasets were generated for the following groups: proliferating cells versus EGF stimulated cells, cetuximab treated cells versus EGF stimulated cells, and gefitinib treated cells versus EGF stimulated cells. Thresholds were set for p-values (≤0.20), total spectral counts (11), and spectral count $\log_2$ rate ratios (fold changes, ≥ 2) generated by this model and were used as criteria to filter comparison datasets. Significance of measured differences for target proteins of all MRM analytes was determined with two-tailed unpaired *t* test using Prism 5.0 (GraphPad Software, San Diego, CA).

Results

EGFR modulation in A431 cells

The A431 cell model of activation and inhibition described in Chapter II was modified to include a longer 4 hour treatment time. Cells proliferating in the presence of serum served as baseline controls, whereas serum-starved cells treated with EGF served as the benchmark for EGFR activation. The phosphorylation status of the EGF receptor as well as global tyrosine phosphorylation was measured by western blot analysis (Figure III-2). After treatment with 30 nM EGF for 4 h, EGFR phosphorylation at residues Y998 and Y1173 increased dramatically, as did global phosphotyrosine levels indicated activation, as measured with the antiphosphotyrosine antibody 4G10. EGFR protein expression inversely varied with activation, which reflects enhanced receptor internalization and down-regulation upon activation (10-13). Increasing concentrations of both cetuximab and gefitinib lead to a decrease of EGFR phosphorylation at Y1173 and Y998 compared to EGF only stimulated cells. At the concentrations used, the tyrosine kinase inhibitor gefitinib produced a more profound inhibition of EGFR phosphorylation than did the ligand binding domain inhibitor cetuximab. The highest concentration of cetuximab (20 μg/mL) only

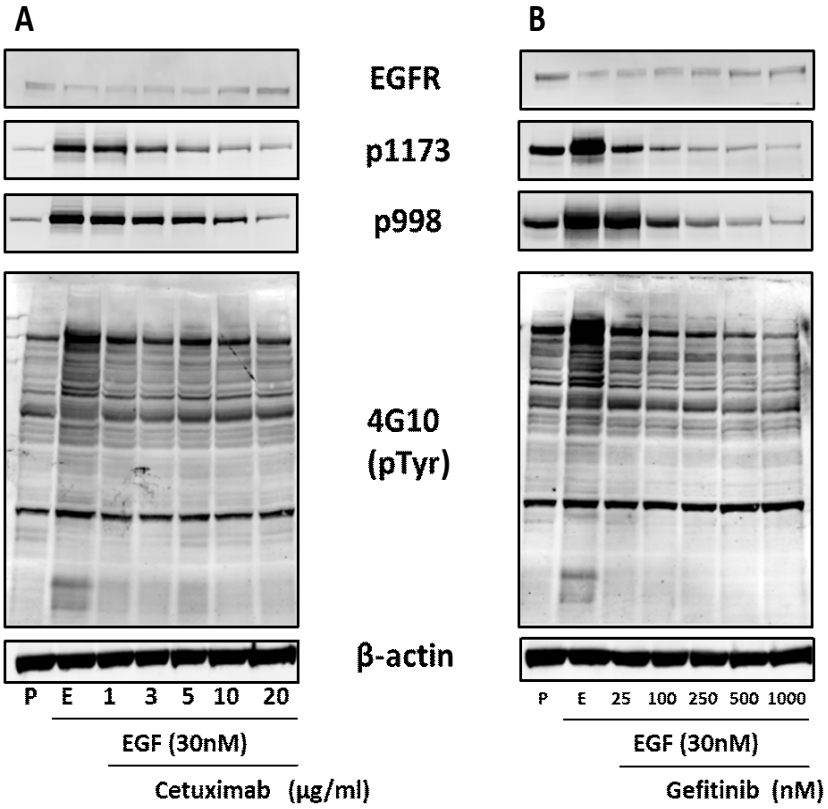

Figure III-2. Activation and inhibition of EGFR in A431 cells. A431 cells were serum-starved overnight before being treated with either 30 nM EGF (E) for 4 hrs or co- treated first with cetuximab (A) or gefitinib (B) at the indicated concentrations for 30 minutes prior to 4 hr treatment with EGF. Proliferating cells (P) were not serum starved and serve as a reference control. Immunoblots were performed for total EGFR, sites of EGFR phosphorylation at pY1173 and pY998 and total tyrosine phosphorylation was detected with the 4G10 antibody. β-Actin was used as a loading control.

reduced EGFR phosphorylation to basal levels (Figure III-2A), whereas gefitinib at 250 nM reduced both Y1173 and Y998 phosphorylation well below basal levels (Figure III-2B). Total tyrosine phosphorylation detected in EGF-stimulated cells showed an increase over signals detected in proliferating cells, and while both inhibitors reduced detected levels of total tyrosine phosphorylation, only gefitinib was capable of reducing tyrosine phosphorylation below basal levels.

With the exception of p998 in cetuximab-treated cells, minimal differences were noted between EGFR and total tyrosine phosphorylation status for the two highest concentrations of each inhibitor (10 and 20 μg/mL for cetuximab or 500 and 1000 nM for gefitinib). Based on these results, a single concentration each for cetuximab (10 μg/mL) and gefitinib (500 nM) was selected for subsequent experiments. Although these doses produced different degrees of inhibition, both drugs reproducibly and significantly inhibited EGFR signaling. At the selected concentrations, both inhibitors significantly and reproducibly inhibited EGFR signaling. While changes in phosphorylation were noted after 4 hours, EGF treatment did not induce apoptosis as determined by caspase 3 and PARP cleavage (Figure B1, Appendix B). A slight rounding of A431 cells in culture was noted for EGF- treated cells, in agreement with previous reports 14, 15, Cells co-treated with inhibitor and EGF retained an unaltered morphology. Neither EGF nor EGFR inhibitors produced significant detachment of cells from the culture dish.

Global protein expression analyses

Shotgun proteomic analyses were performed on the four A431 treatment conditions described above: proliferating cells, EGF-treated, EGF and gefitinib-treated or EGF and cetuximab-treated. A schematic of the sample work-flow can be seen in Figure III-1. Cells were treated, collected and lysed, tryptic digests were prepared and resolved by IEF, and the IEF fractions were analyzed by data-

dependent LC-MS/MS. A summary of the global protein analysis is shown in Table III-1. Values displayed are averaged data from 3 separate cultures and

Table III-1. LC-MS/MS data summary. The table lists confident identifications (# of spectra successfully matched to peptides), protein groups, and %CV of replicate analysis for each of the treatment conditions. Protein group numbers are averages of 6 replicates (three separate cultures, and two process replicates of each) per treatment (30 nM EGF, 10 µg/mL cetuximab, 500 nM gefitinib). A 5% peptide-level FDR and minimum two distinct peptides were required for confident protein identification. *A **protein group** is defined by a set of proteins that cannot be distinguished based on the peptide identifications. A single protein is chosen to represent each protein group.

	Proliferating	**EGF Stimulated**	**Gefitinib + EGF**	**Cetuximab + EGF**
Confident spectral IDs	**32567**	**36156**	**34105**	**35322**
Protein groups	**5203**	**5294**	**5347**	**5250**
Protein group CV (%)	**4.4**	**4.8**	**4.9**	**4.5**

two process replicates of each culture per treatment condition. Similar values for confident spectral IDs (numbers of spectra matched to database sequences at 5% FDR) and protein groups (numbers of indistinguishable protein identifications supported by the identified peptides) and protein group CVs under 5% demonstrate high reproducibility of the analyses across biological replicates. Figure B2 (Appendix B) shows the distribution of peptides identified across all IEF gel fractions for each of the treatment conditions with fractions 7-13 typically displaying the most confident identifications.

Dataset comparisons, data filtering and derivation of a candidate EGFR inhibition signature

Next, protein expression datasets from the four A431 cell conditions were compared to identify proteins whose levels were changed by EGFR activation and for which the changes were reversed by the inhibitors. Protein expression was compared on the basis of spectral counts using QuasiTel, a quasi-likelihood modeling software package (9). QuasiTel performed pair-wise comparison between two treatment/biological conditions based on protein spectral counts and variance across replicate analyses and computed p-values and rate ratios (fold changes) for detected proteins.

Pair-wise comparisons were made between 1) proliferating and EGF stimulated cells, 2) EGF stimulated and EGF/gefitinib treated cells and 3) EGF stimulated and EGF/cetuximab treated cells (Figure III-3, colored boxes). To control the protein-level FDR, comparisons were limited to proteins with ≥11 spectral counts per protein across replicates. Accordingly, the three comparisons included 3783, 3881 and 3750 proteins, which corresponded to protein-level FDRs of 3.3, 3.1 and 3.3% respectively. The colored circles in Figure III-3 represent proteins differentially expressed (both up and down) between treatments with a fold change of ≥ 2.0 and p-values ≤ 0.20. The blue circle (191 proteins) represents proteins differentially expressed between EGF stimulated cells and non-treated, proliferating cells while the green circle (237 proteins) and yellow (133 proteins) circles signify proteins whose EGF-stimulated changes were reversed by gefitinib and cetuximab inhibition, respectively. Tables B1-B3 in

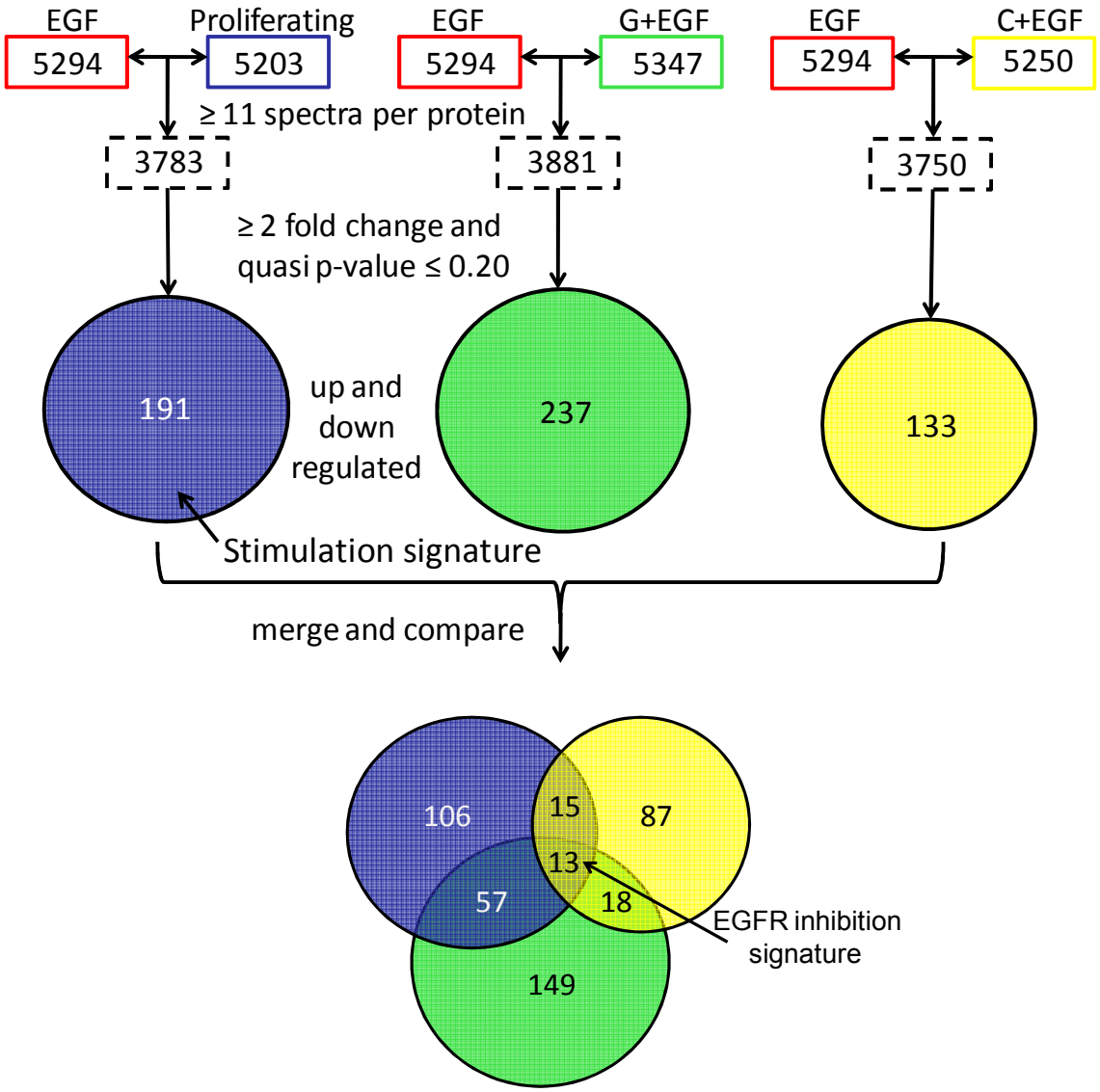

Figure III-3. Filtering and comparison of A431 proteome datasets. Colored rectangles show protein identifications from global proteomic analyses of the four treatment groups. Dashed rectangles show number of proteins in comparison datasets that were filtered to have ≥11 spectral counts per protein across replicates. Comparisons of protein spectral counts between treatment groups were performed by quasi-likelihood analysis; and a p-value and spectral count rate ratio (fold change) were generated. The colored circles represent lists of proteins differentially expressed (both up and down) between treatments with a fold change of ≥2.0 and quasi p-values ≤ 0.20. The resulting protein groups represent proteins differentially expressed in response to EGF (blue), EGF-induced protein changes reversed by gefitinib (green) and EGF-induced protein changes reversed by cetuximab (yellow). The Venn diagram comparison indicates proteins whose expression changes are shared by the different experimental conditions. The central overlap indicates the "EGFR inhibition signature", which refers to EGF-stimulated protein expression changes reversed by both inhibitors.

Appendix B provide a complete list of proteins in each of these groups. The group reversed by cetuximab is only about half as large as the group reversed by gefitinib, which is consistent with the lesser degree of EGFR inhibition produced by cetuximab in the model (Figure III-2), as well as with possible off-target effects of gefitinib due to its inhibition of multiple kinases (16, 17).

The Venn diagram (Figure III-3) compares these three groups of proteins to explore the common protein expression changes associated with EGF stimulation and EGFR inhibition. The three groups comprised 445 proteins, of which 13 proteins were shared between all three groups. Another 90 proteins were shared between two groups and most (342 proteins) belonged to only a single group. The center overlap contained 13 proteins whose expression was significantly changed by EGF treatment and these changes were reversed by both inhibitors. This group is referred to hereafter as the "EGFR inhibition signature". The 13 proteins are: coiled-coiled domain containing 50 (CCDC50), cyclin-dependent kinase inhibitor 1A (CDKN1A, p21), claudin 4 (CLDN4), cordon-bleu-like protein 1(COBLL1), jagged 1 (JAG1), proto-oncogenes c-Jun and JunD (JUN and JUND respectively), DNA primase subunit 1 (PRIM1), RNA binding motif protein 15 (RBM15), translocase of outer mitochondrial membrane 20 (TOMM20), trafficking protein particle complex 3 (TRAPPC3), and tripartite motif containing protein 32 (TRIM 32) and glutamine-fructose-6-phosphatetransaminase 2 (GFPT2).

The Venn diagram also indicates protein subgroups with expression patterns similar to those in the EGFR inhibition signature. For example, EGF-induced expression changes were reversed only by cetuximab for 15 proteins and

only by gefitinib for 57 proteins. Another 18 proteins were reversed by both cetuximab and gefitinib, but these proteins were not significantly elevated by EGF treatment at the selected cut-offs. The proteins found outside of any overlap showed significant differences between EGF stimulation and either non-treated (proliferating) or inhibitor treated cells; however, these protein differentials were unique to individual treatments and comparisons. Table B4 in Appendix B lists the proteins found in each overlapping section of the Venn diagram.

These protein groupings, including the EGFR inhibition signature, depend on the selected thresholds for fold change and p-values. More lenient thresholds may increase detection of false-positive differences, whereas more stringent criteria may decrease detection of true differences. Manipulation of thresholds for p-value and fold change can shift some proteins from one classification to another in the Venn diagram (Figure B3, Appendix B). At all levels of filtering, both CDKN1A and RBM15 meet the cut-off criteria in all three comparison datasets and were found in the center overlap.

MRM verification of EGFR inhibition signature in A431 cells

To verify expression differences for the 13 proteins in the EGFR inhibition signature, MRM analyses using the labeled reference peptide (LRP) method described recently (18) was performed to quantitate target peptides with reference to a labeled β-actin peptide standard. A431 cells were treated as described for global proteome comparisons, but no IEF fractionation was performed. The data generated by MRM analyses is displayed together with spectral count data from

the shotgun analyses (Figure III-4). MRM data (red bar) were from analyses of three separate cultures for each treatment and the normalized peak area (NPA) for a single, proteotypic peptide is shown for each protein. The spectral count

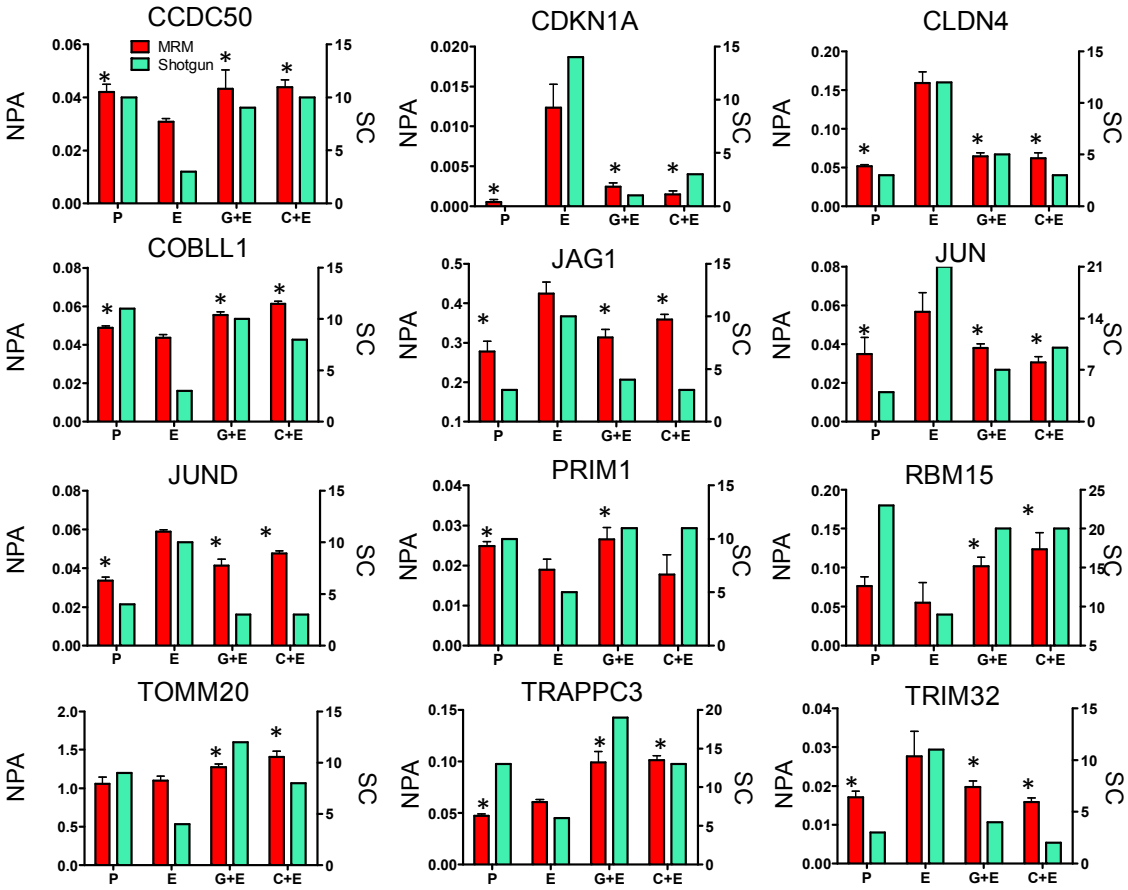

Figure III-4. Normalized MRM data and spectral count correlation of EGFR inhibition signature proteins. Each panel shows both MRM data (red bar) and spectral count data (teal bar) for each protein of interest across four A431 cell treatment conditions: proliferating cells (P), EGF-treated (E), EGF and gefitinib (G+E) and EGF and cetuximab (C+E). The left Y-axis is normalized peak area (NPA), which is the total MRM transition peak area for the target peptide divided by the peak area for the β-actin labeled reference peptide. MRM data is representative of one unique peptide for each target protein across three separate cultures. Spectral counts (SC) are the total number of spectra identified for each protein across replicate analyses. (*) Denotes significant difference compared to EGF treated cells as determined by Student's two-tailed, unpaired t-test.

data (Figure III-4, teal bar) displays the total number of spectra identified for the corresponding protein across six replicate shotgun analyses (three separate cultures and two process replicates of each culture). The peptide sequences, peptide and normalized peak areas, and CVs for the MRM data in Figure III-4 can be found in Table B5 of Appendix B. Calculated CVs for NPA values measured peptides across the treatment conditions for all but two of the peptides were below 30%. For 39 of these, CVs were less than 18%. MRM analyses for a second, unique peptide for 10 of the 12 EGFR inhibition signature proteins produced similar results (Appendix B, Figure B4 and Table B6).

MRM analyses detected peptide transitions corresponding to 12 of the 13 EGFR inhibition signature proteins. None of the peptides monitored for glutamine-fructose-6-phosphatetransaminase 2 (GFPT2) produced detectable signals. This protein was not considered further. For the remaining 12 proteins, MRM analyses verified almost all of the expression differences detected by shotgun analyses (Figure III-4). EGF-induced protein expression compared to proliferating cells was significantly different by MRM in 8 of the 12 cells and the trends in the others were consistent with spectral count differences, except for TOMM20 and RBM15. Significant reversal of EGF-induced expression was verified by MRM for both inhibitors for all 12 proteins, except for the effect of cetuximab on PRIM1, which fell short of statistical significance, although the trend was consistent with the spectral count comparison.

Confirmation of EGFR inhibition signature protein changes in DiFi and HCT-116 cell lines

The next studies analyzed changes in EGFR inhibition signature proteins in cells that differ in response to EGFR inhibitors. MRM analyses was used to measure the 12 EGFR inhibition signature proteins in DiFi and HCT-116 colorectal cancer cell lines. DiFi cells demonstrate both gene amplification and protein overexpression of the EGFR and also harbor an adenomatous polyposis coli (APC) germline mutation found in familial adenomatous polyposis (FAP) (19, 20). DiFi cells thus would be expected to show similar responses to A431 cells. HCT116 cells show increased autocrine production of the EGFR-stimulating ligand transforming growth factor-alpha (TGF-α) and carry a mutant allele (G13D) of the KRAS protoncogene (21, 22). Because KRAS mutations block clinical and cellular responses to EGFR inhibitors, such as cetiximab, I hypothesized that an EGFR inhibition signature would be minimal or absent in the HCT116 cells.

Both cell lines were treated with EGF and inhibitors as described above and the 12 EGFR inhibition signature proteins were analyzed. Peptides for 11 of the 12 proteins were successfully monitored in DiFi cells, whereas peptides for only eight of the proteins were detected in HCT116 cells (Figure III-5 and III-6 respectively). The COBLL1, PRIM1 and RBM15 peptides monitored in HCT116 cells produced no detectable signals and CDKN1A peptide signals were absent in both cell lines. Most of the peptide signals monitored in DiFi cells showed statistically significant differences between EGF only and inhibitor treated cells (Figure III-5) consistent with the trends noted in A431 cell experiments (Figure III-4). Only JUND and PRIM1 failed to show significant changes. HCT116 cells were

largely resistant to changes in EGFR inhibition signature proteins, with significant differences detected only for CCDC50, JUND and TOMM20. CCDC50 peptide

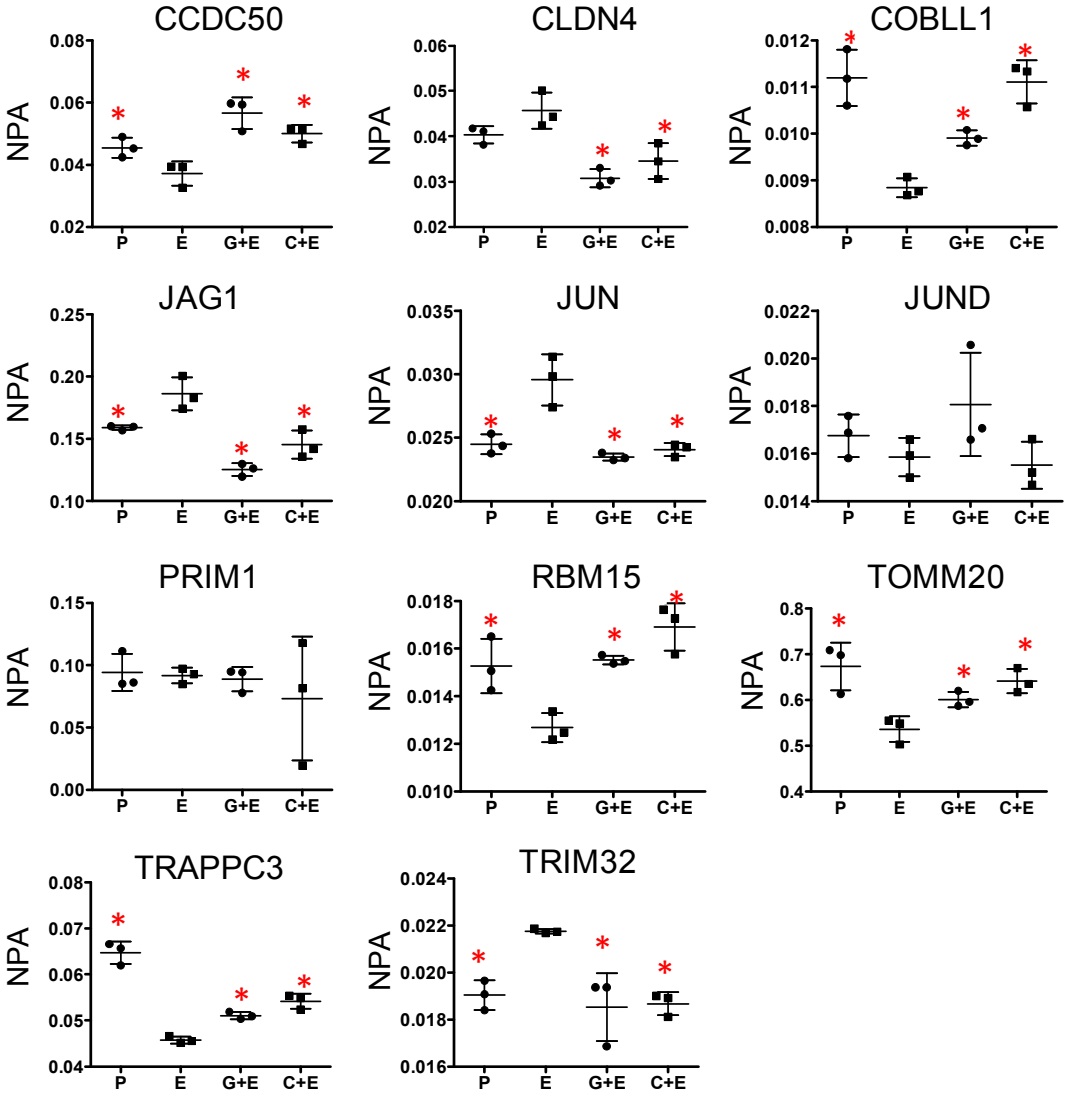

Figure III-5. MRM data for EGFR inhibition signature proteins in DiFi cells. Plots represent data from analysis of three replicate cultures for each treatment condition. Y-axis shows the normalized peak area (NPA), which is the total MRM transition peak area for the target peptide divided by the peak area for the β-actin labeled reference peptide. (*) Denotes statistically significant from EGF treatment condition (determined by Student's two-tailed, unpaired t-test).

signals were significantly upregulated in both inhibitor treated conditions when compared to EGF only samples—in agreement with A431 and DiFi cell MRM data—whereas JUND and TOMM20 peptides showed substantial differences for only gefitinib or cetuximab treatments respectively (Figure III-6). Tables B8 and B9 (Appendix B) list the peptide peak areas, normalized peak areas, averages and CVs for the EGFR inhibition signature peptides monitored in the two cell lines.

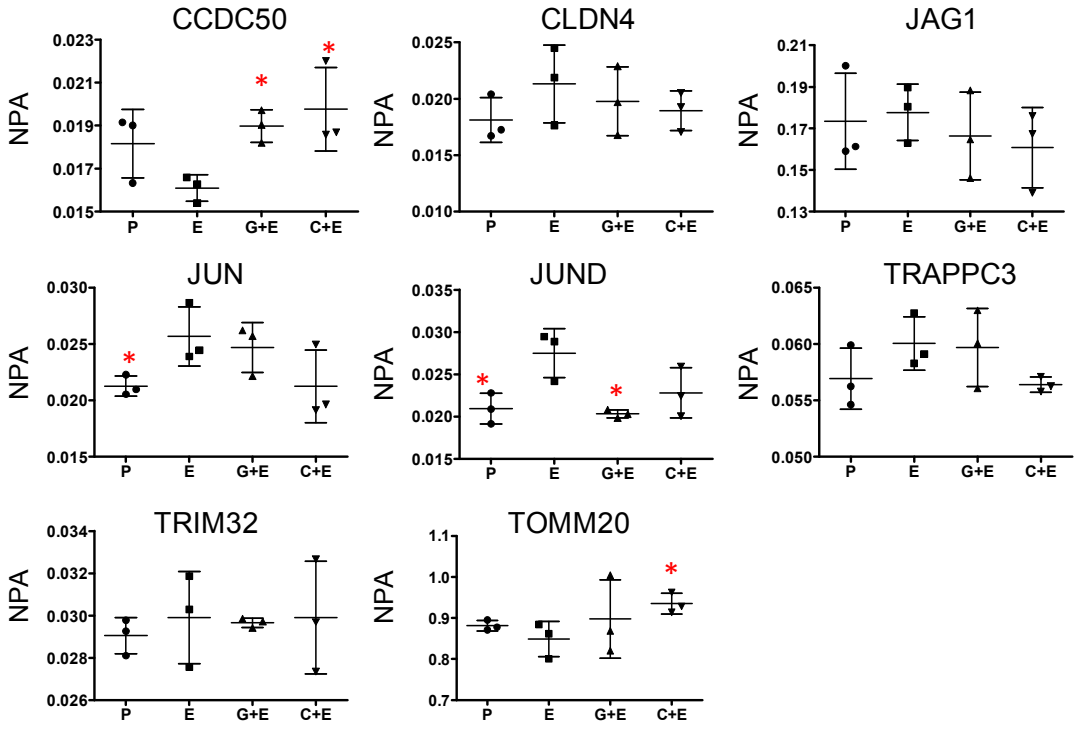

Figure III-6. MRM data for EGFR inhibition signature proteins in HCT116 cells. Plots represent data from analysis of three replicate cultures for each treatment condition. Y-axis shows the normalized peak area (NPA), which is the total MRM transition peak area for the target peptide divided by the peak area for the β-actin labeled reference peptide. (*) Denotes statistically significant from EGF treatment condition (determined by Student's two-tailed, unpaired t-test).

To confirm the expression of the EGFR inhibition signature in the DiFi and HCT116 cells, at least half of the detectable signature proteins were required to show expression changes consistent with changes measured in the A431 model. The MRM data for DiFi cells demonstrate expression changes consistent with those in A431 cell—11 of the 12 signature proteins were detected and 9 showed significant expression differences. None of the proteins showed changes opposite those observed in A431 cells. This result for DiFi cells is consistent with their overexpression of EGFR and responsiveness to EGFR inhibitors. In contrast, the HCT116 cells display expression changes sensitive to both inhibitors in only one of the eight detectable signature proteins (CCDC50) and responded only to a single inhibitor for two others (JUND and TOMM20). By the defined criteria, the HCT116 cells do not display an EGFR inhibition signature, a result that is consistent with the effect of the heterozygous G13D KRAS mutation, which blocks responses to EGFR inhibitors (22).

Immunoblot confirmation of EGFR inhibition signature

Further confirmation of protein changes in response to EGFR perturbation was done by immunoblotting with antibodies to p-EGFR, JAG1, JUN and CLDN4 in the A431, DiFi and HCT116 cell lines across all treatments (Figure III-7). In all cell lines, an increase was observed in p998 and p1173 signals in EGF-treated cells relative to proliferating. In A431 and DiFi cells treated with gefitinib, EGFR p998 and p1173 both were decreased to basal (proliferating) levels, while a less profound, yet still detectable decrease was observed in HCT116 cells. Cetuximab

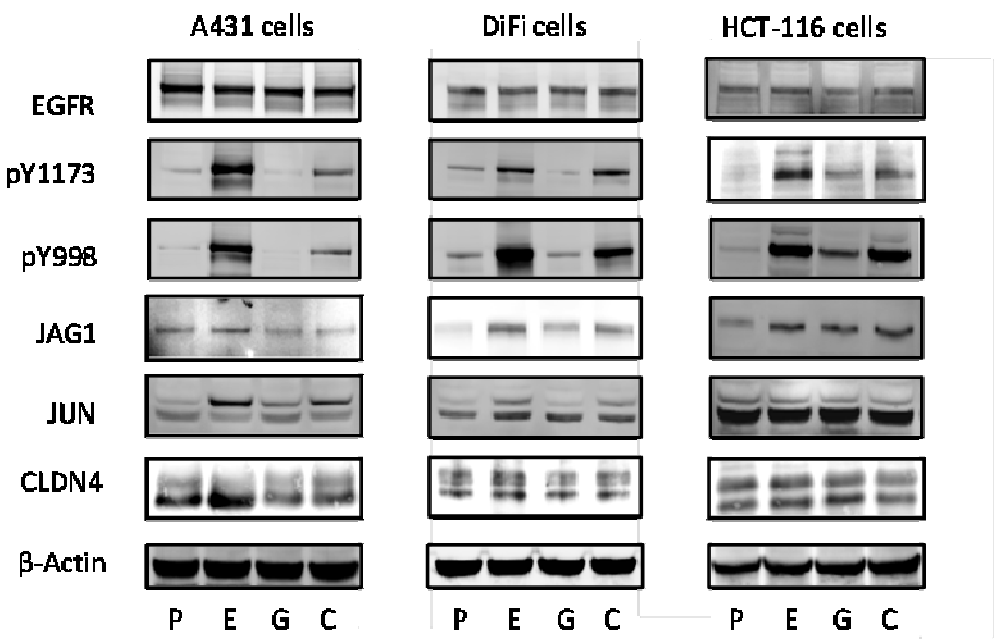

Figure III-7. Western blot analysis of EGFR inhibition signature proteins in treated A431, DiFi and HCT116 cells. P=proliferating cells, E=30 nM EGF for 4 h, G=500 nm gefitinib + 30 nM EGF for 4 h, and C= 10 µg/mL cetuximab + 30nM EGF for 4 h. Each cell line was probed for total EGFR, EGFR tyrosine phosphorylation and three proteins (e.g. JAG1, JUN and CLDN4) from the EGFR inhibition signature. β-Actin was used as a loading control.

treatment (at 10 µg/mL) in all three cell lines partially inhibited EGFR autophosphorylation. For EGFR p1173 in DiFi cells and p998 in HCT116 cells, no change in phosphotyrosine immunoblot signal was detected between EGF only and cetuximab-treated cells (Figure III-7). Protein expression changes in all three cell lines measured by immunoblot were consistent with MRM data. In A431 and DiFi cell lines, JAG1, JUN and CLDN4 were increased in EGF treated compared to proliferating cells. In both A431 and DiFi cells, gefitinib decreased JAG1, JUN and CLDN4 expression, whereas cetuximab produced partial reversal of EGF stimulation for these proteins. In HCT116 cells, EGF elevated JAG1, but the inhibitors did not reverse this effect.

Confirmation of EGFR inhibition signature protein changes in mouse xenograft tumors

To further confirm protein changes in the EGFR inhibition signature in tissue specimens, mouse xenograft tumors derived from DiFi and HCT116 cell lines were analyzed. These xenograft samples come from a previous study, in which novel optical imaging probes were used to study therapeutic responses to cetuximab *in vivo* (4). DiFi and HCT116 xenografts were grown in athymic nude mice. Tumor bearing mice were then treated with 40 mg/kg cetuximab or saline vehicle intraperitoneally every three days for one week (three total injections). Image analysis demonstrated a significant decrease in EGF-probe uptake in DiFi xenografts and increased apoptosis in cetuximab-treated mice, whereas HCT116 xenografts showed neither effect. Gefitinib was not employed in this study.

FFPE sections from the xenograft tumors were analyzed by MRM to measure the 12 EGFR inhibition signature proteins. Analyses of xenograft tumors from vehicle treated mice were used for reference to assess the effects of cetuximab treatment. MRM analyses detected eight of the 12 EGFR inhibition signature proteins in each xenograft type (Figure III-8 and III-9). DiFi derived tumors from cetuximab-treated mice showed decreased expression of CLDN4, JAG1, JUN, and TRIM32 and an increase in TRAPPC3 when compared to tumors from vehicle treated mice. These differences are similar to those between EGF-treated and only to cetuximab/EGF-treated DiFi cells, although the xenograft analyses yielded no statistically significant differences for CCDC50, COBLL1, or RBM15 (Figure III-8).

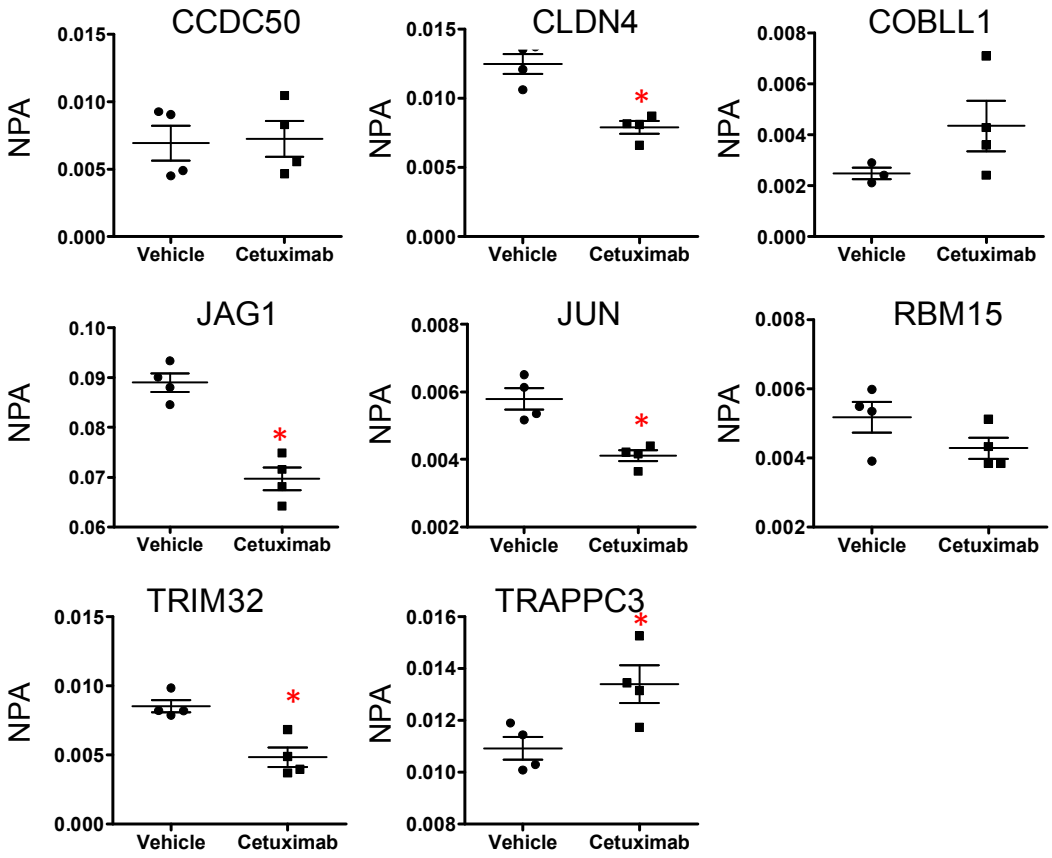

Figure III-8. MRM data for EGFR inhibition signature proteins in mouse xenografts derived from DiFi cells. Plots represent 4 biological replicates and show the average normalized peak area with standard deviation (COBLL1 peptide signal was not detected in one replicate). Y-axis shows the normalized peak area (NPA), which is the total MRM transition peak area for the target peptide divided by the peak area for the β-actin labeled reference peptide. (*) Denotes statistically significant from EGF treatment condition (determined by Student's two-tailed, unpaired t-test).

HCT116 xenografts from cetuximab-treated mice showed a significant increase in TRAPPC3 and RBM15 compared to vehicle treated tumors, but the other proteins in the EGFR inhibition signature were either unchanged or were not detected (Figure III-9). Of note are the differences between the EGFR inhibition signatures for the treated HCT116 cells and the HCT116 mouse tumors. In

HCT116 cells, cetuximab increased CCDC50 and TOMM20, but not in the HCT116 xenografts. The lack of consistent inhibitor-induced protein expression

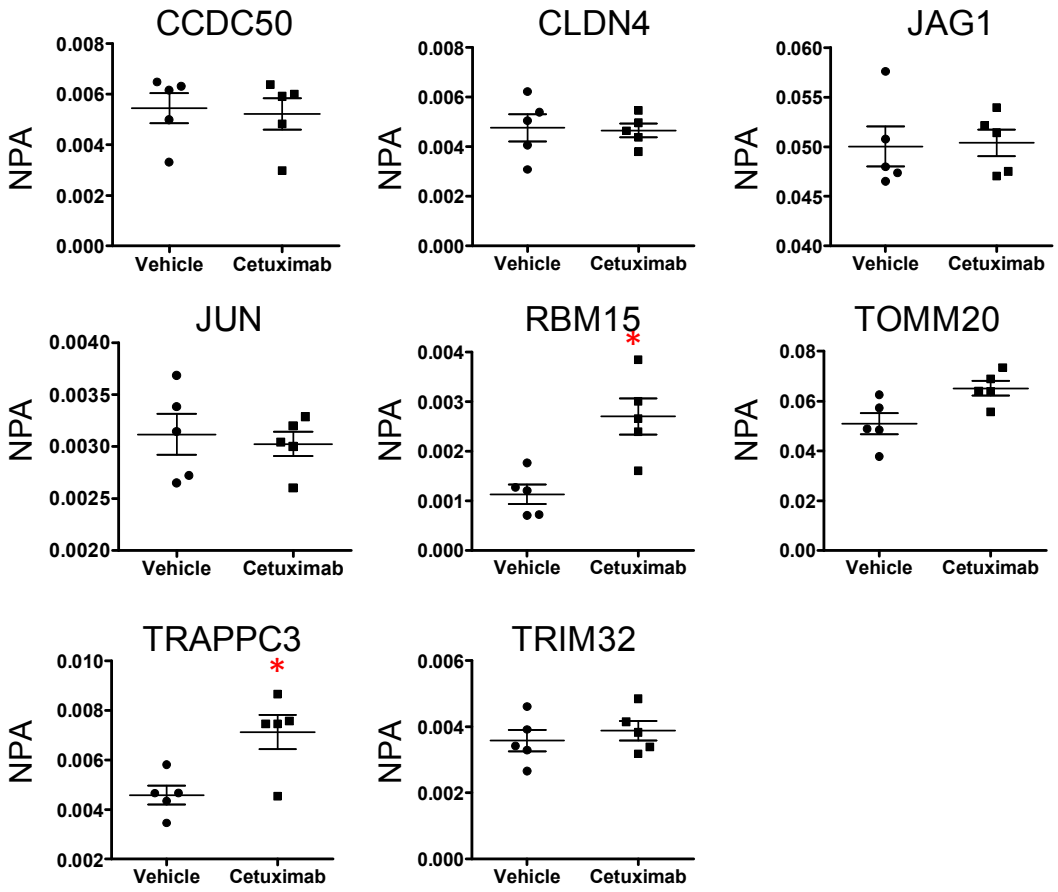

Figure III-9. MRM data for EGFR inhibition signature proteins in mouse xenografts derived from HCT-116 cells. Plots represent five biological replicates and show the average normalized peak area with standard deviation. Y-axis shows the normalized peak area (NPA), which is the total MRM transition peak area for the target peptide divided by the peak area for the β-actin labeled reference peptide. (*) Denotes statistically significant from EGF treatment condition (determined by Student's two-tailed, unpaired t-test).

differences in the HCT116 xenograft samples is consistent with the lack of response to cetuximab *in vivo* (4). MRM data for the DiFi and HCT xenograft

samples are provided in Tables B10 and B11 respectively. An important aspect of this study is the analysis of the EGFR inhibition signature in archival FFPE tissue specimens. Although a few of the measured peptides yielded CVs around 40%, most yielded CVs < 30%.

Confirmation of the EGFR inhibition signature was assessed by the criteria described above—changes concordant with the A431 model in at least 50% of the measurable signature proteins. The signature was confirmed in DiFi xenografts (five concordant changes in eight detectable signature proteins), but not in HCT116 xenografts (two concordant changes in eight detectable signature proteins). A summary of the MRM data for all cell lines and both xenograft models can be seen in Figure III-10.

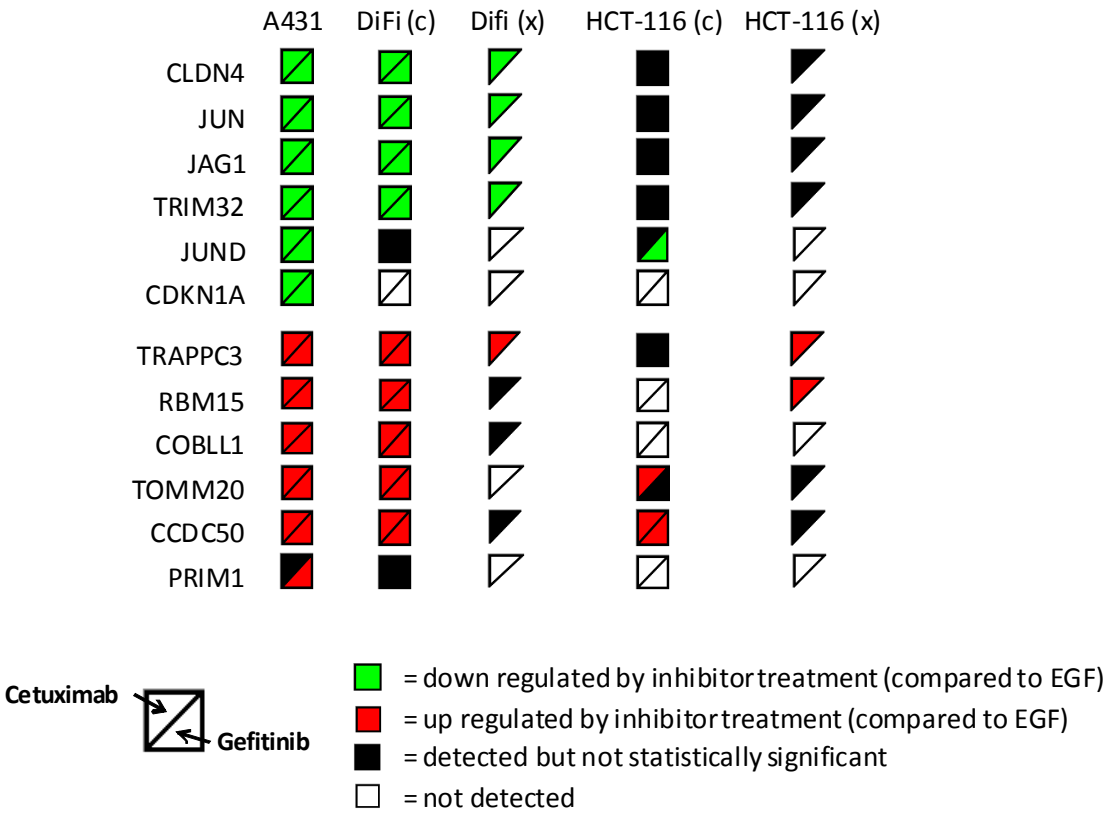

Figure III-10. Summary of expression changes for EGFR inhibition signature proteins in cell lines and mouse xenograft models. Symbol colors indicate decreased expression (green); increased expression (red); detected, but no significant change (black) compared to EGF treatment in cells (c) or compared to vehicle control in xenografts (x); and not detected (white). Only cetuximab treatment was used in xenograft experiments.

Use of the EGFR inhibition signature to assess therapeutic response to cetuximab in Ménétrier's disease

A potential use of the EGFR inhibition signature is to assess response to drug treatment. To test the applicability of the EGFR inhibition signature to assess clinical response to EGFR inhibition, serial biopsies were analyzed from a single Ménétrier's disease patient treated with cetuximab, as described in a recent study (3). Ménétrier's disease is a rare hypertrophic gastropathy characterized at

the molecular level by high expression of transforming growth factor-α (TGFA) and constitutively activated EGFR signaling (23, 24). Symptoms of Ménétrier's disease are highly responsive to cetuximab therapy, which rapidly and dramatically reverses most effects of the disease (3, 25).

One patient from a recent study (3) showed improved symptoms and a histologically normal stomach after the initial one month trial. Baseline (no treatment) specimens as well as serial biopsies from one day and one week post-initial cetuximab treatment were analyzed in triplicate (three separate analyes of pooled biopsies from several sites in the stomach) from this patient. MRM analyses detected peptides from nine of the 12 EGFR inhibition signature proteins (Figure III-11). The MRM data are presented in expanded form in Table B12. Because the cell model for EGFR inhibition reflected an acute response to EGF and inhibitors, I focused on protein expression changes after one day and one week of cetuximab treatment (biopsies were also collected at one and four months of continued treatment). CLDN4, JAG1, and JUN all were significantly decreased relative to baseline after 1 day. JUND and TRIM32 appeared decreased, although the effect was not significant. These changes all are consistent with the effects of cetuximab treatment in the A431 and DiFi cell models. In contrast, CCD50, COBBL1, TOMM20 all were decreased by 1 day of cetuximab treatment, in contrast to the increases in these proteins produced by cetuximab in the A431 and DiFi models. At 1 week cetuximab treatment, CLDN4, JAG1 and JUN were still decreased relative to pretreatment, consistent with responses to cetuximab

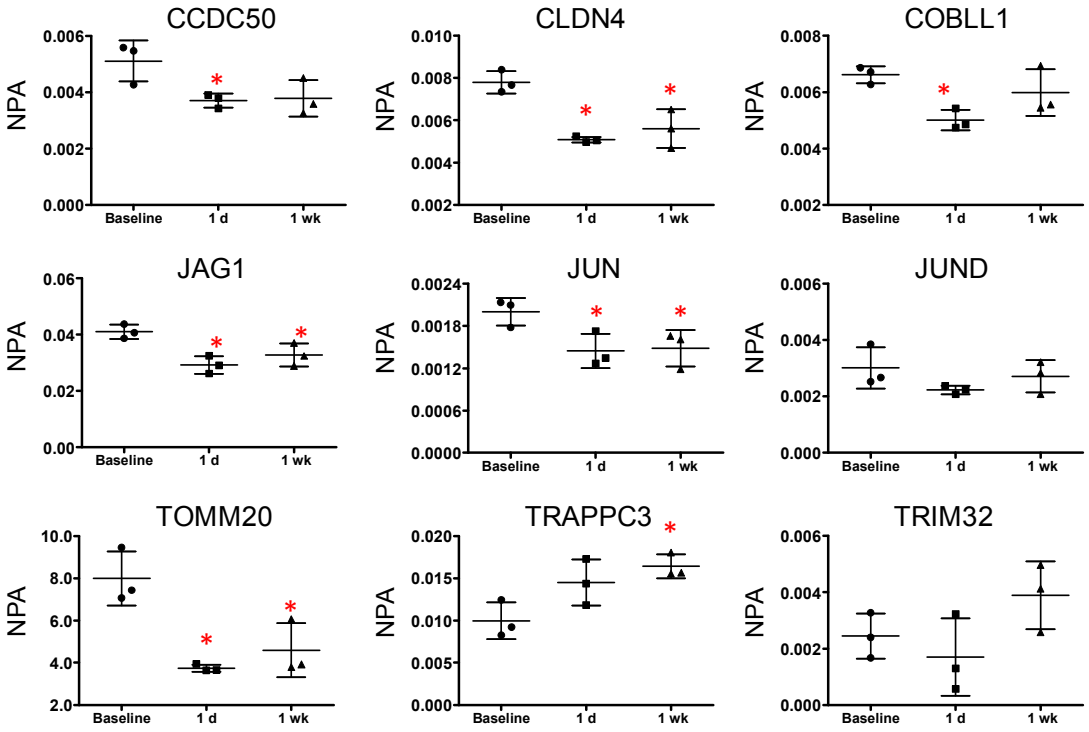

Figure III-11. MRM analyses of EGFR inhibition signature proteins in tissue biopsies from a Ménétrier's disease patient treated with cetuximab. Gastric tissue biopsies were collected from three separate locations prior to treatment (baseline control) and at 1 day and 1 week after treatment with cetuximab. Normalized peak area (NPA), which is the total MRM transition peak area for the target peptide divided by the peak area for the β-actin labeled reference peptide. Data points are representative of three separate biopsies taken from a single patient with mean and standard deviation shown. (*) Denotes significant difference between baseline and time post initial treatment as determined by Student's two-tailed t-test.

treatment in A431 cells, DiFi cells and the DiFi xenograft model. Expression of JAG1, JUN and CLDN4 expression was also measured by immunoblotting (Figure III-12). Consistent with MRM data, JAG1 and CLDN4 were significantly decreased from the baseline sample at one day and one week post-treatment. JUN expression measured by immunoblotting did not change with cetuximab treatment.

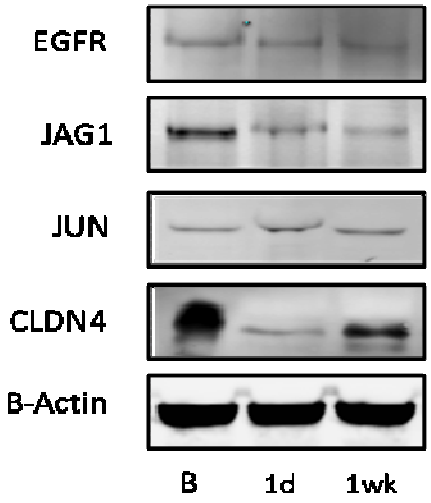

Figure III-12. Western blot analysis of tissue biopsies from a patient with Menetrier's disease. Tissue lysates from a mixture from three individual gastric biopsies taken before treatment (B) and after 1 day and 1 week of treatment with cetuximab. Equal amounts of protein were loaded and analyzed by immunoblotting for total EGFR, JAG1, JUN and CLDN4 proteins. β-Actin was used as a loading control.

By the criteria described above, these results do not confirm the EGFR inhibition signature. Three of the signature proteins (CCD50, COBBL1, TOMM20) showed changes opposite those in the A431 model. Nevertheless, the three proteins (CLDN4, JUN and JAG1) showing changes concordant with the A431 model, were most consistently responsive to EGFR inhibition in all experiments.

Discussion

Direct analysis of phosphorylated receptor proteins and their downstream effectors is the most commonly employed method to assess signaling networks. This approach is complicated by the transient nature of protein post-translational

modifications, their low abundance relative to unmodified proteins and potential artifacts due to uncontrolled pre-analytical variables. I asked whether analysis of changes in protein expression could indicate changes in the status of a signaling network. The rationale for this concept is two-fold. First, protein expression is easier to measure and is less labile than phosphorylation or other post-translational modifications. Second, signaling pathways ultimately drive gene and protein expression changes, which are most directly linked to phenotypes. A protein expression-based analysis could be routinely applied to clinical specimens, including archival FFPE tissues, where direct measurements of phosphorylated intermediates may be neither practical nor valid. Here the hypothesis that manipulation of the EGFR signaling axis with clinically-used drugs generates characteristic protein expression changes was tested. These results confirm the hypothesis and demonstrate a prototypical approach to derive and test protein expression signatures for drug action on signaling networks.

Based on an extensive literature background (26-30) and results described in Chapter II, the A431 cell model was selected as reproducible system to study EGFR-driven signaling events. Four treatment conditions were selected for comparisons: normal proliferating cells, cells stimulated with EGF and cells pre-incubated with either gefitinib or cetuximab and then treated with EGF in the presence of the inhibitors. The initial immunoblot analyses (Figure III-2) confirmed EGFR activation and inhibition. All treated A431 cells were serum-starved overnight to synchronize the cells and to limit potential interference by alternate EGFR ligands, which could complicate results. Serum starving the cells

nevertheless introduced an inherent experimental difference between the proliferating (non-treated) cells harvested in the presence of 10% fetal bovine serum and the EGF treated A431 cells incubated in serum-free media. Shotgun and MRM analyses (Figure B5, Table B7, Appendix B) verified elevation of two proteins (HMGCR and HMCS1) and a decrease of one protein (A2MG) reported to be induced by serum starvation. These proteins were expressed at similar levels in all EGF-treated A431 cells (even in the presence of the inhibitors) compared to proliferating cells. This example illustrates the potential for experimental artifacts and underscores the importance of understanding the underlying biology of the discovery model.

Shotgun proteomic analyses of treated and non-treated A431 cells yielded highly reproducible proteomic inventories—CVs for numbers of protein identifications were less than 5% across three separate cultures for each treatment condition (Table I). The combined inventories comprised nearly 4,300 proteins identified at a protein-level FDR of 4.7%. Quasi-likelihood analyses generated three pairwise comparisons (EGF versus proliferating, EGF versus gefitinib, and EGF versus cetuximab) based on shotgun spectral count data. These datasets were then filtered on the basis of spectral counts (≥ 11), fold-change (≥ 2), and p-value (≤ 0.20) to generate the three protein groups representing EGF-simulated proteins, cetuximab-sensitive proteins and gefitinib-sensitive proteins (Figure III-3). A Venn diagram comparison of these generated the EGFR inhibition signature proteins.

Three important points should be emphasized about the comparison process. First, the application of a minimum spectral count threshold (here ≥11 across all analysis runs in each dataset comparison) is required to control protein-level FDR. Without the threshold, protein FDR exceeded 30%, whereas with the threshold, protein FDR was approximately 3%. Second, an important consideration in dataset comparisons is the stringency of the cut-off criteria applied. A relatively loose p-value threshold (≤0.2) was employed to maximize detection of differences in protein group comparisons. The rationale is that subsequent MRM analyses would identify false positive differences and confirm true positives that might not have been detected in the spectral count comparisons at higher stringency. A 2-fold expression cut-off was employed for the same comparisons. I experimented with different p-value and fold-change thresholds (Figure B3, Appendix B) and ultimately settled on criteria that yielded an EGFR inhibition signature compatible in number of proteins with the capacity to perform subsequent MRM studies. Third, the interplay between p-value and fold-change threshold variation also affected the number and distribution of proteins in the overlap categories in Venn diagram analysis. For example, at thresholds of p ≤0.2 and a 2-fold difference, the central overlap (EGFR inhibition signature) in the Venn diagram contained 13 proteins, but at p ≤0.1, the central overlap contained only 4 proteins (JUN, JUND, CDKN1A, and RBM15) (Figure B3, bottom row middle Venn diagram).

Despite the relatively loose criteria used to derive the EGFR expression signature, 11 of the 13 proteins were verified by MRM with expression changes

similar to those observed from shotgun data (Figure 4). One protein (GFPT2) proved difficult to monitor selectively by MRM and was not further studied and another (PRIM1) did not show significant reversal of EGF-induced change by cetuximab. Although these MRM analyses targeted a single peptide for each of the proteins, a parallel set of analyses targeting a second unique peptide for 10 of the EGFR inhibition signature proteins similarly verified the results of the spectral count comparisons.

Although the shotgun analyses represented an empirical approach to discover a candidate signature, the component proteins have interesting and biologically plausible relations to EGFR signaling. A core group of proteins (e.g. JAG1, JUN, and CLDN4) displayed the most robust responses to EGFR inhibition. JAG1 (Jagged1) is a Notch1 receptor ligand with reported links to EGFR expression (31, 32); moreover, up-regulation of JAG1 expression and Notch1 signaling has been noted in human colon adenocarcinomas and intestinal tumors (33-35) and associated with poor prognosis in breast cancer (36). An increase in JUN detection in EGF-treated samples is consistent with literature reports that indicate an increase in mRNA levels for the transcription factor upon EGF stimulation (37-39). Overexpression of JUN has also been linked with increased invasiveness and hormone resistance in breast cancer cells (40). Increased expression of the tight junction protein CLDN4 upon EGF treatment (41) is in agreement with the data. JUN and CLDN4 also are linked to EGF via the transcription factor Sp1 (42, 43). EGFR manipulation dramatically affected

CDKN1A, a TP53-regulated cyclin dependent kinase inhibitor (44), but only in A431 cells, which lack a functional TP53 protein.

Once a candidate EGFR expression signature was established, I asked whether this set of protein expression changes can consistently represent the output of the EGFR signaling network in cells and tissues that differ in responsiveness to inhibitors. The EGFR inhibition signature in the DiFi cells was nearly identical to that in the A431 model (Figure -10), which is consistent with the high EGFR expression and responsiveness to inhibitors for both lines. In contrast, the HCT116 cells displayed only one consistent change (increase in CCDC50 by both inhibitors) observed in the A431 cells (Figure III-10). This result is consistent with the impact of the KRAS mutant status of these cells, which blocks response to EGFR inhibition (22).

Analyses of DiFi and HCT116 derived mouse xenograft models extended confirmation of the EGFR inhibition signature to tissue specimens. Although fewer targeted EGFR inhibition signature proteins were detected overall (eight of 12 for each xenograft type), there was again a clear difference in response of the signature proteins. Five of eight detected signature proteins displayed the expected expression changes in DiFi xenografts, whereas only two did in HCT116 xenografts (Figure III-10). An important aspect of the xenograft studies is that they demonstrate the potential to analyze protein expression signatures in FFPE specimens. Although it has been previously demonstrated that shotgun proteome inventories of frozen and FFPE tissues are equivalent (2), yield of proteins may be decreased. Indeed, comparison of the cell line and xenograft data also suggests

a “loss of signal”, in that fewer of the signature proteins were quantifiable in the xenografts.

The EGFR inhibition signature was evaluated in Ménétrier’s disease because of the dramatic response of this syndrome to cetuximab therapy (3). The results indicate that the three most consistent elements of the signature (JUN, JAG1 and CLDN4) respond to cetuximab treatment in Ménétrier’s disease. However, CCDC50, COBBL1 and TOMM20 expression changes were opposite to those in the A431 model. This discrepancy could reflect that fact that Ménétrier’s disease is a hyperproliferative disorder, but not a cancer, and thus may differ in other ways from the biology of the A431 discovery model and the DiFi and HCT116 models, which are all cancer cell lines. This point underscores the importance of matching the discovery model as closely as possible to the clinical application of an expression signature.

While the described model of EGFR activation developed in A431 cells might not be representative of all models, the confirmation of several protein changes in various EGFR sensitive models supports the assertion that protein expression changes can represent the effect of drugs on a signaling network. One possible problem with comparing cell models and tissue samples is that endogenous levels of EGF and exposure cannot be controlled in tissues. Moreover, other factors *in vivo* inherent to tissue samples may influence the expression of candidate signature proteins. These reasons could contribute to a lack of complete agreement between cell and *in vivo* models. However, some of most dramatic changes observed (JUN, JAG1 and CLDN4) show consistent

expression patterns in all EGFR inhibitor sensitive systems studied. This suggests the most dramatic changes maybe the most robust across the system. Despite this possible complication, the results support the hypothesis that significant EGFR-driven changes in cell models can be detected in tissue systems.

The main objective in this work was to determine whether protein expression signatures can represent the effects of drugs on a signaling network, rather than to develop and refine a clinically useful EGFR inhibition signature. This latter objective would entail a more elaborate process that includes 1) multiple discovery systems to generate a more broadly-based candidate signature, 2) integration of quantitative measurements with a valid statistical model to establish score thresholds and account for variability and 3) systematic validation in a carefully selected, valid patient cohort. Nevertheless, some of the proteins identified in this study would appear likely to contribute to a clinically useful EGFR inhibition protein profile. These results establish proof of concept for this approach by demonstrating that protein expression signatures detect activation and inhibition of dynamic signaling networks. Clinically useful response signatures developed through this approach could have broad impact in the field of cancer therapeutics.

Acknowledgements

I thank Dr. H. Charles Manning for the xenograft tumor specimens and Dr. Robert J. Coffey for Ménétrier's serial biopsies.

References

1. Slebos, R. J. C., Brock, J. W. C., Winters, N. F., Stuart, S. R., Martinez, M. A., Li, M., Chambers, M. C., Zimmerman, L. J., Ham, A. J., Tabb, D. L., and Liebler, D. C. (2008) Evaluation of Strong Cation Exchange versus Isoelectric Focusing of Peptides for Multidimensional Liquid Chromatography-Tandem Mass Spectrometry. *J. Proteome Res.* **7**, 5286-5294.

2. Sprung, R. W., Brock, J. W. C., Tanksley, J. P., Li, M., Washington, M. K., Slebos, R. J. C., and Liebler, D. C. (2009) Equivalence of Protein Inventories Obtained from Formalin-fixed Paraffin-embedded and Frozen Tissue in Multidimensional Liquid Chromatography-Tandem Mass Spectrometry Shotgun Proteomic Analysis. *Mol. Cell. Proteomics* **8**, 1988-1998.

3. Fiske, W. H., Tanksley, J., Nam, K. T., Goldenring, J. R., Slebos, R. J. C., Liebler, D. C., Abtahi, A. M., La Fleur, B., Ayers, G. D., Lind, C. D., Washington, M. K., and Coffey, R. J. (2009) Efficacy of Cetuximab in the Treatment of Ménétrier's Disease. *Science Translational Medicine* **1**, 8ra18.

4. Manning, H. C., Merchant, N. B., Foutch, A. C., Virostko, J. M., Wyatt, S. K., Shah, C., McKinley, E. T., Xie, J., Mutic, N. J., Washington, M. K., LaFleur, B., Tantawy, M. N., Peterson, T. E., Ansari, M. S., Baldwin, R. M., Rothenberg, M. L., Bornhop, D. J., Gore, J. C., and Coffey, R. J. (2008) Molecular Imaging of Therapeutic Response to Epidermal Growth Factor Receptor Blockade in Colorectal Cancer. *Clin. Cancer Res.* **14**, 7413-7422.

5. Tabb, D. L., Fernando, C. G., and Chambers, M. C. (2007) MyriMatch: Highly Accurate Tandem Mass Spectral Peptide Identification by Multivariate Hypergeometric Analysis. *J. Proteome Res.* **6**, 654-661.

6. Zhang, B., Chambers, M. C., and Tabb, D. L. (2007) Proteomic Parsimony through Bipartite Graph Analysis Improves Accuracy and Transparency. *J. Proteome Res.* **6**, 3549-3557.

7. Qian, W.-J., Liu, T., Monroe, M. E., Strittmatter, E. F., Jacobs, J. M., Kangas, L. J., Petritis, K., Camp, D. G., and Smith, R. D. (2004) Probability-Based Evaluation of Peptide and Protein Identifications from Tandem Mass Spectrometry and SEQUEST Analysis: The Human Proteome. *J. Proteome Res.* **4**, 53-62.

8. Elias, J. E., and Gygi, S. P. (2007) Target-decoy search strategy for increased confidence in large-scale protein identifications by mass spectrometry. *Nat Meth* **4**, 207-214.

9. Li, M., Gray, W., Zhang, H., Chung, C. H., Billheimer, D., Yarbrough, W. G., Liebler, D. C., Shyr, Y., and Slebos, R. J. C. (2010) Comparative Shotgun Proteomics Using Spectral Count Data and Quasi-Likelihood Modeling. *J. Proteome Res.* **9**, 4295-4305.

10. Masui, H., Castro, L., and Mendelsohn, J. (1993) Consumption of EGF by A431 cells: evidence for receptor recycling. *J. Cell Biol.* **120**, 85-93.

11. Liao, H.-J., and Carpenter, G. (2007) Role of the Sec61 Translocon in EGF Receptor Trafficking to the Nucleus and Gene Expression. *Mol. Biol. Cell* **18**, 1064-1072.

12. Liao, H.-J., and Carpenter, G. (2009) Cetuximab/C225-Induced Intracellular Trafficking of Epidermal Growth Factor Receptor. *Cancer Res.* **69**, 6179-6183.

13. Nishimura, Y., Bereczky, B., and Ono, M. (2007) The EGFR inhibitor gefitinib suppresses ligand-stimulated endocytosis of EGFR via the early/late endocytic pathway in non-small cell lung cancer cell lines. *Histochem. Cell Biol.* **127**, 541-553.

14. Chinkers, M., McKanna, J. A., and Cohen, S. (1979) Rapid induction of morphological changes in human carcinoma cells A-431 by epidermal growth factors. *J. Cell Biol.* **83**, 260-265.

15. Chinkers, M., McKanna, J. A., and Cohen, S. (1981) Rapid rounding of human epidermoid carcinoma cells A-431 induced by epidermal growth factor. *J. Cell Biol.* **88**, 422-429.

16. Lu, P. H., Kuo, T. C., Chang, K. C., Chang, C. H., and Chu, C. Y. (2011) Gefitinib-induced epidermal growth factor receptor-independent keratinocyte apoptosis is mediated by the JNK activation pathway. *Br. J. Dermatol.* **164**, 38-46.

17. Mitsos, A., Melas, I. N., Siminelakis, P., Chairakaki, A. D., Saez-Rodriguez, J., and Alexopoulos, L. G. (2009) Identifying Drug Effects via Pathway Alterations using an Integer Linear Programming Optimization Formulation on Phosphoproteomic Data. *PLoS Comput Biol* **5**, e1000591.

18. Zhang, H., Liu, Q., Zimmerman, L. J., Ham, A.-J. L., Slebos, R. J. C., Rahman, J., Kikuchi, T., Massion, P. P., Carbone, D. P., Billheimer, D., and Liebler, D. C. (2011) Methods for Peptide and Protein Quantitation by Liquid Chromatography-Multiple Reaction Monitoring Mass Spectrometry. *Mol. Cell. Proteomics* **10**.

19. Gross, M. E., Zorbas, M. A., Danels, Y. J., Garcia, R., Gallick, G. E., Olive, M., Brattain, M. G., Boman, B. M., and Yeoman, L. C. (1991) Cellular Growth Response to Epidermal Growth Factor in Colon Carcinoma Cells with an Amplified Epidermal Growth Factor Receptor Derived from a Familial Adenomatous Polyposis Patient. *Cancer Res.* **51**, 1452-1459.

20. Olive, M., Untawale, S., Coffey, R. J., Siciliano, M. J., Wildrick, D. M., Fritsche, H., Pathak, S., Cherry, L. M., Blick, M., Lointier, P., and et al. (1993) Characterization of the DiFi rectal carcinoma cell line derived from a familial adenomatous polyposis patient. *In Vitro Cell. Dev. Biol.* **29A**, 239-248.

21. Awwad, R. A., Sergina, N., Yang, H., Ziober, B., Willson, J. K. V., Zborowska, E., Humphrey, L. E., Fan, R., Ko, T. C., Brattain, M. G., and Howell, G. M. (2003) The Role of Transforming Growth Factor-α in Determining Growth Factor Independence. *Cancer Res.* **63**, 4731-4738.

22. van Houdt, W. J., Hoogwater, F. J., de Bruijn, M. T., Emmink, B. L., Nijkamp, M. W., Raats, D. A., van der Groep, P., van Diest, P., Borel Rinkes, I. H., and Kranenburg, O. (2010) Oncogenic KRAS desensitizes colorectal tumor cells to epidermal growth factor receptor inhibition and activation. *Neoplasia (New York, N.Y* **12**, 443-452.

23. Palmer, W. E., Bloch, S. M., and Chew, F. S. (1992) Menetrier disease. *Am. J. Roentgenol.* **158**, 62.

24. Rich, A., Toro, T. Z., Tanksley, J., Fiske, W. H., Lind, C. D., Ayers, G. D., Piessevaux, H., Washington, M. K., and Coffey, R. J. (2011) Distinguishing Menetrier's disease from its mimics. *Gut* **59**, 1617-1624.

25. Burdick, J. S., Chung, E., Tanner, G., Sun, M., Paciga, J. E., Cheng, J. Q., Washington, K., Goldenring, J. R., and Coffey, R. J. (2000) Treatment of Menetrier's disease with a monoclonal antibody against the epidermal growth factor receptor. *N. Engl. J. Med.* **343**, 1697-1701.

26. Wahl, M., and Carpenter, G. (1988) Regulation of epidermal growth factor-stimulated formation of inositol phosphates in A-431 cells by calcium and protein kinase C. *J. Biol. Chem.* **263**, 7581-7590.

27. Xu, Y., Guo, D.-F., Davidson, M., Inagami, T., and Carpenter, G. (1997) Interaction of the Adaptor Protein Shc and the Adhesion Molecule Cadherin. *J. Biol. Chem.* **272**, 13463-13466.

28. Bianco, R., Shin, I., Ritter, C. A., Yakes, F. M., Basso, A., Rosen, N., Tsurutani, J., Dennis, P. A., Mills, G. B., and Arteaga, C. L. (2003) Loss of PTEN//MMAC1//TEP in EGF receptor-expressing tumor cells counteracts the antitumor action of EGFR tyrosine kinase inhibitors. *Oncogene* **22**, 2812-2822.

29. Mariner, D. J., Davis, M. A., and Reynolds, A. B. (2004) EGFR signaling to p120-catenin through phosphorylation at Y228. *J. Cell Sci.* **117**, 1339-1350.

30. Kim, S.-H., Song, Y.-C., Kim, S.-H., Jo, H., and Song, Y.-S. (2009) Effect of Epidermal Growth Factor Receptor Inhibitor Alone and in Combination with Cisplatin on Growth of Vulvar Cancer Cells. *Ann. N. Y. Acad. Sci.* **1171**, 642-648.

31. Choi, K., Ahn, Y.-H., Gibbons, D. L., Tran, H. T., Creighton, C. J., Girard, L., Minna, J. D., Qin, F. X.-F., and Kurie, J. M. (2009) Distinct Biological Roles for the Notch Ligands Jagged-1 and Jagged-2. *J. Biol. Chem.* **284**, 17766-17774.

32. Purow, B. W., Sundaresan, T. K., Burdick, M. J., Kefas, B. A., Comeau, L. D., Hawkinson, M. P., Su, Q., Kotliarov, Y., Lee, J., Zhang, W., and Fine, H. A. (2008) Notch-1 regulates transcription of the epidermal growth factor receptor through p53. *Carcinogenesis* **29**, 918-925.

33. Gao, J., Liu, J., Fan, D., Xu, H., Xiong, Y., Wang, Y., Xu, W., Wang, Y., Cheng, Y., and Zheng, G. (2010) Up-regulated expression of Notch1 and Jagged1 in human colon adenocarcinoma. *Pathol. Biol. (Paris).* **In Press, Corrected Proof**.

34. Reedijk, M., Odorcic, S., Zhang, H., Chetty, R., Tennert, C., Dickson, B. C., Lockwood, G., Gallinger, S., and Egan, S. E. (2008) Activation of Notch signaling in human colon adenocarcinoma. *Int. J. Oncol.* **33**, 1223-1229.

35. Guilmeau, S., Flandez, M., Mariadason, J. M., and Augenlicht, L. H. (2010) Heterogeneity of Jagged1 expression in human and mouse intestinal tumors: implications for targeting Notch signaling. *Oncogene* **29**, 992-1002.

36. Reedijk, M., Odorcic, S., Chang, L., Zhang, H., Miller, N., McCready, D. R., Lockwood, G., and Egan, S. E. (2005) High-level coexpression of JAG1 and NOTCH1 is observed in human breast cancer and is associated with poor overall survival. *Cancer Res.* **65**, 8530-8537.

37. Ben-Ari, E. T., Bernstein, L. R., and Colburn, N. H. (1992) Differential c-jun expression in response to tumor promoters in JB6 cells sensitive or resistant to neoplastic transformation. *Mol. Carcinog.* **5**, 62-74.

38. Kayahara, M., Wang, X., and Tournier, C. (2005) Selective Regulation of c-jun Gene Expression by Mitogen-Activated Protein Kinases via the 12-O-Tetradecanoylphorbol-13-Acetate- Responsive Element and Myocyte Enhancer Factor 2 Binding Sites. *Mol. Cell. Biol.* **25**, 3784-3792.

39. Bartel, D. P., Sheng, M., Lau, L. F., and Greenberg, M. E. (1989) Growth factors and membrane depolarization activate distinct programs of early response gene expression: dissociation of fos and jun induction. *Genes Dev.* **3**, 304-313.

40. Smith, L. M., Wise, S. C., Hendricks, D. T., Sabichi, A. L., Bos, T., Reddy, P., Brown, P. H., and Birrer, M. J. (1999) cJun overexpression in MCF-7 breast cancer cells produces a tumorigenic, invasive and hormone resistant phenotype. *Oncogene* **18**, 6063-6070.

41. Singh, A. B., and Harris, R. C. (2004) Epidermal Growth Factor Receptor Activation Differentially Regulates Claudin Expression and Enhances Transepithelial Resistance in Madin-Darby Canine Kidney Cells. *J. Biol. Chem.* **279**, 3543-3552.

42. Chen, B.-K., and Chang, W.-C. (2000) Functional interaction between c-Jun and promoter factor Sp1 in epidermal growth factor-induced gene expression of human 12(S)-lipoxygenase. *PNAS* **97**, 10406-10411.

43. Ikari, A., Atomi, K., Takiguchi, A., Yamazaki, Y., Miwa, M., and Sugatani, J. (2009) Epidermal growth factor increases claudin-4 expression mediated by Sp1 elevation in MDCK cells. *Biochem. Biophys. Res. Commun.* **384**, 306-310.

44. El-Deiry, W. S., Tokino, T., Velculescu, V. E., Levy, D. B., Parsons, R., Trent, J. M., Lin, D., Mercer, W. E., Kinzler, K. W., and Vogelstein, B. (1993) WAF1, a potential mediator of p53 tumor suppression. *Cell* **75**, 817-825.

CHAPTER IV

SITE-SPECIFIC, QUANTITATIVE COMPARISON OF EGFR PHOSPHORYLATION CHANGES INDUCED BY EGF AND INHIBITOR S

Introduction

Whereas Chapters II and III dealt with identifying global protein expression differences in response to drug treatments, the experiments detailed in Chapter IV describe a mass spectrometry-based approach for quantitation of changes in post-translationally modified proteins. As referenced in the previous chapters, posttranslational protein modifications (PTM), such as phosphorylation, are difficult to quantify because they are highly dynamic and present at low levels. Nevertheless, quantitative analysis of PTMs has been achieved using liquid chromatography tandem mass spectrometry methods (LC-MS/MS) (1-4). Global quantification of phosphorylation or other PTMs typically employs costly isotope labeling methods such as chemical derivatization (*e.g.*, iTRAQ) or metabolic incorporation of stable isotope-labeled amino acids in cell culture (SILAC) (5-8). For targeted quantitation of site-specific phosphorylations, stable isotope dilution has demonstrated the highest precision of quantitation (7-9), but this approach requires costly labeled standards for each peptide of interest.

Additional approaches deemed “Label-free” quantitation methods have been adopted as viable alternatives to stable isotope dilution. These methods fall

broadly into two groups, spectral counting and integrating MS1 peak areas. Although the spectral counting method compares favorably to stable isotope labeling in both precision and accuracy for quantifying proteins in shotgun proteomics analyses (10, 11), the sampling of individual modified peptide spectra by “data-dependent MS/MS” is insufficient in capturing enough spectra to use this method for quantification at the peptide level. Quantification by integrated MS1 signals for specific peptide ions is performed by extraction of selected ion chromatograms from LC-MS datasets. However, the MS1 signal will not distinguish between sites if differentially modified peptides cannot be resolved chromatographically.

In many cases, analysis of PTM is performed on purified proteins or simple mixtures, such as immunoprecipitates, expressed proteins, or proteins purified by chromatography or electrophoresis. In such cases, the need to quantify a stoichiometric change in a modification frequently follows the initial identification of modified forms. Since the modified form has been identified, the MS/MS spectral characteristics of the modified peptides of interest are known. In this context, the goal is targeted quantitation of changes to specific proteins, rather than a quantitative global survey. Here, the validation of a label-free approach to measure quantitative changes in modifications to specific proteins is described. The approach uses targeted LC-MS/MS analysis with extracted selected reaction monitoring (pseudo-SRM or pSRM) using a linear ion trap mass spectrometer to enable selective detection and further quantification of modified peptides. Normalizing pSRM signals for the target peptides to signals from unmodified

reference peptides within the same protein, termed the internal reference peptide (IRP) method, corrects for run-to-run variations in signal intensities. Although other reports have described similar quantification methods previously (12-20), the studies described herein—based on proof-of-concept experiments performed by Dr. Amy-Joan Ham—allowed for validation of the IRP method by defining its performance characteristics and comparing them to stable isotope dilution; a method accepted as the "gold standard" for MRM/SRM-based quantitation. The performance of pSRM was further assessed using both MS/MS and MS^3 data for quantification. The studies described in Chapter IV represent a team project I did with Drs. Stacy D. Sherrod and Dr. Amy-Joan Ham in our laboratory. This project was the development of the IRP method and its application to analyze phosphorylated forms of epidermal growth factor receptor (EGFR) in response to anticancer drugs. My role in this team project was in establishing the EGFR activation and inhibition model described in the previous chapters and in performing analyses to map and quantify differential EGFR phosphorylation. The data demonstrate the utility of the IRP method to quantify site-specific changes in EGFR phosphorylation in response to modulation by EGF and the two tyrosine kinase inhibitors, cetuximab and gefitinib.

Experimental Procedures

Materials and reagents

Acetonitrile and HPLC grade water were from Mallinckrodt Baker (Phillipsburg, NJ) and 98% pure formic acid was from EMD (Darmstadt, Germany). Trypsin gold was purchased from Promega (Madison, WI), dithiothreitol (DTT) from Pierce (Rockford, IL), and iodacetamide was from Sigma (St. Louis, MO). The A431 cell line was obtained from ATCC (Manassas, VA), improved MEM media and PBS were purchased from Invitrogen-GIBCO (Auckland, NZ). Media supplement, fetal bovine serum, was from Atlas Biologicals (Fort Collins, CO). For Western blotting, primary antibodies for phosphotyrosine site 1173 phosphotyrosine site 998 and EGFR were purchased from Cell Signaling Technology (Danvers, MA). Primary antibodies were detected using anti-rabbit and anti-mouse secondary antibodies conjugated with Fluorophore 680 from Invitrogen (Carlsbad, CA) and imaged using the LI-COR Odyssey Imager system with 3.0 application software (Lincoln, NE). All gels (NuPAGE), western blot membranes and gel reagents (LDS, PVDF membrane, and SimplyBlue SafeStain) were purchased from Invitrogen (Carlsbad, CA). Individual components of the NETN lysis buffer, protease inhibitor cocktail and phosphatase inhibitor cocktail (see below) were purchased from Sigma (St. Louis, MO). Beads from immunoprecipitations, Protein A and Protein G were purchased from ThermoScientific (Rockford, IL) and Roche (Indianapolis, IN), respectively.

Synthetic phosphorylated peptides, DRV*pY*IHPF and IKNLQ*pS*LDPSH, were purchased as part of the Phosphopeptide Standard I from Protea Biosciences (Morgantown, WV). Bovine serum albumin (BSA) was purchased from ThermoScientific (Rockford, IL). Four C-terminal isotopically labeled phosphotyrosine peptides containing U-$^{13}C_6$, U-$^{15}N_4$-arginine or U-$^{13}C_6$, U-$^{15}N_2$-lysine from EGFR (Y998 – MHLPSPTDSNF*pY*R, Y1110 – RPAGSVQNPV*pY*HNQPLNPAPSR, Y1173 – GSHQISLDNPD*pY*QQDFFPK and Y1197 – GSTAENAE*pY*LR) were purchased from New England Peptide, LLC (Gardner, MA) at ≥95% chemical purity based on amino acid analysis. EGFR antibody and cetuximab were a gift from Dr. Robert Coffey; gefitinib was a gift from Dr. Carlos Arteaga, both from Vanderbilt-Ingram Cancer Center (Nashville, TN).

Phosphopeptide/BSA spike experiments

The following studies in this section were performed by Dr. Amy-Joan Ham as proof-of-concept experiments for development of the IRP method. Synthetic phosphopeptide mixture (DRV*pY*IHPF and IKNLQ*pS*LDPSH) was resuspended in 0.1% formic acid to a concentration of 500 pmol/mL and peptides were spiked into 100 µL of 6.0 µg/mL (6 ng of BSA) tryptic digest of BSA at concentrations ranging from 0.01-2.0 fmol/ng BSA (which corresponds to 0.064-12.8 fmol/µL) in 0.1% formic acid. The BSA tryptic digest was performed on 200 µg of 2 mg/mL BSA. The sample was diluted in ammonium bicarbonate, reduced in 45 mM DTT at 55°C for 20 min, alkylated in the dark at room temperature for 20 min using 100

mM iodoacetamide and digested with 4 µg of trypsin overnight at 37°C. An aliquot of this digest was diluted with 0.1% formic acid to a final concentration of 6.0 µg/mL.

Cell culture

A human epithelial carcinoma cell line (A431) was cultured in 150 mm culture dishes in improved MEM supplemented with 10% fetal bovine serum at 37°C in 5% CO_2. A431 cells were grown to ~60-70% confluency prior to harvesting (control or treatment). All treated cells were serum-starved (18 hrs), followed by treatment with 30 nmol epidermal growth factor (EGF) for 20 min or incubated with either 10 µg/mL cetuximab) or 500 nmol gefitinib) for 30 min followed by subsequent stimulation with EGF for 20 min. Cells were harvested on ice with Mg and Cl-free PBS supplemented with a phosphatase inhibitor cocktail (1 mM sodium fluoride, 10 mM β-glycerophosphate, 1 mM sodium molybdate, and 1 mM activated sodium orthovanadate), pelleted by centrifugation at ~250 x g, flash-frozen and stored at -80°C.

Immunoprecipitation, western blot, and sample preparation

Cell pellets were lysed by resuspension in NETN lysis buffer (50 mM Tris-HCl, pH 7.5, 150 mM NaCl, 1% Igepal, and 5% glycerol) containing protease inhibitors (0.5 mM 4-(2-Aminoethyl) benzenesulfonyl fluoride hydrochloride, 10 mM aprotinin, 1 mM leupeptin, 1.5 µM E-64, 5µM betastatin and 1 µM pepstatin A) and the phosphatase inhibitor cocktail, and incubated on ice for 25 min prior to

mechanical lysis by sonication. After cell lysis, suspensions were cleared by centrifugation at 9,400 x g for 5 min. The bicinchoninic acid assay (protein standard was bovine serum albumin) was used to measure the protein concentration of the cell lysate. A 100 µg aliquot of total cell lysate was collected as input control and combined with 4X LDS buffer and DTT for a final concentration of 1X and 50 mM, respectively. A 3 mg portion of the remaining cleared lysate was incubated at 4°C for 1.5 hours with cetuximab at a ratio of 5 µg of cetuximab for every 1 mg of cell lysate. A 30 µl portion of pre-equilibrated Protein A and Protein G resin (1:1 v:v) were added to the suspension and incubated with the lysate for 45 min at 4°C. The suspension was then centrifuged at ~200 x g for 2 min at 4°C. The supernatant was removed and the resin washed three times with NETN lysis buffer. Protein(s) were eluted by treating beads for 5 min at 85°C in 2X LDS buffer and 50 mM DTT. Samples were fractionated in NuPAGE 10% Bis-Tris SDS-PAGE gels using MOPS buffer. Gels were either prepared for western blot by transferring proteins to PVDF membrane or stained (for 1 hour) using Simply Blue Safe Stain followed by destaining in deionized water overnight.

Targeted MS analysis was performed on the digested EGFR gel regions. Briefly, the EGFR protein bands were excised and rinsed with 100 mM ammonium bicarbonate (pH 8.0). Gel pieces were reduced with 50 mM DTT at 60°C for 30 min, followed by alkylation with 100 mM iodoacetamide in the dark at ambient temperature for 20 min, and digested with 200 ng trypsin overnight at 37°C. Peptides were extracted from the gel three times with 60% acetonitrile/ 0.1%

formic acid (v/v). Peptides were evaporated *in vacuo* (SpeedVac concentrator, Thermo-Fisher, Waltham, WA) and reconstituted in 30 µL of 5% acetonitrile, 0.1% formic acid with 12.5 fmol/µL of isotopically-labeled peptides spiked in for LC-pSRM-MS analysis.

Mass spectrometry and data analyses

LC-pSRM-MS and MS^3 analyses were performed on a LTQ Velos from ThermoFisher Scientific (San Jose, CA) mass spectrometer equipped with an Eksigent Nano-1D Plus HPLC and AS-1 autosampler (Dublin, CA). Peptides were separated on a 100 µm × 11 cm fused silica capillary column (Polymicro Technologies, LLC., Phoenix, AZ) and 100 µm x 6 cm fused silica capillary pre-column packed with 5 µm, 300 Å Jupiter C_{18} (Phenomenex, Torrance, CA). Liquid chromatography was performed using a 95 min gradient at a flow rate of either 400 or 600 nL/min using a gradient mixture of 0.1% (v/v) formic acid in water (solvent A) and 0.1% (v/v) formic acid in acetonitrile (solvent B). Briefly, a 15 min wash period (100% solvent A) was performed followed by a gradient to 98% A at 15 min (1.2 µl/min) and eluent was diverted to waste prior to the analytical column using a vented column set up similar to that previously described (21). Following removal of residual salts, the flow was redirected to flow through the analytical column and solvent B increased to 75% over 35 minutes and up to 90% in 65 minutes. The column was re-equilibrated to 98% solvent A for 10 minutes after each run. All peptides were analyzed using targeted analysis of doubly and/or triply charged ions to acquire the complete MS/MS spectrum. MS^3 analysis was

performed on the neutral loss of phosphoric acid for phosphopeptides IKNLQ*pS*LDPSH (Protea peptide), MHLP*pS*PTDSNYR and GSHQI*pS*LDNPDYQQDFFPK (both EGFR phosphopeptides) in addition to MS/MS analysis. Typical targeted parameters include an isolation width of 2 bracketed around the *m/z* of interest, a fragmentation time of 10 ms, normalized collision energy of 35.0, spray voltage of 1.8 kV and capillary temperature at 200 ºC.

Data was analyzed using either Xcalibur software (ThermoFisher, San Jose, CA) to determine extracted ion current peak area for 3-5 transitions for each targeted peptide or the full scan MS/MS filtering feature in Skyline 0.7 software (22). Each phosphopeptide was normalized by dividing the individual phosphopeptide (sum of three or four ion transitions/peptide) by either the individual reference peptides (sum of three or four ion transitions/peptide) or to the sum of all the reference (unmodified internal peptides from BSA or EGFR) peptides.

Skyline implementation

Full support for pSRM using chromatograms extracted from targeted MS/MS spectra for peak area calculations was implemented in the Skyline software tool, as shown in Figures C1-2 (Appendix C), and released in version 1.1. These new features included method export for ThermoFisher LTQ instruments as well as chromatogram extraction from MS/MS spectra at targeted product ion mass-to-charge ratios, making available for pSRM many existing

Skyline features proven in SRM experiments with triple quadrupole mass spectrometers.

Statistical methods

The relationship between response and concentration were modeled by applying a weighted least square with the robust linear model using Tukey's bi-weight to down-weight potential outliers. This model (23) assumes that measurement standard deviation increases linearly with concentration. The model also accounts for non-linear behavior at low concentrations by incorporating change-points. Selection of change points is based on Akaike's information criterion (AIC), where the optimal model is the one with the minimum AIC. The fitted model provided three summary statistics: correlation coefficient (r^2), slope and coefficient of variation (CV). The details of the methods have been described previously (8, 23).

Results

Overview of analytical approach

This work describes quantitative analysis of post-translationally-modified peptides by pSRM together with either stable isotope dilution (SID) or a new IRP method. The pSRM experiments are targeted MS/MS analyses performed by producing a full MS/MS spectrum for each precursor *m/z* in a target list using a linear ion trap mass spectrometer (LTQ Velos). Transitions are extracted from the

full MS/MS or MS^3 spectrum and peak areas for transitions are summed and normalized to areas for a reference standard. For stable-isotope dilution (SID), the summed peak area is normalized to summed peak areas for transitions from a stable isotope labeled peptide standard. In the IRP method, one or more unmodified proteotypic peptides from the target protein serve as the reference standard for the modified peptides in the analysis. Because the target modified peptides and the reference standard are present in the same protein, the IRP method corrects for variations in recovery of the protein in the analysis. Normalized signals increase or decrease with a corresponding increase or decrease in the stoichiometry of the modification.

Experiments performed by Dr. Amy Ham establish a proof-of-concept for the IRP method to detect differences in modification stoichiometry. These experiments analyzed synthetic phosphopeptides spiked into a BSA digest background. The peptides, DRV*pY*IHPF (angiotensin II) and IKNLQ*pS*LDPSH (cholecystokinin 10-20), were spiked into the BSA digest at concentrations were chosen to mimic the low abundance phosphorylation events that occur in biological systems (14) represented a 0.12-14% stoichiometry relative to BSA.

Concentration response curves generated on an LTQ Velos linear ion trap using pSRM for modification specific transitions with strong transition signals. These experiments also assess the use of MS^3 measurements for quantification of protein modifications, in which fragmentations from the neutral loss of phosphoric acid from the target phosphopeptide were measured.

These analyses demonstrated that the pSRM method generated measurements that were comparable in linearity and precision to data generated by stable isotope dilution. CV values ranged from 7.3-15.7% (median 10%) and similar values for r^2, slope and CV were obtained for both MS/MS and MS^3 measurements. Although the analyses were done on a linear ion trap with automatic gain control (AGC), which limits filling of the trap at higher ion currents the IRP-normalized signals appeared linear over a 200-fold concentration range, which suggests that AGC has little impact on response under the conditions of our analyses. Dr. Ham's work thus established essential proof-of-concept for the method we applied to quantify site-specific changes in EGFR phosphorylation.

Analysis of six EGFR phosphopeptides in A431 cells

To assess the performance of the IRP method to perform relative quantification of specific phosphorylation sites, the changes in phosphorylation levels of EGFR at four phosphotyrosine sites and two phosphoserine sites were examined. Cell culture experiments using A431 cells and 20 minute treatments similar to those described in Chapter II (e.g., proliferating cells, EGF stimulated, gefitinib treated or cetuximab treated) were performed. Post-treatment, EGFR was immunoprecipitated with cetuximab in the presence of protease and phosphatase inhibitors, resolved on an SDS-PAGE gel, and the EGFR-containing band was excised and digested in-gel with trypsin (Figure IV-1A and B). Modified peptides corresponding to phosphorylation at sites Y998 (MHLPSPTDSNF*pY*R), Y1110 (RPAGSVQNPV*pY*HNQPLNPAPSR), Y1173

(GSHQISLDNPD*pY*QQDFFPK), Y1197 (GSTAENAE*pY*LR), S991 (MHLP*pS*PTDSNFYR) and S1166 (GSHQI*pS*LDNPDYQQDFFPK) within EGFR were targeted for quantification using pSRM. Phosphoserine sites (S991 and S1166) were also monitored using MS^3 of the 98 Da neutral loss ion corresponding to the loss of phosphoric acid. Stable-isotope labeled peptides corresponding to sites Y998, Y1110, Y1173 and Y1197 were spiked in prior to pSRM analysis to enable comparison of the stable-isotope dilution and IRP methods.

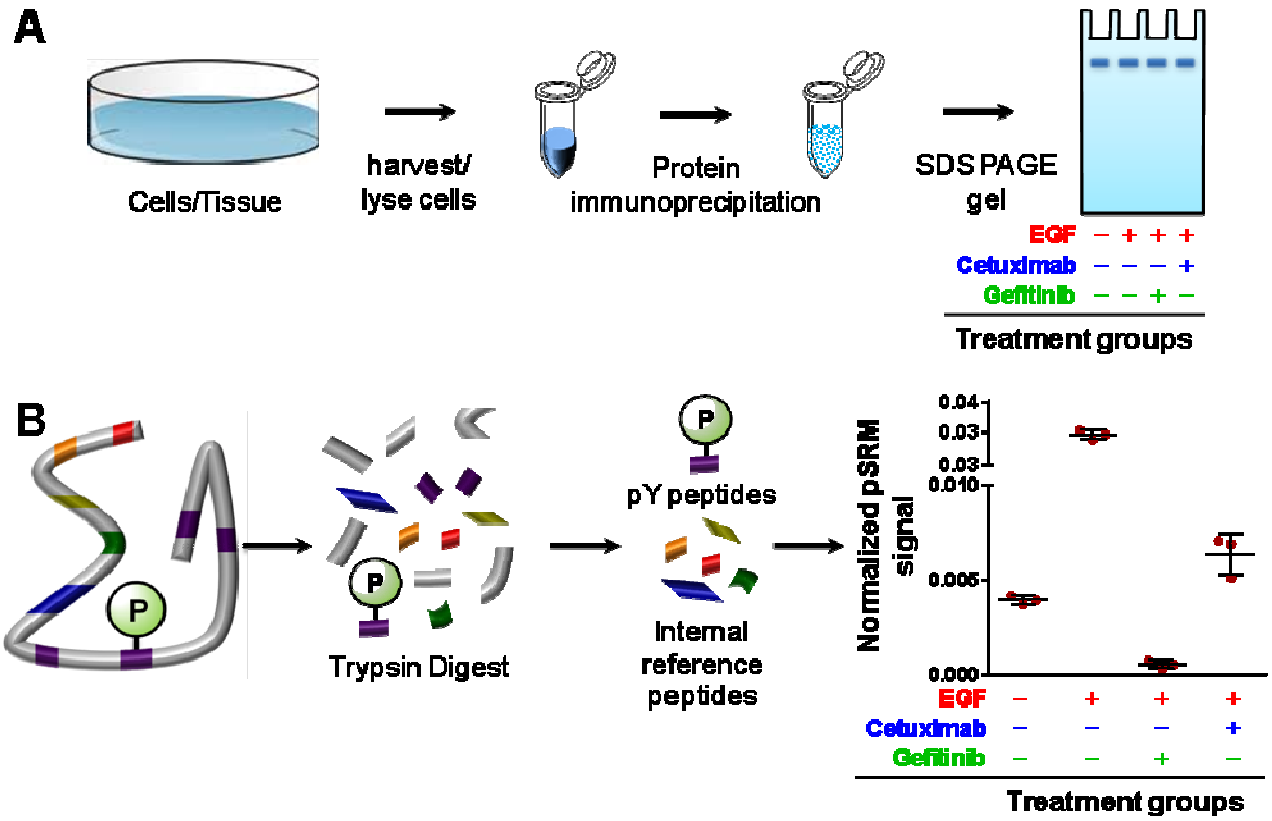

Figure IV-1 Sample work flow and IRP methodology. (A) Illustrates the immunoprecipitation (IP) method for EGFR and treatment groups utilized in these experiments. After IP, EGFR corresponding band on SDS PAGE gel was excised and targeted analysis performed on an LTQ Velos mass spectrometer. (B) Represents analytical approach for normalizing six EGFR phosphorylated peptides to internal reference peptides (IRPs). IRPs are unmodified peptides within the protein of interest, in these experiments EGFR**.**

In addition to the six phosphopeptides, five unmodified peptides from EGFR were selected as internal reference (normalization) peptides. The location and domain position in EGFR (extracellular, juxtamembrane, tyrosine kinase or cytoplasmic) of each reference and phosphorylated peptide are presented in Figure IV-2. Internal reference peptides were selected based on high signal stability, as well as a range of elution times spanning the chromatographic separation (Figure IV-3). For each targeted peptide (phosphorylated and reference), extracted ion current we selected 3-5 transitions that indicate modification specificity and/or generate strong pSRM transition signals. The peptide sequences, precursor *m/z* and specific transitions were extracted and listed in Table C1 in Appendix C. The sum of transitions (peak areas) for phosphopeptides was divided by the sum of transitions for each individual internal reference peptides from EGFR or its stable-isotope labeled counterpart. Three biological replicates were performed for each treatment group and three technical LC-pSRM-MS injections for each sample.

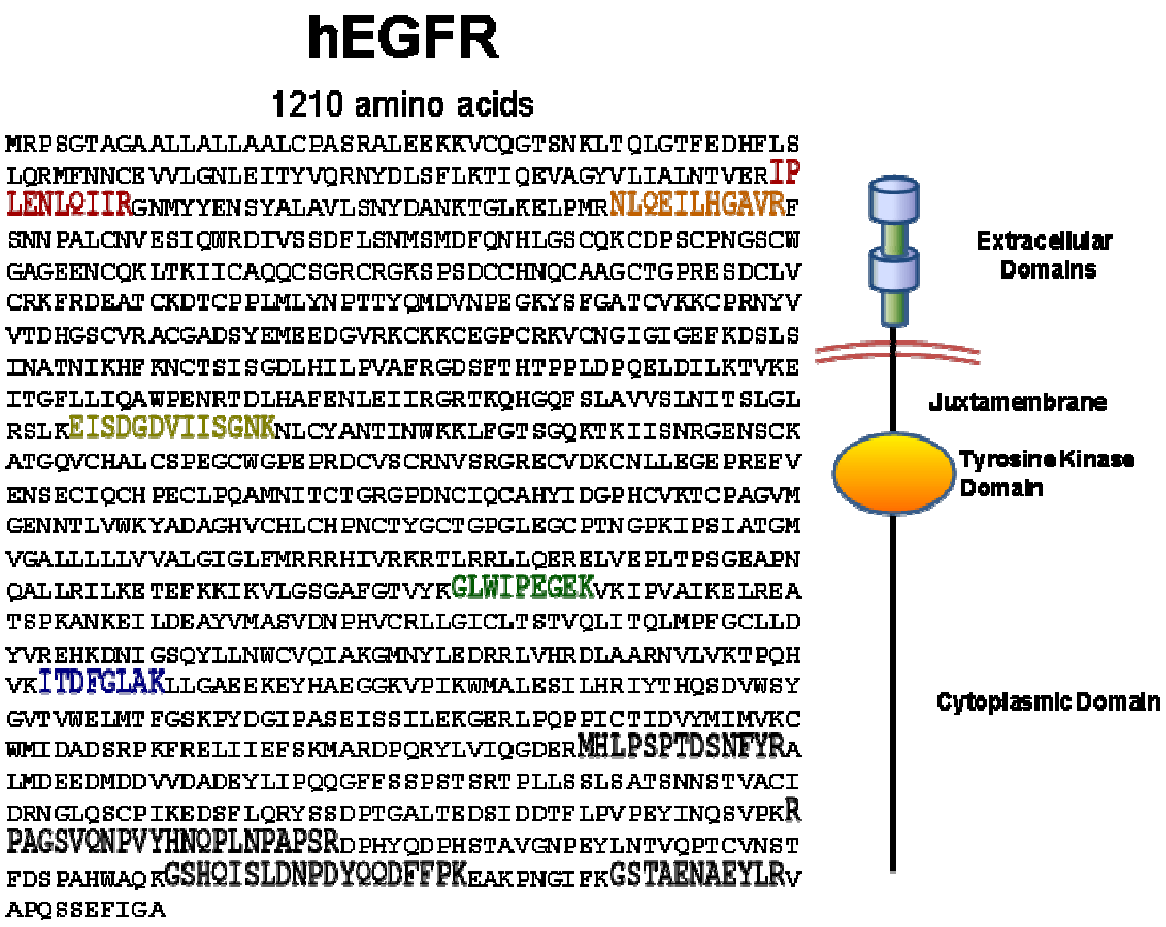

Figure IV-2. Human epidermal growth factor receptor (hEGFR) amino acid sequence. Normalizing and phosphorylated peptides are highlighted in different colors. The nonphosphorylated peptides that were chosen to be used as normalizing peptides are located in the extracellular (IPLENLQIIR, NLQEILHGAVR and EISDGDVIISGNK), juxtamembrane (GLWIPEGEK) and tyrosine kinase domains (ITDFGLAK). Two phosphopeptides that we monitored are located in the tyrosine kinase domain (MHLP*pS*PTDSNFYR and MHLPSPTDSNF*pY*R). The other four phosphopeptides (*pY* and *pS*) that were monitored are located in the cytoplasmic domain (RPAGSVQNPV*pY*HNQPLNPAPSR, GSHQI*pS*LDNPDYQQDFFPK, GSHQISLDNPD*pY*QQDFFPK and GSTAENAE*pY*LR).

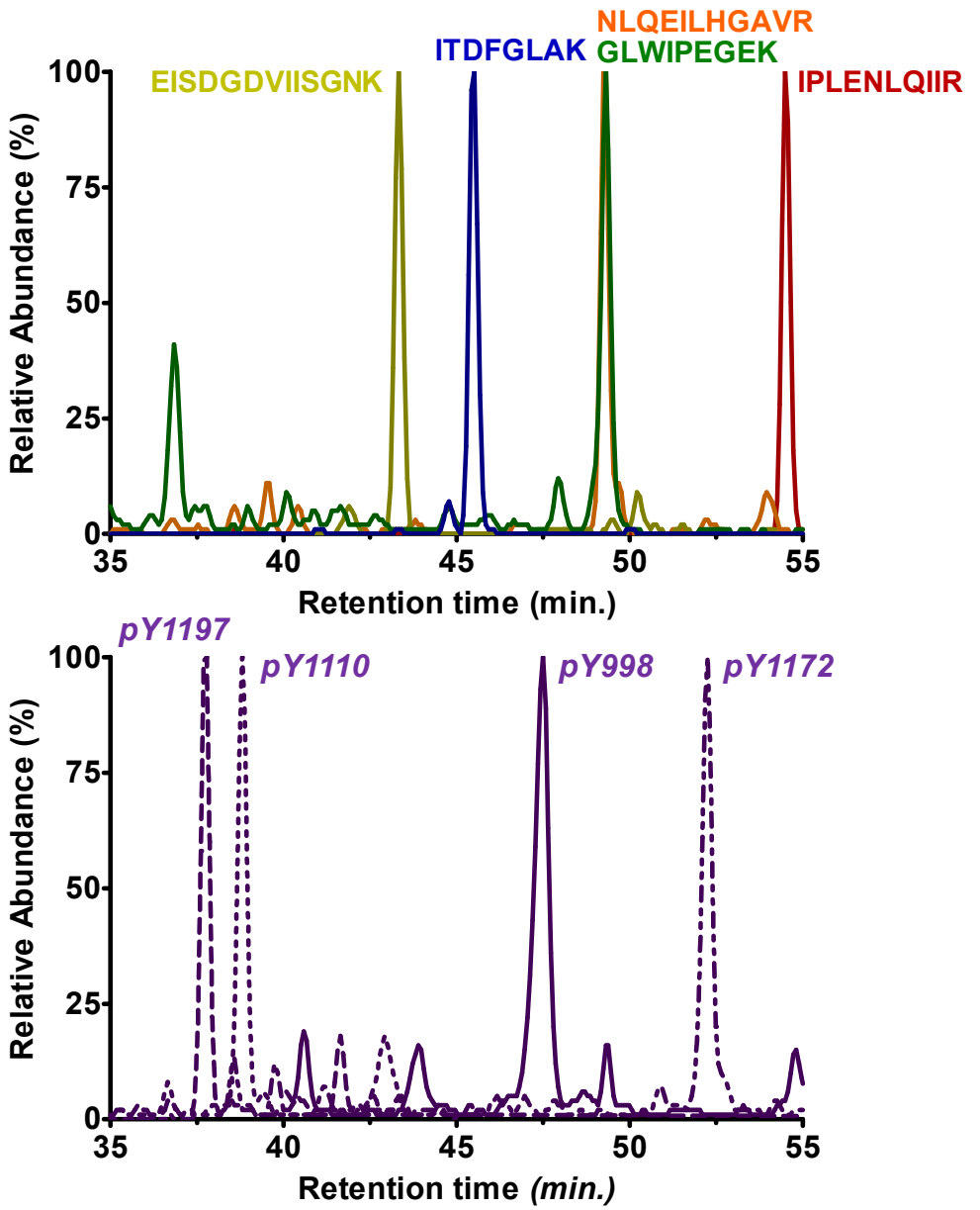

Figure IV-3. The retention time for normalizing peptides ranged across the peptide elution retention time. Retention time plots for all internal nonphosphorylated reference peptides (top) and stable-isotope labeled *pY* peptides, Y998 – MHLPSPTDSNF*p*YR, Y1110 – RPAGSVQNPV*p*YHNQPLNPAPSR, Y1172 – GSHQISLDNPD*p*YQQDFFPK, and Y1197 –GSTAENAE*p*YLR) (bottom). Retention time plots were generated from biological replicate three, technical replicate three. The underlined amino acid indicates which amino acid was stable isotope labeled.

Western blot analysis of EGFR IP

Immunoblot analysis were performed pre- and post IP for each treatment group (proliferating, EGF stimulated, co-treated cetuximab and EGF and co-treated gefitinib and EGF) for total EGFR, and specific pY sites Y998 and Y1173. The amount of receptor phosphorylation at sites Y998 and Y1173 in A431 cells analyzed (Figure IV-4) varied substantially with treatment group. EGF treated

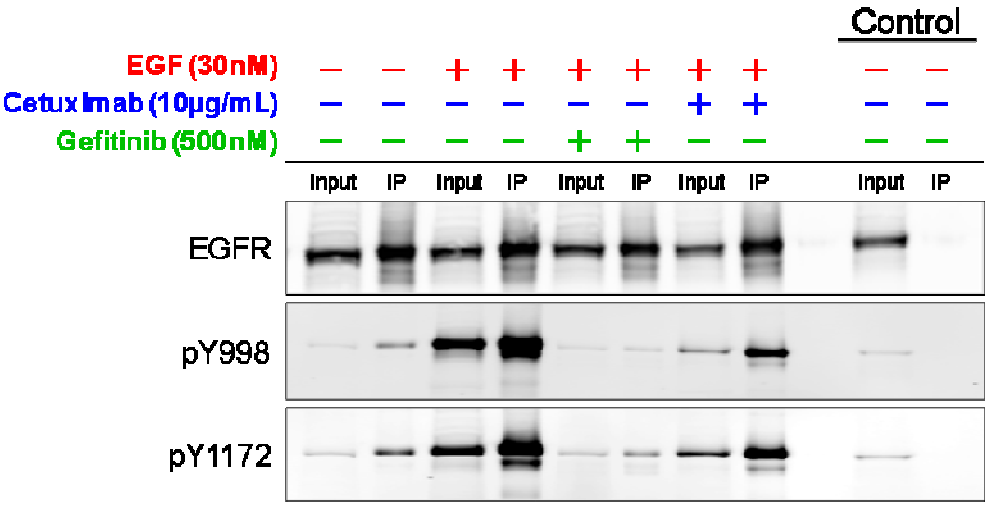

Figure IV-4. EGFR IP in A431 cells. A431 cells not treated, modulated with EGF, or co-treated with inhibitor (cetuximab or gefitinib) followed by EGF exhibit different EGFR activation statuses. Immunoblot showing EGFR activation prior to and after treatment(s) (phosphorylation at Y998 and Y1173). Both phosphorylated forms of the receptor were targeted in the pSRM-MS method. Input lane is 5% of total protein load, and IP lane is post- immunoprecipitation. Control lanes show the IP performed using mouse IgG. All treated cells were serum-starved overnight prior to any treatment.

samples had the highest detected signal for EGFR phosphorylation at both pY998 and pY1173 sites. Consistent with data reported in Chapters II and III, gefitinib at 500 nM for 20 min decreased phosphorylation at both EGFR tyrosine sites near or below basal levels (proliferation), while 10 µg/mL cetuximab

treatment for 20 min was less potent at inhibiting EGFR activation. Thus, EGFR phosphorylation detected for 10 µg/mL cetuximab treatments show signals significantly less than for EGF treatment, but more than basal levels for both pY sites.

Comparison of IRP and SID-based quantitation of site-specific phosphorylation in EGFR

After generating data for three biological replicates and three technical LC-pSRM-MS injections for each sample, median %CV plots were generated for each internal reference peptide and stable isotope labeled peptide. The median %CV plots were calculated using the three technical replicate analyses performed for each treatment, biological replicate and internal reference or stable isotope labeled peptide. Representative data for peptide RPAGSVQNPV*pY*HNQPLNPAPSR can be seen in Figure IV-5. Each panel represents summed peak area signals for one targeted peptide normalized to five individual, internal reference peptides and one SID counterpart. See Appendix C Figures C1-5 (A, B and C) for additional CV plots of technical replicate analysis from each of three separate cultures. Median CV values varied considerably for IRP measurements with different normalization peptides. Normalization to the EGFR peptide IPLENLQIIR yielded the lowest global CV (median 22%), whereas the other normalization peptides NLQEILHGAVR (median 27%), EISDGDVIISGNK (median 27%), GLWIPEGEK (median 26%) and ITDFGLAK (median 32%) displayed modestly greater variation. CV values differed between distinct biological replicate experiments. In these studies, biological replicate

experiments one and two displayed lower variability, with median CVs from different IRP peptides averaging approximately 30%, whereas biological replicate experiment three yielded more variation (≥ 50%). This higher variation was the result of individual technical replicate runs, some of which produced low signal across the chromatogram.

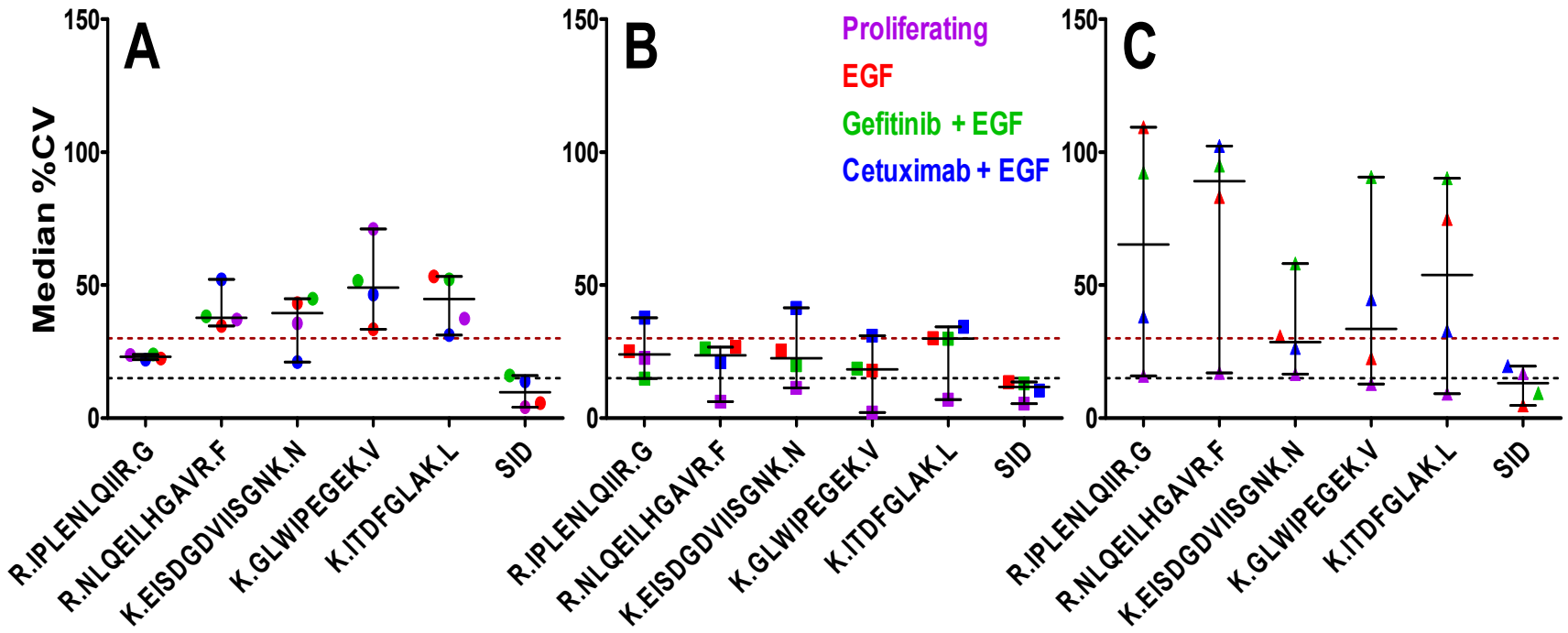

Figure IV-5. **Median CV plots for peptide RPAGSVQNPV*p*YHNQPLNPAPSR.** The CV's were calculated by the technical replicate analysis on a per treatment basis for each internal reference or stable isotope labeled peptide. (A-C) All data (three technical replicates for each treatment) was used to calculate median CV's for biological replicate one (A), two (B) and three (C). The black dashed line represents 15% CV, and the red dashed line represents 30% CV.

Because these pSRM analyses were employed ion trap analyzers, ion injection times could be compared for low-signal versus high-signal runs. Figure IV-6 shows ion injection time plots for all five IRPs and one SID peptide for all technical replicates of biological replicate three only. These time plots should be relatively stable because they represent three technical replicates of the same sample; however, technical replicate one shows a substantial difference (typically at least one order of magnitude longer) compared to technical replicates two and three. Longer ion injection times reflect reduced ion input, typically because of lower sample amounts; Figure IV-6 shows similar differences were obtained for the extracted ion current (XIC) (time vs. relative abundance (%) of the same peptides, *i.e.*, relative abundance (%) was typically ≤10% of technical replicates two and three (Figure IV-6); these XICs should be relatively stable between technical replicates. In comparing Figures IV-6 and 7 to Figures IV-8 and 9, which display ion injection times and XIC plots were stable and similar for samples that did not generate high median CVs. The ion injection time and XIC plots are both performance metrics described in (24), indicate that technical replicate one of biological replicate three was a poor MS analysis. This failed MS analysis is responsible for the overall high median CVs in biological replicate 3. In all of the experiments, the SID method yielded significantly greater measurement precision, with a global median CV of 15%.

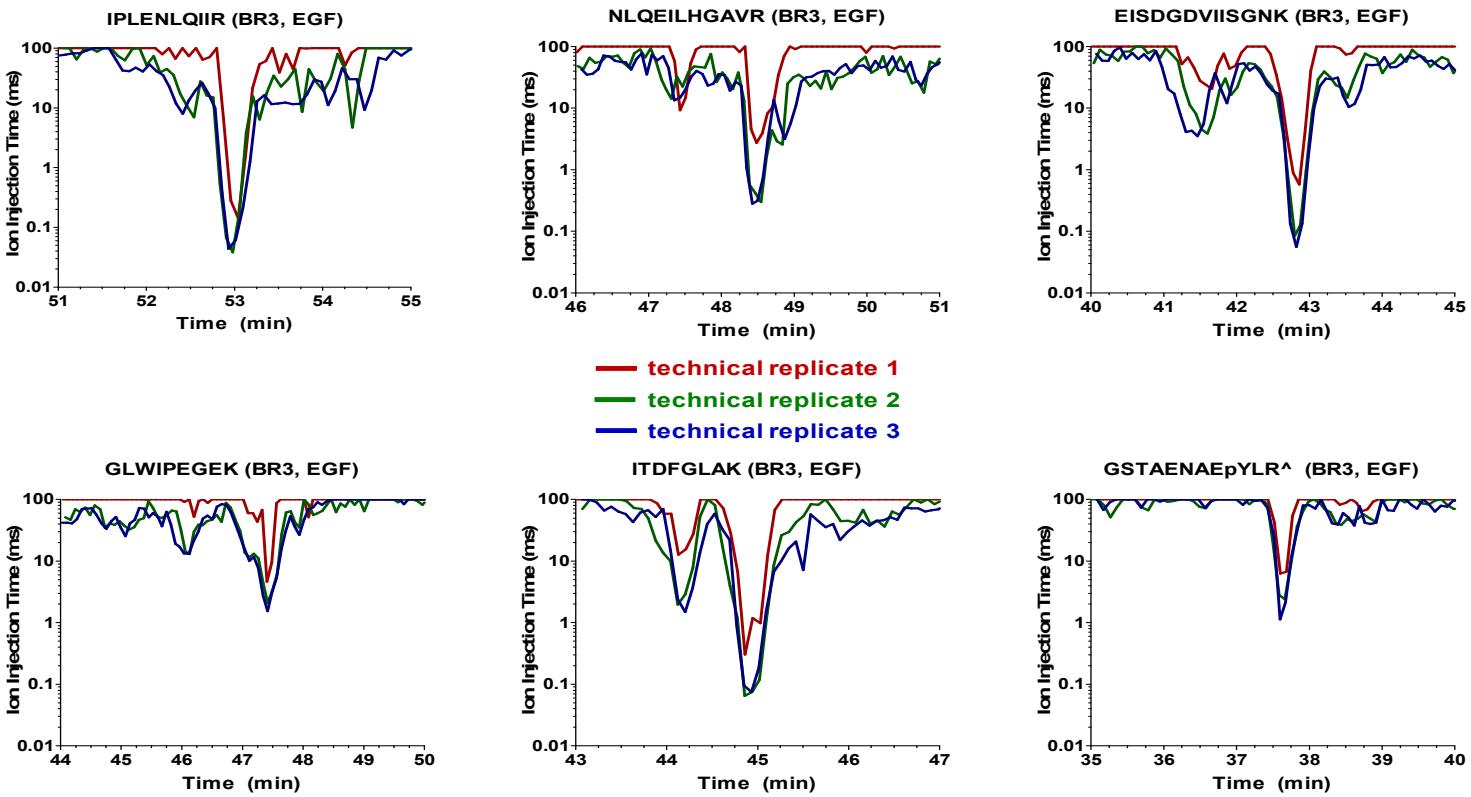

Figure IV-6. **Time vs. ion injection time for EGF treated samples (biological replicate 3).** Data is shown for five internal reference peptides and a stable isotope labeled peptide (GSTAENAE*p*YLR). The maximum allowable ion injection time in these experiments is 100 ms. These data show the ion injection time for technical replicate one (red) was drastically different than both technical replicates two and three, *i.e.*, technical replicate one always required a longer ion injection time for the same sample, suggesting the instrument was behaving differently during the EGF-treated technical replicate one run. These data indicate the reason why large CV values for EGF treated biological replicate three was observed.

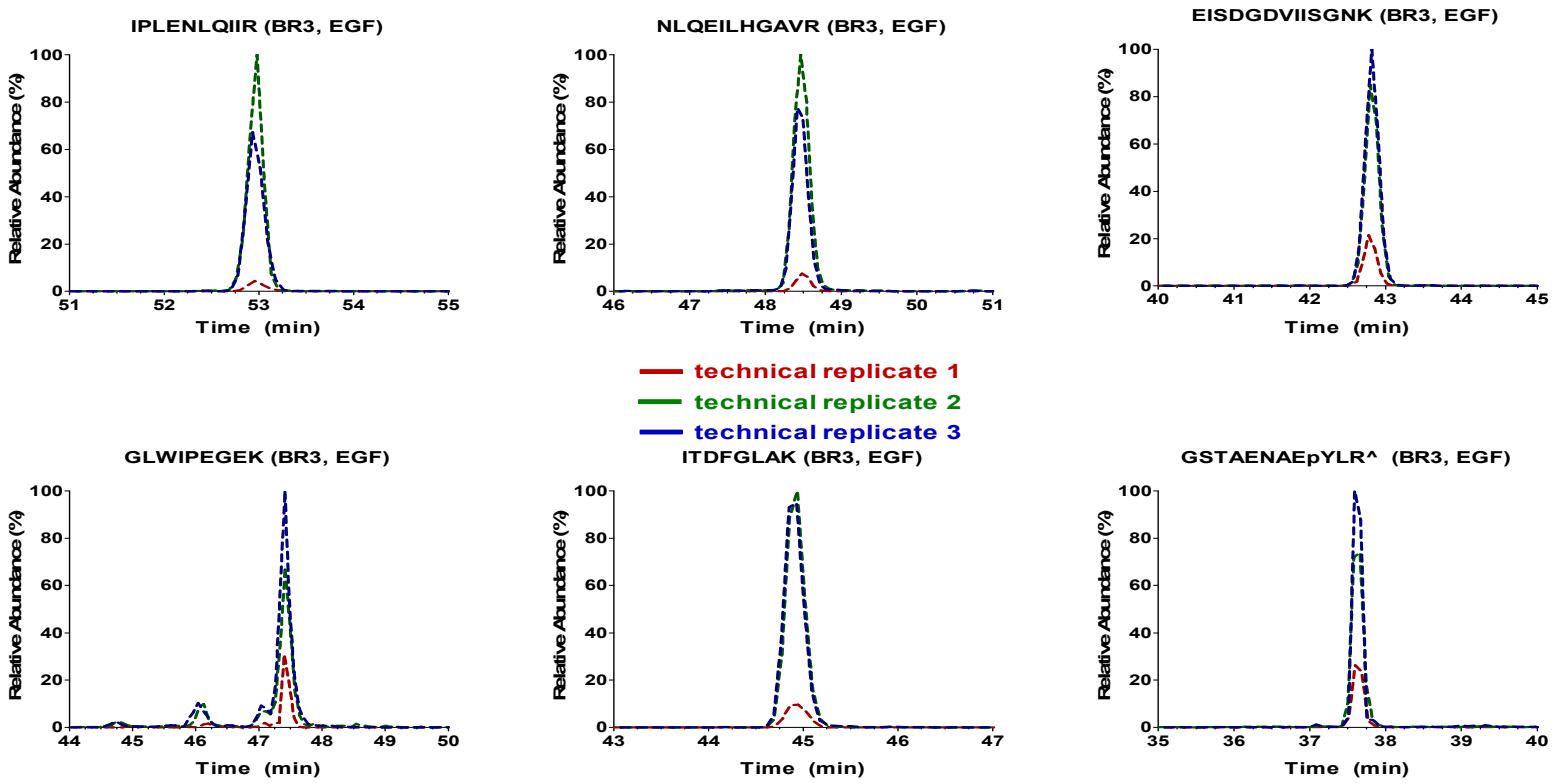

Figure IV-7. Extracted ion chromatograms (time vs. relative abundance (%)) for EGF treated samples (biological replicate 3). Data is shown for five internal reference peptides and a stable isotope labeled peptide (GSTAENAE*p*YLR). These data show that the relative abundance (%) for technical replicate one is drastically different than both technical replicates two and three, *i.e.*, technical replicate 1 has a low intensity for the same sample, suggesting the instrument was behaving significantly different during the EGF treated biological replicate three (technical replicate one run). These data indicate the reason why large CV values for EGF-treated biological replicate three were observed.

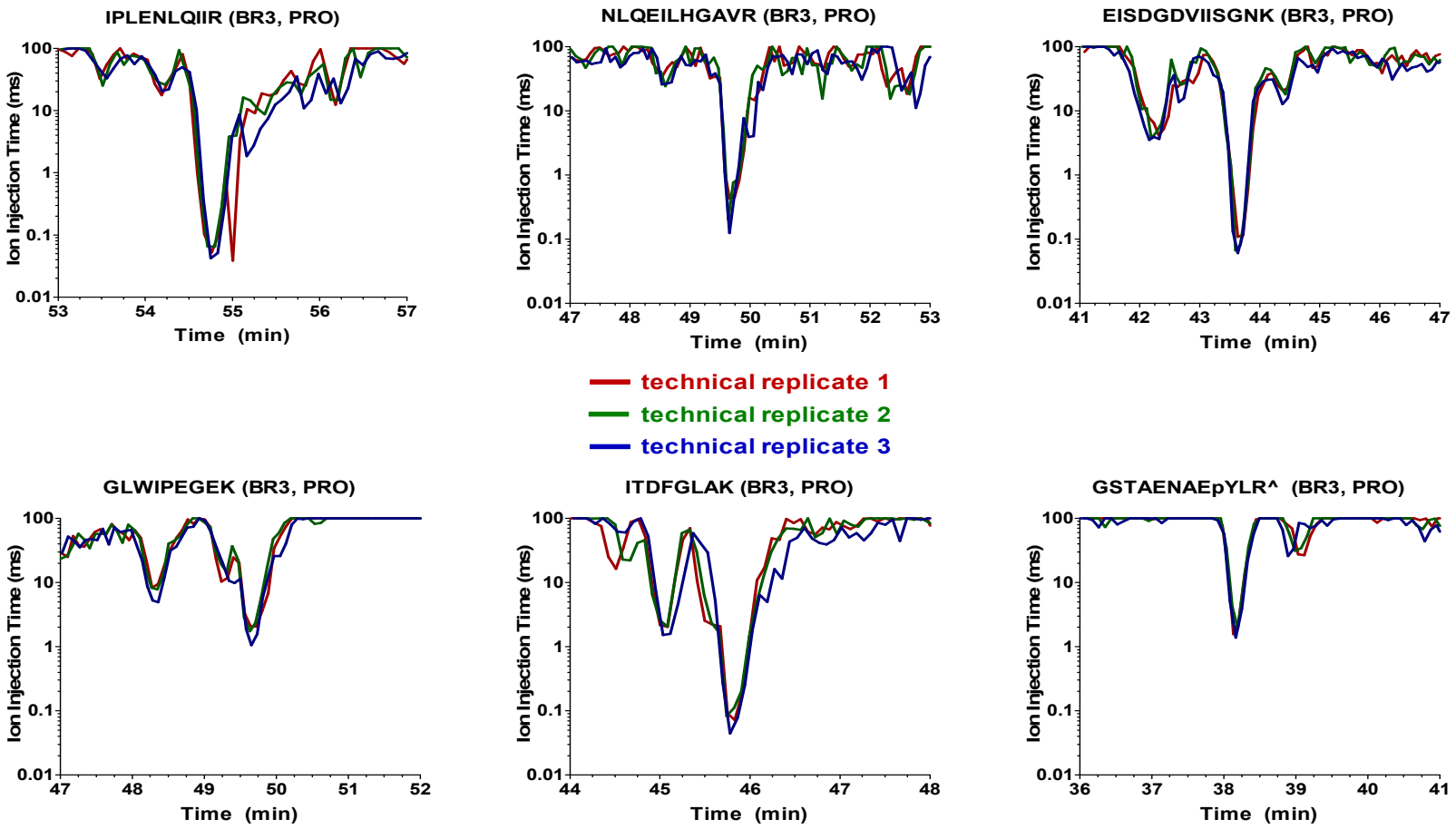

Figure IV-8. Time vs. ion injection time for proliferating samples (biological replicate 3). Data is shown for five internal reference peptides and a stable isotope labeled peptide (GSTAENAE*p*YLR). The maximum allowable ion injection time in these experiments is 100ms. These data show the ion injection time for technical replicate one was similar to both technical replicates two and three, unlike Figure IV-6.

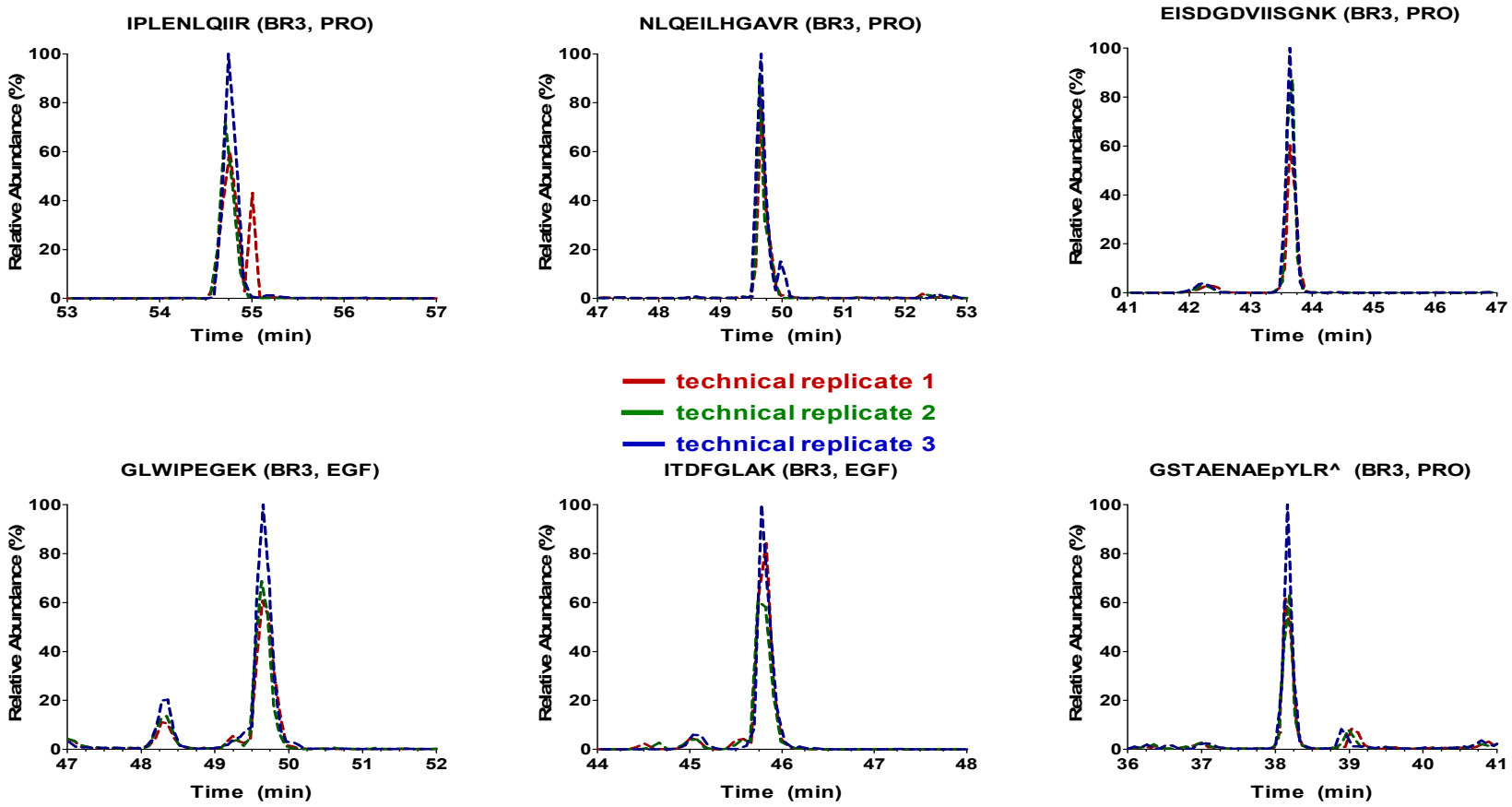

Figure IV-9. Extracted ion chromatograms (time vs. relative abundance (%)) for proliferating samples (biological replicate 3). Data is shown for five internal reference peptides and a stable isotope labeled peptide (GSTAENAE*p*YLR). These data show that the relative abundance (%) for technical replicate one was similar to both technical replicates two and three, unlike technical replicate one in Figure IV-7.

The data generated by analyses of immunoprecipitated EGFR from biological experiment 1 using the IRP and SID methods are shown in Figure IV-10. Both methods yielded similar measures of phosphorylation at Y1173 (GSHQISLDNPD*pY*QQDFFPK), its stimulation by EGF and inhibition by cetuximab and gefitinib (Figure IV-10A and B). The IRP method displayed nearly identical results to SID for all four phosphotyrosine sites (Y998, Y1110, Y1173 and Y1197) (Figure IV-10C and Figures C6-C9). These results also are consistent with the immunoblot analysis for Y1173 shown in Figure IV-3. EGF-treated stimulation produced the highest normalized pSRM signal, whereas samples co-treated with 500 nM gefitinib showed profound decreases in Y1173 phosphorylation to below basal (proliferating) levels. Co-treatment with cetuximab produced less dramatic decreases in Y1173 phosphorylation to near basal levels. Figure IV-10C represents the degree of site-specific phosphorylation relative to that for EGF stimulation by a phosphorylation index, which was calculated as the ratio of the proliferating (P), gefitinib (G+E) or cetuximab (C+E) normalized pSRM signal to the EGF-stimulated normalized pSRM signal (Eq. 1).

$$Phosphorylation\ Index = \frac{normalized\ pSRM\ signal\ of\ P, G+E\ or\ C+E}{normalized\ pSRM\ signal\ of\ EGF}\ x\ 100 \qquad \text{(Eq. 1)}$$

Both IRP and SID approaches yielded similar results and consistently detected similar phosphorylation status differences between the four treatment groups.

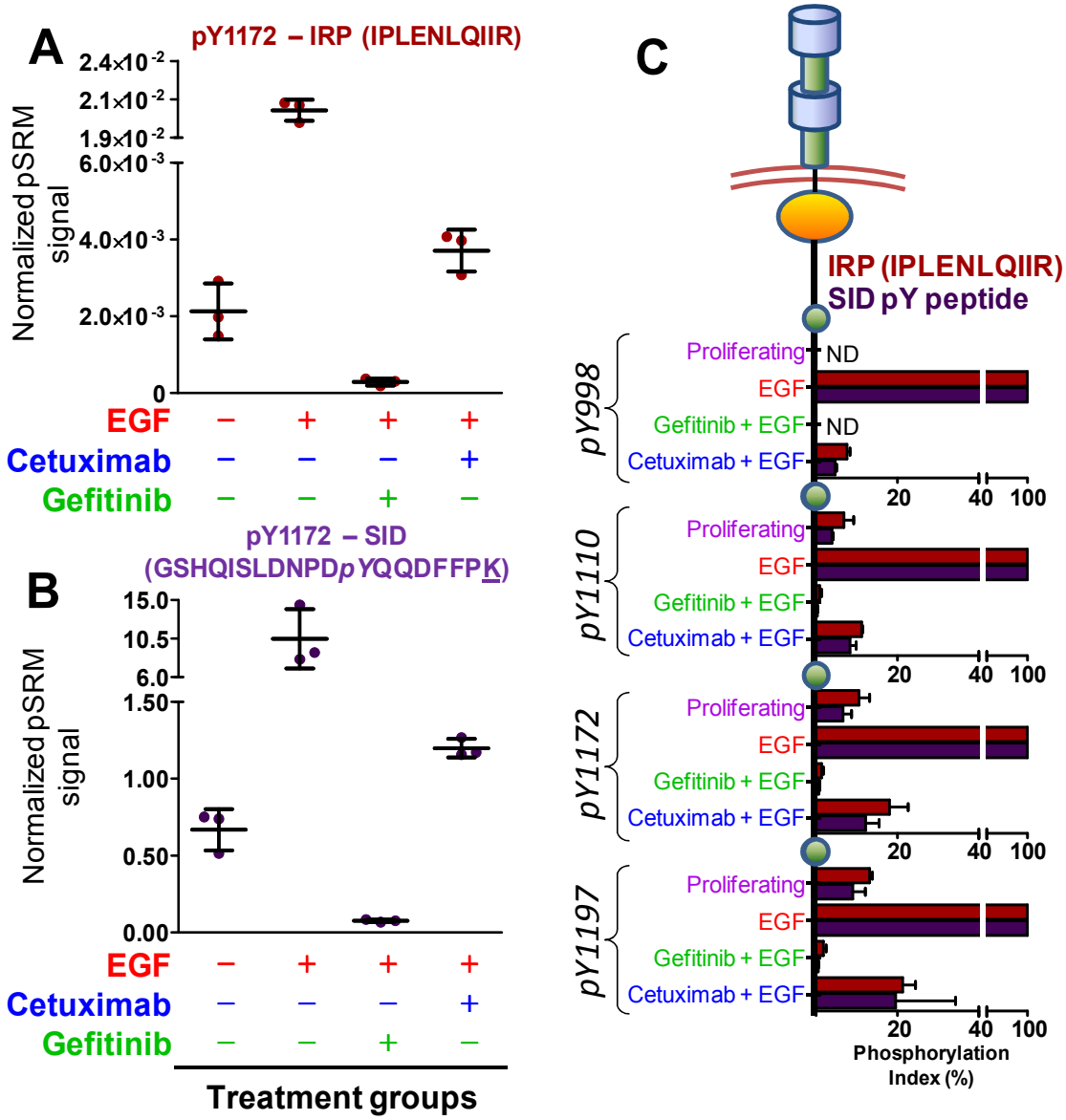

Figure IV-10. Comparison of IRP and SID approaches for (GSHQISLDNPD*pY*QQDFFPK). Treatment groups show the same trends when *pY* peptides are normalized to an internal reference peptide or its stable isotope labeled counterpart. EGFR peptide *pY*1172 (GSHQISLDNPD*pY*QQDFFPK) normalized to an (A) internal reference peptide (IPLENLQIIR) and (B) its *pY* SID peptide standard. (C) Phosphorylation index for each EGFR *pY* peptide and cell treatment group. Similar trends are observed for each *pY* targeted peptide after normalization to an IRP (red) or its stable isotope labeled counterpart (purple). The phosphorylation index is normalized to EGF-stimulated cells(100%). These data represent three technical LC-pSRM-MS injections of biological replicate one. ND, not detected in LC-pSRM-MS experiments. The underlined amino acid indicates which amino acid was stable isotope-labeled.

Analysis of using MS^3 measurements for quantification of EGFR phosphoserine modifications

For *pS* and *pT* peptides MS/MS spectra are dominated by neutral loss of H_3PO_4, measurements based on MS^3 fragmentation of the neutral loss ion offer higher confidence sequence-specific detection. MS^3 measurements for relative quantification of phosphoserine modifications were performed on peptides for EGFR sites S991 (MHLP*pS*PTDSNFYR) $[M+2H-H_3PO_4]^{2+}$ and S1166 (GSHQI*pS*LDNPDYQQDFFPK) $[M+3H-H_3PO_4]^{3+}$. Peak areas from MS^3 measurements were normalized to MS/MS-derived peak areas for the 5 EGFR IRP sequences described above, as well as to the MS/MS-derived peak areas for the isotope-labeled *pY* peptide standards used for SID analyses of the *pY* forms of these sequences (see above). Median CV plots for IRP measurements of S991 and S1166 phosphopeptides (Figures C4 and C5) indicate that normalization to the IPLENLQIIR peptide produced the smallest measurement variation overall, which was comparable to that achieved with normalization to the synthetic *pY* SID peptide sequence analogs. Both analysis methods yielded nearly identical estimates of phosphorylation changes induced by EGF and the effects of cetuximab and gefitinib (Figure IV-11 and Figures C10 and C11).

Phosphorylation levels for S991 display a pattern similar to that for the four phosphotyrosines described above. Phosphorylation at S991 increased after EGF treatment compared to basal (proliferating) levels and were reversed, although not completely, by both inhibitors. This result differs slightly from those seen in Figure IV-10A and B where gefitinib treatment diminished phosphotyrosine signals below basal level. Similar results for S991

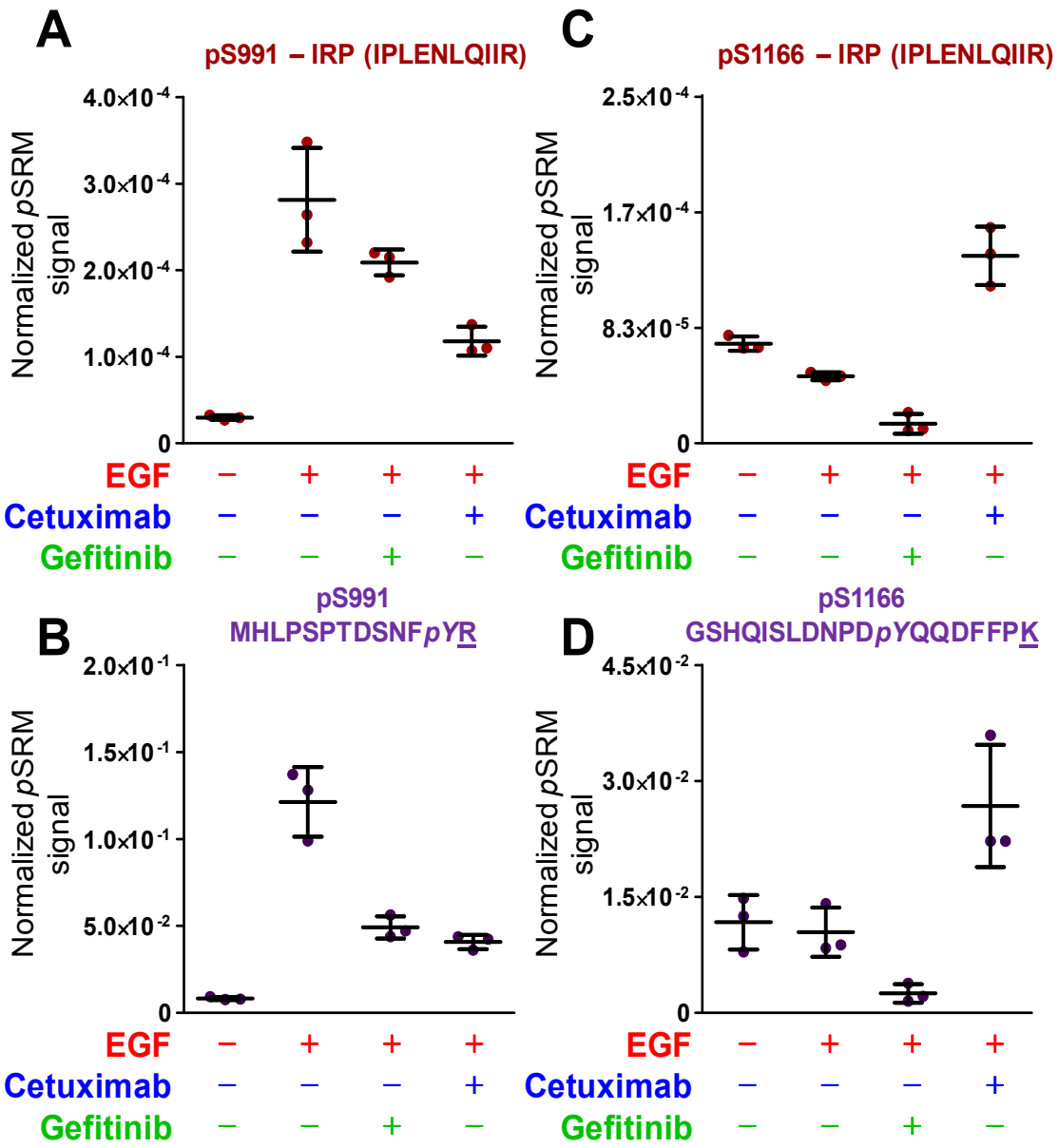

Figure IV-11. MS^3 trend plots for two phosphoserine modified peptides based on treatment group. Phosphopeptide *pS*991 (MHLP*pS*PTDSNFYR) normalized to an (A) IRP or (B) *pY* SID peptide standard (MHLPSPTDSNF*pY*R) show similar trends. These data are similar to trends observed for *pY* peptide MHLPSPTDSNF*pY*R. Phosphopeptide *pS*1166 (GSHQI*pS*LDNPDYQQDFFPK) normalized to an (C) IRP or (D) *pY* SID peptide standard (GSHQISLDNPD*pY*QQDFFPK) show similar trends. These data show that MS^3 measurements can be used for quantification of protein modifications. These data represent three technical injects of biological replicate two. The underlined amino acid indicates which amino acid was stable-isotope labeled.

phosphorylation were reported by Stover et al. (25), who used mass spectrometry analyses to detect S991 phosphorylation induced by EGF stimulation and inhibited by the EGFR inhibitor PK166.

In contrast, similar analyses of phosphorylation at S1166 (GSHQI*pS*LDNPDYQQDFFPK) using both methods indicated a very different pattern. EGF treatment produced little or no S1166 phosphorylation, although gefitinib further decreased phosphorylation at this site. The lack of significant EGF-induced phosphorylation at S1166 is consistent with a previous study that employed a mass spectrometry method (12). On the other hand, combined cetuximab and EGF produced the highest amount of phosphorylation at S1166.

Discussion

The major goal of this work was to evaluate the IRP method for quantifying changes in protein PTMs. Although previous work has reported use of variations of this approach (19, 20), these studies detail performance characteristics of the method in comparison to SID. Furthermore, this work describes the implementation of MS/MS and MS^3-based pSRM measurements on an LTQ Velos ion trap instrument. The pSRM transitions can be extracted from MS/MS and MS^3 data, normalized to peak areas from reference peptides within the same protein, thus affording relative quantification of protein modifications. Unlike MRM, pSRM records a full MS/MS spectrum for each monitored peptide, which allows for spectrum verification by visual inspection as well as the ability to choose different

ions to extract based on PTM site (*e.g.*, *pS*, *pT* vs. *pY*). As with other MS-based methods, IRP analyses can measure multiple site specific phosphorylation sites in parallel without the need for site specific antibodies and without potential concerns for antibody cross-reactivity or lack of phospho–site specificity. The method does not provide the analytical precision of SID; however, the lack of requirement for labeled internal standards, the ease of implementation and the suitability for typical quantitative comparisons—as illustrated with the analyses of EGFR phosphorylation—all make this method suitable for broad application in protein biochemistry.

Previous label-free quantitation approaches have utilized estimated stoichiometry (ES), flyability ratios, the native reference peptide (NRP) method or the selected ion tracing method to quantify post-translational modifications (12-18). In all of these methods, XICs (ion currents) at the MS level are generated for each site specific modification as well as its unmodified peptide complement or an unmodified reference peptide. These methods calculate the stoichiometry (or site abundance) of individual post-translationally modified sites by taking the modified peptide peak area and normalizing to the sum of modified and unmodified peak area (18), to an unmodified reference peptide peak area (15-17) or to the sum of unmodified peak area plus the peak area of any other possible sites of modification on the target peptide (12). A key difference between our approach and previous methods is the use of MS/MS extracted ion chromatograms rather than MS^1 data for each modified and reference peptide. Unlike the ES method and other MS^1-based methods, the pSRM utilizes MS/MS and MS^3 data to obtain

peptide sequence and site specific localization data, thus allowing quantitation even when peptide peaks cannot be resolved by liquid chromatography.

In the EGFR phosphorylation studies, internal reference peptides were chosen such that 1) they were not known to be modified, 2) eluted across the chromatogram, 3) displayed consistent signal stability, 4) were observed in previous data dependent LC-MS/MS data, and 5) contained between 7 and 20 amino acids and lacked methionine and cysteine residues. Phosphopeptides were normalized individually to the each of the five internal reference peptides (ITDFGLAK, IPLENLQIIR, GLWIPEGEK, NLQEILHGAVR and EISDGDVIISGNK). Individual analyses of the internal reference peptides indicated that some internal reference peptides showed large differences in the range and median CV plots (Figures C1-C5). The results show that multiple IRPs should be evaluated to optimize the performance of the IRP method. Ultimately, we chose the internal reference peptide with the lowest median CV in the dataset.

We studied biological variations of EGFR phosphorylation in A431 cells under 4 treatment conditions. IRP analyses with all of the internal reference peptides except GLWIPEGEK detected the same differences between treatments as did SID analyses, which demonstrate that moderate differences in measurement variation do not significantly impact the biological conclusions drawn from these studies. In our SID analysis of 4 analyzed phosphotyrosine sites in EGFR, median CVs ranged from 5-15%, whereas IRP analyses (using reference peptide IPLENLQIIR) of the same 4 sites had median CVs around 20% (Figures C1-C5). Although the median CV for the IRP method was greater than

the SID method, the interpretation of phosphorylation differences with both methods is identical. The phosphorylation sites Y998 and Y1173 were also monitored with commercially available antibodies and these analyses confirmed the mass spectrometry results (Figure IV-4). By all 3 methods (immunoblot, SID and IRP), gefitinib was a more potent inhibitor of EGFR than cetuximab at indicated concentrations—immunoblot analyses for Y998 and Y1173 are barely above background and both SID and IRP methods for sites Y998, Y1110, Y1173, and Y1197 were calculated to have a phosphorylation index <10% when compared to EGF-treated cells.

MS^3 analyses for two *pS* containing peptides in EGFR, MHLP*pS*PTDSNFYR (S991) and GSHQI*pS*LDNPDYQQDFFPK (S1166), yielded results consistent with previous literature reports (12, 25). Phosphoserine peptide S991 follows the same overall changes as the four EGFR *pY* sites (Y998, Y1110, Y1173 and Y1197); with the exception that gefitinib was not a more potent inhibitor than cetuximab. Trends across the different treatment groups were consistent whether the MS^3 *pS* peptides were normalized to the isotope-labeled *pY* SID peptide standard or to the internal reference peptide with the lowest median CV (IPLENLQIIR). The effect of EGFR inhibitors on phosphorylation at site S1166 and site S991 has not previously been reported.

In these experiments, the SID and IRP methods were analyzed on a linear ion trap mass spectrometer (LTQ Velos), which monitors ≤ 20 peptides in a single LC-pSRM-MS experiment. While pSRM measurements do not provide the same throughput as triple quadrupole based MRM analyses (> 30 peptides can be

measured with 4 transitions in a single, unscheduled LC-triple quadrupole MRM analysis), the added benefit of the peptide sequence confirmation from the full MS/MS spectrum and the ability to acquire higher order tandem MS data are significant advantages. The pSRM approach also allows selection of the transition after MS/MS analysis and enables quantitative extension of modification mapping experiments without transferring methods to another platform. Our results suggest several precautions that can improve the reliability of pSRM analyses. First, multiple technical replicate injections enable assessment of instrument performance-based variation due to chromatography, detectors, ion injection times, and signal intensity. Second, an IRP method should incorporate multiple internal reference peptides to provide confirmatory results, to identify peptides with the lowest variation and to minimize error due to ion suppression effects, and co-eluting interferences. In our studies, we observed a consistently poor performing internal reference peptide, GLWIPEGEK, which generated large variations in both CV normalized pSRM signal (Figures C1-C5) and which generated EGF- and inhibitor-related phosphorylation differences inconsistent with analyses using the other internal reference peptides. Arbitrary selection of a single reference peptide would not have detected this effect.

We employ IRP analyses for analyses of modifications on individual proteins in relatively simple samples, such as immunoprecipitated proteins or proteins isolated from SDS-PAGE gel bands. We have not considered and do not recommend the IRP approach for global analyses of modified proteins in complex proteomes. In the appropriate context, the IRP method is intended to estimate

differences in protein modifications between similar samples. The data are comparable in measurement variation to immunoblot analyses (CVs up to 40%). MS-based analyses by both the IRP and SID methods are able to selectively measure many site-specific changes for which reliable antibody reagents are unavailable. IRP analyses display lower precision than SID analyses, but are useful in many applications where high precision is not required. IRP-based methods also do not labeled peptide standards, which add significantly to analysis costs. In the context of targeted biochemical analyses, the IRP method accounts for variations in immunoprecipitation or affinity capture efficiency, gel fractionation and protein digestion. The IRP method also accounts for variability in both biological and technical replicates. These features make the IRP method a flexible, general approach for comparative analysis of protein modifications which can find widespread application in biochemical analyses.

Acknowledgements

I thank Dr. Amy-Joan Ham and Dr. Stacy Sherrod for assistance, guidance and expertise in development and characterization of the IRP method.

References

1. Zhang, G., Spellman, D. S., Skolnik, E. Y., and Neubert, T. A. (2006) Quantitative Phosphotyrosine Proteomics of EphB2 Signaling by Stable Isotope Labeling with Amino Acids in Cell Culture (SILAC). *J. Proteome Res.* **5**, 581-588.

2. Kruger, M., Kratchmarova, I., Blagoev, B., Tseng, Y.-H., Kahn, C. R., and Mann, M. (2008) Dissection of the insulin signaling pathway via quantitative phosphoproteomics. *Proceedings of the National Academy of Sciences* **105**, 2451-2456.

3. Luo, W., Slebos, R. J., Hill, S., Li, M., Bra bek, J., Amanchy, R., Chaerkady, R., Pandey, A., Ham, A.-J. L., and Hanks, S. K. (2008) Global Impact of Oncogenic Src on a Phosphotyrosine Proteome. *J. Proteome Res.* **7**, 3447-3460.

4. Spellman, D. S., Deinhardt, K., Darie, C. C., Chao, M. V., and Neubert, T. A. (2008) Stable Isotopic Labeling by Amino Acids in Cultured Primary Neurons. *Mol. Cell. Proteomics* **7**, 1067-1076.

5. Ow, S. Y., Salim, M., Noirel, J., Evans, C., Rehman, I., and Wright, P. C. (2009) iTRAQ Underestimation in Simple and Complex Mixtures: "The Good, the Bad and the Ugly". *J. Proteome Res.* **8**, 5347-5355.

6. Lill, J. (2003) Proteomic tools for quantitation by mass spectrometry. *Mass Spectrom. Rev.* **22**, 182-194.

7. Kirkpatrick, D. S., Gerber, S. A., and Gygi, S. P. (2005) The absolute quantification strategy: a general procedure for the quantification of proteins and post-translational modifications. *Methods* **35**, 265-273.

8. Zhang, H., Liu, Q., Zimmerman, L. J., Ham, A.-J. L., Slebos, R. J. C., Rahman, J., Kikuchi, T., Massion, P. P., Carbone, D. P., Billheimer, D., and Liebler, D. C. (2011) Methods for Peptide and Protein Quantitation by Liquid Chromatography-Multiple Reaction Monitoring Mass Spectrometry. *Mol. Cell. Proteomics* **10**.

9. Rust, M. J., Markson, J. S., Lane, W. S., Fisher, D. S., and O'Shea, E. K. (2007) Ordered Phosphorylation Governs Oscillation of a Three-Protein Circadian Clock. *Science* **318**, 809-812.

10. Rikova, K., Guo, A., Zeng, Q., Possemato, A., Yu, J., Haack, H., Nardone, J., Lee, K., Reeves, C., Li, Y., Hu, Y., Tan, Z., Stokes, M., Sullivan, L., Mitchell, J., Wetzel, R., MacNeill, J., Ren, J. M., Yuan, J., Bakalarski, C. E., Villen, J., Kornhauser, J. M., Smith, B., Li, D., Zhou, X., Gygi, S. P., Gu, T.-L., Polakiewicz, R. D., Rush, J., and Comb, M. J. (2007) Global Survey of Phosphotyrosine Signaling Identifies Oncogenic Kinases in Lung Cancer. *Cell* **131**, 1190-1203.

11. Liu, H., Sadygov, R. G., and Yates, J. R. (2004) A Model for Random Sampling and Estimation of Relative Protein Abundance in Shotgun Proteomics. *Anal. Chem.* **76**, 4193-4201.

12. Wu, S.-L., Kim, J., Bandle, R. W., Liotta, L., Petricoin, E., and Karger, B. L. (2006) Dynamic Profiling of the Post-translational Modifications and Interaction Partners of Epidermal Growth Factor Receptor Signaling after Stimulation by Epidermal Growth Factor Using Extended Range Proteomic Analysis (ERPA). *Mol. Cell. Proteomics* **5**, 1610-1627.

13. Wu, H.-Y., Tseng, V. S., Chen, L.-C., Chang, H.-Y., Chuang, I. C., Tsay, Y.-G., and Liao, P.-C. (2010) Identification of Tyrosine-Phosphorylated Proteins Associated with Lung Cancer Metastasis using Label-Free Quantitative Analyses. *J. Proteome Res.* **9**, 4102-4112.

14. Zhang, G., Fang, B., Liu, R. Z., Lin, H., Kinose, F., Bai, Y., Oguz, U., Remily-Wood, E. R., Li, J., Altiok, S., Eschrich, S., Koomen, J., and Haura, E. B. (2010) Mass Spectrometry Mapping of Epidermal Growth Factor Receptor Phosphorylation Related to Oncogenic Mutations and Tyrosine Kinase Inhibitor Sensitivity. *J. Proteome Res.* **10**, 305-319.

15. Steen, H., Jebanathirajah, J. A., Springer, M., and Kirschner, M. W. (2005) Stable isotope-free relative and absolute quantitation of protein phosphorylation stoichiometry by MS. *Proc. Natl. Acad. Sci. U. S. A.* **102**, 3948-3953.

16. Ruse, C. I., Willard, B., Jin, J. P., Haas, T., Kinter, M., and Bond, M. (2002) Quantitative Dynamics of Site-Specific Protein Phosphorylation Determined Using Liquid Chromatography Electrospray Ionization Mass Spectrometry. *Anal. Chem.* **74**, 1658-1664.

17. Willard, B. B., Ruse, C. I., Keightley, J. A., Bond, M., and Kinter, M. (2003) Site-Specific Quantitation of Protein Nitration Using Liquid Chromatography/Tandem Mass Spectrometry. *Anal. Chem.* **75**, 2370-2376.

18. Tsay, Y.-G., Wang, Y.-H., Chiu, C.-M., Shen, B.-J., and Lee, S.-C. (2000) A Strategy for Identification and Quantitation of Phosphopeptides by Liquid Chromatography/Tandem Mass Spectrometry. *Anal. Biochem.* **287**, 55-64.

19. Falin, R. A., Morrison, R., Ham, A.-J. L., and Strange, K. (2009) Identification of Regulatory Phosphorylation Sites in a Cell Volume- and Ste20 Kinase-dependent ClC Anion Channel. *The Journal of General Physiology* **133**, 29-42.

20. Erickson, J. R., Joiner, M.-l. A., Guan, X., Kutschke, W., Yang, J., Oddis, C. V., Bartlett, R. K., Lowe, J. S., O'Donnell, S. E., Aykin-Burns, N., Zimmerman, M. C., Zimmerman, K., Ham, A.-J. L., Weiss, R. M., Spitz, D. R., Shea, M. A., Colbran, R. J., Mohler, P. J., and Anderson, M. E. (2008) A Dynamic Pathway for Calcium-Independent Activation of CaMKII by Methionine Oxidation. *Cell* **133**, 462-474.

21. Licklider, L. J., Thoreen, C. C., Peng, J., and Gygi, S. P. (2002) Automation of Nanoscale Microcapillary Liquid Chromatography-Tandem Mass Spectrometry with a Vented Column. *Anal. Chem.* **74**, 3076-3083.

22. MacLean, B., Tomazela, D. M., Shulman, N., Chambers, M., Finney, G. L., Frewen, B., Kern, R., Tabb, D. L., Liebler, D. C., and MacCoss, M. J. (2010) Skyline: an open source document editor for creating and analyzing targeted proteomics experiments. *Bioinformatics* **26**, 966-968.

23. Addona, T. A., Abbatiello, S. E., Schilling, B., Skates, S. J., Mani, D. R., Bunk, D. M., Spiegelman, C. H., Zimmerman, L. J., Ham, A.-J. L., Keshishian, H., Hall, S. C., Allen, S., Blackman, R. K., Borchers, C. H., Buck, C., Cardasis, H. L., Cusack, M. P., Dodder, N. G., Gibson, B. W., Held, J. M., Hiltke, T., Jackson, A., Johansen, E. B., Kinsinger, C. R., Li, J., Mesri, M., Neubert, T. A., Niles, R. K., Pulsipher, T. C., Ransohoff, D., Rodriguez, H., Rudnick, P. A., Smith, D., Tabb, D. L., Tegeler, T. J., Variyath, A. M., Vega-Montoto, L. J., Wahlander, A., Waldemarson, S., Wang, M., Whiteaker, J. R., Zhao, L., Anderson, N. L., Fisher, S. J., Liebler, D. C., Paulovich, A. G., Regnier, F. E., Tempst, P., and Carr, S. A. (2009) Multi-site assessment of the precision and reproducibility of multiple reaction monitoring-based measurements of proteins in plasma. *Nat Biotech* **27**, 633-641.

24. Rudnick, P. A., Clauser, K. R., Kilpatrick, L. E., Tchekhovskoi, D. V., Neta, P., Blonder, N., Billheimer, D. D., Blackman, R. K., Bunk, D. M., Cardasis, H. L., Ham, A. J., Jaffe, J. D., Kinsinger, C. R., Mesri, M., Neubert, T. A., Schilling, B., Tabb, D. L., Tegeler, T. J., Vega-Montoto, L., Variyath, A. M., Wang, M., Wang, P., Whiteaker, J. R., Zimmerman, L. J., Carr, S. A., Fisher, S. J., Gibson, B. W., Paulovich, A. G., Regnier, F. E., Rodriguez, H., Spiegelman, C., Tempst, P., Liebler, D. C., and Stein, S. E. (2010) Performance metrics for liquid chromatography-tandem mass spectrometry systems in proteomics analyses. *Mol Cell Proteomics* **9**, 225-241.

25. Stover, D., Caldwell, J., Marto, J., Root, K., Mestan, J., Stumm, M., Ornatsky, O., Orsi, C., Radosevic, N., Liao, L., Fabbro, D., and Moran, M. (2004) Differential phosphoprofiles of EGF and EGFR kinase inhibitor-treated human tumor cells and mouse xenografts. *Clinical Proteomics* **1**, 69-80.

CHAPTER V

PERSPECTIVE

Contributions and General considerations

Summary

The hypothesis underlying this work was that differences in global protein expression levels can produce distinct protein changes indicative of a cellular response to EGFR signaling modulation. The studies detailed in Chapters II and III prove the hypothesis and present a robust approach to identify differential protein signatures as indicators of anti-EGFR therapy. In addition, Chapter IV defines the performance characteristics of a new quantitative approach for detecting phosphorylated peptides. Together, these approaches represent powerful tools for studying molecular signaling events of EGFR activation and inhibition.

Current practices and limitations

Protein and phosphoprotein analyses in tumor tissues by reverse phase protein array methods have identified putative signatures for EGFR inhibitor responses (1-4). These approaches can be very powerful but require availability of high-quality antibodies for detection and assay development generally lags behind identification of putative targets. Moreover, immunoassays can be

affected by non-specific reactions and can fail if a relevant epitope has been removed by conformational changes, proteolysis, or posttranslational modifications.

Studies in cell models using global phosphoproteomics and targeted analysis of EGF pathway phosphoprotein intermediates have provided the most comprehensive analyses of EGFR-driven signaling networks (5-8). However, phosphoproteomic analysis of tissue specimens is complicated by sample heterogeneity, limiting amounts of available tissue, and low abundance of modified peptides (analyses typically require affinity enrichment of phosphorylated proteins) (5, 9-11). In addition, the transient nature of phosphorylation modifications also presents the challenge of preserving phosphorylation status during sample preparation. Acquisition practices for biopsies and surgical resections do not permit rigorous control of preanalytical variables, such as ischemic time and temperature, which trigger stress responses that may obscure the status of network intermediates *in vivo* (12-14). Despite the rapid growth of information about EGFR signaling networks, identification of robust molecular markers linking network status and therapeutic response remains a challenge.

A new approach

Given above limitations in current practices, more robust approaches to measure signaling networks are needed to overcome the shortcomings of direct phosphoproteome and antibody-based analyses. In this research, a core group

of proteins including Jagged, JUN and CLDN4 shared responses in all of the EGFR inhibitor-sensitive models including mouse xenograft (FFPE blocks) and tissue biopsies from a MD patient. While data for these proteins were in agreement in models, further validation is required to develop a clinically relevant assay. The main objective of this work was to determine whether protein expression signatures can represent the effects of drugs on a signaling network, rather than to develop and refine a clinically useful signature of EGFR sensitivity. The combine results of Chapters II and III illustrate the utility of this approach to identify and verify proteins differences between treatment conditions and across multiple biological systems and illuminate this platform as a viable option to investigate other signaling pathways in a similar systematic approach. A key benefit of using the LRP method to quantitate target peptides is the ease and speed of assay development (i.e., leads identified today can translate into targeted assays tomorrow).

Further investigations specific to this experimental approach should be considered as well. For example, cetuximab and gefitinib inhibit EGFR via two different modes (15-17). Thus, differential proteins found exclusively in one signature or the other could represent the distinctly different molecular events underlying each mechanism of inhibition. In the global shotgun data, clusterin was found to be two fold higher in gefitinib-treated cells than in EGF-treated cells while cetuximab had no effect on expression of clusterin. This is intriguing, as clusterin has been reportedly involved in regulation of cell proliferation and as a pro-survival factor (18, 19).

In addition, further MRM studies of the proposed EGFR inhibition signature should be pursued at a variety of time points in both EGFR-sensitive and EGFR-resistant cell models to better understand the temporal characteristics of the responding proteins. The model presented in this dissertation research represents early signaling responses to acute treatment of a system with EGFR-targeted drugs; however, analyses of the protein signature in longer treatment settings would provide a more complete picture of the underlying biology.

It is unarguable that cultured cells and intact tissues present clear differences that may affect response to EGF and inhibitors. Indeed, a systematic assessment of factors affecting cell versus tissue responses to EGFR modulation is certainly beyond the scope of this work although necessary to illuminate the distinct mechanisms in each system. Global shotgun analysis of the DiFi and HCT-116 cells compared to corresponding xenograft tissue analyses could provide insight into the molecular differences between *in vitro* and *in vivo* models of signaling modulation; however, uncontrollable variables *in vivo* such as endogenous expression of ligands at various concentrations and exposures complicate a direct comparison between models. Furthermore, sample storage must be accounted for in this analysis since the xenograft samples are FFPE while the cell culture samples are flash frozen (20).

Pre-clinical application and companion diagnostics

Perhaps a more far-reaching application of the described platform is as a tool for identifying “companion biomarkers”. The term "companion biomarker"

means that a particular diagnostic test is specifically linked to a therapeutic drug either in drug development or in the clinic. Companion biomarkers assist in the stratification and sub-classification of patient disease types in an effort to optimize therapy (21, 22). For example, an IHC-based test for Her2 (23) is used to determine the suitability of patients for anti-Her2 therapy. However, the ability of Her2 expression status to predict the benefit of trastuzumab is a subject of much debate, as it seems to be modest at best with a positive predictive value (PPV) usually in the region of 25–40% (24). IHC has numerous limitations—technical and interpretative—that impact reproducibility and accuracy as demonstrated by poor correlation between Her2 testing and predicting (25). Furthermore, KRAS mutation was found, in retrospective analyses, to be correlated with absence of response to anti-EGFR therapies (26). Indeed, *KRAS* is considered a predictive drug-response-specific biomarker and anti-EGFR therapies are no longer recommended for patients harboring *KRAS* mutation (27).

The combined global identification and LRP verification platform is well-suited to help fill the gap between cell culture and clinic. The LRP method is a cost-effective approach in the discovery phase when new targets are being identified through *in vitro* models, in a preclinical setting when large numbers of putative candidates are being screened, or in retrospective analyses of archival FFPE tissues. Challenges remain in validating and translating initial markers or signatures generated using defined *in vitro* models to *in vivo* systems. Systematic development of protein signatures for clinical use entails 1) multiple

discovery systems to generate a more broadly-based candidate signature, 2) integration of quantitative measurements with a valid statistical model to establish score thresholds and account for variability and 3) validation in a carefully selected, valid patient cohort.

Indeed more investigations are required for the clinical validation of a specific signature of EGFR inhibitor response. Nevertheless, some of the proteins identified in this study would appear likely to contribute to a clinically useful EGFR inhibition protein profile. This research establishes proof-of-concept for this approach by demonstrating that protein expression signatures detect activation and inhibition of dynamic signaling networks. Clinically useful response signatures developed through this approach could have broad impact in the field of cancer therapeutics. Although the path of translating protein differentials identified *in vitro* to clinically useful biomarkers presents a gauntlet of obstacles prior to candidate validation, this research provides data illustrating the described approach as a progressive step in the rigorous process of identifying companion biomarkers.

Conclusion

In summary, the LRP method was employed to validate protein differences observed from shotgun analyses in EGFR drug treated A431 cells. An EGFR inhibition signature targeted assay developed in a model system was applied across several biological contexts including additional cell models, mouse xenograft models, and human tissues samples. The data show the success of the

approach in detecting differential responses to EGFR stimulation and inhibition and suggest a wide range of applications to investigate other signaling networks as well as a potential use in clinical samples to characterize patient response to drug treatment.

References

1. Hennessy, B. T., Lu, Y., Gonzalez-Angulo, A. M., Carey, M. S., Myhre, S., Ju, Z., Davies, M. A., Liu, W., Coombes, K., Meric-Bernstam, F., Bedrosian, I., McGahren, M., Agarwal, R., Zhang, F., Overgaard, J., Alsner, J., Neve, R. M., Kuo, W. L., Gray, J. W., Borresen-Dale, A. L., and Mills, G. B. (2010) A Technical Assessment of the Utility of Reverse Phase Protein Arrays for the Study of the Functional Proteome in Non-microdissected Human Breast Cancers. *Clin Proteomics* **6**, 129-151.

2. Pernas, F. G., Allen, C. T., Winters, M. E., Yan, B., Friedman, J., Dabir, B., Saigal, K., Mundinger, G. S., Xu, X., Morris, J. C., Calvo, K. R., Van Waes, C., and Chen, Z. (2009) Proteomic Signatures of Epidermal Growth Factor Receptor and Survival Signal Pathways Correspond to Gefitinib Sensitivity in Head and Neck Cancer. *Clin. Cancer Res.* **15**, 2361-2372.

3. Pierobon, M., Calvert, V., Belluco, C., Garaci, E., Deng, J., Lise, M., Nitti, D., Mammano, E., Marchi, F. D., Liotta, L., and Petricoin, E. (2009) Multiplexed Cell Signaling Analysis of Metastatic and Nonmetastatic Colorectal Cancer Reveals COX2-EGFR Signaling Activation as a Potential Prognostic Pathway Biomarker. *Clin Colorectal Cancer* **8**, 110-117.

4. Tsavachidou-Fenner, D., Tannir, N., Tamboli, P., Liu, W., Petillo, D., Teh, B., Mills, G. B., and Jonasch, E. (2011) Gene and protein expression markers of response to combined antiangiogenic and epidermal growth factor targeted therapy in renal cell carcinoma. *Ann. Oncol.* **21**, 1599-1606.

5. Zhang, Y., Wolf-Yadlin, A., Ross, P. L., Pappin, D. J., Rush, J., Lauffenburger, D. A., and White, F. M. (2005) Time-resolved Mass Spectrometry of Tyrosine Phosphorylation Sites in the Epidermal Growth Factor Receptor Signaling Network Reveals Dynamic Modules. *Mol. Cell. Proteomics* **4**, 1240-1250.

6. Thelemann, A., Petti, F., Griffin, G., Iwata, K., Hunt, T., Settinari, T., Fenyo, D., Gibson, N., and Haley, J. D. (2005) Phosphotyrosine signaling networks in epidermal growth factor receptor overexpressing squamous carcinoma cells. *Mol Cell Proteomics* **4**, 356-376.

7. Pandey, A., Podtelejnikov, A. V., Blagoev, B., Bustelo, X. R., Mann, M., and Lodish, H. F. (2000) Analysis of receptor signaling pathways by mass spectrometry: Identification of Vav-2 as a substrate of the epidermal and platelet-derived growth factor receptors. *PNAS* **97**, 179-184.

8. Guo, A., Villen, J., Kornhauser, J., Lee, K. A., Stokes, M. P., Rikova, K., Possemato, A., Nardone, J., Innocenti, G., Wetzel, R., Wang, Y., MacNeill, J., Mitchell, J., Gygi, S. P., Rush, J., Polakiewicz, R. D., and Comb, M. J. (2008) Signaling networks assembled by oncogenic EGFR and c-Met. *PNAS* **105**, 692-697.

9. Rexer, B. N., Ham, A. J. L., Rinehart, C., Hill, S., de Matos Granja-Ingram, N., Gonzalez-Angulo, A. M., Mills, G. B., Dave, B., Chang, J. C., Liebler, D. C., and Arteaga, C. L. (2011) Phosphoproteomic mass spectrometry profiling links Src family kinases to escape from HER2 tyrosine kinase inhibition. *Oncogene* **30**, 4163-4174.

10. Li, X., Gerber, S. A., Rudner, A. D., Beausoleil, S. A., Haas, W., Villén, J., Elias, J. E., and Gygi, S. P. (2007) Large-Scale Phosphorylation Analysis of Î±-Factor-Arrested Saccharomyces cerevisiae. *J. Proteome Res.* **6**, 1190-1197.

11. Wolf-Yadlin, A., Hautaniemi, S., Lauffenburger, D. A., and White, F. M. (2007) Multiple reaction monitoring for robust quantitative proteomic analysis of cellular signaling networks. *PNAS* **104**, 5860-5865.

12. Espina, V., Edmiston, K. H., Heiby, M., Pierobon, M., Sciro, M., Merritt, B., Banks, S., Deng, J., VanMeter, A. J., Geho, D. H., Pastore, L., Sennesh, J., Petricoin, E. F., 3rd, and Liotta, L. A. (2008) A portrait of tissue phosphoprotein stability in the clinical tissue procurement process. *Mol Cell Proteomics* **7**, 1998-2018.

13. Espina, V., Mueller, C., Edmiston, K., Sciro, M., Petricoin, E. F., and Liotta, L. A. (2009) Tissue is alive: New technologies are needed to address the problems of protein biomarker pre-analytical variability. *Proteomics Clin Appl* **3**, 874-882.

14. Silvestri, A., Colombatti, A., Calvert, V. S., Deng, J., Mammano, E., Belluco, C., De Marchi, F., Nitti, D., Liotta, L. A., Petricoin, E. F., and Pierobon, M. (2010) Protein pathway biomarker analysis of human cancer reveals requirement for upfront cellular-enrichment processing. *Lab. Invest.* **90**, 787-796.

15. Li, S., Schmitz, K. R., Jeffrey, P. D., Wiltzius, J. J., Kussie, P., and Ferguson, K. M. (2005) Structural basis for inhibition of the epidermal growth factor receptor by cetuximab. *Cancer cell* **7**, 301-311.

16. Bremer, E., Samplonius, D. F., van Genne, L., Dijkstra, M. H., Kroesen, B. J., de Leij, L. F. M. H., and Helfrich, W. (2005) Simultaneous Inhibition of Epidermal

Growth Factor Receptor (EGFR) Signaling and Enhanced Activation of Tumor Necrosis Factor-related Apoptosis-inducing Ligand (TRAIL) Receptor-mediated Apoptosis Induction by an scFv:sTRAIL Fusion Protein with Specificity for Human EGFR. *J. Biol. Chem.* **280**, 10025-10033.

17. Averbuch, S. D. (2003) The impact of gefitinib on epidermal growth factor receptor signaling pathways in cancer. *Clin Lung Cancer* **5 Suppl 1**, S5-S10.

18. Zhou, W., Janulis, L., Park, I. I., and Lee, C. (2002) A novel anti-proliferative property of clusterin in prostate cancer cells. *Life Sci.* **72**, 11-21.

19. Criswell, T., Beman, M., Araki, S., Leskov, K., Cataldo, E., Mayo, L. D., and Boothman, D. A. (2005) Delayed Activation of Insulin-like Growth Factor-1 Receptor/Src/MAPK/Egr-1 Signaling Regulates Clusterin Expression, a Pro-survival Factor. *J. Biol. Chem.* **280**, 14212-14221.

20. Sprung, R. W., Brock, J. W. C., Tanksley, J. P., Li, M., Washington, M. K., Slebos, R. J. C., and Liebler, D. C. (2009) Equivalence of Protein Inventories Obtained from Formalin-fixed Paraffin-embedded and Frozen Tissue in Multidimensional Liquid Chromatography-Tandem Mass Spectrometry Shotgun Proteomic Analysis. *Mol. Cell. Proteomics* **8**, 1988-1998.

21. La Thangue, N. B., and Kerr, D. J. (2011) Predictive biomarkers: a paradigm shift towards personalized cancer medicine. *Nat Rev Clin Oncol* **8**, 587-596.

22. Ross, J. S. (2011) Cancer biomarkers, companion diagnostics and personalized oncology. *Biomarkers in Medicine* **5**, 277-279.

23. Allison, M. (2010) The HER2 testing conundrum. *Nat Biotech* **28**, 117-119.

24. Phillips, K. A., Marshall, D. A., Haas, J. S., Elkin, E. B., Liang, S.-Y., Hassett, M. J., Ferrusi, I., Brock, J. E., and Van Bebber, S. L. (2009) Clinical practice patterns and cost effectiveness of human epidermal growth receptor 2 testing strategies in breast cancer patients. *Cancer* **115**, 5166-5174.

25. Perez, E. A., Roche, P. C., Jenkins, R. B., Reynolds, C. A., Halling, K. C., Ingle, J. N., and Wold, L. E. (2002) HER2 Testing in Patients With Breast Cancer: Poor Correlation Between Weak Positivity by Immunohistochemistry and Gene Amplification by Fluorescence In Situ Hybridization. *Mayo Clin. Proc.* **77**, 148-154.

26. Linardou, H., Dahabreh, I. J., Kanaloupiti, D., Siannis, F., Bafaloukos, D., Kosmidis, P., Papadimitriou, C. A., and Murray, S. (2008) Assessment of somatic k-RAS mutations as a mechanism associated with resistance to EGFR-targeted agents: a systematic review and meta-analysis of studies in advanced non-small-cell lung cancer and metastatic colorectal cancer. *The Lancet Oncology* **9**, 962-972.

27. Mack, G. S. (2009) FDA holds court on post hoc data linking KRAS status to drug response. *Nat Biotech* **27**, 110-112.

APPENDIX A

Data to Chapter II:

CELL MODELS FOR EGFR ACTIVATION AND INHIBITION AND INITIAL EVALUATION OF GLOBAL PROTEIN EXPRESSION CHANGES

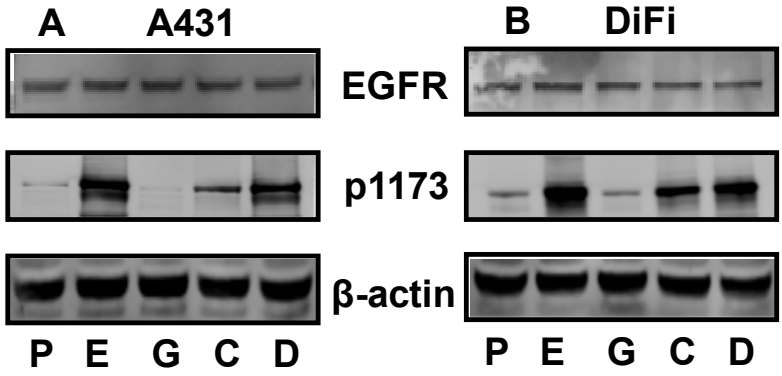

Figure A1. No effect from gefitinib DMSO control. Proliferating cells (P), EGF-stimulated (E), Gefitinib (500 nM) plus EGF (G) Cetuximab (10 μg/mL) plus EGF (C), and DMSO plus EGF control (D). Treated A431 and DiFi cells were serum-starved overnight before being treated with either 30 nM EGF alone or co-treated with inhibitor and EGF for 4 h. Proliferating cells were not serum starved and serve as a reference control for basal level signaling. Immunoblots were performed for total EGFR and phosphorylation at Y1173 (Cell signaling #4267s, 4407s). β-actin was used as a loading control.

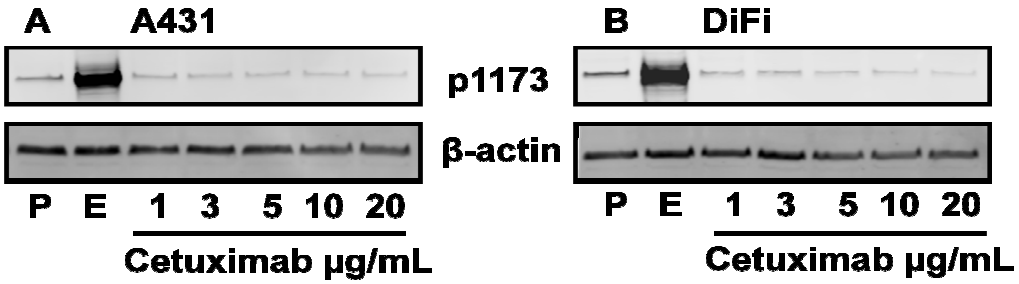

Figure A2. No effect from cetuximab control. Proliferating cells (P) and EGF stimulated (E). Treated A431 and DiFi cells were serum-starved overnight before being treated with 30 nM EGF or indicated concentrations of cetuximab only for 4 h. Proliferating cells were not serum starved and serve as a reference control for basal level signaling. Immunoblots were performed for EGFR phosphorylation at Y1173 (Cell Signaling #4407s). β-Actin (Abcam # ab8224) was used as a loading control.

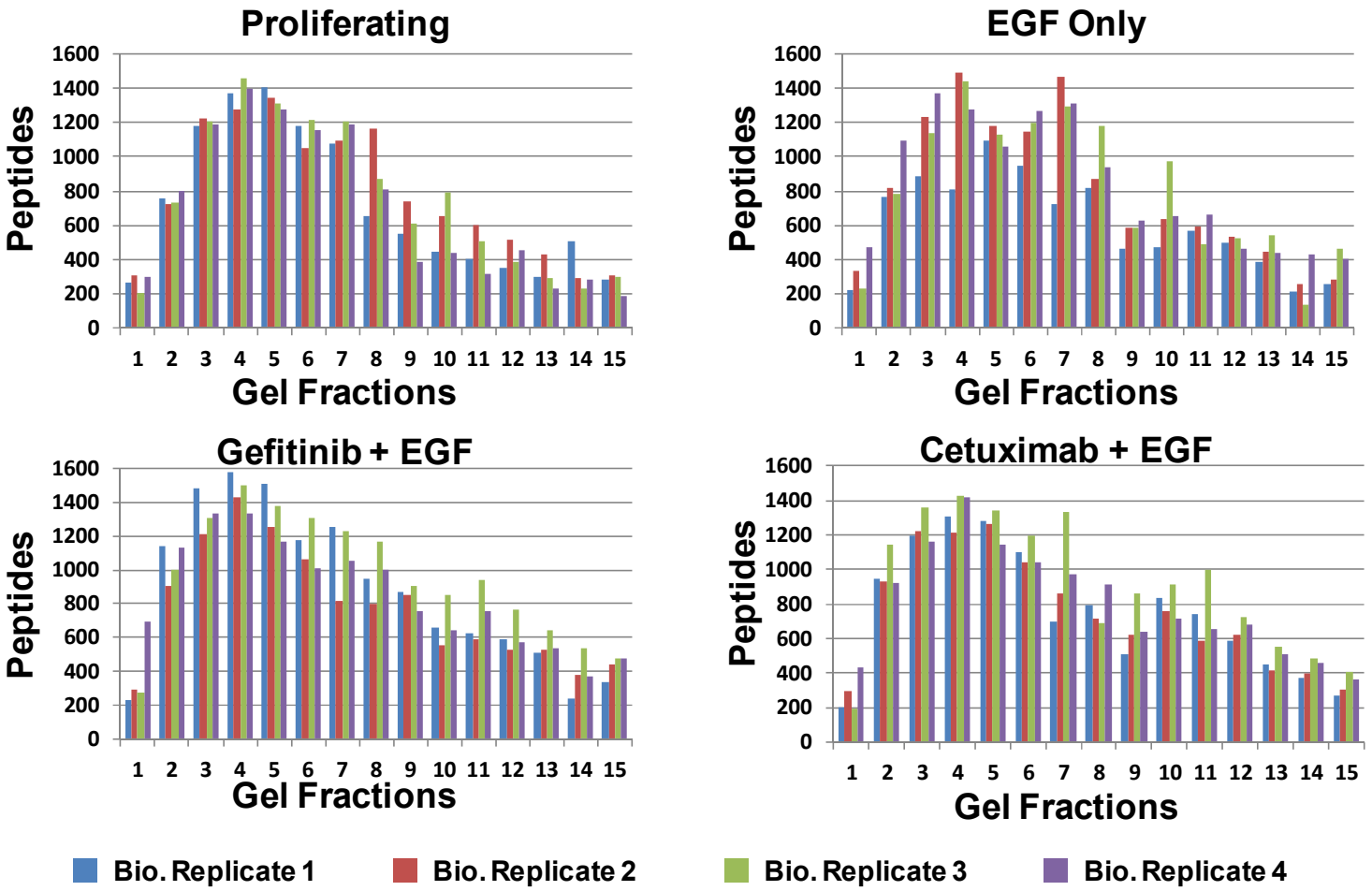

Figure A3. Peptide identification distribution. Treated A431 cells were serum-starved overnight before being treated for 30 min with 30 nM EGF or gefitinib (500 nM) plus EGF or cetuximab (10 μg/mL) plus EGF. Proliferating cells were not serum-starved. Graphs show number of peptides identified per gel fraction. Each bar is representative of a single MS analysis.

Comparison	EGF Stimulated vs Proliferating	EGF stimulated vs Gefitinib+EGF	EGF stimulated vs Cetuximab+EGF
Proteins	2298	2488	2393
FDR(%)	2.2	1.7	1.7

Proteins filtered for a Quasi p-value ≤ 0.05 & ≥ 1.5 Fold Change

Proteins	42

ATP6V0D1	ATPase, H+ transporting, lysosomal 38kDa, V0 subunit d1
ATP6V1B2	ATPase, H+ transporting, lysosomal 56/58kDa, V1 subunit B2
CD47	CD47 molecule
COL12A1	collagen, type XII, alpha 1
CUL2	cullin 2
EIF2S1	eukaryotic translation initiation factor 2, subunit 1 alpha, 35kDa
FARSA	phenylalanyl-tRNA synthetase, alpha subunit
LPCAT1	lysophosphatidylcholine acyltransferase 1
MSH2	mutS homolog 2, colon cancer, nonpolyposis type 1 (E. coli)
NOC3L	nucleolar complex associated 3 homolog (S. cerevisiae)
NT5DC1	5'-nucleotidase domain containing 1
PSMC1	proteasome (prosome, macropain) 26S subunit, ATPase, 1
PSMD7	proteasome (prosome, macropain) 26S subunit, non-ATPase, 7
RAB21	RAB21, member RAS oncogene family
REEP5	receptor accessory protein 5
RPS26	Ribosomal protein S26
SARNP	SAP domain containing ribonucleoprotein
UGP2	UDP-glucose pyrophosphorylase 2

HYOU1	hypoxia up-regulated 1
ATP1A2	ATPase, Na+/K+ transporting, alpha 2 (+) polypeptide
L2HGDH	L-2-hydroxyglutarate dehydrogenase
PACSN2	protein kinase C and casein kinase substrate in neurons 2
ACAT1	acetyl-Coenzyme A acetyltransferase 1
RPS23	ribosomal protein S23
SH3GLB1	SH3-domain GRB2-like endophilin B1
LTF	Lactotransferrin
PLIN3	perilipin 3
CHP	calcium binding protein P22
SUCLG2	succinate-CoA ligase, GDP-forming, beta subunit
OGFR	opioid growth factor receptor
ARPC1B	actin related protein 2/3 complex, subunit 1B, 41kDa
NDUFV1	NADH dehydrogenase (ubiquinone) flavoprotein 1, 51kDa
ACO2	aconitase 2, mitochondrial
CYB5B	cytochrome b5 type B (outer mitochondrial membrane)
HIBCH	3-hydroxyisobutyryl-Coenzyme A hydrolase
IDH2	isocitrate dehydrogenase 2 (NADP+), mitochondrial
SPCS3	signal peptidase complex subunit 3 homolog (S. cerevisiae)
SR140	U2-associated SR140 protein
MRPL47	mitochondrial ribosomal protein L47
SEC23IP	SEC23 interacting protein
CAPR1	Carpin-1 Isoform 2
RRFM	Ribosome recyling factor

Figure A4. Proteins up- and down-regulated in EGF versus proliferating conditions. Up (red) and down (green) regulated proteins (relative to EGF) with ≥6 spectra per protein, ≥1.5 fold change and quasi p-value ≤ 0.05 identified from EGF versus proliferating comparison datasets.

Comparison	EGF Stimulated vs Proliferating	EGF stimulated vs Gefitinib+EGF	EGF stimulated vs Cetuximab+EGF
Proteins	2298	2488	2393
FDR(%)	2.2	1.7	1.7

Proteins filtered for a Quasi p-value ≤ 0.05 & ≥ 1.5 Fold Change

		60	31

ACSL4	acyl-CoA synthetase long-chain family member 4
BRIX1	BRX1, biogenesis of ribosomes, homolog (S. cerevisiae)
CYB5B	cytochrome b5 type B (outer mitochondrial membrane)
DDX23	DEAD (Asp-Glu-Ala-Asp) box polypeptide 23
FUS	fusion (involved in t(12;16) in malignant liposarcoma)
H2AFY2	H2A histone family, member Y2
HYOU1	hypoxia up-regulated 1
MCM3	minichromosome maintenance complex component 3
ME1	malic enzyme 1, NADP(+)-dependent, cytosolic
NLRP2	NLR family, pyrin domain containing 2
NOLC1	nucleolar and coiled-body phosphoprotein 1
PGM1	phosphoglucomutase 1
PSMD2	proteasome (prosome, macropain) 26S subunit, non-ATPase, 2
PYGB	phosphorylase, glycogen; brain
SFRS9	splicing factor, arginine/serine-rich 9
Stat3	Signal transducer and activator of transcription 3
STIP1	stress-induced-phosphoprotein 1
TBL1XR1	transducin (beta)-like 1 X-linked receptor 1
TIAL1	TIA1 cytotoxic granule-associated RNA binding protein-like 1
USP10	ubiquitin specific peptidase 10
USP5	ubiquitin specific peptidase 5 (isopeptidase T)
VPS29	vacuolar protein sorting 29 homolog (S. cerevisiae)
WDR77	WD repeat domain 77

CHD3	Chromodomain-helicase DNA binding protein
HIST1H1A	histone cluster 1, H1a
MACF1	microtubule-actin crosslinking factor 1
MAT2B	methionine adenosyltransferase II, beta
NOSIP	nitric oxide synthase interacting protein
NT5DC1	5'-nucleotidase domain containing 1
RPS26	Ribosomal protein S26
RPS6	ribosomal protein S6

Figure A5. Proteins up- and down-regulated in EGF versus cetuximab-treated conditions. Up (red) and down (green) regulated proteins (relative to EGF) with ≥6 spectra per protein, ≥1.5 fold change and quasi p-value ≤0.05 identified from EGF versus cetuximab comparison datasets.

Comparison	EGF Stimulated vs Proliferating	EGF stimulated vs Gefitinib+EGF	EGF stimulated vs Cetuximab+EGF
Proteins	**2298**	**2488**	**2393**
FDR(%)	**2.2**	**1.7**	**1.7**
		Proteins filtered for a Quasi p-value ≤ 0.05 & ≥ 1.5 Fold Change	
		60	**31**

ARPC4	actin related protein 2/3 complex, subunit 4, 20kDa
BTAF1	BTAF1 RNA polymerase II, B-TFIID transcription factor-associated,
DNM2	dynamin 2
DNM3	dynamin 3
EIF2S3	eukaryotic translation initiation factor 2, subunit 3 gamma, 52kD
EVPL	envoplakin
KRAS	v-Ki-ras2 Kirsten rat sarcoma viral oncogene homolog
MAP4	microtubule-associated protein 4
MYH14	myosin, heavy chain 14
PAFAH1B3	platelet-activating factor acetylhydrolase, isoform Ib, subunit 3
PPP1R12A	protein phosphatase 1, regulatory (inhibitor) subunit 12A

ABCD3	ATP-binding cassette, D (ALD), member	NLRP2	NLR family, pyrin domain containing 2	SAR1A	SAR1 homolog A (S. cerevisiae)
AGK	acylglycerol kinase	NPEPPS	aminopeptidase puromycin sensitive	SCARB1	scavenger receptor class B, member 1
AP2M1	adaptor-related protein complex 2, mu 1	OGFR	opioid growth factor receptor	SCP2	sterol carrier protein 2
BRIX1	BRX1, biogenesis of ribosomes,	P4HA1	prolyl 4-hydroxylase, alpha polypeptide I	SDHB	succinate dehydrogenase, subunit B, iron sulfur (Ip)
COASY	Coenzyme A synthase	PGM1	phosphoglucomutase 1	SLC25A10	solute carrier family 25 dicarboxylate transporter-10)
CSNK2A2	casein kinase 2, alpha prime polypeptide	PIGT	phosphatidylinositol glycan anchor, class	SPTBN2	spectrin, beta, non-erythrocytic 2
CTBL1	Beta-catinin protein like-1	PLRG1	pleiotropic regulator 1 (PRL1)	SRP72	signal recognition particle 72kDa
DAK	dihydroxyacetone kinase 2	POLR2H	polymerase (RNA) II polypeptide H	SRPRB	signal recognition particle receptor, B subunit
EPCAM	epithelial cell adhesion molecule	PPP1R10	protein phosphatase 1, regulatory subuni	STIP1	stress-induced-phosphoprotein 1
ETF1	eukaryotic translation termination factor	PSB5	Proteosome subunit bet S5	TIAL1	TIA1 cytotoxic granule-associated RBP-like 1
HIBCH	3-hydroxyisobutyryl-Coenzyme A hydrola	PSIP1	PC4 and SFRS1 interacting protein 1	TNPO1	transportin 1
HSDL2	hydroxysteroid dehydrogenase like 2	PSMD2	Proteasome 26S subunit, non-ATPase, 2	TTLL12	tubulin tyrosine ligase-like family, member 12
LSR	lipolysis stimulated lipoprotein receptor	PSMD4	Proteasome 26S subunit, non-ATPase, 4	UCHL5	ubiquitin carboxyl-terminal hydrolase L5
LYZ	lysozyme (renal amyloidosis)	PYGB	phosphorylase, glycogen; brain	USP5	ubiquitin specific peptidase 5 (isopeptidase T)
MAPK3	mitogen-activated protein kinase 3	RCN1	reticulocalbin 1, EF-hand calcium binding	WDR18	WD repeat domain 18
MRPL47	mitochondrial ribosomal protein L47	ROA3	Nuclear Riboprotein A3		
NDUFV1	NADH dehydrogenase flavoprotein 1,	RPL23A	ribosomal protein L23a		

Figure A6. Proteins up- and down-regulated in EGF versus gefitinib-treated conditions. Up (red) and down (green) regulated proteins (relative to EGF) with ≥6 spectra per protein, ≥1.5 fold change and quasi p-value ≤0.05 identified from EGF versus gefitinib comparison datasets.

Table A1. MRM data for LC-MRM targeted proteins depicted in Figure II- 8. Pre. *m/z* = precursor mass to charge ratio, Protein = HUGO name, NPA = normalized peak area, Std. Dev. = standard deviation, CV = coefficient of variation. Pro = proliferating cells, EGF = EGF-stimulated (30 nM for 30 min), GEF = gefitinib (500 nM) and EGF treated, CET = cetuximab (10 µg/mL) and EGF-treated. Data is representative of three separate cultures. All precursor *m/z* have a charge of 2+ unless otherwise noted.

PeptideSequence	Pre. m/z	Protein	NPA PRO	Std. Dev. PRO	CV (%) PRO	NPA EGF	Std. Dev. EGF	CV (%) EGF	NPA GEF	Std. Dev. GEF	CV (%) GEF	NPA CET	Std. Dev. CET	CV (%) CET
FNPETDYLTGTDGK	926.9832	ACO2	0.0547	0.0051	9.38	0.0632	0.0088	13.90	0.0537	0.0072	13.44	0.0621	0.0032	5.17
ALAPSAECPIAEENLAR	906.4515	MCM3A	0.0836	0.0045	5.38	0.1511	0.0347	22.95	0.1491	0.0225	15.11	0.2576	0.0675	26.20
AIYHDLEQSIR	672.8490	PACN2	0.1133	0.0133	11.74	0.0886	0.0014	1.59	0.1201	0.0226	18.84	0.0925	0.0233	25.16
VDLGVLGK	400.7475	PGM1	0.1959	0.0075	3.84	0.1840	0.0521	28.30	0.1855	0.0191	10.28	0.1925	0.0019	1.00
HNALIQEVISQSR	747.9048	CUL2	0.2267	0.0125	5.49	0.3254	0.0472	14.50	0.3949	0.0369	9.34	0.3409	0.0380	11.14
DFYELEPEK	585.2717	PYGB	0.3135	0.0042	1.33	0.3170	0.0849	26.78	0.3424	0.0481	14.05	0.3747	0.0607	16.19
TDLHAFENLEIIR	524.2790	EGFR	0.5447	0.0375	6.89	0.5360	0.0388	7.23	0.5509	0.0942	17.10	0.5869	0.0227	3.87
YFDLGLPNR	547.785	IDH2	0.550	0.035	6.34	0.437	0.013	3.01	0.452	0.016	3.56	0.422	0.049	11.70
GIFASGSPFK	505.7689	ME1	0.7881	0.0559	7.09	0.9736	0.1578	16.20	0.9597	0.0539	5.62	0.9371	0.1074	11.46
MATEVAADALGEEWK	810.8823	RPS6	0.8953	0.0108	1.20	2.2385	0.0465	2.08	1.5933	0.2071	13.00	1.3998	0.1400	10.00
CGPMVLDALIK	608.8251	SDHB	1.1818	0.0401	3.39	1.3417	0.1479	11.02	1.2692	0.1166	9.18	1.4737	0.1117	7.58

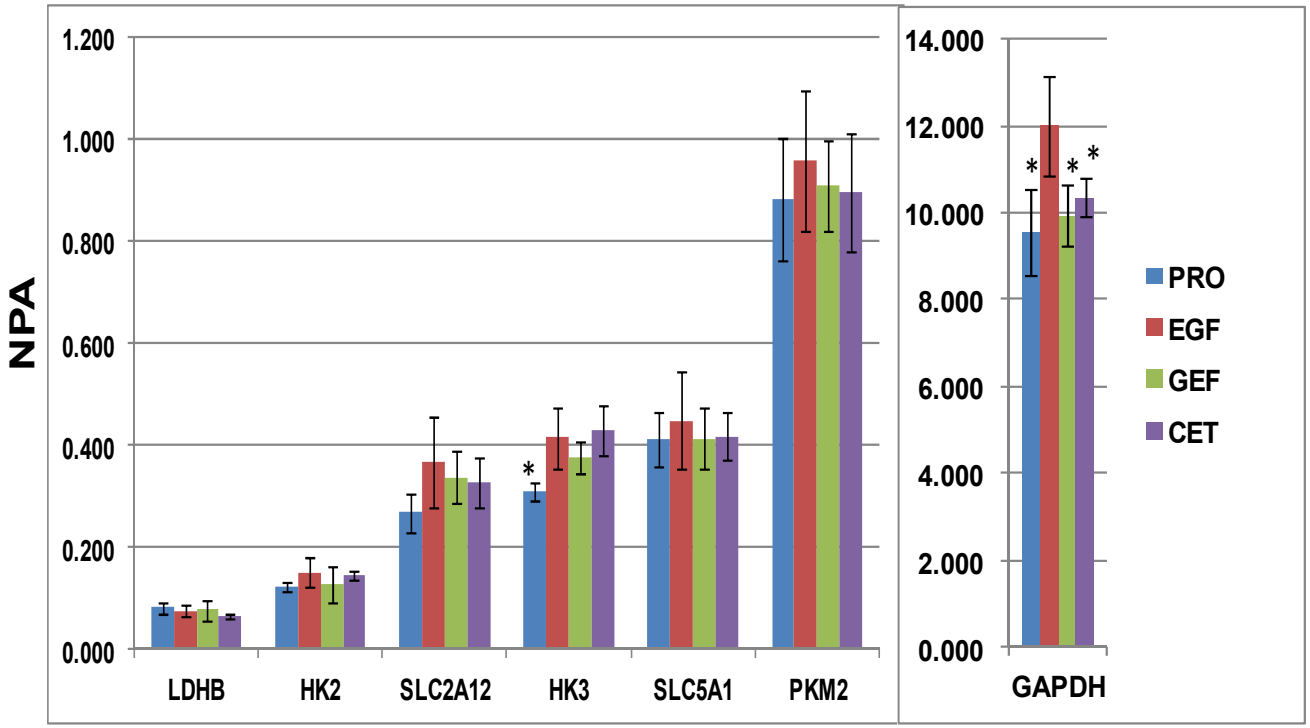

Figure A7. MRM data for analysis of glycolysis pathway-associated proteins. Shows normalized peak area (NPA) quantified from one unique peptide for each target protein across three separate cultures. Pro=proliferating cells, EGF=EGF stimulated (30 nM) for 30 min, GEF=gefitinib (500 nM) and EGF-treated for 30 min, CET=cetuximab (10 µg/mL) and EGF-treated for 30 min. LDHB=lactate dehydrogenase B, HK2=hexokinase 2, SLC2A12=solute carrier family 2 member 12, HK3=hexokinase 3, SLC5A1=solute carrier family 5 member 1, PKM2=pyru8vate kinase (muscle), GAPDH=glyceraldehyde-3-phosphate dehydrogenase. (*) Denotes significant difference between EGF-treated A431 cells as determined by Student's two-tailed, unpaired t-test.

Table A2. MRM data for glycolysis pathway-associated proteins depicted in Figure A7. Pre. *m/z* = precursor mass to charge ratio, Protein = HUGO name, NPA = normalized peak area, Std. Dev. = standard deviation, CV = coefficient of variation. Pro = proliferating cells, EGF = EGF-stimulated (30 nM for 30 min), GEF = gefitinib (500 nM) and EGF treated, CET = cetuximab (10 μg/mL) and EGF-treated. Data is representative of three separate cultures. All precursor *m/z* have a charge of 2+ unless otherwise noted.

PeptideSequence	Pre. *m/z*	Protein	NPA	Std. Dev.	CV (%)	NPA	Std. Dev.	CV (%)	NPA	Std. Dev.	CV (%)	NPA	Std. Dev.	CV (%)
			Pro	Pro	Pro	EGF	EGF	EGF	GEF	GEF	GEF	CET	CET	CET
DYSVTANSK	492.735	LDHB	0.0822	0.0105	12.72	0.0762	0.0120	15.69	0.0775	0.0212	27.39	0.0671	0.0042	6.26
NVELVEGEEGR	615.802	HK2	0.1246	0.0072	5.78	0.1528	0.0285	18.64	0.1285	0.0344	26.75	0.1455	0.0086	5.89
ALSDTTEELTVIK	710.382	SLC2A12	0.2697	0.0377	13.97	0.3676	0.0877	23.86	0.3380	0.0510	15.09	0.3284	0.0509	15.51
ATPDGSER	416.693	HK3	0.3108	0.0183	5.90	0.4160	0.0596	14.34	0.3790	0.0309	8.15	0.4302	0.0483	11.22
GTVGGFFLAGR	541.293	SLC5A1	0.4119	0.0535	12.98	0.4503	0.0967	21.47	0.4133	0.0596	14.42	0.4178	0.0463	11.08
EAEAAIYHLQLFEELR	644.667	PKM2	0.8823	0.1197	13.57	0.9597	0.1386	14.45	0.9094	0.0878	9.65	0.8979	0.1148	12.79
AAFNSGK	347.680	GAPDH	9.5663	0.9951	10.40	11.9845	1.1479	9.58	9.9483	0.7025	7.06	10.3648	0.4264	4.11

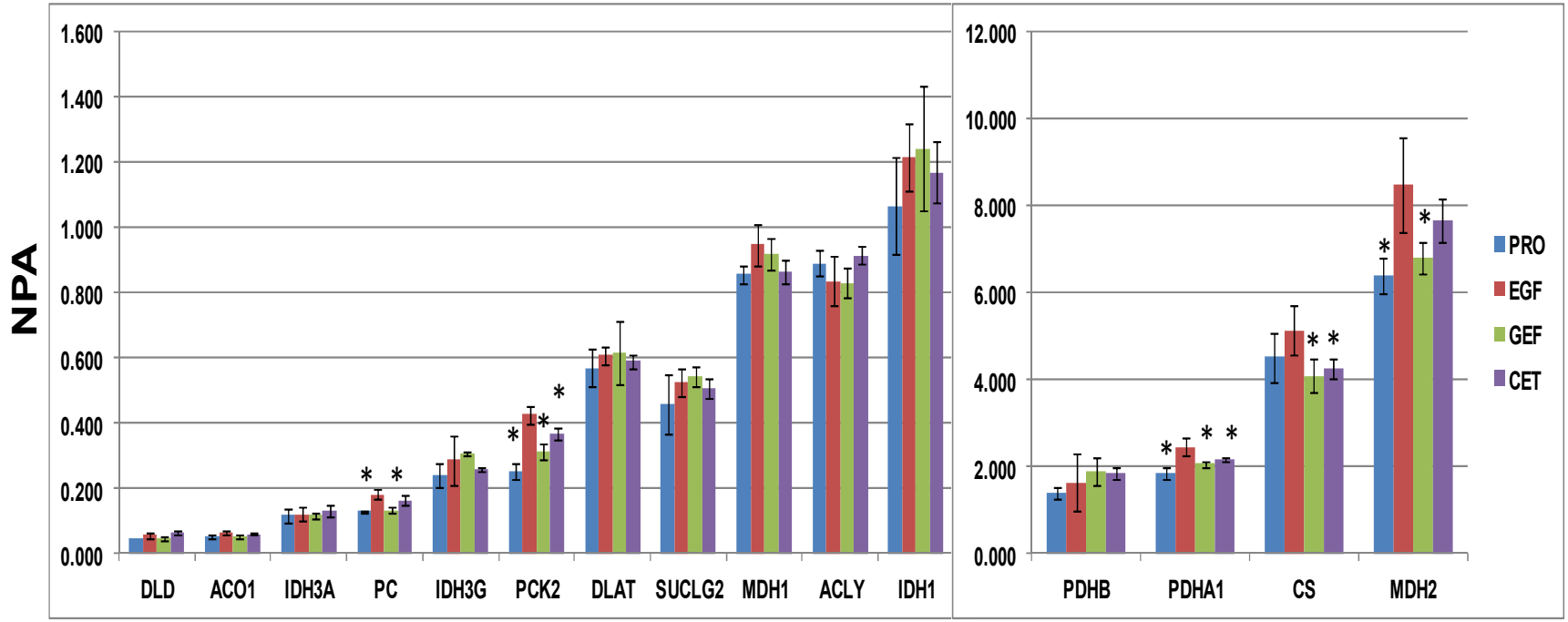

Figure A8. MRM data for analysis of tricarboxylic acid cycle-associated proteins. Shows normalized peak area (NPA) quantified from one unique peptide for each target protein across three separate cultures. Pro = proliferating cells, EGF = EGF-stimulated (30 nM) for 30 min, GEF = gefitinib (500 nM) and EGF-treated for 30 min, CET = cetuximab (10 µg/mL) and EGF-treated for 30 min. DLD=dihydrolipoamide dehydrogenase, ACO1=aconitase 1, IDH3A=isocitrate dehydrogenase 3A, PC=pyruvate carboxylase, IDH3G=isocitrate dehydrogenase 3 (NAD+) gamma PCK2=phosphoenolpyruvate carboxykinase 2, DLAT=dihydrolipoamide S-acetyltransferase, SUCLG2=succinate-CoA ligase, GDP-forming, beta subunit, MDH1=malate dehydrogenase 1, ACLY=ATP citrate lyase, IDH1=isocitrate dehydrogenase 1, PDHB=pyruvate dehydrogenase beta, PDHA1=pyruvate dehydrogenase alpha 1, CS=citrate synthase and MDH2=malate dehydrogenase 1. (*) Denotes significant difference between EGF treated A431 cells as determined by Student's two-tailed, unpaired t-test.

Table A3. MRM data for tricarboxylic acid cycle-associated proteins depicted in Figure A8. Pre. *m/z* = precursor mass to charge ratio, Protein = HUGO name, NPA = normalized peak area, Std. Dev. = standard deviation, CV = coefficient of variation. Pro = proliferating cells, EGF = EGF-stimulated (30 nM for 30 min), GEF = gefitinib (500 nM) and EGF-treated, CET = cetuximab (10 µg/mL) and EGF-treated. Data is representative of three separate cultures. All precursor *m/z* have a charge of 2+ unless otherwise noted.

PeptideSequence	Pre. m/z	Protein	NPA	Std. Dev.	CV (%)	NPA	Std. Dev.	CV (%)	NPA	Std. Dev.	CV (%)	NPA	Std. Dev.	CV (%)
			PRO	PRO	PRO	EGF	EGF	EGF	GEF	GEF	GEF	CET	CET	CET
ADGGTQVIDTK	552.780	DLD	0.0500	0.0006	1.28	0.0577	0.0097	16.85	0.0469	0.0062	13.29	0.0656	0.0068	10.31
FVEFFGPGVAQLSIAI	926.983	ACO1	0.0547	0.0051	9.38	0.0663	0.0088	13.26	0.0537	0.0072	13.44	0.0621	0.0032	5.17
NVTAIQGPGGK	521.288	IDH3A	0.1183	0.0214	18.08	0.1217	0.0210	17.22	0.1189	0.0084	7.04	0.1342	0.0177	13.17
DFTATFGPLDSLNTF	827.907	PC	0.1303	0.0049	3.76	0.1829	0.0161	8.79	0.1353	0.0109	8.02	0.1641	0.0143	8.74
LGDGLFLQCCR	669.818	IDH3G	0.2441	0.0362	14.84	0.2876	0.0777	27.02	0.3088	0.0046	1.50	0.2612	0.0059	2.27
EVLAELEALER	636.346	PCK2	0.2522	0.0244	9.68	0.4270	0.0279	6.52	0.3161	0.0229	7.23	0.3684	0.0197	5.36
GVETIANDVVSLATK	758.914	DLAT	0.5712	0.0578	10.12	0.6084	0.0248	4.08	0.6180	0.0967	15.65	0.5904	0.0188	3.19
EQIDIFEGIK	596.316	SUCLG2	0.4621	0.0911	19.71	0.5258	0.0434	8.26	0.5421	0.0302	5.56	0.5068	0.0297	5.86
GEFVTTVQQR	582.804	MDH1	0.8579	0.0276	3.22	0.9482	0.0619	6.52	0.9192	0.0495	5.39	0.8649	0.0364	4.21
FGGALDAAAK	460.745	ACLY	0.8922	0.0390	4.38	0.8374	0.0770	9.20	0.8301	0.0458	5.51	0.9162	0.0255	2.78
DIFQEIYDK	585.788	IDH1	1.0673	0.1500	14.05	1.2144	0.1035	8.52	1.2435	0.1895	15.24	1.1705	0.0956	8.17
DFLIPIGK	451.771	PDHB	1.3994	0.1392	9.94	1.6418	0.6547	39.88	1.9155	0.3073	16.04	1.8533	0.1351	7.29
EILAELTGR	501.285	PDHA1	1.8516	0.1383	7.47	2.4620	0.1940	7.88	2.0650	0.0666	3.22	2.1777	0.0509	2.34
FVEGLPINDFSR	697.359	MDH1	2.3160	0.2803	12.10	0.3200	0.0355	11.11	0.2454	0.0117	4.75	2.9115	0.2677	9.19
GLVYETSVLDPDEGI	881.947	CS	4.5215	0.5809	12.85	5.1485	0.5491	10.67	4.1054	0.3759	9.16	4.2636	0.2184	5.12
GYLGPEQLPDCLK	745.371	MDH2	6.3996	0.4287	6.70	8.4708	1.0878	12.84	6.8216	0.3710	5.44	7.6578	0.4968	6.49

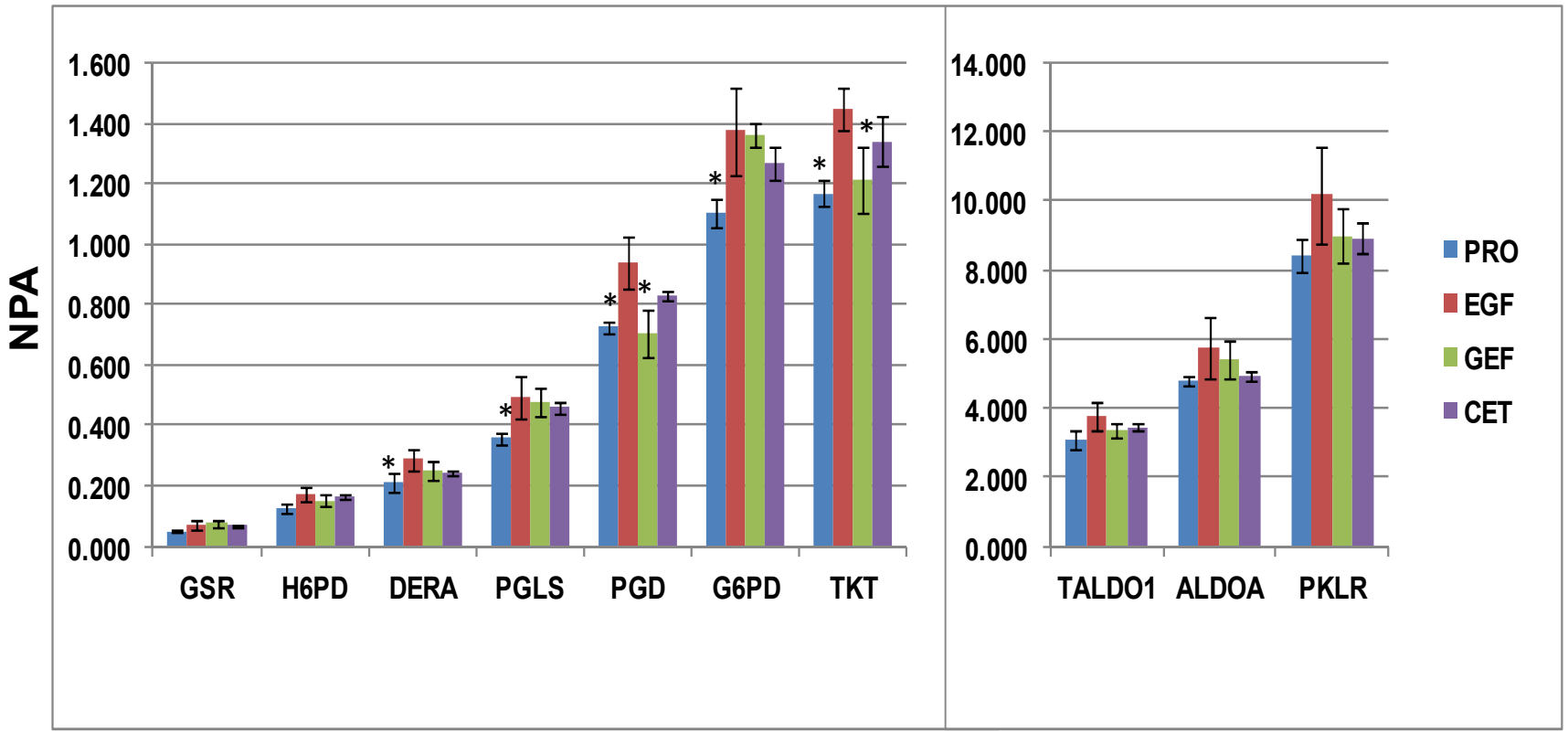

Figure A9. MRM data for analysis of pentose phosphate pathway-associated proteins. Shows normalized peak area (NPA) quantified from one unique peptide for each target protein across three separate cultures. Pro = proliferating cells, EGF = EGF-stimulated (30 nM) for 30 min, GEF = gefitinib (500 nM) and EGF treated for 30 min, CET = cetuximab (10 µg/mL) and EGF-treated for 30 min. GSR=glutathione reductase, H6PD=hexose-6-phosphate dehydrogenase, DERA=deoxyribose-phosphate aldolase, PGLS=6-phosphogluconolactonase, PGD=phosphogluconate dehydrogenase, G6PD=glucose-6-phosphate dehydrogenase, TKT=transketolase, TALDO1=transaldolase 1, ALDOA=aldolase A, fructose-bisphosphate and PKLR=pyruvate kinase, liver and RBC. (*) Denotes significant difference between EGF-treated A431 cells as determined by Student's two-tailed, unpaired t-test.

Table A4. MRM data for pentose phosphate pathway-associated proteins depicted in Figure A9. Pre. *m/z* = precursor mass to charge ratio, Protein = HUGO name, NPA = normalized peak area, Std. Dev. = standard deviation, CV = coefficient of variation. Pro = proliferating cells, EGF = EGF-stimulated (30 nM for 30 min), GEF = gefitinib (500 nM) and EGF-treated, CET = cetuximab (10 µg/mL) and EGF-treated. Data is representative of three separate cultures. All precursor *m/z* have a charge of 2+ unless otherwise noted.

Peptide Sequence	Pre. m/z	Protein	NPA	Std. Dev.	CV (%)	NPA	Std. Dev.	CV (%)	NPA	Std. Dev.	CV (%)	NPA	Std. Dev.	CV (%)
			Pro	Pro	Pro	EGF	EGF	EGF	GEF	GEF	GEF	CET	CET	CET
YGIENVK	411.721	GSR	0.0509	0.0025	4.96	0.0701	0.0131	18.69	0.0754	0.0106	14.06	0.0685	0.0060	8.82
LLDFEFSSGR	585.793	H6PD	0.1248	0.0132	10.61	0.1731	0.0254	14.66	0.1522	0.0172	11.32	0.1660	0.0071	4.26
IGASTLLSDIER	637.851	DERA	0.2113	0.0344	16.29	0.2885	0.0355	12.31	0.2481	0.0321	12.94	0.2426	0.0106	4.38
TVIFVATGEGK	561.314	PGLS	0.3583	0.0203	5.67	0.4956	0.0706	14.24	0.4742	0.0472	9.96	0.4584	0.0169	3.68
NPELQNLLLDDFFK	853.443	PGD	0.7246	0.0186	2.56	0.9382	0.0854	9.10	0.7062	0.0803	11.37	0.8297	0.0121	1.45
DGLLPENTFIVGYAR	832.936	G6PD	1.1034	0.0457	4.14	1.3762	0.1442	10.48	1.3590	0.0381	2.80	1.2679	0.0538	4.25
AVELAANTK	458.759	TKT	1.1682	0.0438	3.75	1.4472	0.0697	4.82	1.2164	0.1099	9.03	1.3416	0.0842	6.28
AAQASDLEK	466.738	TALDO1	3.0914	0.2649	8.57	3.7777	0.4124	10.92	3.3789	0.1936	5.73	3.4561	0.1287	3.72
ELSDIAHR	470.746	ALDOA	4.7904	0.1443	3.01	5.7731	0.8979	15.55	5.4072	0.5647	10.44	4.9287	0.1521	3.09
GDLGIEIPAEK	571.309	PKLR	8.4288	0.5006	5.94	10.1709	1.4182	13.94	8.9897	0.7784	8.66	8.9241	0.4471	5.01

APPENDIX B

Data to Chapter III:

PROTEIN EXPRESSION SIGNATURES FOR INHIBITION OF EPIDERMAL GROWTH FACTOR RECEPTOR-MEDIATED SIGNALING

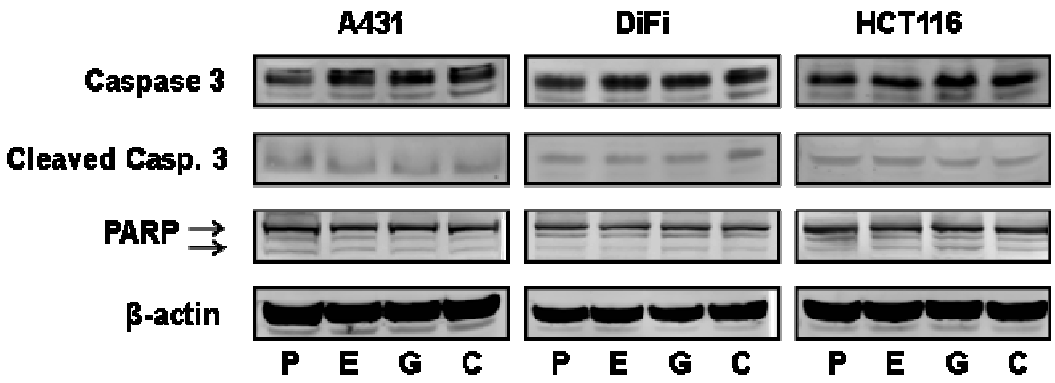

Figure B1. Western blot analysis of caspase 3 and PARP cleavage in treated A431, DiFi and HCT116 cells. P=proliferating cells, E=30nM EGF for 4 h, G=500 nm gefitinib + 30nM EGF for 4 h, and C= 10 μg/mL cetuximab + 30nM EGF for 4 h. Each cell line was probed with antibodies for full length caspase 3 (32 kDa), cleaved caspase 3 (19 kDa) and an antibody that recognizes both full length PARP (116kDa) and cleaved PARP (89 kDa). β-Actin was used as a loading control.

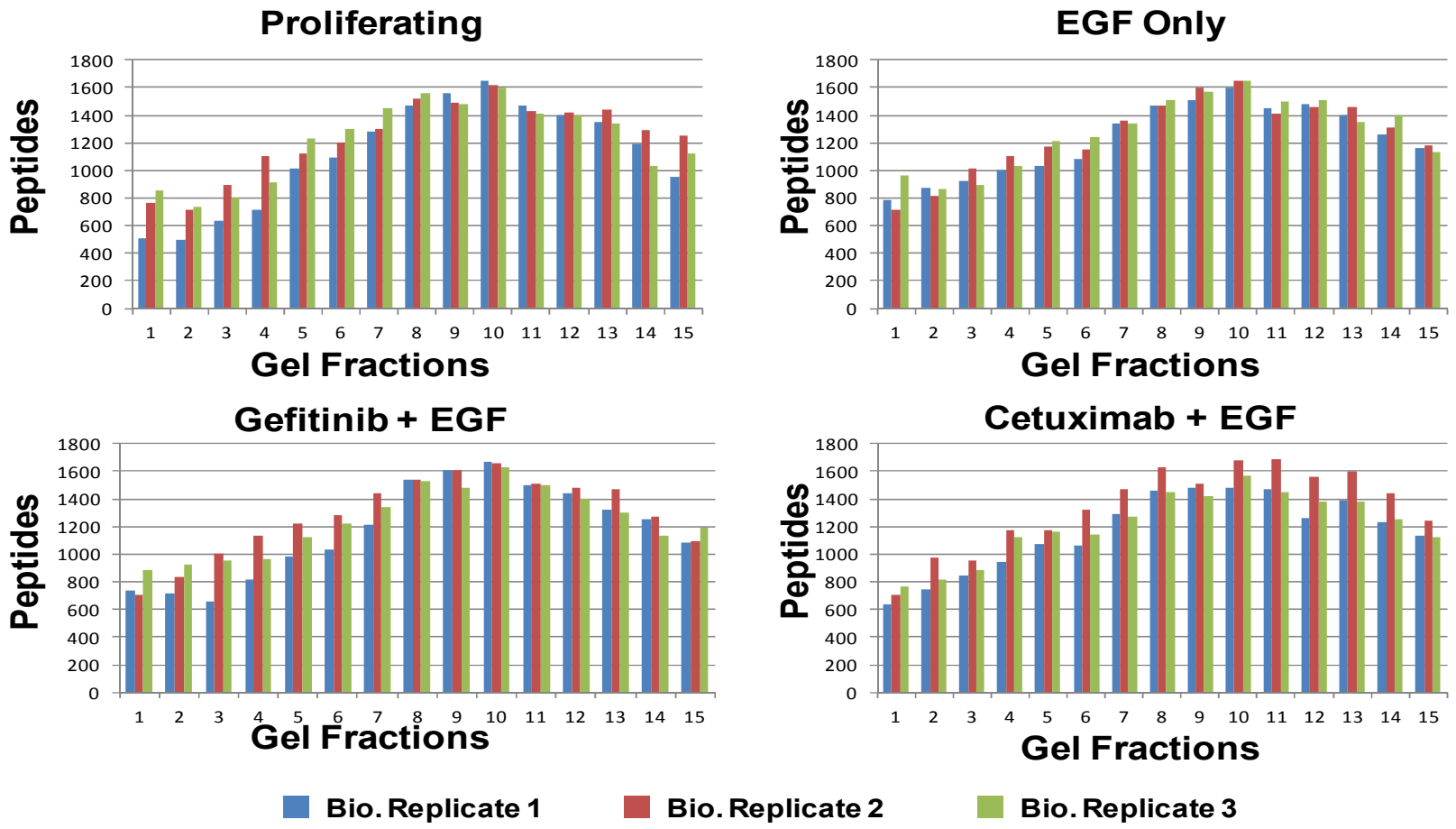

Figure B2. Peptide identification distribution. Treated A431 were serum-starved overnight before being treated with 30 nM EGF or gefitinib (500 nM) plus EGF or cetuximab (10 µg/mL) plus EGF. Proliferating cells were not serum-starved. Graphs show number of peptides identified per each IEF gel fraction. Each bar is representative of a MS single analysis.

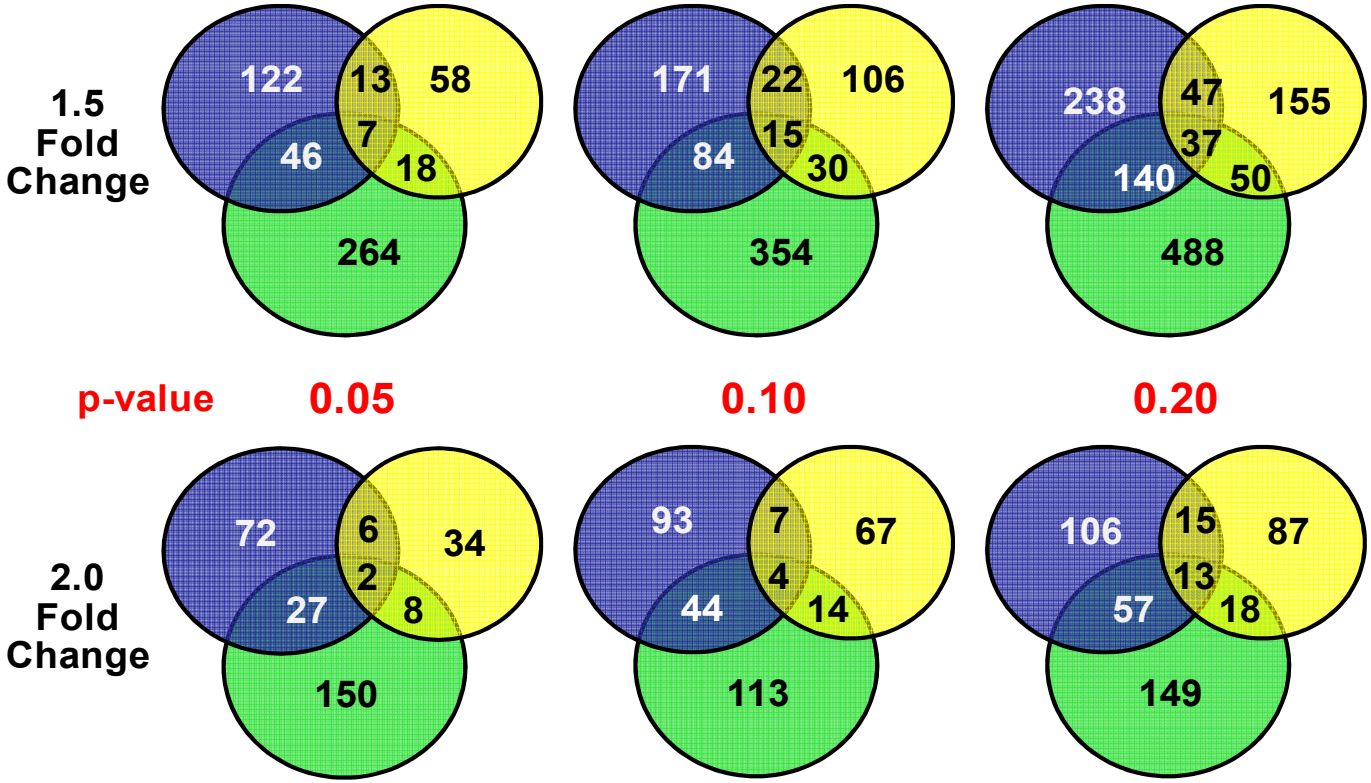

Figure B3. **Varying the thresholds for filtering comparison datasets.** The colored circles represent lists of proteins differentially expressed (both up and down) at varying criteria between differently treated A431 cells. The resulting protein groups represent proteins differentially expressed in response to EGF (blue), EGF-induced protein changes reversed by gefitinib (green) and EGF-induced protein changes reversed by cetuximab (yellow). Fold changes were kept static at either 1.5 or 2.0 while p-values were varied from 0.05 – 0.20.

Table B1. Stimulation signature. Accession numbers, HUGO names, % coverage, spectral counts, fold-change and p-values for proteins identified from QuasiTel comparison of EGF-stimulated and proliferating A431 cell proteomes. Results were filtered to have at least 11 spectra across all analysis (12), a fold change ≥ 2 (base 2 log rate ratio of 1.0) and a p-value ≤ 0.20. rev_ prefix indicates reverse database hit. Protein-level FDR = 11.9%.

Protein	HUGO	Coverage	EGF counts	Pro counts	Fold Change	Quasi p-value	Total Counts
rev_IPI00940099.1		11	1	16	17.763	0.001	17
rev_IPI00845353.2		4	3	9	3.331	0.044	12
rev_IPI00477426.3		4	3	8	2.961	0.021	11
rev_IPI00247295.4		2	6	11	2.035	0.121	17
rev_IPI00385267.4		2	6	11	2.035	0.079	17
rev_IPI00027180.1		4	70	29	2.174	0.065	99
rev_IPI00741537.5		2	20	7	2.574	0.074	27
rev_IPI00293200.3		2	9	3	2.702	0.076	12
rev_IPI00642259.2		2	9	3	2.702	0.129	12
rev_IPI00010903.2		2	15	5	2.702	0.024	20
rev_IPI00645369.2		3	9	3	2.702	0.184	12
rev_IPI00302270.3		1	10	1	9.007	0.025	11
rev_IPI00023868.1		1	12	1	10.809	0.013	13
IPI00478003.1	A2M	2	4	43	11.935	0.000	47
IPI00217272.7	AACS	9	11	4	2.477	0.110	15
IPI00413730.4	ACSS2	7	24	7	3.088	0.006	31
IPI00019901.1	ADD1	11	7	13	2.062	0.035	20
IPI00022431.2	AHSG	4	14	30	2.379	0.010	44
IPI00413641.7	AKR1B1	4	4	8	2.220	0.152	12
IPI00296183.7	ALDH3A1	18	26	9	2.602	0.038	35
IPI00032516.5	AP1M1	11	9	4	2.027	0.159	13
IPI00337741.4	APEH	13	12	22	2.035	0.016	34
IPI00022229.1	APOB	1	2	11	6.106	0.039	13
IPI00013988.2	ARHGAP5	5	3	9	3.331	0.033	12
IPI00472160.5	ARHGEF2	9	10	4	2.252	0.041	14
IPI00014232.1	ARL6IP1	8	19	6	2.852	0.071	25
IPI00170548.1	ATAD2	21	29	53	2.029	0.025	82
IPI00059139.1	ATP6V1E2	18	10	4	2.252	0.080	14
IPI00296191.1	ATP6V1H	21	12	3	3.603	0.130	15
IPI00396074.2	ATP8B2	4	6	11	2.035	0.108	17
IPI00180154.4	ATXN2	6	3	8	2.961	0.026	11
IPI00514611.1	BCAP29	10	5	11	2.442	0.118	16
IPI00294158.1	BLVRA	7	3	8	2.961	0.139	11
IPI00218054.2	C11orf31	25	3	15	5.551	0.001	18

IPI00782974.1	C17orf85	8	3	9	3.331	0.009	12
IPI00027898.3	C21orf70	16	5	11	2.442	0.025	16
IPI00014516.1	CALD1	13	20	9	2.002	0.009	29
IPI00060148.3	CCDC127	6	4	12	3.331	0.092	16
IPI00217059.5	CCDC50	16	3	10	3.701	0.029	13
IPI00657752.1	CD81	11	3	9	3.331	0.052	12
IPI00005822.2	CDC23	14	5	12	2.664	0.017	17
IPI00303099.2	CDCA8	9	3	11	4.071	0.004	14
IPI00645518.1	CDIPT	14	8	17	2.359	0.040	25
IPI00015713.4	CDKAL1	7	4	11	3.053	0.045	15
IPI00009384.5	CDKN1A	18	14	0	4.369	0.000	14
IPI00101532.5	CEP55	15	6	13	2.405	0.034	19
IPI00238469.6	CEP97	6	3	8	2.961	0.178	11
IPI00398992.6	CHD8	4	11	3	3.303	0.040	14
IPI00021944.1	CLDN4	12	12	3	3.603	0.072	15
IPI00000692.2	CLIC3	23	28	11	2.293	0.001	39
IPI00006615.3	CLPB	9	10	22	2.442	0.002	32
IPI00291262.3	CLU	26	17	6	2.552	0.085	23
IPI00216682.5	CNN3	17	24	9	2.402	0.094	33
IPI00807339.2	COBLL1	8	3	11	4.071	0.024	14
IPI00010133.3	CORO1A	10	4	9	2.498	0.107	13
IPI00419731.4	CRELD2	12	6	13	2.405	0.021	19
IPI00295387.5	CRLF3	20	2	12	6.661	0.001	14
IPI00647073.1	CUL2	13	6	15	2.776	0.032	21
IPI00013892.1	CYTH3	8	8	3	2.402	0.200	11
IPI00071483.1	DDX4	4	21	9	2.102	0.022	30
IPI00015799.2	DGAT1	10	3	12	4.441	0.007	15
IPI00006433.6	DNAJC16	8	10	3	3.002	0.082	13
IPI00830108.1	DNAJC2	21	25	9	2.502	0.006	34
IPI00257508.4	DPYSL2	22	26	6	3.903	0.006	32
IPI00293251.5	DST	6	12	23	2.128	0.028	35
IPI00185038.3	DUOX1	10	16	7	2.059	0.020	23
IPI00096972.5	EHMT2	4	3	8	2.961	0.049	11
IPI00003921.2	EPB41	11	7	13	2.062	0.043	20
IPI00384975.4	EPB41L1	8	16	7	2.059	0.077	23
IPI00010338.1	F3	26	41	16	2.308	0.021	57
IPI00031670.6	FAM114A1	10	4	8	2.220	0.196	12
IPI00178750.3	FAM192A	25	5	10	2.220	0.166	15
IPI00910530.1	FGFR2	2	8	3	2.402	0.188	11
IPI00456630.6	FNDC3A	2	4	9	2.498	0.071	13
IPI00009057.2	G3BP2	11	14	4	3.153	0.046	18
IPI00552587.1	GADD45GIP1	35	13	25	2.135	0.005	38
IPI00030229.4	GALE	15	5	10	2.220	0.128	15

IPI00216159.14	GFPT2	8	4	10	2.776	0.029	14
IPI00005132.3	GNL3L	10	4	11	3.053	0.074	15
IPI00005677.1	GNPAT	6	4	9	2.498	0.139	13
IPI00186721.2	GOPC	10	3	11	4.071	0.014	14
IPI00478657.4	GRSF1	21	17	7	2.188	0.080	24
IPI00012948.3	HBEGF	10	0	14	4.648	0.000	14
IPI00010590.2	HELLS	20	13	33	2.818	0.006	46
IPI00029193.1	HGFAC	5	4	26	7.216	0.000	30
IPI00021770.1	HMGCR	14	26	4	5.855	0.002	30
IPI00008475.1	HMGCS1	28	169	57	2.671	0.000	226
IPI00008934.1	HMGCS2	3	21	5	3.783	0.001	26
IPI00011970.3	HSD17B7	17	12	4	2.702	0.007	16
IPI00555915.1	HSP90AB6P	7	31	12	2.327	0.035	43
IPI00024284.5	HSPG2	3	8	18	2.498	0.100	26
IPI00220014.2	IDI1	28	17	5	3.063	0.006	22
IPI00293735.2	IKBKAP	12	5	11	2.442	0.079	16
IPI00290198.3	IL18	17	4	8	2.220	0.100	12
IPI00759472.1	INCENP	10	5	15	3.331	0.020	20
IPI00099650.2	JAG1	5	10	3	3.002	0.109	13
IPI00008965.1	JUN	13	21	4	4.729	0.010	25
IPI00289547.4	JUND	10	10	4	2.252	0.042	14
IPI00299554.3	KIF14	9	9	19	2.344	0.008	28
IPI00044751.5	KIF20B	12	7	24	3.806	0.001	31
IPI00000769.2	KIF22	16	3	10	3.701	0.010	13
IPI00001458.1	KNTC1	5	5	12	2.664	0.132	17
IPI00016458.2	L2HGDH	6	5	10	2.220	0.052	15
IPI00000070.1	LDLR	15	38	15	2.282	0.005	53
IPI00937839.1	LOC100293655	19	16	31	2.151	0.006	47
IPI00847670.1	LOC440043	20	53	21	2.273	0.061	74
IPI00385128.3	LPCAT4	10	7	13	2.062	0.055	20
IPI00020557.1	LRP1	6	17	38	2.482	0.001	55
IPI00007321.2	LYPLA1	9	5	10	2.220	0.142	15
IPI00301082.1	MAGEA1	7	13	3	3.903	0.041	16
IPI00065350.1	MAGEB18	8	8	3	2.402	0.119	11
IPI00297989.4	MAGEB6	5	9	3	2.702	0.162	12
IPI00009542.1	MAGED2	19	8	16	2.220	0.043	24
IPI00025323.7	MAP9	3	11	1	9.908	0.051	12
IPI00185037.9	MARK1	6	5	10	2.220	0.103	15
IPI00064797.1	MARK4	5	3	9	3.331	0.048	12
IPI00029275.1	MFI2	9	14	26	2.062	0.052	40
IPI00024266.3	MGST3	22	8	3	2.402	0.107	11
IPI00418290.1	MRPL14	21	10	4	2.252	0.043	14
IPI00010278.6	MRPS30	7	8	3	2.402	0.052	11

IPI00030273.1	MST1R	6	3	10	3.701	0.023	13
IPI00022498.1	MT2A	61	21	7	2.702	0.059	28
IPI00022745.1	MVD	11	14	5	2.522	0.039	19
IPI00007858.1	MYH13	3	31	13	2.148	0.082	44
IPI00027255.1	MYL6B	24	62	25	2.234	0.060	87
IPI00747787.2	NCAPD3	9	3	9	3.331	0.111	12
IPI00641645.1	NFIA	5	3	8	2.961	0.144	11
IPI00643720.3	OGDHL	6	13	3	3.903	0.096	16
IPI00015143.1	ORC5L	17	4	9	2.498	0.153	13
IPI00014301.3	OXA1L	4	8	3	2.402	0.091	11
IPI00432527.1	PABPCP2	8	15	6	2.252	0.181	21
IPI00027009.2	PACSIN2	16	5	13	2.887	0.007	18
IPI00240675.2	PDCD4	26	16	31	2.151	0.001	47
IPI00168698.1	PDZD8	6	3	8	2.961	0.054	11
IPI00219568.4	PGK2	13	50	18	2.502	0.018	68
IPI00025463.3	PHLDA1	8	5	10	2.220	0.076	15
IPI00022149.1	PIP5K1A	10	13	4	2.927	0.045	17
IPI00030362.1	PLP2	8	18	36	2.220	0.014	54
IPI00024129.1	PPIC	8	10	4	2.252	0.159	14
IPI00006298.2	PPIG	5	7	14	2.220	0.006	21
IPI00045550.4	PPP1R9B	14	10	2	4.504	0.016	12
IPI00026994.3	PRAF2	11	3	8	2.961	0.127	11
IPI00027704.5	PRIM1	20	5	10	2.220	0.153	15
IPI00295988.4	PROM2	10	13	30	2.562	0.001	43
IPI00028006.1	PSMB2	30	10	4	2.252	0.165	14
IPI00107831.4	PTPRF	9	4	15	4.163	0.005	19
IPI00014376.5	RAB31	12	6	13	2.405	0.010	19
IPI00102752.2	RBM15	17	9	23	2.837	0.000	32
IPI00000686.2	RBM19	9	4	8	2.220	0.064	12
IPI00021626.2	RBM42	9	12	22	2.035	0.010	34
IPI00154352.2	RER1	27	3	11	4.071	0.036	14
IPI00465059.4	RHOT2	16	5	10	2.220	0.029	15
IPI00002408.4	RPAP3	26	8	20	2.776	0.058	28
IPI00893680.1	RPL10	22	54	15	3.243	0.004	69
IPI00868816.1	RPL12P38	38	32	12	2.402	0.030	44
IPI00219153.4	RPL22	32	56	22	2.293	0.053	78
IPI00030179.3	RPL7P32	40	122	54	2.035	0.022	176
IPI00008527.3	RPLP1	68	20	6	3.002	0.024	26
IPI00013296.3	RPS18	39	176	79	2.007	0.054	255
IPI00012493.1	RPS20	26	100	30	3.002	0.010	130
IPI00187140.1	RPS26P11	19	33	12	2.477	0.073	45
IPI00746004.2	RPS27L	35	44	16	2.477	0.020	60
IPI00302740.8	RPS4Y1	24	94	42	2.016	0.001	136

IPI00017526.1	S100P	39	35	11	2.866	0.025	46
IPI00329108.4	SCEL	14	18	3	5.404	0.002	21
IPI00106642.4	SDF2L1	23	22	3	6.605	0.005	25
IPI00871605.2	SELT	28	5	10	2.220	0.189	15
IPI00216139.3	SEPT6	13	13	24	2.050	0.014	37
IPI00307733.5	SETD2	3	13	4	2.927	0.122	17
IPI00103419.4	SF4	12	4	9	2.498	0.086	13
IPI00022649.3	SLC12A2	7	7	14	2.220	0.070	21
IPI00015473.3	SLC1A3	11	6	13	2.405	0.019	19
IPI00023035.2	SLC20A1	5	9	4	2.027	0.088	13
IPI00154528.3	SMC6	14	6	14	2.590	0.105	20
IPI00297714.2	SNCG	48	14	6	2.102	0.139	20
IPI00438170.3	SNX12	12	5	10	2.220	0.079	15
IPI00012645.1	SPTBN2	16	27	53	2.179	0.002	80
IPI00219168.7	SPTBN5	2	9	2	4.053	0.036	11
IPI00218486.5	SSH3	10	12	3	3.603	0.049	15
IPI00004312.1	STAT2	9	9	2	4.053	0.023	11
IPI00299149.1	SUMO2	35	55	21	2.359	0.038	76
IPI00328144.6	TAF2	9	5	11	2.442	0.021	16
IPI00159322.4	TCF20	5	4	10	2.776	0.041	14
IPI00296099.6	THBS1	25	128	36	3.203	0.003	164
IPI00478062.2	TLE2	9	11	3	3.303	0.089	14
IPI00743888.2	TMUB2	11	9	4	2.027	0.163	13
IPI00170752.5	TNS4	9	12	0	2.709	0.000	12
IPI00941588.1	TOM1	12	10	3	3.002	0.030	13
IPI00328178.3	TOM1L2	19	6	12	2.220	0.068	18
IPI00016676.1	TOMM20	16	4	9	2.498	0.093	13
IPI00301631.5	TOR3A	7	3	8	2.961	0.044	11
IPI00004324.1	TRAPPC3	28	6	13	2.405	0.103	19
IPI00426252.1	TRIM27	14	4	13	3.608	0.023	17
IPI00297113.1	TRIM32	4	11	3	3.303	0.126	14
IPI00003505.3	TRIP13	14	5	10	2.220	0.132	15
IPI00216293.6	TST	14	6	11	2.035	0.024	17
IPI00300504.5	UPF2	7	6	11	2.035	0.147	17
IPI00009329.2	UTRN	8	8	15	2.082	0.021	23
IPI00334159.6	VBP1	33	21	8	2.364	0.016	29
IPI00090327.1	VPS45	15	19	36	2.104	0.055	55
IPI00017160.3	VTA1	21	16	7	2.059	0.110	23
IPI00002564.3	XRCC1	9	7	13	2.062	0.056	20
IPI00477949.1	ZMYM4	9	6	12	2.220	0.193	18
IPI00418316.6	ZMYND8	9	3	8	2.961	0.110	11

Table B2. Gefitinib inhibition signature. Accession numbers, spectral counts, fold changes, and p-values for proteins identified from QuasiTel comparison of EGF stimulated and gefitinib-treated cell proteomes. Results were filtered to have at least 11 spectra across all analysis, ≥ 2.0 fold change (base 2 log rate ratio of 1.0) and a p-value ≤ 0.20. rev_ prefix indicates reverse database hit. Protein-level FDR = 9.2%

Protein	HUGO	Coverage	EGF counts	GEF counts	Fold change	Quasi p-value	Total Counts
rev_IPI00007175.3		14	32	9	3.354	0.024	41
rev_IPI00010903.2		2	15	3	4.716	0.003	18
rev_IPI00023868.1		1	12	1	11.319	0.012	13
rev_IPI00027180.1		4	70	26	2.540	0.019	96
rev_IPI00102678.2		1	10	1	9.433	0.101	11
rev_IPI00171087.7		7	8	3	2.515	0.165	11
rev_IPI00217602.5		8	8	3	2.515	0.191	11
rev_IPI00291800.1		2	10	27	2.862	0.019	37
rev_IPI00301395.4		4	19	6	2.987	0.041	25
rev_IPI00302270.3		1	10	2	4.716	0.041	12
rev_IPI00642259.2		2	9	3	2.830	0.180	12
rev_IPI00741537.5		2	20	5	3.773	0.035	25
IPI00015826.2	ABCB10	6	3	11	3.887	0.020	14
IPI00329245.7	ANKLE2	19	9	2	4.245	0.120	11
IPI00253323.3	ANKRD57	24	3	8	2.827	0.093	11
IPI00014232.1	ARL6IP1	8	19	1	17.922	0.003	20
IPI00328526.6	ARPP19	39	6	13	2.297	0.109	19
IPI00940046.1	ASAH1	11	7	15	2.272	0.005	22
IPI00102575.4	ATAD5	6	3	8	2.827	0.147	11
IPI00289499.3	ATIC	31	18	38	2.238	0.062	56
IPI00034277.1	ATP13A1	8	1	11	11.661	0.005	12
IPI00847139.1	ATP13A3	6	4	9	2.385	0.189	13
IPI00294158.1	BLVRA	7	3	8	2.827	0.142	11
IPI00020017.1	C10orf116	67	42	17	2.330	0.016	59
IPI00016925.1	C12orf57	34	4	9	2.385	0.143	13
IPI00107728.4	C16orf62	5	4	8	2.120	0.199	12
IPI00554560.4	C16orf88	17	13	30	2.446	0.048	43
IPI00016634.1	C20orf11	29	6	13	2.297	0.014	19
IPI00797771.1	C20orf117	9	10	3	3.144	0.101	13
IPI00027898.3	C21orf70	16	5	10	2.120	0.152	15
IPI00299387.3	C3orf1	24	15	33	2.332	0.006	48
IPI00419575.6	C7orf20	11	5	11	2.332	0.110	16
IPI00514301.3	CASK	11	7	21	3.180	0.004	28
IPI00220857.3	CAST	28	37	70	2.006	0.007	107

IPI00302647.4	CC2D1A	7	12	5	2.264	0.130	17
IPI00641630.1	CC2D1B	9	3	10	3.534	0.008	13
IPI00217059.5	CCDC50	16	3	9	3.180	0.136	12
IPI00334743.4	CCNY	13	6	12	2.120	0.087	18
IPI00185371.5	CCNYL1	11	4	9	2.385	0.023	13
IPI00298851.4	CD151	8	10	4	2.358	0.163	14
IPI00374740.3	CD47	8	9	4	2.122	0.043	13
IPI00657752.1	CD81	11	3	10	3.534	0.009	13
IPI00005822.2	CDC23	14	5	12	2.544	0.017	17
IPI00465387.2	CDCA2	7	2	9	4.771	0.062	11
IPI00303099.2	CDCA8	9	3	10	3.534	0.006	13
IPI00031681.1	CDK2	23	14	6	2.201	0.089	20
IPI00009384.5	CDKN1A	18	14	1	13.206	0.001	15
IPI00101532.5	CEP55	15	6	12	2.120	0.027	18
IPI00238469.6	CEP97	6	3	8	2.827	0.022	11
IPI00306853.2	CHST3	8	8	3	2.515	0.159	11
IPI00021944.1	CLDN4	12	12	5	2.264	0.159	17
IPI00101942.1	CLMN	6	8	3	2.515	0.146	11
IPI00291262.3	CLU	26	17	36	2.245	0.026	53
IPI00303158.3	CMAS	16	15	7	2.021	0.048	22
IPI00430812.6	CNBP	29	41	13	2.975	0.010	54
IPI00216682.5	CNN3	17	24	10	2.264	0.029	34
IPI00807339.2	COBLL1	8	3	10	3.534	0.059	13
IPI00009365.3	COX16	20	6	12	2.120	0.091	18
IPI00645310.1	CPNE2	9	30	7	4.043	0.011	37
IPI00295469.5	CPNE6	4	29	6	4.559	0.006	35
IPI00332395.2	CPNE9	3	29	6	4.559	0.006	35
IPI00027713.1	CREB1	17	14	6	2.201	0.042	20
IPI00797918.1	CRELD2	13	3	8	2.827	0.066	11
IPI00019918.5	DDX19A	20	5	10	2.120	0.074	15
IPI00008943.3	DDX19B	18	5	10	2.120	0.179	15
IPI00007208.4	DDX41	17	13	25	2.039	0.015	38
IPI00015799.2	DGAT1	10	3	10	3.534	0.087	13
IPI00909589.1	DHX38	15	4	10	2.650	0.115	14
IPI00006433.6	DNAJC16	8	10	1	9.433	0.021	11
IPI00010348.1	DNASE2	6	9	2	4.245	0.046	11
IPI00816460.2	DST	10	13	39	3.180	0.000	52
IPI00029658.1	EFEMP1	12	3	9	3.180	0.116	12
IPI00096972.5	EHMT2	4	3	13	4.594	0.011	16
IPI00374054.3	ENAH	23	17	33	2.058	0.023	50
IPI00029631.1	ERH	31	70	31	2.130	0.027	101
IPI00024167.1	ESF1	14	9	19	2.238	0.048	28
IPI00019427.4	EXOC1	7	3	10	3.534	0.042	13

IPI00070643.6	FAF1	21	13	25	2.039	0.063	38
IPI00031670.6	FAM114A1	10	4	9	2.385	0.178	13
IPI00178750.3	FAM192A	25	5	15	3.180	0.017	20
IPI00030098.5	FAM50A	13	5	10	2.120	0.158	15
IPI00302641.1	FAT2	11	35	68	2.060	0.000	103
IPI00216159.14	GFPT2	8	4	8	2.120	0.125	12
IPI00010130.3	GLUL	6	4	10	2.650	0.053	14
IPI00328744.6	GNA12	7	19	7	2.560	0.019	26
IPI00027243.1	GNA15	14	3	8	2.827	0.134	11
IPI00031115.4	GOLGA1	9	5	10	2.120	0.139	15
IPI00186721.2	GOPC	10	3	8	2.827	0.047	11
IPI00218002.6	GPR110	8	4	10	2.650	0.017	14
IPI00011989.1	GRIN1	3	5	11	2.332	0.159	16
IPI00016725.2	GTF3C4	21	11	22	2.120	0.016	33
IPI00010463.5	GTPBP1	10	5	10	2.120	0.129	15
IPI00021924.1	H1FX	22	26	11	2.230	0.114	37
IPI00220994.3	H2AFY2	21	12	25	2.209	0.000	37
IPI00014220.2	HAUS5	5	3	8	2.827	0.070	11
IPI00170924.2	HINT3	35	5	10	2.120	0.028	15
IPI00171903.2	HNRNPM	50	441	199	2.090	0.003	640
IPI00555957.1	HSP90AA4P	17	87	37	2.218	0.035	124
IPI00555915.1	HSP90AB6P	7	31	12	2.437	0.026	43
IPI00008494.4	ICAM1	13	38	17	2.109	0.036	55
IPI00446765.2	INTS4	6	3	10	3.534	0.032	13
IPI00099650.2	JAG1	5	10	4	2.358	0.126	14
IPI00008965.1	JUN	13	21	7	2.830	0.025	28
IPI00289547.4	JUND	10	10	3	3.144	0.069	13
IPI00748360.2	KIAA1797	4	4	8	2.120	0.163	12
IPI00044751.5	KIF20B	12	7	18	2.726	0.019	25
IPI00375910.2	KRT26	7	153	63	2.291	0.023	216
IPI00019359.4	KRT9	13	72	28	2.426	0.011	100
IPI00296922.4	LAMB2	8	5	11	2.332	0.134	16
IPI00009030.1	LAMP2	4	31	11	2.658	0.003	42
IPI00005724.1	LANCL1	8	3	8	2.827	0.101	11
IPI00939286.1	LDHA	47	315	148	2.008	0.006	463
IPI00148061.3	LDHAL6A	10	69	24	2.712	0.031	93
IPI00554498.3	LDHC	8	65	23	2.666	0.035	88
IPI00004758.5	LDLRAP1	15	3	8	2.827	0.124	11
IPI00029397.5	LEPROTL1	9	3	9	3.180	0.028	12
IPI00791938.1	LLGL1	6	4	9	2.385	0.059	13
IPI00847670.1	LOC440043	20	53	16	3.125	0.012	69
IPI00397575.3	LRRC41	5	11	4	2.594	0.049	15
IPI00007321.2	LYPLA1	9	5	11	2.332	0.104	16

IPI00152900.2	LZIC	36	5	11	2.332	0.036	16
IPI00301082.1	MAGEA1	7	13	4	3.066	0.058	17
IPI00046955.9	MAGEB17	3	8	3	2.515	0.106	11
IPI00065350.1	MAGEB18	8	8	3	2.515	0.106	11
IPI00297989.4	MAGEB6	5	9	3	2.830	0.080	12
IPI00299085.3	MAGEC1	1	8	3	2.515	0.106	11
IPI00025323.7	MAP9	3	11	2	5.188	0.087	13
IPI00297191.2	MED14	5	9	4	2.122	0.097	13
IPI00027310.5	MEGF8	3	3	9	3.180	0.053	12
IPI00783001.1	METT5D1	14	4	8	2.120	0.135	12
IPI00293276.10	MIF	16	53	16	3.125	0.009	69
IPI00455518.5	MORC2	15	8	17	2.253	0.072	25
IPI00218495.3	MPG	17	3	8	2.827	0.102	11
IPI00007001.1	MRPL11	25	5	11	2.332	0.149	16
IPI00032872.3	MRPS16	26	3	8	2.827	0.030	11
IPI00006440.6	MRPS7	28	11	22	2.120	0.026	33
IPI00030273.1	MST1R	6	3	8	2.827	0.030	11
IPI00027255.1	MYL6B	24	62	17	3.440	0.002	79
IPI00018968.2	NAE1	13	9	17	2.002	0.111	26
IPI00747787.2	NCAPD3	9	3	9	3.180	0.102	12
IPI00644022.5	NCAPH2	8	4	8	2.120	0.162	12
IPI00005966.6	NDUFA12	16	4	9	2.385	0.080	13
IPI00180559.3	NET1	4	12	5	2.264	0.139	17
IPI00004845.4	NIPSNAP3	17	11	5	2.075	0.100	16
IPI00432527.1	PABPCP2	8	15	5	2.830	0.065	20
IPI00027009.2	PACSIN2	16	5	10	2.120	0.114	15
IPI00014808.1	PAFAH1B3	10	4	8	2.120	0.037	12
IPI00030009.4	PAPSS2	18	17	7	2.291	0.018	24
IPI00064457.4	PARP10	4	5	10	2.120	0.031	15
IPI00640304.1	PBRM1	13	14	30	2.272	0.009	44
IPI00240675.2	PDCD4	26	16	38	2.518	0.000	54
IPI00022095.3	PEG10	5	3	8	2.827	0.145	11
IPI00004534.4	PFAS	6	3	9	3.180	0.144	12
IPI00219568.4	PGK2	13	50	17	2.774	0.018	67
IPI00382788.6	PHF15	9	4	13	3.445	0.019	17
IPI00022149.1	PIP5K1A	10	13	6	2.044	0.032	19
IPI00010676.1	PLAUR	19	10	2	4.716	0.038	12
IPI00440688.4	POLDIP3	22	3	8	2.827	0.145	11
IPI00031960.2	POLR1A	11	13	25	2.039	0.044	38
IPI00006113.1	POLR2I	30	1	11	11.661	0.001	12
IPI00024698.1	PQBP1	11	10	20	2.120	0.060	30
IPI00027704.5	PRIM1	20	5	11	2.332	0.090	16
IPI00012322.1	PRKG2	4	35	16	2.063	0.010	51

IPI00329538.3	PRSS8	11	5	12	2.544	0.071	17
IPI00171199.5	PSMA3	22	26	9	2.725	0.002	35
IPI00926491.1	PTCD1	6	12	2	5.660	0.006	14
IPI00016373.3	RAB13	25	88	39	2.128	0.002	127
IPI00028481.1	RAB8A	26	71	22	3.044	0.001	93
IPI00024282.1	RAB8B	19	65	23	2.666	0.006	88
IPI00449923.1	RAI1	5	2	10	5.301	0.016	12
IPI00643041.3	RANP1	33	152	70	2.048	0.001	222
IPI00102752.2	RBM15	17	9	20	2.356	0.000	29
IPI00000686.2	RBM19	9	4	8	2.120	0.178	12
IPI00017367.6	RDX	19	100	29	3.253	0.000	129
IPI00154352.2	RER1	27	3	9	3.180	0.039	12
IPI00926466.1	RHOA	27	17	8	2.004	0.066	25
IPI00641330.1	RING1	17	4	8	2.120	0.174	12
IPI00017373.1	RPA3	33	18	7	2.426	0.013	25
IPI00002408.4	RPAP3	26	8	17	2.253	0.159	25
IPI00893680.1	RPL10	22	54	14	3.638	0.001	68
IPI00868816.1	RPL12P38	38	32	10	3.019	0.011	42
IPI00219153.4	RPL22	32	56	24	2.201	0.008	80
IPI00010153.5	RPL23	41	128	49	2.464	0.003	177
IPI00456758.4	RPL27A	32	74	21	3.324	0.001	95
IPI00219335.10	RPL3L	11	46	6	7.232	0.001	52
IPI00030179.3	RPL7P32	40	122	36	3.197	0.001	158
IPI00013296.3	RPS18	39	176	63	2.635	0.002	239
IPI00012493.1	RPS20	26	100	23	4.101	0.001	123
IPI00218606.7	RPS23	31	18	8	2.122	0.140	26
IPI00012750.3	RPS25	37	70	24	2.751	0.007	94
IPI00187140.1	RPS26P11	19	33	13	2.394	0.041	46
IPI00746004.2	RPS27L	35	44	19	2.184	0.025	63
IPI00302740.8	RPS4Y1	24	94	43	2.062	0.001	137
IPI00465287.2	RREB1	8	13	5	2.453	0.198	18
IPI00021766.5	RTN4	8	41	16	2.417	0.007	57
IPI00418394.2	RXRA	12	5	11	2.332	0.091	16
IPI00017526.1	S100P	39	35	6	5.502	0.017	41
IPI00303343.7	SCAF1	9	7	17	2.575	0.014	24
IPI00002441.2	SDC1	15	24	47	2.076	0.004	71
IPI00301618.6	SDCCAG1	10	9	17	2.002	0.163	26
IPI00307733.5	SETD2	3	13	4	3.066	0.156	17
IPI00005978.8	SFRS2	27	107	39	2.588	0.002	146
IPI00022649.3	SLC12A2	7	7	15	2.272	0.081	22
IPI00010420.2	SLC25A31	11	34	10	3.207	0.006	44
IPI00007188.5	SLC25A5	45	306	143	2.018	0.007	449
IPI00291467.7	SLC25A6	44	262	111	2.226	0.002	373

IPI00029267.1	SNRPB2	24	45	21	2.021	0.002	66
IPI00016572.1	SNRPG	24	17	37	2.307	0.016	54
IPI00045914.1	SPEN	9	13	35	2.854	0.002	48
IPI00012645.1	SPTBN2	16	27	59	2.317	0.028	86
IPI00219168.7	SPTBN5	2	9	2	4.245	0.034	11
IPI00004312.1	STAT2	9	9	4	2.122	0.066	13
IPI00386786.5	STX5	22	2	13	6.891	0.020	15
IPI00299149.1	SUMO2	35	55	14	3.706	0.004	69
IPI00216137.4	SYCP1	3	10	3	3.144	0.011	13
IPI00154565.14	SYTL1	6	4	9	2.385	0.085	13
IPI00296099.6	THBS1	25	128	59	2.046	0.019	187
IPI00742863.2	THEMIS	7	15	5	2.830	0.188	20
IPI00063729.4	THOC3	16	3	10	3.534	0.020	13
IPI00328985.1	THOC6	19	3	10	3.534	0.030	13
IPI00221206.1	TLE3	10	9	4	2.122	0.047	13
IPI00063334.3	TMEM41A	8	2	10	5.301	0.004	12
IPI00386760.2	TMEM48	9	5	10	2.120	0.027	15
IPI00419856.1	TNPO2	6	6	12	2.120	0.029	18
IPI00170752.5	TNS4	9	12	3	3.773	0.053	15
IPI00016676.1	TOMM20	16	4	12	3.180	0.022	16
IPI00000980.1	TOMM7	31	4	9	2.385	0.099	13
IPI00395631.3	TRAF7	10	3	12	4.241	0.012	15
IPI00004324.1	TRAPPC3	28	6	19	3.357	0.004	25
IPI00426252.1	TRIM27	14	4	8	2.120	0.195	12
IPI00297113.1	TRIM32	4	11	4	2.594	0.173	15
IPI00024151.3	TRUB2	21	3	8	2.827	0.027	11
IPI00000171.1	TSC22D4	13	9	3	2.830	0.097	12
IPI00386354.1	TTLL3	40	13	4	3.066	0.102	17
IPI00017454.4	TUBA4B	18	114	38	2.830	0.010	152
IPI00908469.1	TUBB6	37	243	102	2.247	0.010	345
IPI00409659.2	UBQLN2	8	4	9	2.385	0.131	13
IPI00305303.3	UFSP2	11	6	14	2.474	0.003	20
IPI00000733.4	UTP18	6	4	8	2.120	0.159	12
IPI00009329.2	UTRN	8	8	19	2.518	0.014	27
IPI00031804.1	VDAC3	38	103	41	2.370	0.002	144
IPI00063784.3	VTI1B	17	2	9	4.771	0.057	11
IPI00170786.1	WBP11	16	17	33	2.058	0.024	50
IPI00218240.3	WHSC1	5	2	12	6.361	0.002	14
IPI00009326.1	YAP1	11	4	9	2.385	0.122	13
IPI00004337.2	ZBTB11	7	3	8	2.827	0.155	11
IPI00329547.3	ZC3H13	6	4	13	3.445	0.009	17
IPI00010833.1	ZNF148	14	6	16	2.827	0.021	22
IPI00011631.6	ZW10	15	2	13	6.891	0.007	15

Table B3. Cetuximab inhibition signature. Accession numbers, spectral counts, fold changes, and p-values for proteins identified from QuasiTel comparison of EGF-stimulated and cetuximab-treated cell proteomes. Results were filtered to have at least 11 spectra across all analysis, ≥ 2.0 fold change (base 2 log rate ratio of 1.0) and a p-value ≤ 0.20. rev_ prefix indicates reverse database hit. Protein-level FDR = 10.0%

Protein	HUGO	Coverage	EGF counts	GEF counts	Fold Change	quasi p-value	Total Counts
rev_IPI00003923.1		6	9	3	2.931	0.067	12
rev_IPI00023283.3		2	20	8	2.442	0.080	28
rev_IPI00023868.1		1	12	5	2.345	0.170	17
rev_IPI00740019.2		4	3	8	2.730	0.092	11
rev_IPI00302270.3		1	10	3	3.256	0.071	13
rev_IPI00642126.3		1	4	11	2.815	0.105	15
rev_IPI00012345.2		5	8	3	2.605	0.150	11
IPI00002938.1	ABT1	16	9	4	2.198	0.063	13
IPI00020226.2	ACOX3	9	5	10	2.047	0.035	15
IPI00019353.4	AGK	12	8	3	2.605	0.066	11
IPI00152898.1	AP1S1	23	5	14	2.866	0.050	19
IPI00031030.1	APLP2	7	2	9	4.606	0.025	11
IPI00021841.1	APOA1	25	0	15	3.704	0.032	15
IPI00186903.4	APOL1	13	19	6	3.094	0.006	25
IPI00042580.4	APOO	17	15	6	2.442	0.040	21
IPI00218648.2	ARID4A	6	3	9	3.071	0.046	12
IPI00328526.6	ARPP19	39	6	13	2.218	0.039	19
IPI00008161.8	ATP12A	4	8	20	2.559	0.073	28
IPI00647099.2	ATP1A4	13	8	21	2.687	0.061	29
IPI00012851.2	ATP8B1	4	11	5	2.149	0.110	16
IPI00180154.4	ATXN2	6	3	10	3.412	0.011	13
IPI00554756.2	BLK	3	7	15	2.193	0.101	22
IPI00218054.2	C11orf31	25	3	8	2.730	0.104	11
IPI00031526.3	C19orf43	26	8	17	2.175	0.010	25
IPI00816419.1	C1orf151	44	7	14	2.047	0.067	21
IPI00797771.1	C20orf117	9	10	4	2.442	0.082	14
IPI00015101.2	C9orf167	16	16	7	2.233	0.030	23
IPI00641630.1	CC2D1B	9	3	8	2.730	0.062	11
IPI00217059.5	CCDC50	16	3	9	3.071	0.075	12
IPI00298851.4	CD151	8	10	3	3.256	0.055	13
IPI00017529.1	CD58	13	11	5	2.149	0.162	16
IPI00007811.1	CDK4	12	9	18	2.047	0.077	27
IPI00023530.7	CDK5	7	7	14	2.047	0.147	21
IPI00009384.5	CDKN1A	18	14	3	4.559	0.002	17

IPI00021944.1	CLDN4	12	12	3	3.908	0.025	15
IPI00303158.3	CMAS	16	15	7	2.093	0.056	22
IPI00807339.2	COBLL1	8	3	8	2.730	0.137	11
IPI00027988.1	CTCF	12	16	6	2.605	0.006	22
IPI00216003.4	CUL5	7	2	12	6.142	0.013	14
IPI00013892.1	CYTH3	8	8	3	2.605	0.090	11
IPI00291032.7	CYTSB	9	11	4	2.687	0.027	15
IPI00027547.2	DCD	61	0	15	2.659	0.000	15
IPI00335385.4	DCPS	16	11	5	2.149	0.057	16
IPI00063408.7	DHTKD1	11	12	5	2.345	0.074	17
IPI00031508.1	DHX8	13	19	9	2.062	0.002	28
IPI00004459.1	DIMT1L	13	10	4	2.442	0.100	14
IPI00010348.1	DNASE2	6	9	3	2.931	0.074	12
IPI00015905.1	EXOSC2	23	12	3	3.908	0.028	15
IPI00745613.2	EXOSC4	8	4	8	2.047	0.194	12
IPI00216605.1	FGFR2	2	7	15	2.193	0.095	22
IPI00170778.4	FNBP4	7	8	3	2.605	0.115	11
IPI00217490.5	FNDC3B	8	9	3	2.931	0.091	12
IPI00552587.1	GADD45GIP1	35	13	27	2.126	0.002	40
IPI00292753.7	GAPVD1	10	8	16	2.047	0.011	24
IPI00296635.5	GBE1	10	4	10	2.559	0.096	14
IPI00028565.4	GBP2	10	9	2	4.396	0.092	11
IPI00789740.1	GEMIN4	10	10	4	2.442	0.026	14
IPI00216159.14	GFPT2	8	4	11	2.815	0.017	15
IPI00002496.2	GMPPB	5	5	10	2.047	0.058	15
IPI00005677.1	GNPAT	6	4	10	2.559	0.096	14
IPI00011989.1	GRIN1	3	5	13	2.661	0.086	18
IPI00008494.4	ICAM1	13	38	16	2.320	0.010	54
IPI00018305.4	IGFBP3	21	8	3	2.605	0.155	11
IPI00399007.7	IGHG2	14	0	59	65.235	0.000	59
IPI00941837.1	IGHM	8	0	55	42.126	0.000	55
IPI00423463.1	IGHV4-31	16	1	90	92.126	0.000	91
IPI00185146.5	IPO9	10	13	29	2.283	0.028	42
IPI00099650.2	JAG1	5	10	3	3.256	0.040	13
IPI00008965.1	JUN	13	21	10	2.052	0.051	31
IPI00289547.4	JUND	10	10	3	3.256	0.017	13
IPI00060715.1	KCTD12	13	5	10	2.047	0.167	15
IPI00154283.4	KIAA1524	12	17	7	2.373	0.006	24
IPI00299554.3	KIF14	9	9	18	2.047	0.003	27
IPI00004758.5	LDLRAP1	15	3	8	2.730	0.060	11
IPI00552510.2	LMO7	18	30	10	2.931	0.002	40
IPI00025489.1	MAK	3	7	14	2.047	0.147	21
IPI00005741.1	MAPK13	16	8	3	2.605	0.123	11

IPI00028932.7	MAST3	5	4	8	2.047	0.185	12
IPI00028954.1	MCM3AP	10	5	16	3.276	0.021	21
IPI00556494.3	MED4	20	11	5	2.149	0.150	16
IPI00000784.1	MEF2D	12	5	10	2.047	0.143	15
IPI00300763.4	METAP2	24	18	8	2.198	0.089	26
IPI00073713.3	MSI2	21	3	9	3.071	0.046	12
IPI00031109.4	NDUFAF2	30	10	1	9.769	0.014	11
IPI00012315.2	NME3	10	3	8	2.730	0.078	11
IPI00604756.2	NRBP1	5	8	3	2.605	0.118	11
IPI00010196.1	NRIP1	3	8	3	2.605	0.042	11
IPI00306305.9	OBSL1	6	4	8	2.047	0.150	12
IPI00014301.3	OXA1L	4	8	3	2.605	0.161	11
IPI00030009.4	PAPSS2	18	17	8	2.076	0.023	25
IPI00064457.4	PARP10	4	5	12	2.457	0.018	17
IPI00072541.4	PCID2	16	9	3	2.931	0.125	12
IPI00922194.1	PCTK1	10	7	14	2.047	0.147	21
IPI00394661.4	PCTK3	11	7	15	2.193	0.093	22
IPI00552367.3	PDLIM5	26	8	3	2.605	0.123	11
IPI00419263.3	PECI	24	12	1	11.723	0.003	13
IPI00025463.3	PHLDA1	8	5	11	2.252	0.122	16
IPI00019551.1	PHLDA2	35	7	14	2.047	0.015	21
IPI00001813.5	PHRF1	9	9	4	2.198	0.198	13
IPI00010676.1	PLAUR	19	10	3	3.256	0.110	13
IPI00007948.2	POLR3C	14	10	2	4.885	0.057	12
IPI00301689.7	PPFIBP2	4	12	4	2.931	0.037	16
IPI00045550.4	PPP1R9B	14	10	3	3.256	0.018	13
IPI00027704.5	PRIM1	20	5	11	2.252	0.065	16
IPI00219616.7	PRPS1	23	6	12	2.047	0.138	18
IPI00028006.1	PSMB2	30	10	4	2.442	0.134	14
IPI00000787.1	PSMB9	9	7	19	2.778	0.004	26
IPI00218604.6	PTPN6	15	17	8	2.076	0.089	25
IPI00550882.3	PYCR1	19	5	11	2.252	0.162	16
IPI00102752.2	RBM15	17	9	20	2.275	0.000	29
IPI00009737.1	RRAGD	11	8	3	2.605	0.101	11
IPI00412713.4	SAMM50	14	9	18	2.047	0.009	27
IPI00023649.3	SBNO1	5	3	8	2.730	0.165	11
IPI00303343.7	SCAF1	9	7	15	2.193	0.055	22
IPI00103419.4	SF4	12	4	9	2.303	0.163	13
IPI00015476.1	SLC1A4	10	10	4	2.442	0.147	14
IPI00024305.1	SMAD3	13	8	3	2.605	0.087	11
IPI00386786.5	STX5	22	2	11	5.630	0.010	13
IPI00216137.4	SYCP1	3	10	2	4.885	0.006	12
IPI00159322.4	TCF20	5	4	8	2.047	0.172	12

IPI00005563.1	TINAGL1	4	5	12	2.457	0.131	17
IPI00221206.1	TLE3	10	9	2	4.396	0.015	11
IPI00307572.1	TMEM165	20	5	16	3.276	0.040	21
IPI00180240.2	TMSL3	41	11	2	5.373	0.156	13
IPI00016676.1	TOMM20	16	4	8	2.047	0.177	12
IPI00166704.1	TOMM5	31	9	4	2.198	0.150	13
IPI00004324.1	TRAPPC3	28	6	13	2.218	0.095	19
IPI00018971.8	TRIM21	10	5	12	2.457	0.048	17
IPI00297113.1	TRIM32	4	11	2	5.373	0.068	13
IPI00005634.3	TTC37	8	6	12	2.047	0.194	18
IPI00385712.3	TTF1	10	2	9	4.606	0.048	11
IPI00033516.1	TUBGCP3	10	10	4	2.442	0.144	14
IPI00305303.3	UFSP2	11	6	16	2.730	0.008	22
IPI00300504.5	UPF2	7	6	12	2.047	0.114	18
IPI00020515.3	USE1	20	9	4	2.198	0.040	13
IPI00419844.3	USP39	12	17	8	2.076	0.003	25
IPI00376439.1	VPS13B	2	4	10	2.559	0.151	14
IPI00418316.6	ZMYND8	9	3	9	3.071	0.106	12
IPI00328737.2	ZNF598	14	7	16	2.340	0.013	23
IPI00011631.6	ZW10	15	2	9	4.606	0.018	11

Table B4. Up- and down-regulated proteins from Venn diagram (Figure III-3) overlaps.

Proteins common in all three signatures EGFR inhibition Signature (13)	Proteins common between stimulation and cetuximab inhibition signature (15)	Proteins shared between cetuximab and gefitinib inhibition signature (18)	Proteins shared between gefitinib inhibition signature and stimulation signature (57)		
CCDC50	ATXN2	ARPP19	ARL6IP1	HSP90AB6P	RPAP3
CDKN1A	C11orf31	C20orf117	BLVRA	KIF20B	RPL10
CLDN4	CYTH3	CC2D1B	C21orf70	LOC440043	RPL12P38
COBLL1	FGFR2	CD151	CD81	LYPLA1	RPL22
GFPT2	GADD45GIP1	CMAS	CDC23	MAGEA1	RPL7P32
JAG1	GNPAT	DNASE2	CDCA8	MAGEB18	RPS18
JUN	KIF14	GRIN1	CEP55	MAGEB6	RPS20
JUND	OXA1L	ICAM1	CEP97	MAP9	RPS26P11
PRIM1	PHLDA1	LDLRAP1	CLU	MST1R	RPS27L
RBM15	PPP1R9B	PAPSS2	CNN3	MYL6B	RPS4Y1
TOMM20	PSMB2	PARP10	CRELD2	NCAPD3	S100P
TRAPPC3	SF4	PLAUR	DGAT1	PABPCP2	SETD2
TRIM32	TCF20	SCAF1	DNAJC16	PACSIN2	SLC12A2
	UPF2	STX5	DST	PDCD4	SPTBN2
	ZMYND8	SYCP1	EHMT2	PGK2	SPTBN5
		TLE3	FAM114A1	PIP5K1A	STAT2
		UFSP2	FAM192A	RBM19	SUMO2
		ZW10	GOPC	RER1	THBS1
			TNS4	TRIM27	UTRN

Table B5. A431 EGFR inhibition signature MRM data depicted in Figure III-4. Pre. *m/z* = precursor mass to charge ratio, Protein = HUGO name, NPA = normalized peak area, Std. D. = standard deviation, CV = coefficient of variation. Pro = proliferating cells, EGF = EGF-stimulated (30 nM for 4 h), GEF = gefitinib (500 nM) and EGF-treated, CET = cetuximab (10 µg/mL) and EGF-treated. Data is representative of three separate cultures. All precursor *m/z* have a charge of 2+ unless otherwise noted.

Peptide Sequence	Protein	Pre. *m/z*	NPA PRO	Std. D. PRO	CV (%) PRO	NPA EGF	Std. D. EGF	CV (%) EGF	NPA GEF	Std. D. GEF	CV (%) GEF	NPA CET	Std. D. CET	CV (%) CET
DQEWYDAEIAR	CCDC50	698.3124	0.042	0.003	6.88	0.031	0.001	3.52	0.043	0.007	16.77	0.044	0.003	6.31
SGEQAEGSPGGPGDSQGR	CDKN1A	836.8615	0.001	0.000	54.89	0.012	0.003	23.58	0.002	0.001	20.60	0.001	0.000	29.18
CTNCLEDESAK	CLDN4	663.7687	0.052	0.002	3.65	0.159	0.015	9.32	0.064	0.005	7.14	0.062	0.002	2.78
DQTASAPATPLVNK	COBL1	706.8726	0.049	0.001	1.95	0.044	0.002	3.63	0.055	0.002	2.76	0.061	0.001	2.01
DLESAQSLNR	JAG1	566.7833	0.278	0.025	9.02	0.424	0.030	6.99	0.314	0.020	6.39	0.359	0.013	3.60
NVTDEQEGFAEGFVR	JUN	849.3919	0.035	0.009	24.80	0.057	0.010	17.28	0.038	0.002	5.75	0.031	0.003	9.74
SQNTELASTASLLR	JUND	745.8941	0.034	0.002	5.55	0.059	0.001	1.58	0.041	0.003	7.76	0.047	0.001	3.12
VFEHFLENLDK	PRIM1	695.8537	0.025	0.001	4.23	0.019	0.003	14.33	0.027	0.003	11.01	0.018	0.005	27.69
LWVGGLGPWVPLAALAR	RBM15	888.5196	0.067	0.003	4.69	0.052	0.023	43.87	0.095	0.002	1.80	0.124	0.021	17.35
LPTISQR	TOMM20	407.7427	1.061	0.087	8.23	1.098	0.061	5.59	1.274	0.042	3.28	1.406	0.078	5.51
GALEMVQMAVEAK	TRAPPC3	688.8493	0.047	0.002	3.46	0.061	0.001	2.63	0.099	0.010	10.54	0.101	0.004	2.49
ELTLQDVELLK	TRIM32	650.8716	0.017	0.002	8.79	0.028	0.006	23.18	0.020	0.002	8.08	0.016	0.001	6.78

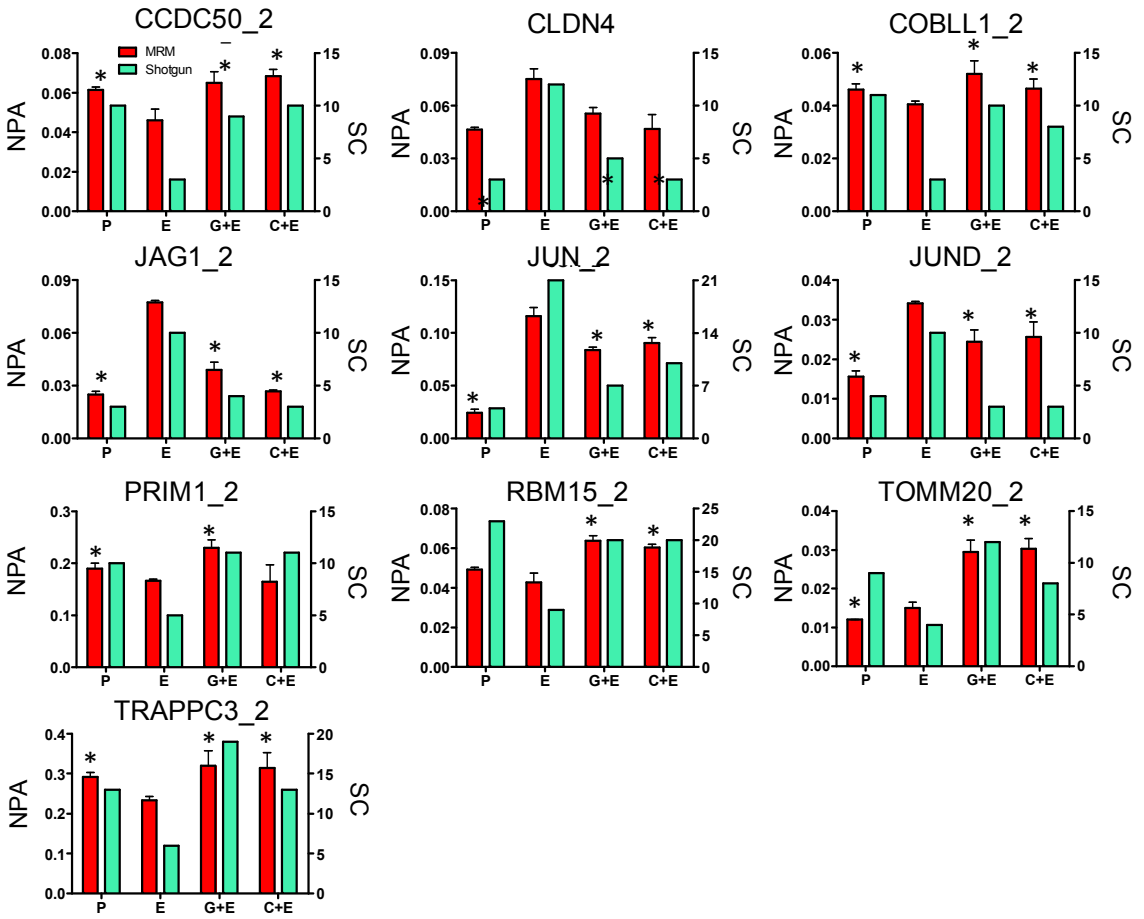

Figure B4. MRM and spectral count data for analysis of EGFR inhibition signature proteins using a second unique peptide in A431 cells. Each panel shows both MRM data (red bar-normalized to β-actin labeled reference peptide) and spectral count data (teal bar-total spectra identified in global proteome analyses) for each protein of interest across four A431 cell treatment conditions (see Table I legend for treatment conditions). MRM data shows normalized peak area quantified from one unique peptide for each target protein across three separate cultures. (*) Denotes significant difference between EGF-treated A431 cells as determined by Student's two-tailed, unpaired t-test.

Table B6. A431 EGFR inhibition signature MRM data depicted in Figure B4 for second unique peptide. Pre. *m/z* = precursor mass to charge ratio, Protein = HUGO name, NPA = normalized peak area, Std. Dev. = standard deviation, CV = coefficient of variation. Pro = proliferating cells, EGF = EGF-stimulated (30 nM for 4 h), GEF = gefitinib (500 nM) and EGF treated, CET = cetuximab (10 µg/mL) and EGF treated. Data is representative of three separate cultures. All precursor *m/z* have a charge of 2+ unless otherwise noted.

Peptide Sequence	Protein	Pre. m/z	NPA PRO	Std. Dev. PRO	CV (%) PRO	NPA EGF	Std. Dev. EGF	CV (%) EGF	NPA GEF	Std. Dev. GEF	CV (%) GEF	NPA CET	Std. Dev. CET	CV (%) CET
LQEEELLATQVDMR	CCDC50	837.9220++	0.061	0.002	2.52	0.046	0.006	12.46	0.065	0.006	8.78	0.068	0.004	5.16
VYDSLLALPQDLQAAR	CLDN4	886.9807++	0.046	0.001	3.08	0.075	0.006	7.63	0.055	0.003	6.21	0.047	0.008	17.45
DYQSQEPLDLTK	COBL1	718.8488++	0.046	0.002	4.76	0.040	0.001	3.29	0.052	0.005	9.72	0.046	0.004	7.60
QNTGVAHFEYQIR	JAG1	781.8891++	0.025	0.002	7.13	0.077	0.001	1.51	0.039	0.004	11.24	0.027	0.001	2.58
NSDLLTSPDVGLLK	JUN	736.4038++	0.024	0.003	13.09	0.116	0.008	7.04	0.084	0.002	2.95	0.090	0.005	5.86
VAASEEQEFAEGFVK	JUND	820.8938++	0.016	0.001	9.43	0.034	0.000	1.27	0.024	0.003	12.25	0.026	0.004	14.83
SGIVEYLSLVK	PRIM1	604.3503++	0.215	0.019	8.76	0.183	0.010	5.37	0.241	0.010	4.04	0.165	0.032	19.44
TAATSVPAYEPLDSLDR	RBM15	903.4494++	0.054	0.003	8.10	0.043	0.005	11.05	0.064	0.004	4.06	0.060	0.003	2.50
IVSAQSLAEDDVE	TOMM20	688.3330++	0.012	0.001	0.66	0.015	0.002	0.66	0.029	0.003	10.37	0.030	0.003	8.87
LIEDFLAR	TRAPPC3	488.7767++	0.292	0.011	3.75	0.234	0.001	0.22	0.320	0.037	11.62	0.314	0.039	12.25

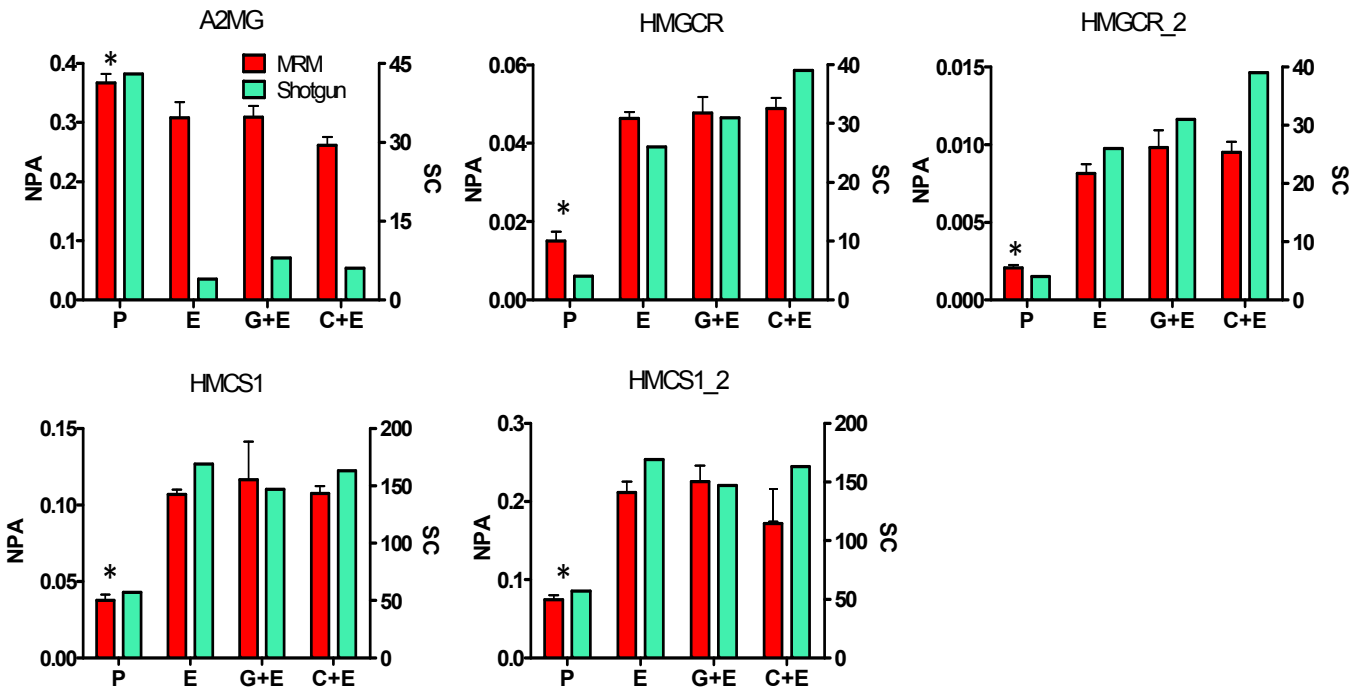

Figure B5. MRM and spectral count data for analysis of additional proteins in A431 cells. Each panel shows both MRM data (red bar-normalized to β-actin labeled reference peptide) and spectral count data (teal bar-total spectra identified in global proteome analyses) for each protein of interest across four A431 cell treatment conditions (see Table I legend for treatment conditions). MRM data shows normalized peak area quantified from one unique peptide for each target protein across three separate cultures. (*) Denotes significant difference between EGF-treated A431 cells as determined by Student's two-tailed, unpaired t-test.

Table B7. A431 MRM data for additional proteins depicted in Figure B5. Pre. *m/z* = precursor mass to charge ratio, Protein = HUGO name, NPA = normalized peak area, Std. Dev. = standard deviation, CV = coefficient of variation. Pro = proliferating cells, EGF = EGF-stimulated (30 nM for 4 h), GEF = gefitinib (500 nM) and EGF-treated, CET = cetuximab (10 μg/mL) and EGF-treated. Data is representative of three separate cultures. All precursor *m/z* have a charge of 2+ unless otherwise noted.

Peptide Sequence	Protein	Pre. m/z	NPA PRO	Std. Dev PRO	CV (%) PRO	NPA EGF	Std. Dev EGF	CV (%) EGF	NPA GEF	Std. Dev GEF	CV (%) GEF	NPA CET	Std. Dev CET	CV (%) CET
AAQVTIQSSGTFSSK	A2MG	756.3886++	0.3667	0.0150	4.08	0.3085	0.0260	8.44	0.3093	0.0188	6.09	0.2615	0.0145	5.53
FALSSNSQDEVR	HMGCR	676.8257++	0.0150	0.0023	15.25	0.0463	0.0017	3.60	0.0477	0.0040	8.46	0.0489	0.0026	5.34
VLEEEENKPNPVTQR	HMGCR	891.4550++	0.0021	0.0002	7.82	0.0082	0.0006	7.16	0.0098	0.0011	11.21	0.0095	0.0007	7.29
IGVFSYGSGLAATLYSLK	HMCS1	924.0011++	0.0377	0.0038	10.05	0.1069	0.0031	2.94	0.1164	0.0252	21.60	0.1075	0.0050	4.61
NSIYSGLEAFGDVK	HMCS1	750.3725++	0.0741	0.0063	8.57	0.2116	0.0140	6.61	0.2257	0.0203	9.01	0.1716	0.0027	1.56

Table B8. DiFi cell EGFR inhibition signature MRM data depicted in Figure III-5. Pre. *m/z* = precursor mass to charge ratio, Protein = HUGO name, NPA = normalized peak area, Std. Dev. = standard deviation, CV = coefficient of variation. Pro = proliferating cells, EGF = EGF-stimulated (30 nM for 4 h), GEF = gefitinib (500 nM) and EGF-treated, CET = cetuximab (10 µg/mL) and EGF-treated. Data is representative of three separate cultures. All precursor *m/z* have a charge of 2+ unless otherwise noted.

Peptide Sequence	Protein	Pre. m/z	NPA PRO	Std. Dev. PRO	CV (%) PRO	NPA EGF	Std. Dev. EGF	CV (%) EGF	NPA GEF	Std. Dev. GEF	CV (%) GEF	NPA CET	Std. Dev. CET	CV (%) CET
DQEWYDAEIAR	CCDC50	698.3124++	0.045	0.003	7.14	0.037	0.004	10.50	0.057	0.005	8.90	0.050	0.003	5.56
CTNCLEDESAK	CLDN4	663.7687++	0.040	0.002	4.73	0.046	0.004	8.73	0.031	0.002	6.47	0.035	0.004	11.45
DQTASAPATPLVNK	COBL1	706.8726++	0.011	0.001	5.39	0.009	0.000	2.31	0.010	0.000	1.61	0.011	0.000	0.44
DLESAQSLNR	JAG1	566.7833++	0.159	0.002	1.10	0.186	0.013	7.17	0.125	0.005	4.13	0.145	0.011	7.88
NVTDEQEGFAEGFVR	JUN	849.3919++	0.024	0.001	3.16	0.030	0.002	6.77	0.023	0.000	1.21	0.024	0.001	2.12
SQNTELASTASLLR	JUND	745.8941++	0.017	0.001	5.34	0.016	0.001	5.06	0.018	0.002	12.02	0.016	0.001	6.40
VFEHFLENLDK	PRIM1	695.8537++	0.094	0.015	15.72	0.092	0.006	6.83	0.089	0.010	10.91	0.073	0.050	67.90
LWVGGLGPWVPLAALAR	RBM15	888.5196++	0.015	0.001	7.46	0.013	0.001	4.83	0.016	0.000	1.17	0.017	0.001	5.87
GALEMVQMAVEAK	TRAPPC3	688.8493++	0.065	0.002	3.73	0.046	0.001	1.60	0.051	0.001	1.53	0.054	0.002	2.94
ELTLQDVELLK	TRIM32	650.8716++	0.019	0.001	3.29	0.022	0.000	0.44	0.019	0.001	7.80	0.019	0.000	2.63
LPTISQR	TOMM20	407.7427++	0.673	0.052	7.79	0.536	0.028	5.24	0.601	0.017	2.83	0.641	0.027	4.13

Table B9. HCT-116 cells EGFR inhibition signature MRM data depicted in Figure III-6. Pre. *m/z* = precursor mass to charge ratio, Protein = HUGO name, NPA = normalized peak area, Std. Dev. = standard deviation, CV = coefficient of variation. Pro = proliferating cells, EGF = EGF-stimulated (30 nM for 4 h), GEF = gefitinib (500 nM) and EGF-treated, CET = cetuximab (10 µg/mL) and EGF-treated. Data is representative of three separate cultures. All precursor *m/z* have a charge of 2+ unless otherwise noted.

Peptide Sequence	Protein	Pre. m/z	NPA PRO	Std. Dev. PRO	CV (%) PRO	NPA EGF	Std. Dev. EGF	CV (%) EGF	NPA GEF	Std. Dev. GEF	CV (%) GEF	NPA CET	Std. Dev. CET	CV (%) CET
DQEWYDAEIAR	CCDC50	698.3124++	0.018	0.002	8.781	0.016	0.001	3.835	0.019	0.001	4.009	0.020	0.002	9.861
CTNCLEDESAK	CLDN4	663.7687++	0.018	0.002	11.012	0.021	0.003	16.189	0.020	0.003	15.486	0.019	0.002	9.239
DLESAQSLNR	JAG1	566.7833++	0.173	0.023	13.317	0.178	0.014	7.606	0.166	0.021	12.716	0.161	0.019	12.002
NVTDEQEGFAEGFVR	JUN	849.3919++	0.021	0.001	4.257	0.026	0.003	10.257	0.025	0.002	8.971	0.021	0.003	15.174
SQNTELASTASLLR	JUND	745.8941++	0.021	0.002	8.732	0.027	0.003	10.541	0.020	0.000	2.354	0.023	0.003	12.982
GALEMVQMAVEAK	TRAPPC3	688.8493++	0.057	0.003	4.759	0.047	0.024	52.209	0.060	0.003	5.823	0.056	0.001	1.197
ELTLQDVELLK	TRIM32	650.8716++	0.029	0.001	2.949	0.030	0.002	7.284	0.030	0.000	0.757	0.030	0.003	8.906
LPTISQR	TOMM20	407.7427++	0.882	0.013	1.426	0.849	0.043	5.086	0.898	0.096	10.672	0.898	0.096	10.672

Table B10. DiFi xenograft MRM data depicted in Figure III-8. Pre. *m/z* = precursor mass to charge ratio, Protein = HUGO name, NPA = normalized peak area, Std. Dev. = standard deviation, CV = coefficient of variation. Tumor bearing mice were treated with 40 mg/kg cetuximab (CET) or saline (vehicle) intraperitoneally every three days for one week (three total injections). Data is representative of four separate tissue biopsies. All precursor *m/z* have a charge of 2+ unless otherwise noted.

Peptide Sequence	Protein	Pre. m/z	NPA Vehicle	Std. Dev. Vehicle	CV (%) Vehicle	NPA CET	Std. Dev. CET	CV (%) CET
DQEWYDAEIAR	CCDC50	698.3124++	0.0069	0.0026	37.1862	0.0072	0.0026	36.4968
CTNCLEDESAK	CLDN4	663.7687++	0.0125	0.0014	11.5945	0.0079	0.0009	11.4793
DQTASAPATPLVNK	COBL1	706.8726++	0.0025	0.0004	15.9557	0.0043	0.0020	45.6175
DLESAQSLNR	JAG1	566.7833++	0.0890	0.0037	4.1588	0.0697	0.0046	6.5510
NVTDEQEGFAEGFVR	JUN	849.3919++	0.0058	0.0006	10.9894	0.0041	0.0003	7.7912
LWVGGLGPWVPLAALAR	RBM15	888.5196++	0.0052	0.0009	17.1928	0.0043	0.0006	14.0857
GALEMVQMAVEAK	TRAPPC3	688.8493++	0.0109	0.0009	8.0546	0.0140	0.0011	8.1909
ELTLQDVELLK	TRIM32	650.8716++	0.0085	0.0009	10.3832	0.0048	0.0014	29.4158

Table B11. HCT-116 xenograft MRM data depicted in Figure III-9. Pre. *m/z* = precursor mass to charge ratio, Protein = HUGO name, NPA = normalized peak area, Std. Dev. = standard deviation, CV = coefficient of variation. Tumor bearing mice were treated with 40 mg/kg cetuximab (CET) or saline (vehicle) intraperitoneally every three days for one week (three total injections). Data is representative of four separate tissue biopsies. All precursor *m/z* have a charge of 2+ unless otherwise noted.

Peptide Sequence	Protein	Pre. m/z	NPA	Std. Dev.	CV (%)	NPA	Std. Dev.	CV (%)
			Vehicle	Vehicle	Vehicle	CET	CET	CET
DQEWYDAEIAR	CCDC50	698.3124++	0.0055	0.0013	24.4692	0.0052	0.0014	26.4362
CTNCLEDESAK	CLDN4	663.7687++	0.0048	0.0012	25.5800	0.0046	0.0006	13.3858
DLESAQSLNR	JAG1	566.7833++	0.0500	0.0045	9.0159	0.0504	0.0030	5.9767
NVTDEQEGFAEGFVR	JUN	849.3919++	0.0031	0.0004	14.0274	0.0030	0.0003	8.7231
LWVGGLGPWVPLAALAR	RBM15	888.5196++	0.0011	0.0004	38.8846	0.0027	0.0008	30.3899
GALEMVQMAVEAK	TRAPPC3	688.8493++	0.0046	0.0008	18.3772	0.0071	0.0015	21.5939
ELTLQDVELLK	TRIM32	650.8716++	0.0036	0.0007	20.4497	0.0039	0.0007	17.0449
LPTISQR	TOMM20	407.7427++	0.0509	0.0094	18.5009	0.0651	0.0066	10.1000

Table B12. MRM data from Ménétrier's disease patient for EGFR inhibition signature proteins depicted in Figure III-11. Pre. *m/z* = precursor mass to charge ratio, Protein = HUGO name, NPA = normalized peak area, Std. Dev. = standard deviation, CV = coefficient of variation. All precursor *m/z* have a charge of 2+ unless otherwise noted. Normalized peak areas, standard deviations and CVs from are shown for each of the three separate biopsies (from a single patient); and the average, standard deviation, and %CV have been calculated for each timepoint. Baseline = prior to cetuximab-treatment, 1 day, 1 week, 1 month and 4 months = time post initial cetuximab treatment.

Peptide Sequence	Protein	Pre. m/z	NPA Baseline	Std. Dev. Baseline	CV (%) Baseline	NPA 1 day	Std. Dev. 1 day	CV (%) 1 day	NPA 1 week	Std. Dev. 1 week	CV (%) 1 week
DQEWYDAEIAR	CCDCC50	698.3124++	0.0051	0.0007	14.2532	0.0037	0.0003	6.8715	0.0038	0.0006	17.1559
CTNCLEDESAK	CLDN4	663.7687++	0.0078	0.0005	6.8395	0.0051	0.0001	2.6273	0.0056	0.0009	16.3332
DQTASAPATPLVNK	COBL1	706.8726++	0.0066	0.0003	4.6491	0.0050	0.0004	7.2467	0.0060	0.0008	13.8583
DLESAQSLNR	JAG1	566.7833++	0.0410	0.0026	6.2662	0.0292	0.0032	10.8415	0.0328	0.0041	12.4525
NVTDEQEGFAEGFVR	JUN	849.3919++	0.0014	0.0002	16.8748	0.0014	0.0002	16.8748	0.0015	0.0003	17.5052
SQNTELASTASLLR	JUND	745.8941++	0.0030	0.0007	24.3173	0.0022	0.0001	6.6875	0.0027	0.0006	21.3102
GALEMVQMAVEAK	TRAPPC3	688.8493++	0.0100	0.0022	21.9320	0.0145	0.0027	18.7889	0.0164	0.0014	8.6232
ELTLQDVELLK	TRIM32	650.8716++	0.0024	0.0008	32.7586	0.0017	0.0014	80.6941	0.0039	0.0012	31.0642
LPTISQR	TOMM20	407.7427++	7.9892	1.2856	16.0912	3.7432	0.1697	4.5340	4.5989	1.2768	27.7624

APPENDIX C

Data to Chapter IV:

SITE-SPECIFIC, QUANTITATIVE COMPARISON OF EGFR PHOSPHORYLATION CHANGES INDUCED BY EGF AND INHIBITORS

Table C1. EGFR phosphorylated and nonphosphorylated peptides and transitions selected for LC-pSRM-MS. Peptides marked with *p* are phosphorylated. Those marked with ^ are isotopically labeled at the indicated amino acid.

Peptide[1]	Precursor *m/z*	Product *m/z*
MHLPSPTDSNF *p*YR	822.8	1263.5 (y_{10}), 1079.4 (y_8), 766.3 (y_5), 688.8 (y_{11}^{2+}), 382.2 (b_3)
MHLPSPTDSNFYR	782.9	1296.6 (y_{11}), 1183.5 (y_{10}), 648.8 (y_{11}^{2+}), 592.3 (y_{10}^{2+}), 1390.6 (b_{12})
MHLP*p*SPTDSNFYR – MS^3	822.84 → 773.85	534.7 (y_9^{2+}), 639.8 (y_{11}^{2+}), 861.4 (b_8), 1165.5 (y_{10}), 1278.6 (y_{11})
RPAGSVQNPV *p*YHNQPLNPAPSR	827.1	1473.7 (y_{12}), 1113.5 (y_{20}^{2+}), 1078.0 (y_{19}^{2+}), 892.4 (y_{15}^{2+}), 977.0 (b_{17}^{2+})
RPAGSVQNPVYHNQPLNPAPSR	800.4	851.5 (y_8), 1009.5 (y_{18}^{2+}), 710.9 (b_{13}^{2+}), 774.9 (b_{14}^{2+}), 937.0 (b_{17}^{2+})
GSHQISLDNPD *p*YQQDFFPK	772.7	1267.5 (y_9), 1152.5 (y_8), 797.3 (y_{12}^{2+}), 739.8 (y_{11}^{2+}), 682.8 (y_{10}^{2+})
GSHQISLDNPDYQQDFFPK	746.0	1072.5 (y_8), 642.8 (y_{10}^{2+}), 952.5 (b_9), 923.4 (b_{16}^{2+}), 996.9(b_{17}^{2+})
GSHQI*p*SLDNPDYQQDFFPK – MS^3	772.7 → 740.01	914.4 (b_{16}^{2+}), 934.4 (b_9), 987.9 (b_{17}^{2+})
GSTAENAE *p*YLR	645.8	845.4 (y_6), 731.3 (y_5), 660.3 (y_4), 531.2 (y_3), 573.8 (y_9^{2+})
GSTAENAEYLR	605.78	894.4 (y_7), 765.4 (y_6), 580.3 (y_4), 451.3 (y_3), 533.8 (y_9^{2+})
IPLENLQIIR	**604.9**	**998.6 (y_8), 885.5 (y_7), 756.5 (y_6), 529.4 (y_4), 548.3 (y_9^{2+})**
NLQEILHGAVR	**625.4**	**894.5 (y_8), 765.5 (y7), 652.4 (y_6), 539.3 (y_5), 402.3 (y_4)**
EISDGDVIISGNK	**673.8**	**1104.6 (y_{11}), 631.4 (y_6), 518.3 (y_5), 405.2 (y_4), 502.2 (b_5^{2+})**
GLWIPEGEK	**514.8**	**858.4 (y_7), 672.4 (y_6), 559.3 (y_5), 429.7 (y_7^{2+}), 470.3 (b_4)**
ITDFGLAK	**432.7**	**751.4 (y_7), 650.4 (y_6), 535.3 (y_5), 388.3 (y_4), 215.1 (b_2)**
MHLPSPTDSNF*p*YR^	**827.9**	**1273.5 (y_{10}), 1089.4 (y_8), 776.3 (y_5), 693.8 (y_{11}^{2+}), 382.2 (b_3)**
RPAGSVQNPV*p*Y HNQPLNPAPSR^	**830.4**	**1483.7 (y_{12}), 1118.5 (y_{20}^{2+}), 1083.0 (y_{19}^{2+}), 897.4 (y_{15}^{2+}), 976.9 (b_{17}^{2+})**
GSHQISLDNPD*p*YQQDFFPK^	**775.3**	**1275.5 (y_9), 1160.5 (y_8), 807.3 (y_{12}^{2+}), 743.8 (y_{11}^{2+}), 686.8 (y_{10}^{2+})**
GSTAENAE*p*YLR^	**650.8**	**855.4 (y_6), 741.3 (y_5), 670.3 (y_4), 541.2 (y_3), 578.8 (y_9^{2+})**

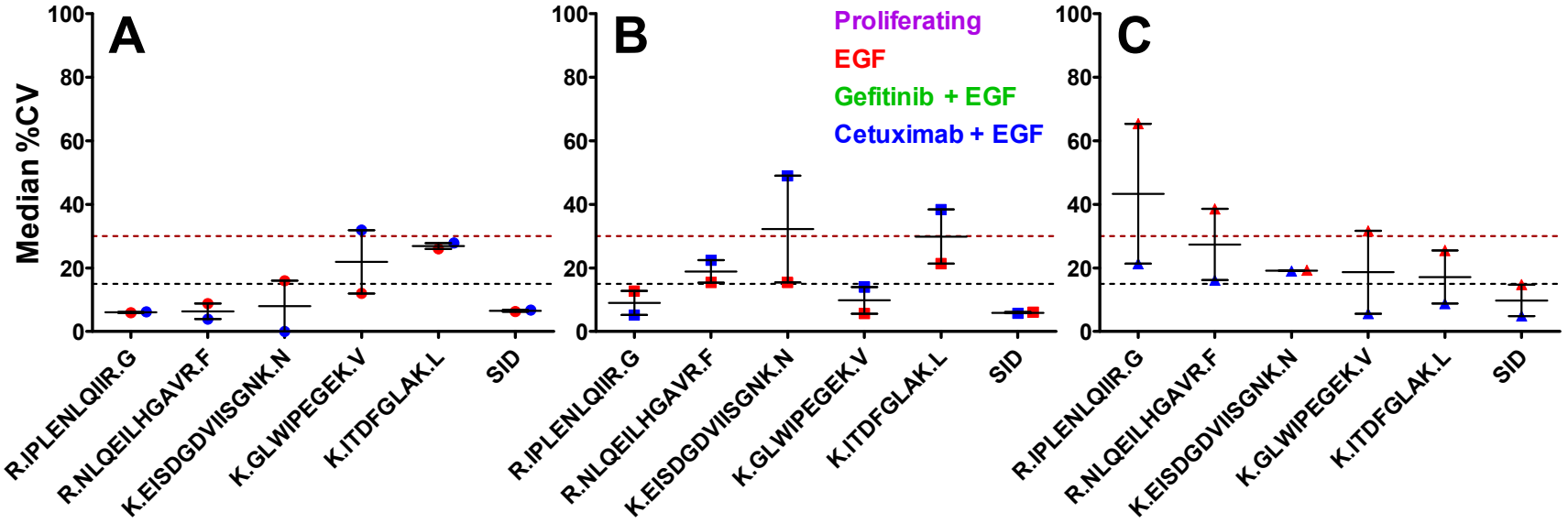

Figure C1. **Median CV plots for peptide MHLPSPTDSNF*pY*R.** The CV's were calculated by the technical replicate analysis on a per treatment basis for each internal reference and stable isotope labeled peptide. (A-C) All data (three technical replicates for each treatment) was used to calculate median CV's for biological replicate one (A), two (B) and three (C). The black dashed line represents 15% CV, and the red dashed line represents 30% CV. Data was not detected in proliferating or gefitinib co-treated samples.

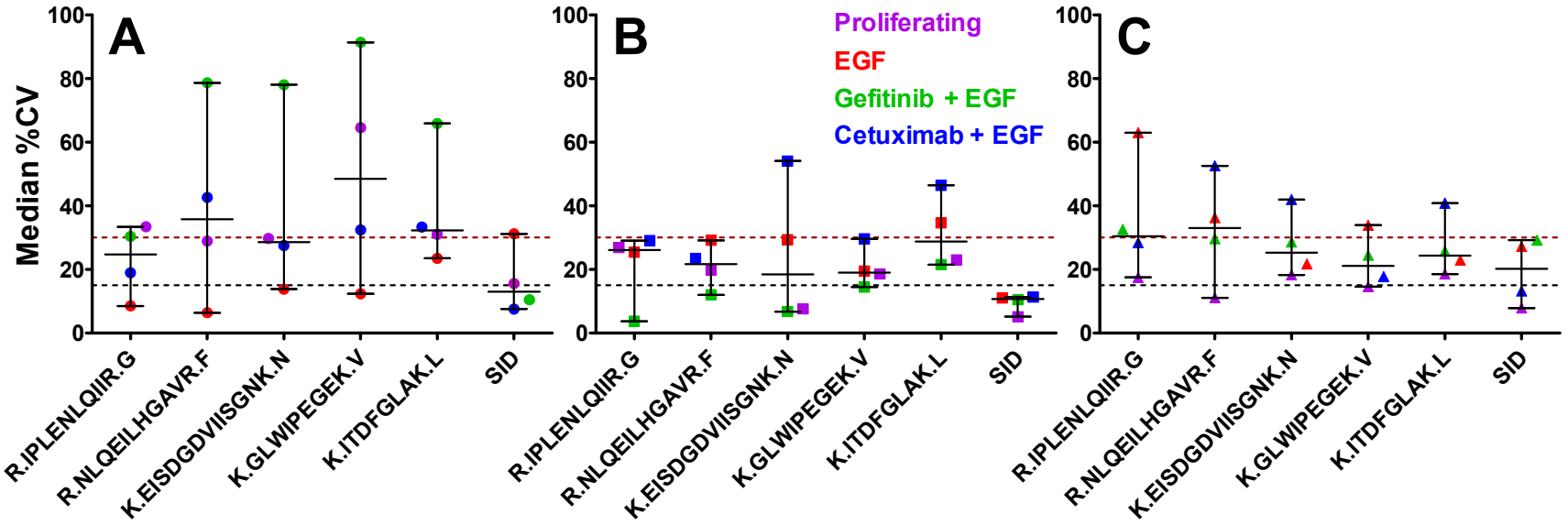

Figure C2. **Median CV plots for peptide GSHQISLDNPD*pY*QQDFFPK.** The CV's were calculated by the technical replicate analysis on a per treatment basis for each internal reference and stable isotope labeled peptide. (A-C) All data (three technical replicates for each treatment) was used to calculate median CV's for biological replicate one (A), two (B) and three (C). The black dashed line represents 15% CV, and the red dashed line represents 30% CV.

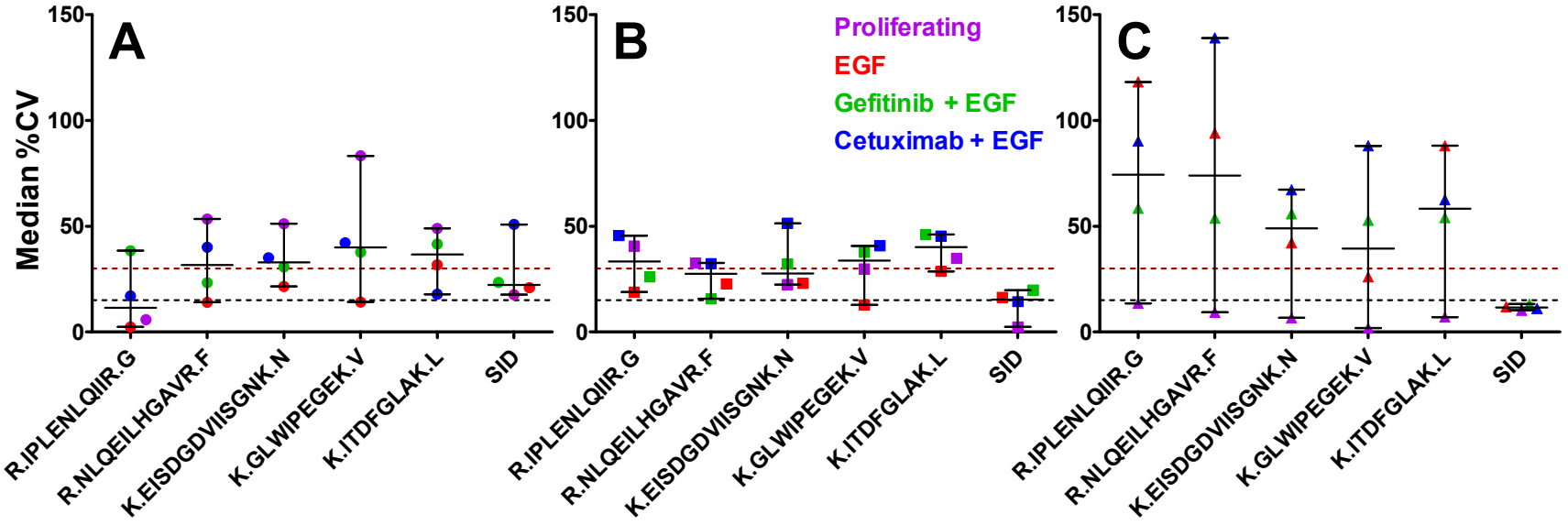

Figure C3. **Median CV plots for peptide GSTAENAE*pY*LR.** The CV's were calculated by the technical replicate analysis on a per treatment basis for each internal reference and stable isotope labeled peptide. (A-C) All data (three technical replicates for each treatment) was used to calculate median CV's for biological replicate one (A), two (B) and three (C). The black dashed line represents 15% CV, and the red dashed line represents 30% CV.

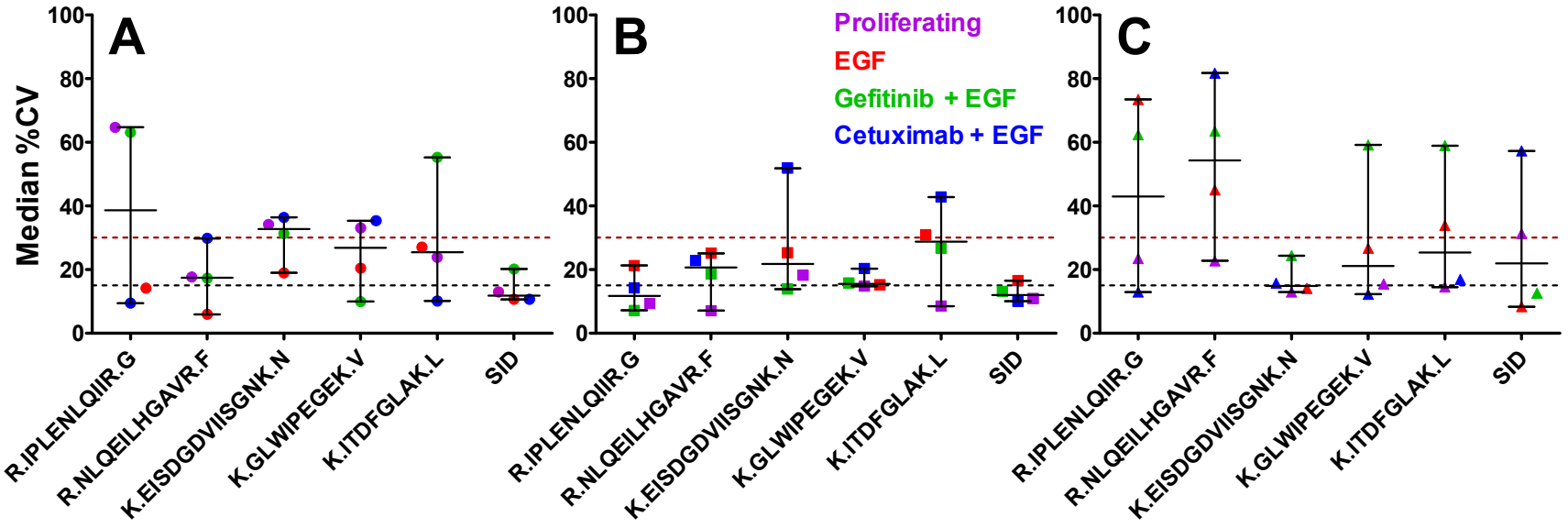

Figure C4. **Median CV plots for MS^3 of MHLP*pS*PTDSNFYR peptide.** The CV's were calculated by the technical replicate analysis on a per treatment basis for each internal reference and stable isotope labeled peptide. (A-C) All data (three technical replicates for each treatment) was used to calculate median CV's for biological replicate one (A), two (B) and three (C). The black dashed line represents 15% CV, and the red dashed line represents 30% CV.

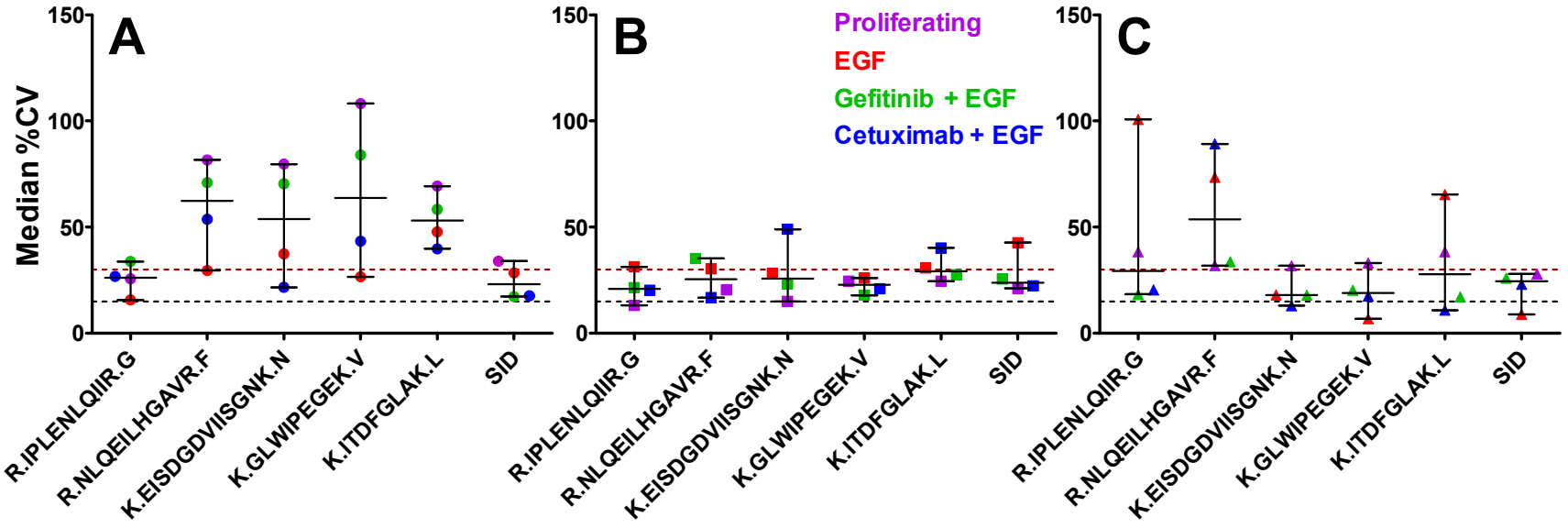

Figure C5. **Median CV plots for MS^3 of GSHQI*p*SLDNPDYQQDFFPK peptide.** The CV's were calculated by the technical replicate analysis on a per treatment basis for each internal reference and stable isotope labeled peptide. (A-C) All data (three technical replicates for each treatment) was used to calculate median CV's for biological replicate one (A), two (B) and three (C). The black dashed line represents 15% CV, and the red dashed line represents 30% CV.

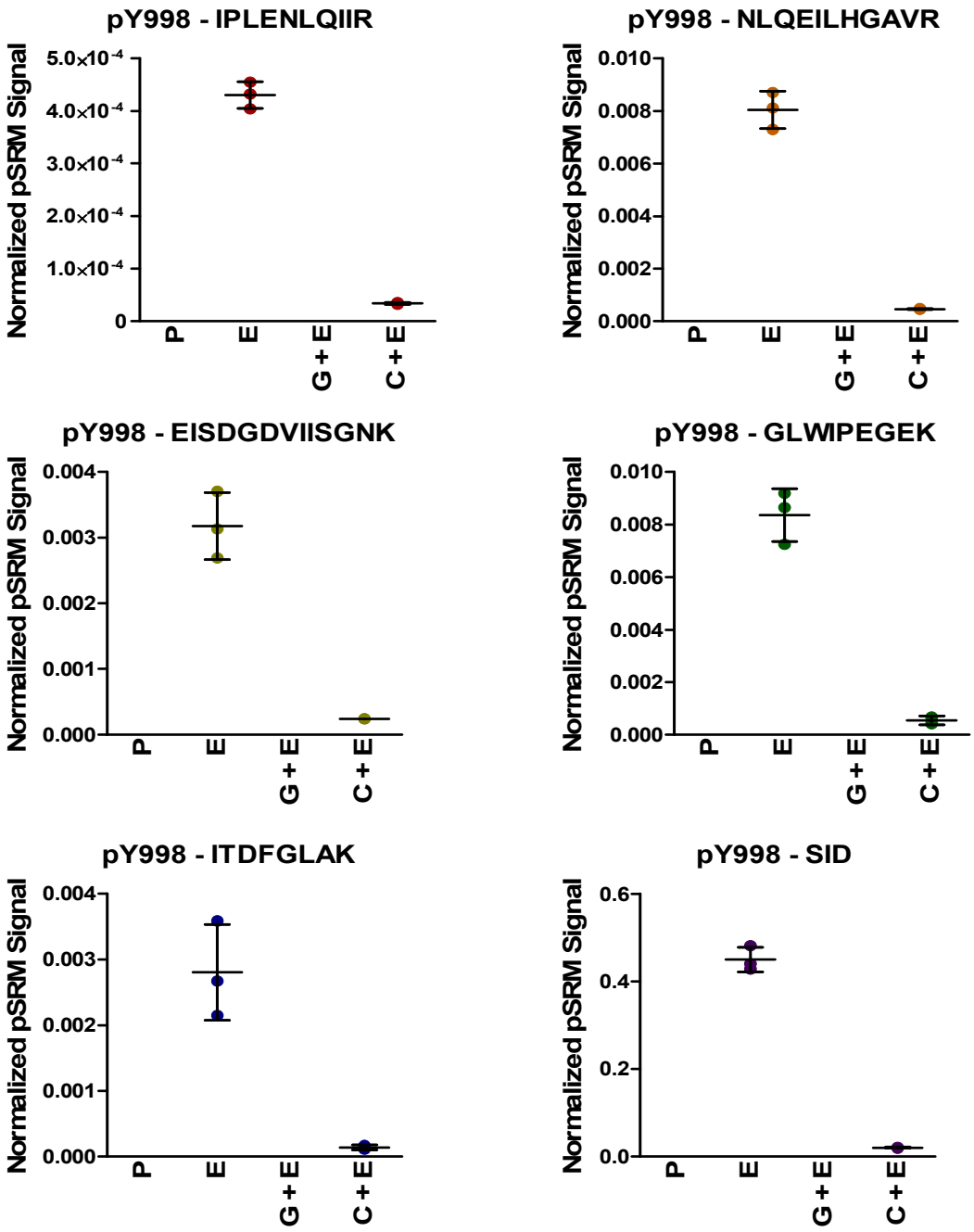

Figure C6. **Normalized pSRM plots of MHLPSPTDSNF*pY*R for each internal reference peptide and SID peptide**. (P – proliferating, E – EGF-stimulated, G + E – gefitinib-treatment followed by EGF and C + E – Cetuximab-treatment followed by EGF). Data from biological replicate one (biological replicate two and three generate similar results), three technical replicates. Data was "not detected" for P and G + E samples.

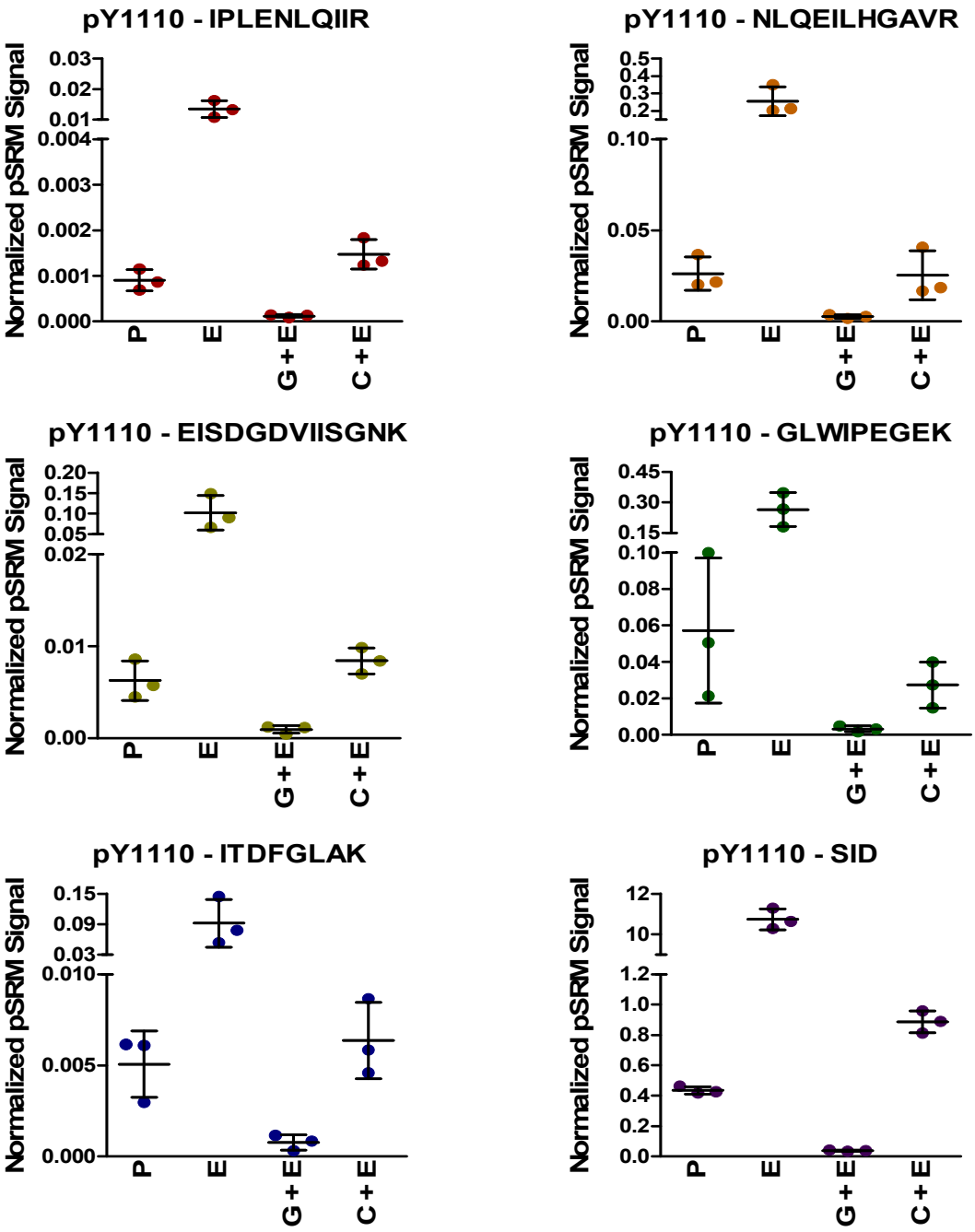

Figure C7. Normalized pSRM plots of RPAGSVQNPV*pY*HNQPLNPAPSR for each internal reference peptide and SID peptide. (P – proliferating, E – EGF stimulated, G + E – Gefitinib-treatment followed by EGF and C+ E – Cetuximab-treatment followed by EGF). Data from biological replicate one (biological replicate two and three generate similar results), three technical replicates.

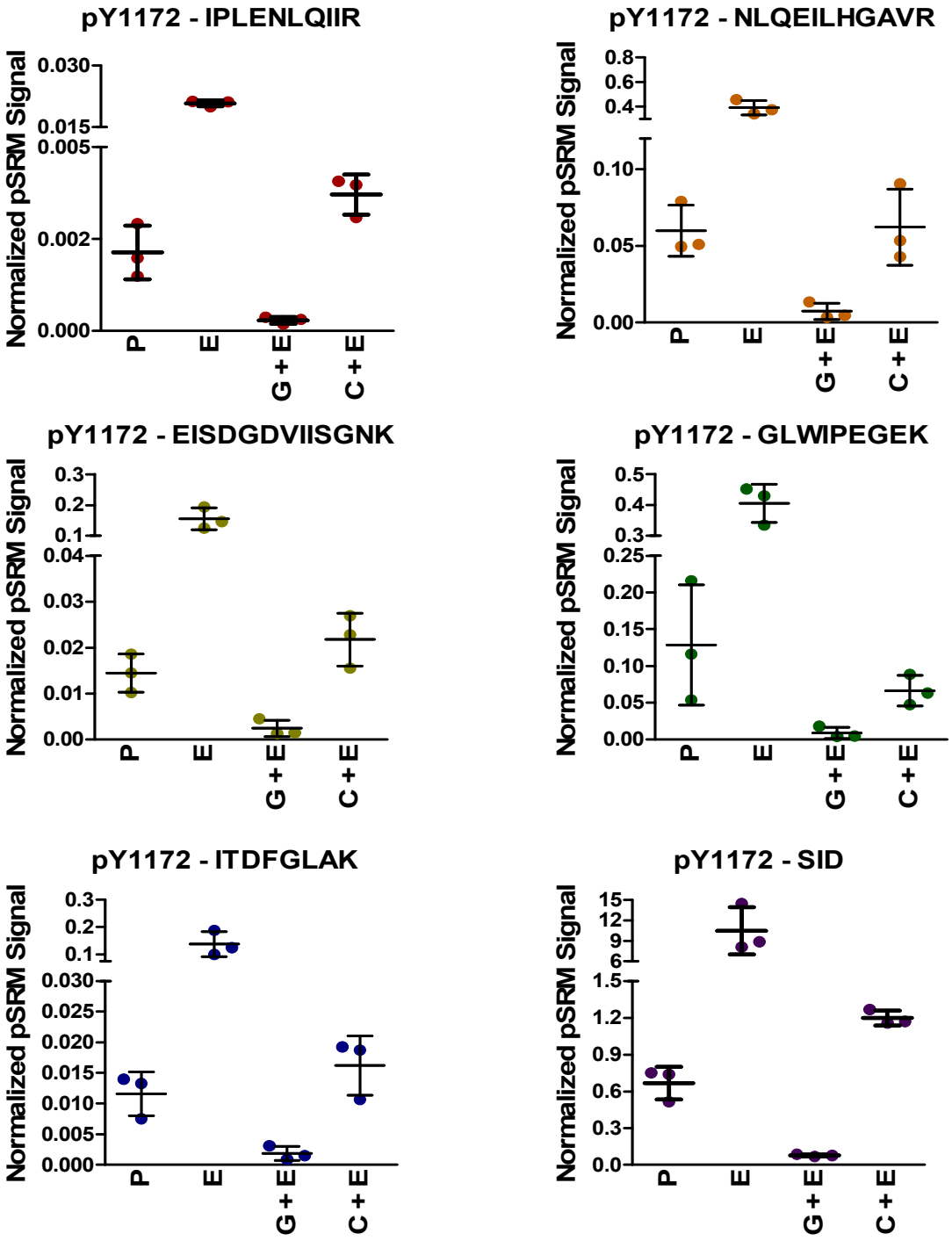

Figure C8. Normalized pSRM plots of GSHQISLDNPD*pY*QQDFFPK for each internal reference peptide and SID peptide. P – proliferating, E – EGF-stimulated, G + E – gefitinib-treatment followed by EGF and C + E – cetuximab-treatment followed by EGF). Data from biological replicate one, three technical replicates (biological replicate two and three generate similar results).

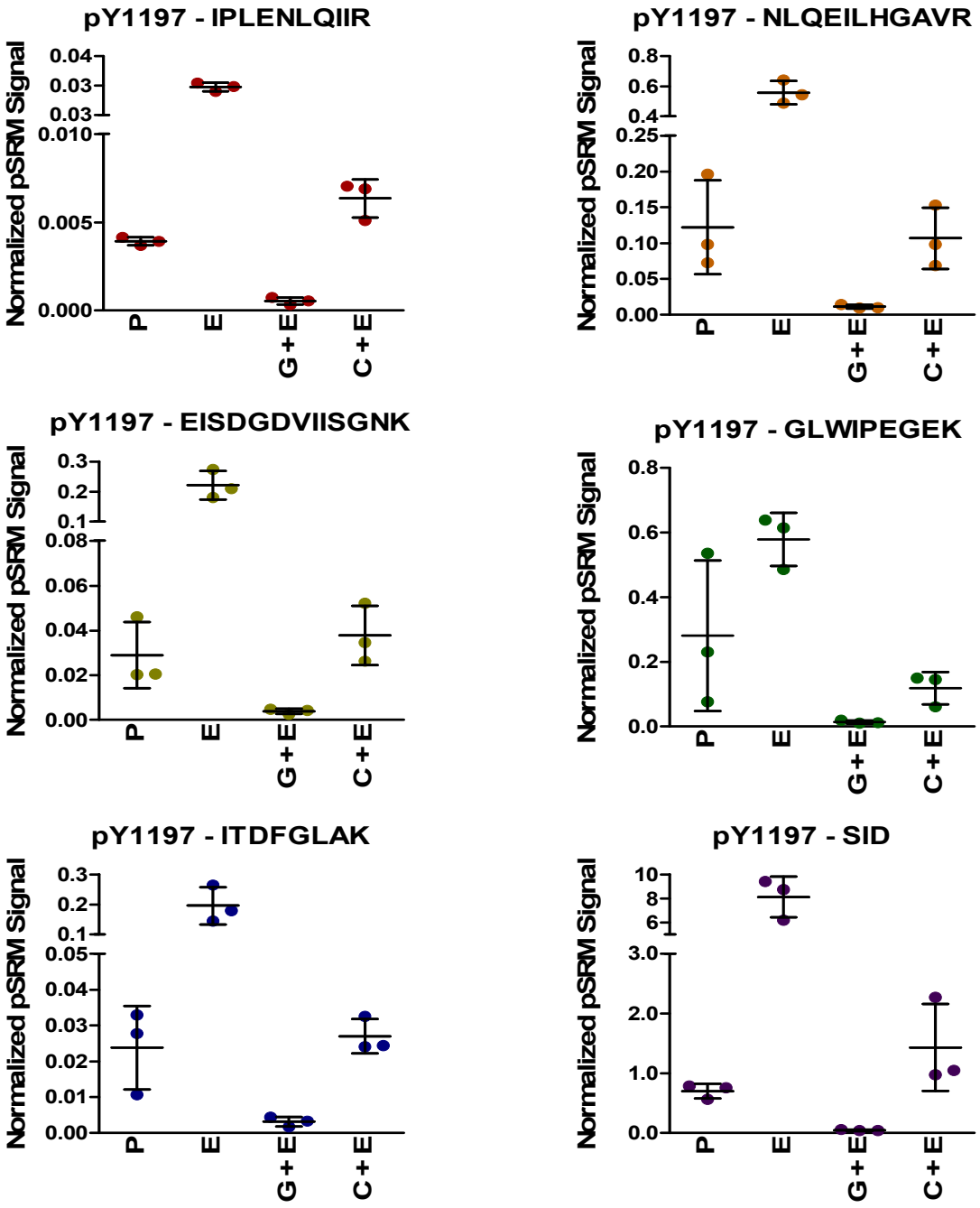

Figure C9. Normalized pSRM plots (GSTAENAE*pY*LR) for each internal reference peptide and SID peptide P – proliferating, E – EGF-stimulated, G + E – gefitinib-treatment followed by EGF and C + E – cetuximab-treatment followed by EGF). Data from biological replicate one, three technical replicates (biological replicate two and three generate similar results).

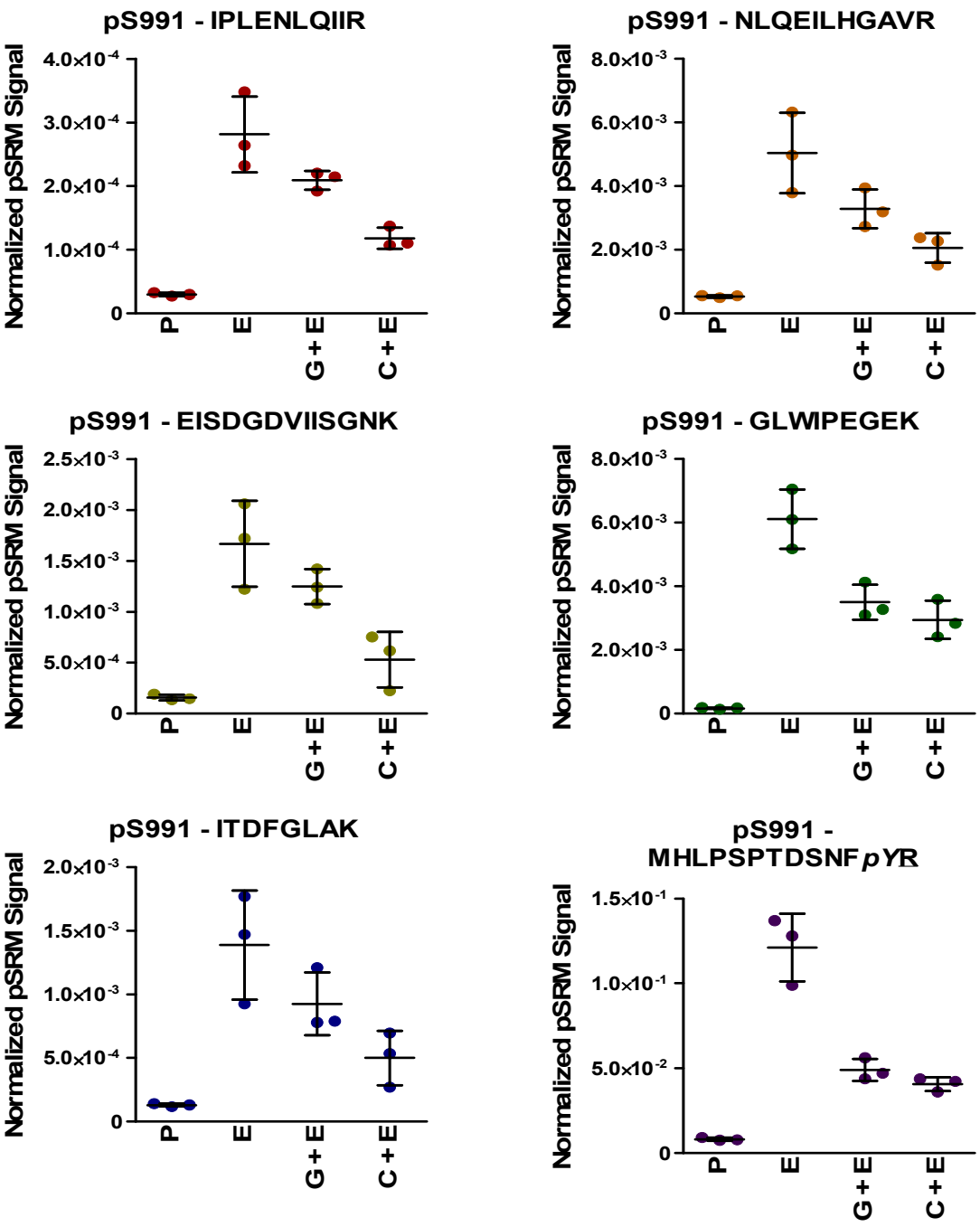

Figure C10. Normalized MS^3 pSRM plots (MHLP*pS*PTDSNFYR) for each internal reference peptide and *pY* peptide complement. (P – proliferating, E – EGF-stimulated, G + E – Gefitinib-treatment followed by EGF and C + E – Cetuximab-treatment followed by EGF). Data from biological replicate two, three technical replicates. The underlined amino acid indicates which amino acid was stable isotope labeled.

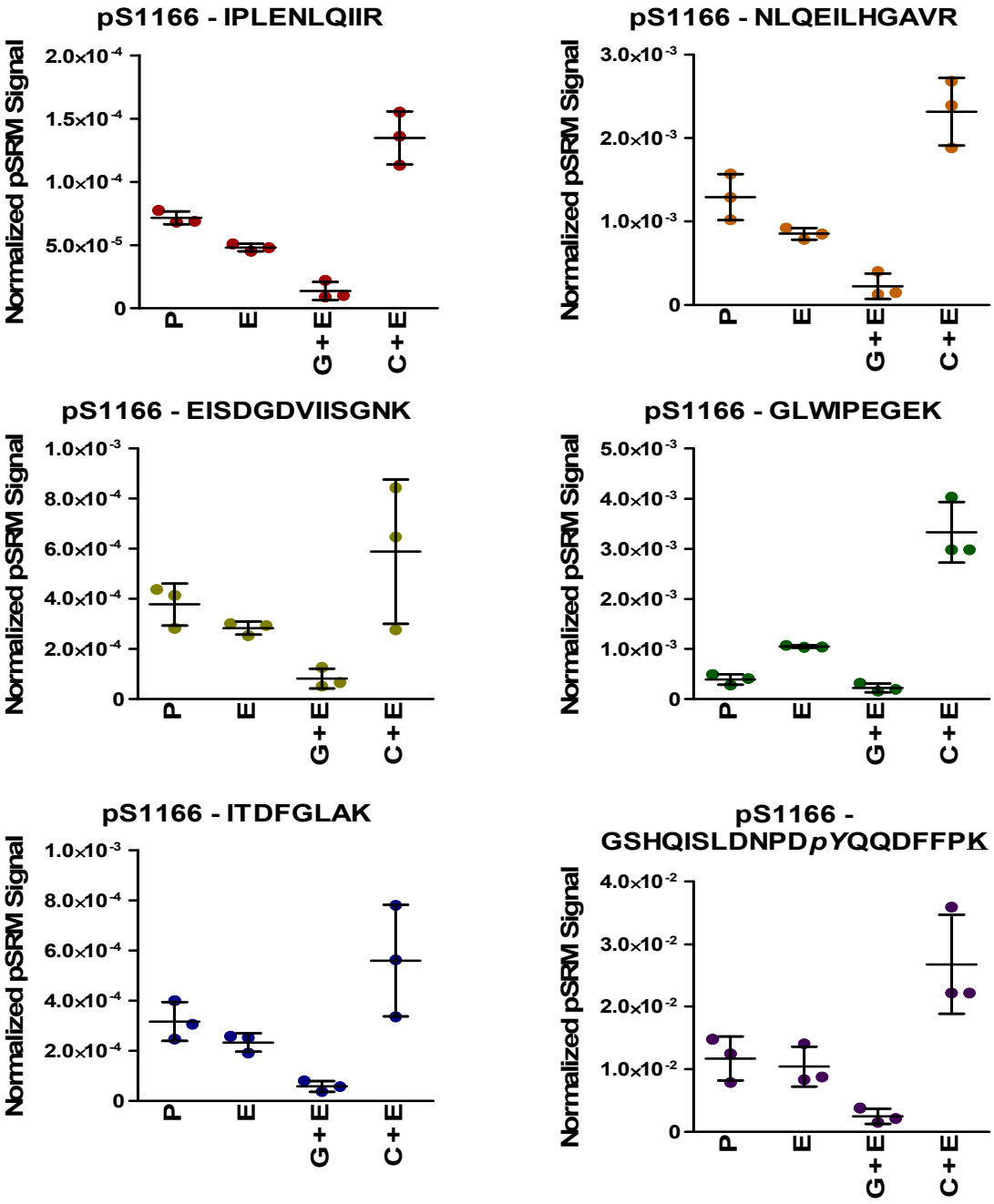

Figure C11. Normalized MS^3 pSRM plots (GSHQI*pS*LDNPDYQQDFFPK) for each internal reference peptide and *pY* peptide complement. (P – proliferating, E – EGF-stimulated, G + E – Gefitinib-treatment followed by EGF- and C + E – Cetuximab-treatment followed by EGF). Data from biological replicate two, three technical replicates. The underlined amino acid indicates which amino acid was stable isotope labeled.